Heinrich Heine
Universität
Düsseldorf

RNA-cleaving DNAzymes: an approach to treat viral infections?

Inaugural-Dissertation

zur Erlangung des Doktorgrades der
Mathematisch-Naturwissenschaftlichen Fakultät der
Heinrich-Heine-Universität Düsseldorf

vorgelegt von

Nina Maria Kirchgässler

aus Mettmann

Düsseldorf, März 2024

aus dem Institut für Physikalische Biologie
der Heinrich-Heine-Universität Düsseldorf

Gedruckt mit der Genehmigung der
Mathematisch-Naturwissenschaftlichen Fakultät der
Heinrich-Heine-Universität Düsseldorf

Berichterstattende:

1. Prof. Dr. Ingrid Span
2. Prof. Dr. Ilka Axmann

Tag der mündlichen Prüfung: 18. Juni 2024

The virtues of science are scepticism and independence of thought.
Walter Gilbert

CONTENTS

ABBREVIATIONS

3D	Three-dimensional
6-FAM	6-carboxyfluorescein
Å	Angstrom
ANA	Arabino nucleic acid
ASO	Antisense oligonucleotide
ATP	Adenosine triphosphate
AuNP	Gold nanoparticle
BHQ-1	Black Hole Quencher-1
BSA	Bovine serum albumin
CD	Circular dichroism
CeNA	Cyclohexene nucleic acid
CuAAC	Copper-catalyzed alkyne-azide cycloaddition
D	Cavity size
Da	Dalton (g/mol)
dex	Dextran
DNA	Deoxyribonucleic acid
DRz	Deoxyribozyme, DNAzyme
Dz	10-23 DNAzyme
EG	Ethylene glycol
FANA	2'-fluoroarabino nucleic acid
FCS	Fluorescence correlation spectroscopy
F-Q pair	Fluorophore-quencher pair
FRET	Förster Resonance Energy Transfer
g	Gram
h	Hour
HeNA	Hexitol nucleic acid
HIV-1	Human immunodeficiency virus type 1
k_{obs}	Rate constant (observed)
k_{rel}	Relative rate constant
L	Litre
LNA	Locked nucleic acid
m	Metre
M	Molar
M^{+}	Monovalent metal ion
M^{2+}	Divalent metal ion
MBS	Metal ion binding site
MC	Molecular crowding
MD	Molecular dynamic
min	Minute

miRNA	microRNA
mRNA	Messenger RNA
MΩ	Mega-Ohm
M_W	Molecular weight
$M_{W,\,av}$	Average molecular weight
N	Nucleocapsid protein
NA	Nucleic acid
NMR	Nuclear magnetic resonance
nt	Nucleotide
PAGE	Polyacrylamide gel electrophoresis
PCR	Polymerase chain reaction
PEG	Polyethylene glycol
PLL-*g*-Dex	Poly(L-lysine)-*graft*-dextran
PrP	Prion protein (human)
PS	Phosphorothioate
R	Purine (adenine (A), guanine (G))
RCD	RNA-cleaving DNAzyme
RFD	RNA-cleaving fluorescent DNAzyme
r_g	Gyration radius
r_h	Hydrodynamic radius
RNA	Ribonucleic acid
RNAi	RNA interference
s	Second
SAXS	Small-angle X-ray scattering
SELEX	Systematic evolution of ligands by exponential enrichment
siRNA	Small interfering RNA
smFRET	Single-molecule FRET
T	RNA substrate only (samples)
τ_D	Diffusion time
TBE	Tris-borate EDTA buffer
TCSPC	Time-correlated single photon counting
TDz	DNAzyme:RNA complex (samples)
T_m	Melting temperature
TMAO	Trimethylamine-N-oxide
TNA	α-L-threofuranosyl nucleic acid
u_{10}	Mean pairing probability
UTR	Untranslated region
VHS	Viral hemorrhagic septicaemia
VHSV	Viral hemorrhagic septicaemia virus
WOAH	World Organisation for Animal Health (OIE)
XNA	Xeno nucleic acid
Y	Pyrimidine (cytosine (C), thymine (T), uracil (U))

ABSTRACT

DNAzymes are artificially obtained, single-stranded DNA molecules that are capable of catalyzing chemical reactions. For therapeutic approaches, RNA-cleaving DNAzymes are of particular interest, which catalyze the site-specific cleavage of RNA substrates depending on divalent metal ions as cofactor. One of the most prominent RNA-cleaving DNAzymes is the 10-23 DNAzyme (Dz). The Dz consists of a catalytic core that is flanked by two substrate binding arms, of which the latter can be designed to target almost any sequence of interest. Recent high resolution structural data on the Dz:RNA complex shed light on the Dz's cleavage mechanism and closed a long lasting gap of missing information. Although the Dz was discovered more than 20 years ago by *in vitro* selection, low *in vivo* activity remains a persisting challenge. Despite promising progress using chemically modified building blocks, it is poorly understood how the cellular environment is able to interfere with Dz activity. Here, molecular crowding is suspected as cause, which summarizes physicochemical consequences that result from unspecific interactions within the heterogeneous and densely packed environment in cells. Thus, the present work aims at investigating effects by molecular crowding on the activity and structure of the Dz. The goal is to contribute to a better understanding of the molecular interplay that might point towards new modification strategies to help overcome *in vivo* limitations.

In order to investigate molecular crowding *in vitro*, it is key to simulate conditions that resemble cells. The first article (Kirchgässler *et al.* (2022) Protocol for molecular crowding analyses) provides a protocol for mimicking a cell-like environment *in vitro* and analyzing a Dz's stability and activity in presence of them. Additional hints for handling crowded solutions and DNAzymes are given. The simulation of crowded conditions is obtained using osmolytes and polymers polyethylene glycol and dextran as cosolutes. The protocol includes detailed instructions for a Förster Resonance Energy Transfer-based cleavage assay, denaturing urea polyacrylamide gel electrophoresis, and circular dichroism spectroscopy.

In the second article (Molecular crowding: impacts on the activity of the 10-23 DNAzyme), studies on the Dz under crowded conditions, including the methods presented in article one, are pursued and expanded by determining physicochemical solution properties and providing first information on the Dz:RNA complex structure. The latter was obtained by fluorescence correlation spectroscopy and small-angle X-ray scattering. The data show that depending on the cosolute's nature and concentration, Dz activity is reduced or at certain conditions even increased. In a promoting surrounding, preferences in crowded conditions tend to differ between cofactors Mg^{2+} and Mn^{2+}. Analyses on the size and shape of the Dz:RNA complex indicate less structural impact by molecular crowding. This study provides important first insights on how cellular conditions potentially influence the performance of the Dz and presents cofactor dependencies for the first time.

As cells contain a diversity of biomolecules, resembling their complexity *in vitro* is challenging. Thus, in a perspective, article 3 (Extending crowding *in vitro*), the conditions under which previous crowding studies with the focus on DNAzymes have been performed are compared and discussed with regard to the applied cosolute and buffer as well as used RNA

substrate length. The critical analysis outlines options for adjustment to gradually increase system complexity, which will help to gain deeper insights on molecular crowding effects in future attempts.

Apart from molecular crowding analyses, this work also deals with examining the therapeutic potential of the Dz to target viral infections beyond human pathogens, in which fish farming is selected as field of interest (Article 4: Use of the 10-23 DNAzyme to target fish viruses). One of the most dominating diseases is mediated by the viral hemorrhagic septicaemia virus, which is selected as target. Dz are designed to bind and cleave the RNA sequence that codes for the nucleocapsid protein due to its crucial function in viral replication. For the very first time, we present three potential candidates that are stable and able to perform site-specific cleavage under the tested conditions targeting VHSV. The results provide an initial base to further explore the antiviral potential of DNAzymes in fish.

ZUSAMMENFASSUNG

DNAzyme sind artifizielle, einzelsträngige DNA-Moleküle, die in der Lage sind, chemische Reaktionen zu katalysieren. Für therapeutische Zwecke sind RNA-spaltende DNAzyme von besonderem Interesse, die die sequenzspezifische Spaltung von RNA-Substraten in Abhängigkeit von divalenten Kationen als Cofaktoren katalysieren. Eines der bekanntesten RNA-spaltenden DNAzyme ist das 10-23 DNAzym (Dz). Das Dz besteht aus einem katalytischem Kern, der von zwei Substratbindearmen flankiert wird. Letztere lassen sich in ihrer Sequenz variable an nahezu jedes RNA-Substrat anpassen. Eine erst kürzlich veröffentlichte, hochaufgelöste Struktur des Dz:RNA-Komplexes liefert neue Hinweise auf den Katalysemechanismus und schließt damit eine lang bestehende Informationslücke. Obwohl das Dz bereits vor mehr als zwei Jahrzehnten mittels *in vitro*-Selektion selektiert wurde, ist dessen geringe *in vivo*-Aktivität eine bestehende Herausforderung. Trotz vielversprechender Fortschritte bei der Verwendung von chemisch modifizierten Bausteinen, ist es nur unzureichend geklärt, inwiefern das zelluläre Umfeld die Aktivität des Dz beeinflussen kann. Hier wird das molekulare Gedränge (Molecular Crowding) als eine mögliche Ursache vermutet, welches die physikochemischen Konsequenzen zusammenfasst, die aus den unspezifischen Wechselwirkungen innerhalb des heterogenen und dicht gepackten Umfelds in Zellen resultieren. Ziel dieser Arbeit ist es daher die Auswirkungen des molekularen Gedränges in Zellen auf die Aktivität und Struktur des Dz zu untersuchen, die zu einem besseren Verständnis des molekularen Zusammenspiels beitragen sollen und neue, mögliche Modifizierungsstrategien öffenbaren könnten.

Um das molekulare Gedränge *in vitro* untersuchen zu können, ist es wichtig zellnahe Bedingungen zu simulieren. Der erste Artikel (Kirchgässler *et al.* (2022) Protocol for molecular crowding analyses) beinhaltet ein Protokoll um solche *in vitro* zu simulieren und die Aktivität und Stabilität des Dz unter diesen zu untersuchen. Darüber hinaus werden Hinweise zum Umgang mit gedrängten Lösungen und DNAzymen aufgeführt. Die gedrängten Bedingungen werden unter Verwendung von Osmolyten und den Polymeren Polyethylenglykol und Dextran als Kosolute simuliert. Das Protokoll enthält detaillierte Anweisungen für eine Förster-Resonanz-Energie-Transfer-basierte Spaltungsanalyse, denaturierende Harnstoff-Polyacrylamid-Gelelektrophorese und Zirkulardichroismus-Spektroskopie.

Im zweiten Artikel (Molecular crowding: impacts on the activity of the 10-23 DNAzyme) werden die Untersuchungen des Dz unter gedrängten Bedingungen, einschließlich der in Artikel 1 vorgestellten Methoden, fortgeführt und durch die Bestimmung von physikochemischen Lösungseigenschaften und der Lieferung erster Informationen zur Struktur des Dz:RNA-Komplexes erweitert. Letztere wurden mittels Fluoreszenzkorrelationsspektroskopie und Kleinwinkel-Röntgenstreuung gewonnen. Die Daten zeigen, dass in Abhängigkeit von der Art und Konzentration des Kosolutes die Aktivität des Dz reduziert oder unter bestimmten Bedingungen sogar erhöht wird. In einer aktivitätsfördernden Umgebung zeigen die von den beiden Cofaktoren Mg^{2+} und Mn^{2+} bevorzugten Bedingungen unterschiedliche Tendenzen auf. Die Analysen zur Größe und Form des Dz:RNA-Komplexes deuten auf einen geringen, strukturellen Einfluss durch das molekulare Gedränge hin. Diese Studie liefert erste, wich-

tige Erkenntnisse darüber, wie zelluläre Bedingungen die Leistung des Dz möglicherweise beeinflussen und zeigt zum ersten Mal Kofaktor-Abhängigkeiten auf.

Da sich Zellen aus einer Vielzahl von verschiedenen Biomolekülen zusammensetzen, ist es eine Herausforderung ihre Komplexität *in vitro* widerzuspiegeln. Daher werden in Artikel 3 (Extending crowding *in vitro*) die Bedingungen, unter denen bisherige Studien unter gedrängten Bedingungen mit Schwerpunkt auf DNAzymen durchgeführt wurden, verglichen und im Hinblick auf die verwendeten Kosolute und Puffer, sowie RNA-Substratlängen diskutiert. Die kritische Analyse arbeitet Anpassungsmöglichkeiten heraus, um eine graduelle Erhöhung der Systemkomplexität zu gewährleisten, die es in zukünftigen Studien ermöglichen soll noch tiefere Einblicke in die Einflüsse des molekularen Gedränges zu gewinnen.

Neben diesen Analysen befasst sich die vorliegende Arbeit auch mit der Untersuchung des therapeutischen Potenzials des Dz zur Bekämpfung von Virusinfektionen jenseits von Humanpathogenen, wobei die Fischzucht als Interessensgebiet betrachtet wird (Artikel 4: Use of the 10-23 DNAzyme to target fish viruses). Eine der dominierenden Krankheiten wird durch das virale hämorrhagische Septikämievirus hervorgerufen, das als Ziel ausgewählt wurde. Dz wurden zur Bindung und Spaltung der RNA-Sequenz des Nukleokapsidproteins entworfen, welches eine entscheidende Funktion bei der viralen Replikation einnimmt. Zum ersten Mal stellen wir drei potenzielle Kandidaten vor, die unter den getesteten Bedingungen stabil und in der Lage sind, die RNA des VHSV sequenzspezifisch zu spalten. Die Ergebnisse bilden eine erste Grundlage für die weitere Untersuchung des antiviralen Potenzials von DNAzymen in Fischen.

1

General Introduction

1.1 Catalytic properties of nucleic acids

Prior to discovering nucleic acid catalysts in the early 1980s, biocatalysis was solely attributed to proteins, better known as enzymes. Proteins mostly consist of 20 amino acids that are classified as non-polar, polar, hydrophobic, hydrophilic, and negatively or positively charged, depending on their side chain properties. These provide a vast repertoire of interactions and define the process of co-operative folding to achieve the thermodynamically most favored structure, which results in proteins of differently charged surfaces (Bhagavan, 2002). Thus, diversity in amino acid sequence–primary structure–paired with variability in structural organization–secondary and tertiary–promised broad functionality.

On the contrary, nucleic acids (NA) are composed of four building blocks, two double-ringed purine bases, adenine (A) and guanine (G), and two single-ringed pyrimidine bases, uracil (U) and cytosine (C). In deoxyribonucleic acid (DNA), uracil is exchanged to thymine (T) and the ribose moiety lacks the 2'-hydroxyl group (OH, Tinoco and Bustamante, 1999; Minchin and Lodge, 2019). In comparison to proteins, NA present a rather restricted number of functional groups, thus chemical diversity, and interactions, which include hydrogen bonding and base stacking (Tinoco and Bustamante, 1999). Their composition and uniformly negatively charged surface due to a regular phosphate backbone made nucleic acid-mediated catalysis counterintuitive (Minchin and Lodge, 2019; Silverman, 2016).

Despite, for the first time in 1981, Cech and co-workers reported a ribonucleic acid (RNA) sequence with self-splicing activity in absence of proteins in *Tetrahymena* (Cech *et al.*, 1981; Kruger *et al.*, 1982). With a second report of an RNA-cleaving RNA sequence emerging in 1983 (Guerrier-Takada *et al.*, 1983), speculations and discussions were triggered assuming a world with RNA as a central molecule prior to DNA and proteins. In such an 'RNA world', first introduced in 1986 (Gilbert, 1986), RNA is supposed to store genetic information as well as to perform chemical reactions (Robertson and Joyce, 2012; Higgs and Lehman, 2015). Today, such RNA catalysts are better known as ribozymes and several classes of naturally occurring and artificial ribozymes have been identified over the past decades (Müller *et al.*, 2016; Doudna and Cech, 2002; Tanner, 1999; Ward *et al.*, 2014). The key feature is adopting a three-dimensional (3D) structure that uses bound metal ions as primary cofactors and includes recognition sites as well as catalytic regions to allow for an activity similar to enzymes (Robertson and Joyce, 2012; Lilley, 2011).

Since RNA and DNA share many compositional and structural similarities, although occupying markedly different cellular functions (Minchin and Lodge, 2019; Raina and Ibba, 2014; Valadkhan and Gunawardane, 2013; O'Brien *et al.*, 2018; Van Lint *et al.*, 2013), speculations quickly arose questioning the existence of DNA molecules with alike catalytic properties. However, to this day, DNA catalysts have not been found in nature. Thus, naturally occurring DNA molecules maintain only the function as long-term storage of genetic information (Thomas *et al.*, 2021).

Early methodical achievements made NA catalysts gain major advantage that quickly expanded their research and functionalization. In 1967, a report by Spiegelman marked the beginning of *in vitro* evolution methods (Mills *et al.*, 1967). The development of the polymerase chain reaction (PCR) nine years later, which is a widely established tool, highlights an important breakthrough allowing for quick and exponential amplification of RNA and DNA (Mullis *et al.*, 1986). Though amplification requires DNA polymerases and reverse transcriptase as enzymes, their frequent and established use makes such attempts feasible (Garibyan and Avashia, 2013). In this regard, ribozymes with RNA polyermase properties offered a second option for RNA amplification in a PCR-like manner (Ekland and Bartel, 1996; Horning and Joyce, 2016). Furthermore, the development of phosphoramidite chemistry in the 1980s, better known as solid-phase synthesis, further facilitated easy and quick synthesis of random as well as sequence-specific oligonucleotides (Caruthers, 2013; Beaucage and Caruthers, 1981; Matteucci and Caruthers, 1981). Today, this method is an automated and cost-effective standard in commercial NA synthesis, which provides the option to simply introduce chemical modifications and/or labels, and enables low batch to batch variation (Hughes and Ellington, 2017; Caruthers, 2013; Ma and Liu, 2021). Finally, in 1990, the process of systematic evolution of ligands by exponential enrichment (SELEX) was first described as *in vitro* selection method. This approach allows for the selection of nucleic acids with desired properties and function, without knowing any sequence requirements, and has advanced and adapted over the years (Tuerk and Gold, 1990; Joyce, 2007; Müller *et al.*, 2016).

In comparison, such approaches do not exist for proteins. Due to the above mentioned composition and folding, randomized amino acid sequences will most unlikely fold into tertiary structures that provide the desired function. Thus, protein optimization by directed evolution still relies on known structures and properties (Silverman, 2016). Moreover, secondary structure elements such as α-helices, β-sheets or random coils may not form in solution when isolated (Tinoco and Bustamante, 1999). On the contrary, secondary structures of NA, such as helices, are stable by themselves, enabling a hierarchical and sequential folding for RNA and DNA molecules (Tinoco and Bustamante, 1999; Wada and Suyama, 1986). In addition, high thermostability is a favorable property of NA compared to proteins (El-Murr *et al.*, 2012; Guo *et al.*, 2017; Nelson *et al.*, 2005). After denaturation by heating, NA are able to renature after cooling. Proteins, however, are often denatured irreversibly, leaving them inactive (Ma and Liu, 2021). These prerequisites, coupled with flexible programmability and sequence-specific cleavage (Silverman, 2016; Weinberg *et al.*, 2019), made NA catalysts become versatile tools.

1.2 Deoxyribozymes

The discovery of catalytically active RNA sequences expanded the spectrum of naturally occurring biocatalysts with ribozymes. In 1994, the first report of a DNA molecule with catalytic properties emerged, which was obtained by *in vitro* selection and performed the lead ion (Pb^{2+})-dependent cleavage of an RNA phosphodiester linkage within its oligonucleotide sequence (*cis*-cleavage, Breaker and Joyce, 1994). Since then, deoxyribozymes or DNAzymes (DRz) describe single-stranded DNA molecules that are able to adopt a three-dimensional structure, by which they obtain catalytic activity (Silverman, 2016; Achenbach *et al.*, 2005). To this day, however, DNA catalysts have not been found in nature (Ma and Liu, 2020). Compared to their RNA counterparts, DRz presented advantageous features, as DNA is not immunoactive or stimulatory (Uehata and Takeuchi, 2020) and lacks the 2'-OH at the sugar moiety. The latter makes them less prone to hydrolysis and consequently lowers the costs and necessary protective measures during synthesis (Javadi-Zarnaghi and Höbartner, 2020).

For almost three decades, continuous interest and attention in DRz have opened up new research areas and resulted in a pool of DNA catalysts of different function and application. In this regard, several review articles have been published that capture DRz versatility (e. g. Silverman, 2005, 2016; Baum and Silverman, 2008; Hollenstein, 2015; Morrison *et al.*, 2018; Ma and Liu, 2020).

1.2.1 RNA-cleaving DNAzymes

Even though DRz catalyze a broad spectrum of reactions (Section 1.3.1), variants that perform RNA cleavage still have been considered the most interesting. Besides applications in biosensing (Section 1.3.3), their ability to manage RNA knockdown highlighted their potential to function in medical applications including cancer treatment (Section 1.3.2).

Currently, the two most extensively studied RNA-cleaving DNAzymes (RCD) are the 8-17 and 10-23 DNAzyme (Santoro and Joyce, 1997). Both were named after the respective round of *in vitro* selection and clone number, from which they derive: thus, the 8-17 DNAzyme derived from the 17^{th} clone in selection round 8 and the 10-23 DNAzyme from the 23^{rd} clone in round 10. This thesis focuses on the latter, which is known as one of the most catalytically active variants (Nedorezova *et al.*, 2020, section 1.2.3).

Mechanistically, RCD are assumed to perform catalysis similar to the transesterification mediated by the hammerhead ribozyme (Santoro and Joyce, 1998; Emilsson *et al.*, 2003). The long lasting lack of structural information left researchers with insufficient mechanistic understanding. Today, new structural insights support the initial hypothesis of a general acid-base mechanism (Cortés-Guajardo *et al.*, 2021; Cepeda-Plaza and Peracchi, 2020; Cepeda-Plaza *et al.*, 2018; Borggräfe *et al.*, 2023, for further information see section 1.2.3).

1.2.2 *In vitro* selection

The isolation of DNAzymes and artificial ribozymes via *in vitro* selection generally starts with a library of 10^{14} - 10^{15} random sequences, in which each randomized sequence of length n provides 4^n different possible sequences. The aim of such process is to iteratively narrow down the initial pool to a few sequences that provide the desired function (Breaker and Joyce, 1994; Wilson and Szostak, 1999). In general, this procedure is based on the assumption that single-stranded oligonucleotide sequences are able to adopt a three-dimensional structure, by which they obtain catalytic function. Since this thesis focuses on the 10-23 DNAzyme, the applied *in vitro* selection strategy, which gave rise to it, is described below (Figure 1.1). Overall, this experiment is very similar to that applied for aptamer selection, better known as SELEX (Tuerk and Gold, 1990). In comparison, aptamers are single-stranded RNA or DNA molecules that provide ligand-binding properties and are able to bind to a specific target with high affinity (Jijakli *et al.*, 2016; Ellington and Szostak, 1992).

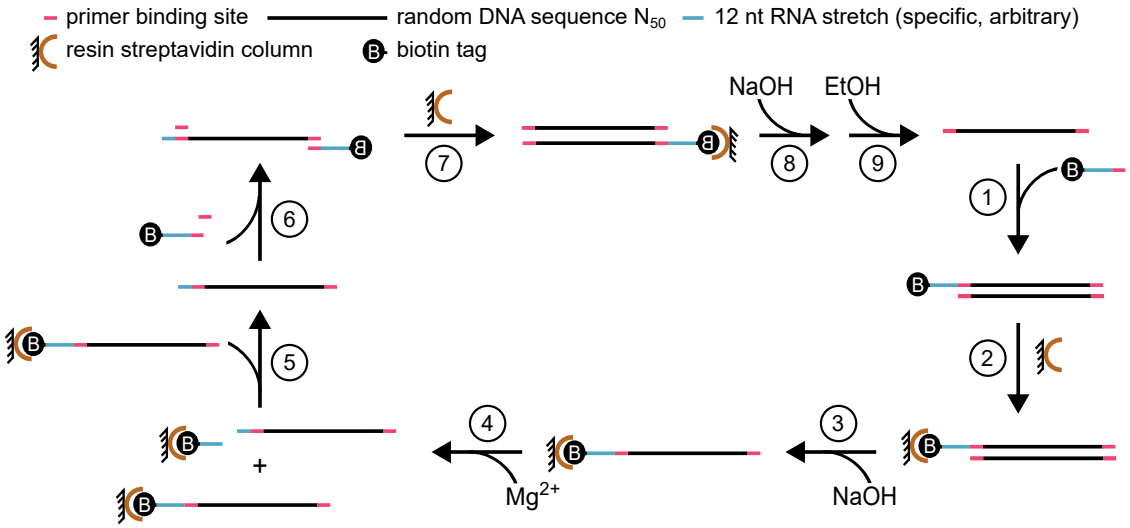

Figure 1.1: Strategy of *in vitro* selection applied to identify the 10-23 and 8-17 DNAzyme. A pool of 10^{14} randomized DNA sequences of 50 nt in length (black) and with constant primer binding sites (pink) on each end enters the selection cycle. **(1)** Annealing with a primer that contains a 12 nt RNA stretch (blue) as recognition and cleavage site and a biotin-tag at the 5'-end, followed by enzymatic primer extension. **(2)** Immobilization of double-stranded products on a streptavidin column. **(3)** Denaturation by treatment with NaOH to remove non-biotinylated strands. **(4)** Elution of RNA-cleaving DNA sequences using a magnesium ion (Mg^{2+})-containing buffer. Sequences that are able to adopt a catalytically active structure in presence of Mg^{2+} will elute from the column. **(5)** Inactive DNA sequences will remain attached to the column and are discarded. **(6)** Recovery of eluted sequences by primer annealing and amplification by PCR. **(7)** Immobilization of PCR products on a streptavidin column. **(8)** Treatment with NaOH to denature and elute non-biotinylated strands that will enter the next selection round as templates, followed by **(9)** precipitation with EtOH. Modified after Silverman (2005); Kumar *et al.* (2019); Breaker and Joyce (1994), based on Santoro and Joyce (1997).

The process started with a library of 10^{14} random nucleic acid sequences, each of 50 nucleotides (nt) in length (Santoro and Joyce, 1997). After annealing of a 5' biotinylated primer, which contained a 12 nt stretch of RNA as cleavage site, and template-directed extension, each sequence contained a biotin-label at the 5'-end, followed by the 12 nt stretch of RNA (Silverman, 2005). Next, sequences were attached to the solid phase of a streptavidin column, double-strands were denatured by sodium hydroxide (NaOH) treatment, and unlabeled strands were removed. Site-specific cleavage of an RNA phosphodiester bond was induced using a buffer composed of 10 mM $MgCl_2$, 1 M NaCl, and 50 mM Tris-HCl, pH 7.5. Sequences that

were presumably capable of cleaving RNA, detach from the column and elute. Subsequent recovery of such and amplification by PCR allowed immobilization to a streptavidin column again. Washing with NaOH, followed by ethanol precipitation led to the isolation of the non-biotinylated sequences that entered and started a new selection cycle. Since each round separates active from inactive sequences, the pool becomes enriched in sequences of desired function (Santoro and Joyce, 1997; Silverman, 2005).

Nowadays, several strategies evolved and SELEX-based techniques were adapted to meet the needs of DNAzyme diversity (Kumar *et al.*, 2019; Huang and Liu, 2020). Since chemical modifications are on the rise to overcome challenges in applications (Section 1.4.2), evolution and selection methods focused on facilitating their incorporation (Huang and Liu, 2020; Nguyen *et al.*, 2023; Taylor *et al.*, 2022). Another procedure, which has only been reported for nucleobase-modified aptamer selection so far, but may present an alternative for DNAzyme-selection as well, is click-SELEX. This versatile tool allows facilitated and modular introduction of modified building blocks using copper-catalyzed alkyne-azide cycloaddition (CuAAC), better known as click chemistry (Pfeiffer *et al.*, 2018; Tolle *et al.*, 2015).

1.2.3 The 10-23 DNAzyme

The 10-23 DNAzyme (Dz) is composed of a fixed catalytic core of 15 nt, flanked by two substrate binding arms of 6 to 12 nt each, by which the Dz binds its substrate through Watson-Crick base pairing (for an example and numbering of nucleotides see Figure 1.3A). The latter can be designed to recognize almost any target RNA of interest (Santoro and Joyce, 1998). Since increasing the arm length and GC-content influence positively the association, but negatively the dissociation of the Dz:RNA complex, which limits the use of Dz as catalysts, it is recommended to aim for a predicted binding free energy ($\Delta G_{37\,^\circ\mathrm{C}}$) of -8 to $-10\,\mathrm{kcal/M}$ for each arm during the design (Joyce, 2001; Sugimoto *et al.*, 1995; Fokina *et al.*, 2012). Cleavage of a phosphodiester bond requires a) a central purine-pyrimidine junction as cleavage site (5'-R↓Y-3', R = {G, A}; Y = {U, C}), in which the purine nucleotide is left unpaired (Santoro and Joyce, 1998), and b) divalent metal ions (M^{2+}) as cofactors, preferably manganese ions (Mn^{2+}) and Mg^{2+} (Joyce, 2001; Sugimoto *et al.*, 1999). Activity and substitution experiments revealed a dinucleotide preference of AU = GU $\geq$ GC $\gg$ AC as cleavage site (Santoro and Joyce, 1998).

Similarity to the hammerhead ribozyme and pH-dependent analyses led to the initial assumption that the Dz performs RNA-cleavage via a transesterification mechanism (Joyce, 2001; Breaker *et al.*, 2003). Here, initial proton abstraction by a Brønstedt base at the 2'-OH of the unpaired purine nucleotide enables the resulting oxyanion to perform a nucleophilic 'in-line attack' on the adjacent phosphorus center of the phosphodiester bond. In this 'in-line attack' conformation the O2' is placed opposite to the leaving 5' oxygen and aligned in the direction of the to be cleaved P-O5' bond (Przybilski and Hammann, 2006; Martick and Scott, 2006; Min *et al.*, 2007). Subsequently, the penta-coordinated phosphorane intermediate degrades and yields two RNA fragments with a 2',3'-cyclic phosphate and 5'-OH terminus (Santoro and Joyce, 1998; Breaker *et al.*, 2003, Figure 1.2).

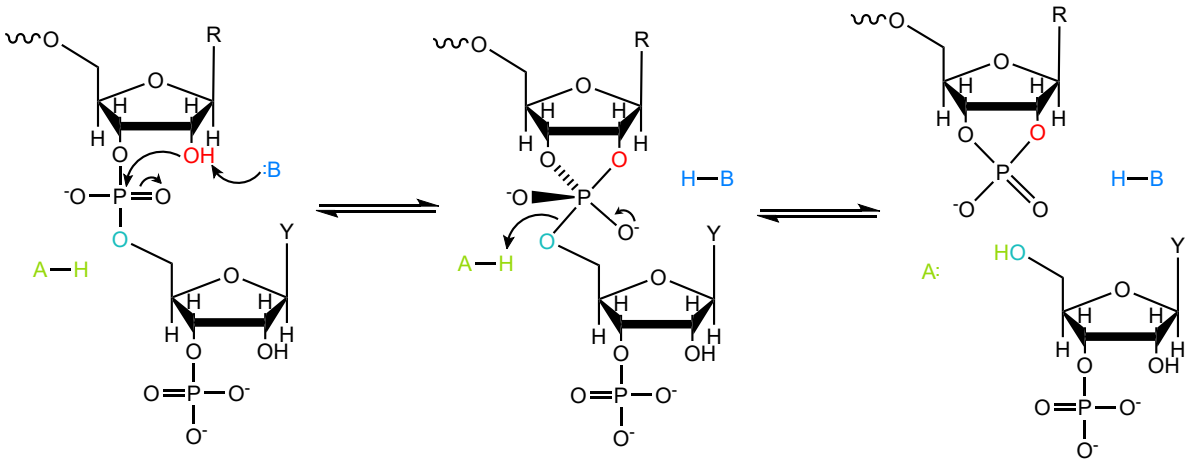

Figure 1.2: Proposed catalytic mechanism of RNA cleavage mediated by the 10-23 DNAzyme. Abstraction of a proton at the 2'-OH group of the ribose of the unpaired purine (R) at position '0' by a Brønstedt base (B), allows for a nucleophilic attack by the 2'-oxygen on the adjacent phosphodiester bond. After formation of a penta-coordinated intermediate, two fragments evolve with a 2',3'-cyclic phosphate and 5'-OH terminus. A Brønstedt acid (A) in close proximity, for instance, a hydrated metal ion (Borggräfe *et al.*, 2023), provides a proton. Adapted from Rosenbach *et al.* (2020b).

Even though several groups performed substitution and systematic deletion studies to investigate the function and involvement of the residues within the catalytic core during RNA cleavage, the long lasting lack of high-resolution structural data left the exact mechanism unknown (Cairns *et al.*, 2000; Zaborowska *et al.*, 2002, 2005; Wang *et al.*, 2010). A first crystal structure of the Dz in 1999 (Nowakowski *et al.*, 1999) and another one, just recently published in 2023 (Cramer *et al.*, 2023), reflect a conformation without catalytic relevance due to the palindromic sequence within the catalytic core (Figure 1.3A). In order to disrupt the palindrome and prevent homodimer formation, without losing catalytic activity, single point mutations proved to be sufficient (Zaborowska *et al.*, 2002; Borggräfe *et al.*, 2021).

In 2021, Borggräfe *et al.* (2021) published the first representative structure of the Dz bound to an RNA substrate in a pre-catalytic complex conformation using nuclear magnetic resonance (NMR) spectroscopy and molecular dynamics (MD) simulations (PDB 7PDU). The structure displays one possible conformation and presents a partly restrained and overall condensed catalytic core, which is wrapped around the RNA by an additional turn. This alignment locks the RNA in place and fully exposes the cleavage site to the catalytic core (Figure 1.3D). Experiments in presence of Mg^{2+} led to the identification of three metal ion binding sites (MBSI–III, Figure 1.3B), which supported previous results (Victor *et al.*, 2018). Simultaneous occupation of all three MBS was required to allow for catalysis. Exchanging divalent to solely monovalent ions, provided complex stabilization and partly conformational activation, but did not make the Dz gain catalytic function, which is referred to as state B_1 by the authors (Figure 1.3C).

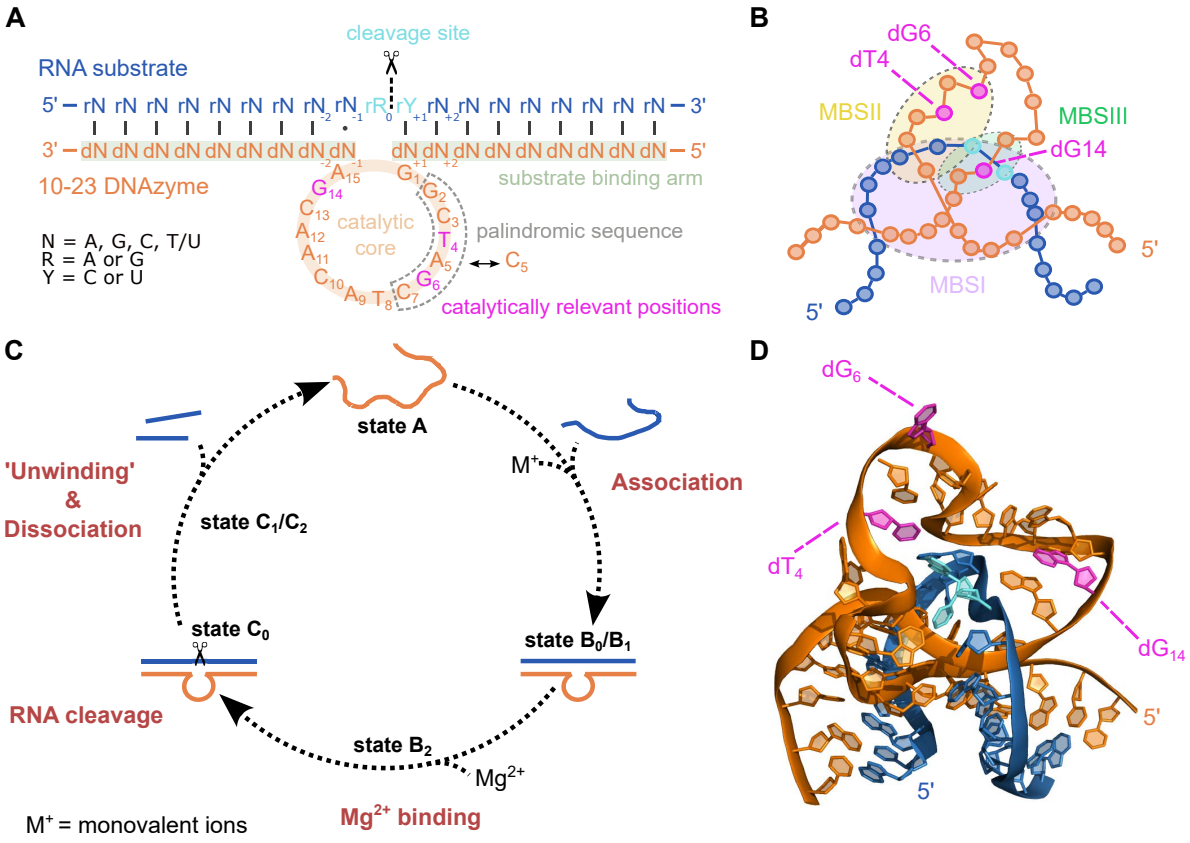

Figure 1.3: Architecture of and catalysis mediated by the 10-23 DNAzyme. **A** Schematic illustration of the Dz (orange) in complex with a complementary RNA substrate (blue). RNA cleavage requires a purine-pyrimidine (RY) junction as cleavage site (cyan). The Dz comprises a catalytic core, which includes a self-complementary sequence (grey), flanked by two substrate binding arms (green). Activity enhancement is achieved, when the Dz engages wobble interactions (•) with the nucleotide at position −1 (Cairns *et al.*, 2000). The mutation A5C eliminates dimerization. Positions important for catalysis are highlighted in pink (Borggräfe *et al.*, 2021). Adapted from Borggräfe *et al.* (2023). **B** Schematic representation of metal binding sites (MBS) I to III within the three-dimensional structure of the Dz:RNA complex. Modified after Borggräfe *et al.* (2023). **C** Catalytic cycle of the Dz. Modified after Larcher *et al.* (2023); Rosenbach *et al.* (2020b). **D** Tertiary structure of the pre-catalytic Dz:RNA complex (PBD 7PDU, Borggräfe *et al.*, 2021). Folding of the Dz locks the RNA in place with the cleavage site (cyan) fully exposed to the catalytic loop.

MBSI is located at the crossing of both binding arms and Mg^{2+}-binding in this area is proposed to counter electrostatic repulsion, thus aiming for charge compensation. This results in complex stabilization as well as condensation, to which the authors refer to as ‘scaffolding’. MBSII is located at the 5’-side of the catalytic core. Here, binding of Mg^{2+} induces conformational rearrangements, which is proposed to switch the Dz into an ‘on-conformation’. In particular, T4 is assumed to function as Mg^{2+}-triggered switch, since its rearrangements seem to promote π-π-stacking between G6 and the cleavage site, facilitating the formation of an ‘in-line attack’ conformation (Borggräfe *et al.*, 2021, 2023). Previous studies already identified residues G1, G2, T4, G6, and G14 to be essential for activity (Zaborowska *et al.*, 2002). The third MBS is located at the more flexible 3’-side of the catalytic core and moves towards the cleavage site upon ‘scaffolding’. In this area, especially C13 and G14 demonstrate stronger interactions with Mg^{2+}, assuming one or both to be directly involved in catalysis. Recent reports on the 8-17 DNAzyme provided evidence that RNA cleavage follows a general acid-base mechanism, which supports initial assumptions (Cepeda-Plaza *et al.*, 2018). Here, G14 is believed to function as general base and a hydrated metal ion as general acid (Cortés-Guajardo *et al.*, 2021). The data obtained by NMR spectroscopy

and MD simulations also suggest G14 as general base for the 10-23 DNAzyme to perform the nucleophilic attack and metal ion-coordinated water as general acid (Borggräfe *et al.*, 2021, 2023).

Furthermore, the authors were able to identify transient intermediate states (Figure 1.3C). After association of the Dz and RNA substrate (state B_0) and subsequent stabilization by sodium ions (Na^+, state B_1), the complex is fully activated after saturation of MBSI-III with Mg^{2+} (state B_2). In this regard, the authors suggest that the transition from state B_2 to state C_0, in which RNA cleavage occurs, is rather limiting than MBS occupancy with Mg^{2+} (Borggräfe *et al.*, 2021, 2023). Prior to dissociation and product release, the complex is able to transient into state C_1 or C_2, of which the latter predominantly occurs at temperatures above 37 °C, but may also remain in state C_0. Finally, the Dz is able to enter a new catalytic cycle and bind another RNA substrate under multiple turnover (state A).

1.3 Diversity of DNAzyme-based applications

1.3.1 The spectrum of DNAzyme-mediated catalysis

Even though RNA-cleaving DNAzymes have been receiving a lot of attention in medical approaches (Larcher *et al.*, 2023), the repertoire of DNAzyme-mediated reactions goes far beyond. In this regard, selection techniques have evolved and were adapted to meet the respective requirements. Depending on the type of substrate, catalysis can be roughly grouped into reactions with an oligonucleotide or non-oligonucleotide substrate.

Reactions, in which the DNAzyme interacts with an oligonucleotide substrate, include for example the phosphorylation (Li and Breaker, 1999), adenylation (Li *et al.*, 2000), site-specific thymidine excision (Wang *et al.*, 2014), ligation (Cuenoud and Szostak, 1995), or cleavage (Carmi *et al.*, 1998) of DNA, and ligation of RNA (Flynn-Charlebois *et al.*, 2003). On the other hand, DNAzymes with non-oligonucleotide substrates are able to perform, for example, porphyrin metallation (Li and Sen, 1996), thymine dimer photoreversion (Chinnapen and Sen, 2004), Diels-Alder reactions (Chandra and Silverman, 2008), azide-alkyne cycloaddition (CuAAC, Liu *et al.*, 2020), the modification of proteins (Pradeepkumar *et al.*, 2008; Wong *et al.*, 2011; Silverman, 2015), or mimicry of peroxidase activity (Travascio *et al.*, 1999). Some articles that reviewed the reaction scope of DNAzymes were published by Hollenstein in 2015, by Silverman in 2016, and by Ma and Liu in 2020.

1.3.2 RNA-cleaving DNAzymes in therapy

To date, several oligonucleotide-based strategies have been tested for gene therapy, including antisense oligonucleotides (ASOs, Fusco *et al.*, 2019; Egli and Manoharan, 2023), small interfering RNAs (siRNAs, Hu *et al.*, 2020), microRNAs (miRNAs, Christopher *et al.*, 2016), ribozymes (Wong *et al.*, 2022; Lewin and Hauswirth, 2001; Kashani-Sabet, 2002), and DNAzymes (Thomas *et al.*, 2021; Cho *et al.*, 2013; Cao *et al.*, 2014). For the majority of applications, the aim is to specifically recognize, bind, and cleave messenger RNA (mRNA) to allow targeted RNA knockdown and regulate gene expression.

ASOs are short, single-stranded DNA molecules that are designed to complementary and selectively bind an mRNA and either induce its degradation by recruiting the endonuclease

RNase H (see section 1.4.2, Figure 1.8), modulate splicing, or prevent translation by blocking and hindering ribosome movement (Fusco *et al.*, 2019; Crooke, 2017). siRNAs are double-stranded RNA molecules of 20 to 25 nt in length that contain two nucleotide overhangs at the 3'-end and 5' phosphate groups. They operate via the cellular process RNA interference (RNAi). Integrated into a multi-protein component complex, better known as RNA-induced silencing complex (RISC), the double-stranded molecule unwinds and the antisense strand guides the complex to bind the target mRNA, while the sense strand is degraded. Binding of the respective target sequence finally induces its cleavage by the endonuclease Argonaute 2 and triggers further fragment degradation by exonucleases (Chery, 2016; Dana *et al.*, 2017). miRNAs are evolutionary conserved, single-stranded RNA molecules of 20 to 25 nt in length, that bind to the 3' untranslated region (UTR) of mRNA in a sequence specific manner and regulate gene expression through the RNAi machinery (MacFarlane and R. Murphy, 2010; Christopher *et al.*, 2016). Despite, NA therapies often face off-target effects, low stability, when oligonucleotides are unmodified, and restricted efficiency in delivery due to their negatively charged backbone (Dhuri *et al.*, 2020; Khan *et al.*, 2023).

In comparison, ribozymes and DNAzymes provide several advantages, which make them attractive alternatives: (i) both catalysts are self-sufficient, which makes them independent of protein cofactors, (ii) the ability for multi-turnover, and (iii) evolving algorithms/tools facilitated the *in situ* design of artificial catalysts for almost any target of interest (Tafer *et al.*, 2008; Steger and Victor, 2022; Mohammadi-Arani *et al.*, 2022; Pine *et al.*, 2023, chapter 5). Moreover, higher biostability and lower costs during synthesis made DNAzymes even more beneficial for therapy compared to ribozymes (Thomas *et al.*, 2021; Xu *et al.*, 2012; Fokina *et al.*, 2017).

Over the years, several DNAzymes were designed to address viral infections such as the human immunodeficiency virus (HIV, Jakobsen *et al.*, 2007), influenza A (Kumar *et al.*, 2015), hepatitis C (Lee *et al.*, 2010) or, with regard to recent years, the severe acute respiratory syndrome coronavirus type 2 (SARS-CoV-2, Gerber *et al.*, 2022). Further applications include the desire of anti-inflammatory (Chakravarthy *et al.*, 2017) and anti-cancer (Taube *et al.*, 2005) properties, or the treatment of cardiovascular (Benson *et al.*, 2008) and central nervous system diseases (Mastroyiannopoulos *et al.*, 2010; Yan *et al.*, 2023a).

So far, five DNAzymes are reported that have entered clinical trials: (i) the DNAzyme Dz13 to treat nodular basal-cell carcinoma (Phase I completed, Cho *et al.*, 2013), (ii) the DNAzyme Dz1 to treat nasopharyngeal carcinoma (Phase I, II completed, Cao *et al.*, 2014), (iii) the DNAzyme SB010 to treat bronchial asthma (Phase I, IIa completed, Krug *et al.*, 2015, 2017) as well as chronic obstructive pulmonary disease (COPD, phase IIa completed, Greulich *et al.*, 2018), (iv) the DNAzyme SB011 to treat atopic dermatitis (Phase I, IIa completed, Xiao *et al.*, 2023), and (v) the DNAzyme SB012 to treat ulcerative colitis (Phase I, IIa completed, Xiao *et al.*, 2023). The increasing versatility of DNAzymes made them not only evolve as therapeutics, but also in diagnostics (He *et al.*, 2015).

Despite numerous reports of DNAzymes as therapeutic agents, currently approved NA therapies are dominated by ASOs and siRNAs, without any DNA catalyst amongst them (Egli and Manoharan, 2023; Larcher *et al.*, 2023; Nedorezova *et al.*, 2020). To explain this discrepancy, DNAzymes are suggested to face similar challenges, which limit their *in vivo* performance, including cellular uptake, retention, stability, targeted delivery (Fokina *et al.*, 2017; Thomas *et al.*, 2021), or a cell's environment in general (Section 1.4). Furthermore, the choice of RNA substrate is considered as source of error, since cancer markers that presented favorable for detection and recognition, do not necessarily have to be equally promising as substrates in gene silencing (Nedorezova *et al.*, 2020). In order to increase *in vivo* competence

and make DNAzymes accessible for therapy, different promising strategies evolved including chemical modifications (Section 1.4.2). Nevertheless, a more detailed understanding of a DNAzyme's catalytic mechanism and its interactions within cells is vital to improve current and open up new design options, of which investigating its cellular behaviour is the main objective of this thesis.

To this day, therapeutic DNAzymes have been designed to primarily target pathogens or diseases that threaten humans. Few examples of DNAzymes, that were designed for biosensing, expand the horizon to detect bacterial or viral pathogens with impacts on plants or fish (Wang *et al.*, 2019b; Gu *et al.*, 2019). However, fish farming, for instance, as one huge sector to provide and secure food supply on earth, faces challenges in biological control. Over the years, infections have become more frequent and, although few vaccines are administered, widely approved, used, and commercially available options are needed urgently (Ma *et al.*, 2019). One key prerequisite for suitable treatments is large-scalability. Since DNAzyme synthesis meets this requirement, they may provide an alternative to not only detect fish pathogens, but also treat them, which will be explored in this thesis (Chapter 5).

1.3.3 DNAzymes as biosensors

Given their beneficial properties, RNA-cleaving DNAzymes became also attractive to function in biosensing (McConnell *et al.*, 2021; Ma and Liu, 2021; Ma *et al.*, 2021; Yang *et al.*, 2023). A biosensor consists of two components: a molecular recognition element (MRE), which selectively binds a target analyte, and a signal reporting element (SRE), which translates the occurring events into a detectable signal (McConnell *et al.*, 2021; Ma and Liu, 2021; Gong *et al.*, 2015). Since RNA-cleaving DNAzymes provide the capability to function as MRE as well as reporter, DNAzyme-based sensing strategies have been focussing on RCD systems so far (McConnell *et al.*, 2021; Khan *et al.*, 2021).

Over time, a plethora of biosensors has been designed and applied to detect metal ions (Zhang *et al.*, 2011; Cheng *et al.*, 2022), pathogens or bacteria (Gu *et al.*, 2019; Ali *et al.*, 2017), nucleic acids (e. g. miRNA, Peng *et al.*, 2017, or DNA (Wang *et al.*, 2019a)), small molecules such as adenosine triphosphate (ATP, Cai *et al.*, 2023) or glucose (Liu *et al.*, 2015), and beyond. Depending on the respective sensor, different signalling mechanisms have been established including fluorescence (Li and Lu, 2000), colour (Liu and Lu, 2003), electrochemistry (Wu *et al.*, 2017), chemiluminescence (Gao *et al.*, 2013), or surface-enhanced Raman scattering (SERS, He *et al.*, 2020). Here, fluorescence-based sensors have been used most widely due to high sensitivity, reproducibility, simple operational procedure, and versatility (Ma and Liu, 2021; Kumar *et al.*, 2019). Since DNA lacks the property of intrinsic fluorescence, a fluorophore has to be incorporated. This can be either achieved by direct labeling, usually using fluorophore-quencher (F–Q) pairs (Liu and Lu, 2006) or indirectly by making use of intercalating fluorescent dyes such as SYBR Green (Zhang *et al.*, 2013; Kumar *et al.*, 2019). As the variability in biosensor design, strategy, and application exceeds this thesis by far, only a small selection of RCD-based sensors will be demonstrated below (Figure 1.4, 1.5). Several review articles on the sensing repertoire of DNAzymes have been published (Zhang *et al.*, 2011; Gong *et al.*, 2015; Zhou *et al.*, 2017b; Kumar *et al.*, 2019; McConnell *et al.*, 2021; Khan *et al.*, 2021; Ma and Liu, 2021).

One major field in biosensing is the detection of metal ions in environmental samples and cells due to their indispensability and pivotal role as cofactors or in process regulation (Zhou *et al.*, 2017b; Young *et al.*, 2010; McGhee *et al.*, 2017; Xiang and Lu, 2014). As elevated

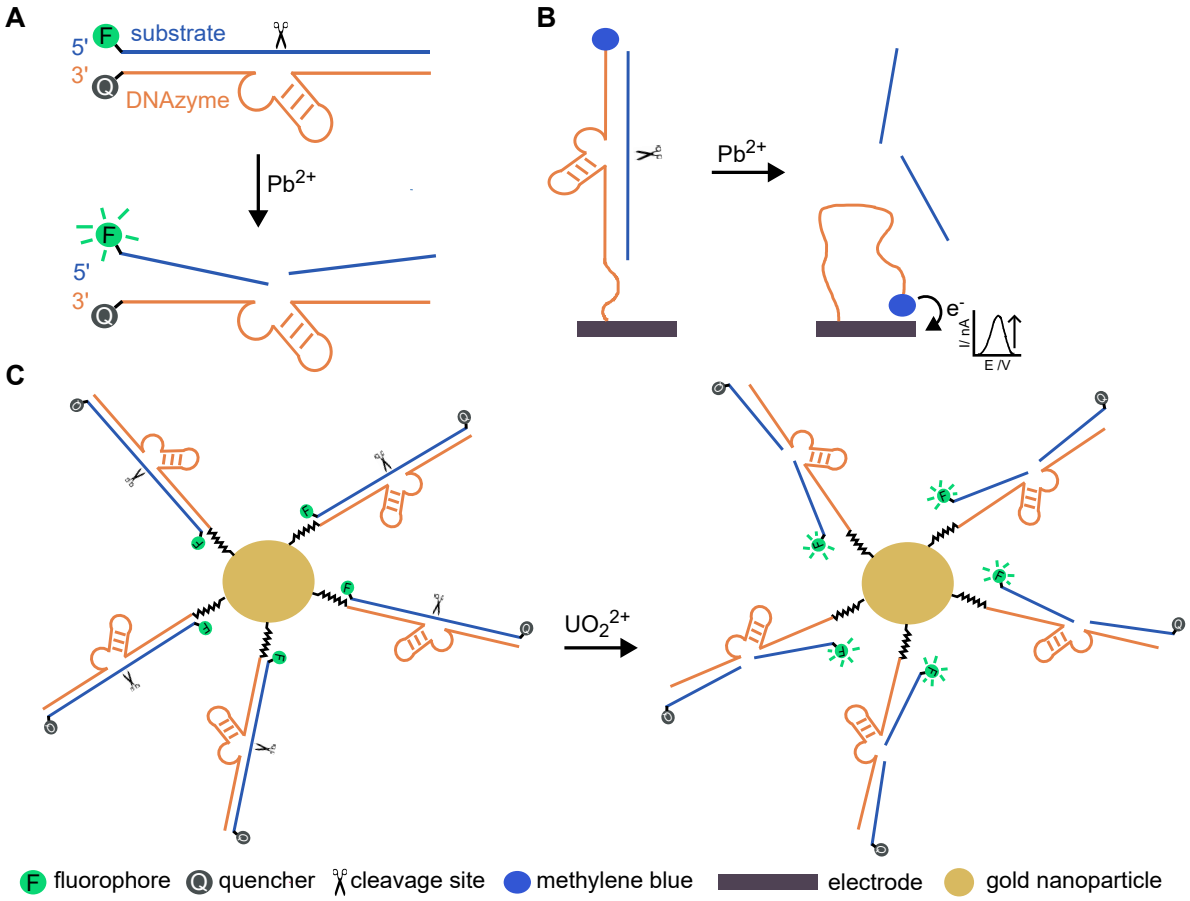

Figure 1.4: Selection of DNAzyme-based biosensors for sensing of metal ions. **A** Biosensor for lead detection using a variant of the 8-17 DNAzyme. In presence of Pb^{2+}, cleavage and subsequent complex dissociation spatially separate the fluorophore and quencher generating a fluorescent signal. Based on Li and Lu (2000). **B** Electrochemical sensor for lead detection using the 8-17 DNAzyme. After Pb^{2+}-induced cleavage, the RNA fragments dissociate and the DNAzyme unfolds, which allows the methylene blue to transfer electrodes to the electrode, when in close proximity. Based on Xiao *et al.* (2007). **C** DNAzyme-gold nanoparticle sensor for specific uranyl ion detection using a variant of the 8-17 DNAzyme. UO_2^{2+} induced cleavage and subsequent dissociation spatially separates F and Q of the double-labeled substrate, leading to increased fluorescence. Based on Wu *et al.* (2013).

levels and accumulation of some ions have cytotoxic effects, their spatial distribution and quantification is of special interest (Zhou *et al.*, 2017b; Zhang *et al.*, 2011). One example is the initially reported sensor for Pb^{2+}-detection, a common environmental contaminant. The sensor contains a fluorophore-quencher pair, of which Q is linked to the 3'-end of the DNAzyme and F is linked to the 5'-end of the complementary substrate (Li and Lu, 2000, Figure 1.4A). In absence of Pb^{2+}, close proximity of Q and F results in a quenched fluorescence signal. This principle is better known as Förster Resonance Energy Transfer (FRET, Förster, 1965). Pb^{2+}-induced cleavage separates F and Q and allows for detection of an increased signal. Since this F–Q arrangement faced temperature-dependencies in the extent of background noise, additional designs derived to allow an overall low background signal (Liu and Lu, 2006; Gong *et al.*, 2015). In the following, the majority of the described examples are FRET-based.

In an electrochemical approach for Pb^{2+}-sensing, the DNAzyme binds its substrate and is chemisorbed to a gold electrode via a 5' terminal thiol and carries a methylene blue (MB) modification at the other end (Figure 1.4B). Pb^{2+}-induced cleavage and subsequent complex

dissociation allow the DNAzyme to unfold and make the MB come close to the electrode. As a result, an increase in electron transfer can be detected (Xiao *et al.*, 2007).

In a different approach, sensing of uranyl ions (UO_2^{2+}) in living cells was achieved by the design of DNAzyme-gold nanoparticle probes (Wu *et al.*, 2013, Figure 1.4C). In general, nanoparticles of different materials became attractive for sensor design, as they provide quenching properties and facilitate targeted delivery (Gong *et al.*, 2015). However, efficient immobilization is the key to ensure functionalization (Khan *et al.*, 2021). UO_2^{2+} is the most water stable form of uranium, a highly toxic and carcinogen element (Ma and Liu, 2021). DNAzymes were immobilized onto 13 nm large gold nanoparticles (AuNP) and hybridized to double-labeled substrates, which contained a F at the 5'- and a Q at the 3'-end (Wu *et al.*, 2013). The latter was added to further improve the signal to noise ratio (S/N). Subsequent incubation of uranyl treated cells with DNAzyme-AuNPs induced substrate cleavage and resulted in an increased fluorescence. As several DNAzyme conjugates cover the particle's surface, this design allows for signal amplification.

Besides metal ions, Wang *et al.* designed a sensor based on a hybridization-triggered DNAzyme cascade (HTDC) for efficient DNA detection (Wang *et al.*, 2019a, Figure 1.5A). The DNAzyme's substrate binding arms are designed to asymmetrically bind to a double-labeled substrate, of which nine nt bind complementary on the one and only three nt on the other side, leaving the shorter side inefficient to build a stable and active DNAzyme:substrate complex. The substrate is labeled with a Q at the 3'-end and a F in close proximity to the cleavage site, which is a single ribonucleotide. Simultaneous hybridization of a target DNA, which is partly complementary to the cleavable substrate as well as the second binding arm of the DNAzyme, is necessary to form a stable and active complex. Zinc ion (Zn^{2+})-induced cleavage results in an elevated fluorescence.

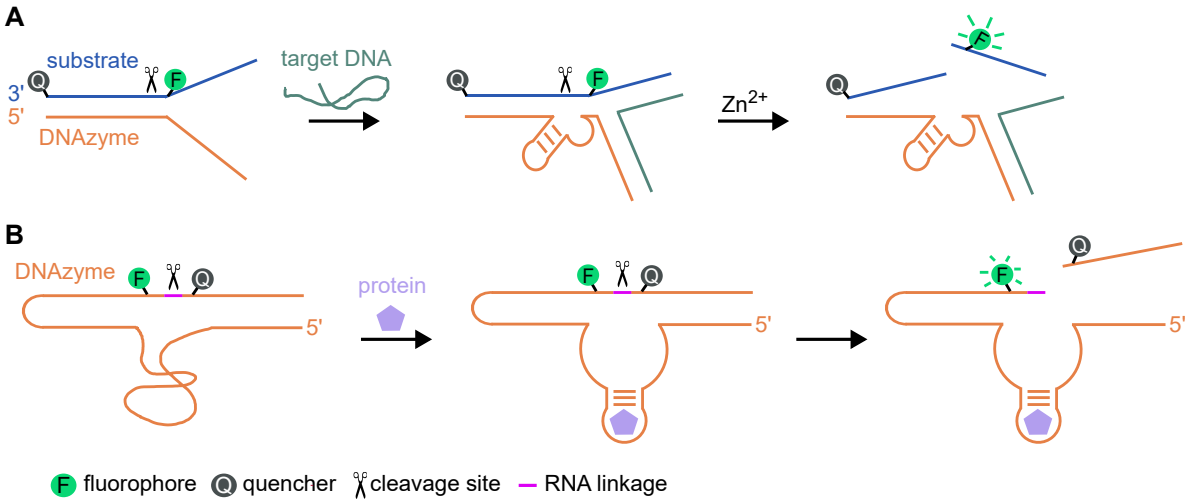

Figure 1.5: Examples of further applications of DNAzyme-based sensors. **A** Design of a DNAzyme sensor for a hybridization-triggered cascade assay for specific DNA detection. Based on Wang *et al.* (2019a). **B** Pathogenic bacterial detection using an RNA-cleaving fluorescent DNAzyme. Here, a protein is selected as possible target molecule to convert the DNAzyme into its active form. Based on Ali *et al.* (2011, 2017).

Lastly, biosensor designs also target the detection of pathogenic bacteria, as they cause severe infections and environmental pollutions. Thus, early detection and prevention is crucial (Ma *et al.*, 2021). Here, Ali *et al.* directly isolated DNA probes from a crude extracellular mixture (CEM) or crude intracellular mixture (CIM) of a bacterial pathogen by *in vitro* selection (Ali *et al.*, 2011). The DNAzyme consists of one DNA chain, that performs cleavage

at a lone RNA linkage embedded into it. The cleavage site is flanked by a F–Q pair, resulting in an RNA-cleaving fluorescent DNAzyme (RFD, Figure 1.5B). In presence of CEM or CIM, any molecule may become a target and can allosterically convert the inactive RFD upon interaction into its active form. When activated, the RFD performs cleavage, which results in an increased signal (Ali *et al.*, 2011, 2017). This set up is also applied to perform real-time monitoring of food contaminations (Yousefi *et al.*, 2018).

1.4 Restricted *in vivo* success

Despite the increasing number of *in vivo* applications using RNA-cleaving DNAzymes, consistent success in cells remains limited, facing several obstacles. To explain the discrepancy between high *in vitro* and low *in vivo* activity, cellular challenges have been mainly attributed to inefficient uptake (Zhang, 2018), risk of degradation (Xiao *et al.*, 2023), and cofactor availability (Victor *et al.*, 2018).

As mentioned above, DRz require additional delivery systems to successfully cross cell borders due to their polyanionic character (Santoro and Joyce, 1998; Akhtar *et al.*, 2000; Zhang, 2018). However, such require high uptake efficiency as well as the ability to perform subcellular delivery with targeted and precise spatiotemporal control, which already made progress, but remains an area of great interest. Depending on the chosen delivery system, cytotoxicity needs to be considered and eliminated (Zhang, 2018; Xiao *et al.*, 2023; Larcher *et al.*, 2023).

In biological samples, the single-stranded character of DRz makes them susceptible to degradation by cellular nucleases, limiting their life time. Therefore, for instance, chemical modifications (Section 1.4.2) and conjugation strategies of DRz to nanostructures became promising tools to improve biological stability and catalytic activity (Etzkorn and Span, 2023; Larcher *et al.*, 2023; Xiao *et al.*, 2023). In all this, low cofactor availability at physiological relevant concentrations is suspected to be one main limitation (Victor *et al.*, 2018). In cells, the abundance of Mg^{2+} is relatively high, but other potential interaction partners, such as ATP (Victor *et al.*, 2018), lower the availability to an approximate free Mg^{2+} concentration of $0.5 - 1\,\mathrm{mM}$ (Pechlaner and Sigel, 2012). However, cofactor requirement of DRz often turns out higher (Zhou *et al.*, 2017a). Thus, some attempts aimed at lowering cofactor requirement suggesting direct selection at respective concentrations, the change of cofactor species (Roth and Breaker, 1998), or the change of the design to DRz that operate in absence of them (Sidorov *et al.*, 2004; Hollenstein *et al.*, 2009). Pursuing investigations on effects by metal ions on DRz activity demonstrated additional catalysis modulating properties by monovalent ions (Rosenbach *et al.*, 2021). A decrease in activity in presence of monovalent ions and low Mg^{2+} concentration, was already observed in the mid 1990s (Breaker and Joyce, 1995). Potassium ions (K^+) are the most abundant monovalent cations in mammalian cells with a concentration of 140 mM. Na^+ make up to 10 mM within cells (Pechlaner and Sigel, 2012). Even though both ions usually play an unspecific role in charge neutralization for nucleic acid stabilization, Rosenbach *et al.* propose a more complex interplay with different modes of action depending on the type of divalent ion involved as cofactor (Rosenbach *et al.*, 2021).

1.4.1 The crowded environment in cells

Pioneering work on volume exclusion in 1981 by Minton (1981) led to the introduction of molecular crowding and associated events as a cell phenomenon in the early 1990s (Zimmerman and Minton, 1993; Minton, 1992, Figure 1.6). Ever since, this field of research attracts great interest. Compared to *in vitro* conditions, cells are composed of various biomolecules that create a heterogeneous and densely packed environment. The diversity in molecule properties is suspected to have thermodynamic and kinetic consequences, which determine cell processes (Zhou *et al.*, 2008; Miyoshi and Sugimoto, 2008, for further information see chapter 4). Several reports of *in vitro* analyses on biocatalysts (Kuznetsova *et al.*, 2014; Hingorani and Gierasch, 2014; Sasaki *et al.*, 2007), including ribozymes (DasGupta, 2020; DasGupta *et al.*, 2023; Paudel and Rueda, 2014; Paudel *et al.*, 2018; Desai *et al.*, 2014; Nakano *et al.*, 2008), demonstrated consequences on folding, activity, and stability in presence of a crowded, more cell-like environment.

These events fired discussions and speculations whether DNAzymes are also affected and let assume a much more complex network of factors potentially limiting their cellular activity. So far, the main approach in investigating such effects is to mimic crowded conditions *in vitro* using natural and artificial cosolutes such as polyethylene glycol (PEG), dextran or Ficoll (DasGupta, 2020; Model *et al.*, 2021; Benny and Raghunath, 2017, for further information see chapter 4). Though first reports on DRz have been published in recent years (Wang *et al.*, 2023; Gao *et al.*, 2015; Rudeejaroonrung *et al.*, 2020), still little is known if and how a crowded environment impacts their activity. To shed more light on this interplay such analyses play a major part in this thesis (see chapters 2, 3).

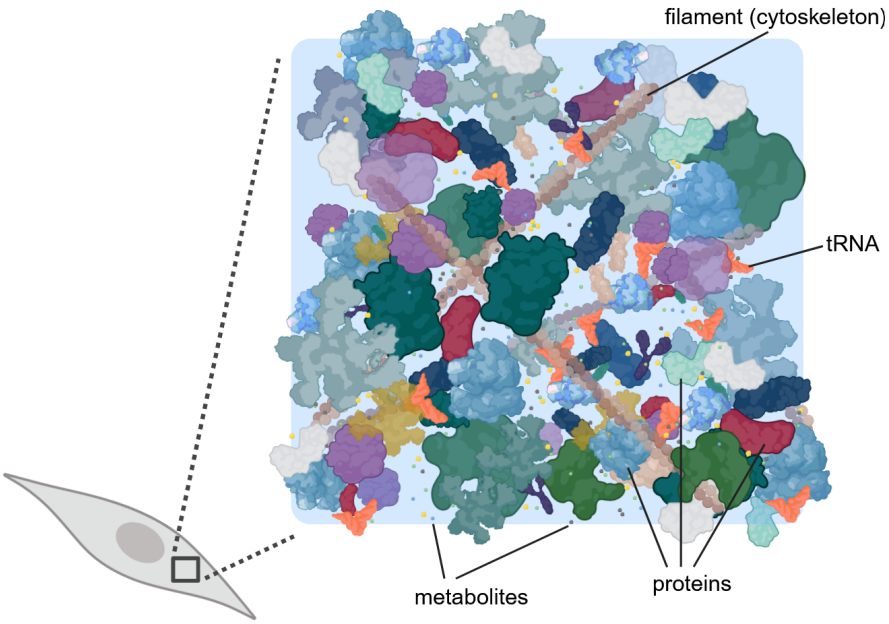

Figure 1.6: Illustration of a cell's interior. A diversity of biomolecules generates a heterogeneous and densely packed (crowded) environment. Created with BioRender.com

1.4.2 Modification strategies towards DNAzymes with enhanced activity

Aiming at overcoming persisting limitations and improve DRz performance under physiological conditions, promising progress has been made using different approaches: a) covalent attachment of DRz to nanostructures (Seferos *et al.*, 2009; Zhou *et al.*, 2017a; Yan *et al.*, 2023a), b) change of design to, for example, hairpin or photoactivated DRz (Larcher *et al.*, 2023; Young *et al.*, 2010), and c) incorporation of chemically modified building blocks (Nguyen *et al.*, 2023; Chiba *et al.*, 2023; Taylor *et al.*, 2022; Gerber *et al.*, 2022; Wang *et al.*, 2021; Huang and Liu, 2020; Fokina *et al.*, 2012; Schubert *et al.*, 2003). This chapter will focus on the latter due to their evolving diversity and increasing number of promising reports over the years (Figure 1.7).

In general, modifications should meet the requirement to at least maintain, but favourably enhance DRz activity without significantly disturbing or changing their active conformation (Schubert *et al.*, 2003). Although the optimization of binding arm length also provides an option to enhance catalytic properties (Schubert *et al.*, 2003), the chemical range to positively impact DRz efficiency is significantly restricted in sole presence of the standard four nucleotides (Huang and Liu, 2020; Etzkorn and Span, 2023). Thus, the incorporation of non-standard (non-natural and natural) nucleotides has become more frequent, which resulted in enhanced biostability, low toxicity, and high substrate affinity. However, the outcome depends on the type of modification and its inserted amount, a combination of different modifications, and their respective position–binding arm and/or catalytic core (Fokina *et al.*, 2012; Schubert *et al.*, 2003; Fokina *et al.*, 2015). Most of currently applied chemical modifications in DRz have already been used in antisense technology (Kurreck, 2003) and can be categorized into three classes: alteration of phosphate backbone, ribose moiety, and functional groups of the nucleobase itself (Etzkorn and Span, 2023). Here, changes within the sugar moiety mainly focus on the 2'-OH, since changes at this position showed preservation of NA function and interaction, but significantly lowered the risk of hydrolysis (Freund *et al.*, 2023).

In nature, the bridging phosphate group of a phosphodiester bond in a DNA dinucleotide is coordinated by four oxygen atoms in a tetrahedral configuration (Etzkorn and Span, 2023; Pauling and Corey, 1953). Substitution of one of the non-bridging oxygen atoms by a sulfur leads to a phosphorothioate (PS) linkage (Javadi-Zarnaghi and Höbartner, 2020; Akhtar *et al.*, 2000, Figure 1.7). Even though PS linkages showed increased stability towards nuclease degradation (Schubert *et al.*, 2003; Reyes-Gutiérrez and Alvarez-Salas, 2009) and allowed for a change in binding preferences to softer metal ions (according to Pearson concept) such as cadmium (Cd^{2+}, Huang and Liu, 2020), catalytic activity was significantly reduced, when applied throughout the substrate binding arms (Schubert *et al.*, 2003). In addition, PS linkages resulted in decreased substrate affinity and cytotoxicity, which limits their utility (Schubert *et al.*, 2003; Larcher *et al.*, 2023). Replacing the 3'-oxygen by a 3'-amino group results in N3'-P5' phosphoramidite linkages (Figure 1.7). Such alterations also provided enhanced exonuclease resistance, when introduced at the 3'- and 5'- end of the DRz's binding arms (Takahashi *et al.*, 2004).

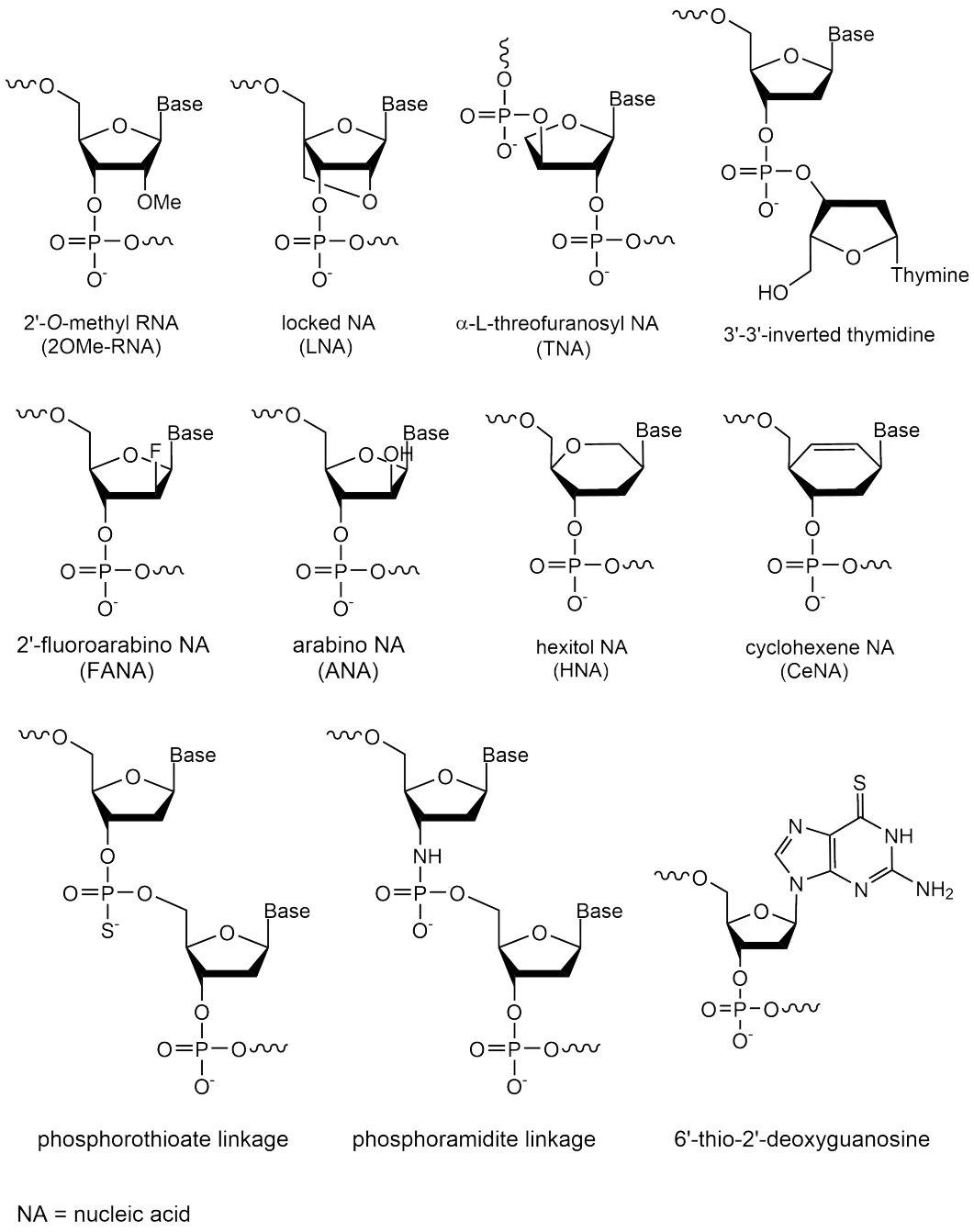

Figure 1.7: Selection of chemically modified nucleotides that have been introduced into DNAzymes.

Besides both backbone analogues, the incorporation of naturally occurring 2'-O-methyl RNA (Schubert *et al.*, 2003; Larcher *et al.*, 2023; Schubert and Kurreck, 2005; Fokina *et al.*, 2012; Freund *et al.*, 2023), 3'-3'-inverted thymidine nucleotides (Schubert *et al.*, 2003), and locked nucleic acids (LNAs, Schubert *et al.*, 2003; Vester *et al.*, 2002; Jakobsen *et al.*, 2007; Wang *et al.*, 2021) have also enhanced the stability to exonucleolytic and/or endonucleolytic digestion. In the case of 2'-O-methyl RNA and LNAs, modified DRz additionally demonstrated elevated target affinity and catalytic activity (Vester *et al.*, 2002; Fokina *et al.*, 2012). LNAs, which consist of a methylene bridge that connects the 2'O and the 4'C, further gained attention due to their property of elevated thermostability, but faced significant cell toxicity as downside (Jakobsen *et al.*, 2007; Wang *et al.*, 2021; Javadi-Zarnaghi and Höbartner, 2020). In 2021,

Borggräfe *et al.* (2021) used 6-thio-2'dG as nucleobase modification, which resulted in increased activity, but simultaneously decreased Mg^{2+} affinity (Borggräfe *et al.*, 2021).

In general, most of the above mentioned modifications have mainly been incorporated at the end or within a DRz's binding arms to aim for increased biostability and target affinity. Only few exceptions, for example 2'-O-methyl-RNA (Schubert *et al.*, 2003; Fokina *et al.*, 2012), have also been incorporated into the catalytic core. Depending on the exchanged nucleotide position (Zaborowska *et al.*, 2002), such are assumed to not significantly change tertiary folding. On the one hand, increasing a DRz's target affinity is beneficial for association, thus DRz:RNA complex formation. On the other hand, however, complex dissociation can be hampered severely above a certain degree of modification, which impacts catalytic activity under multiple turnover and often leads to product inhibition (Schubert *et al.*, 2003; Wang *et al.*, 2021).

To face these limitations and avoid product inhibition, synthetic building blocks with altered physiochemical properties, so-called xeno nucleic acids (XNAs), have emerged within previous years (Wang *et al.*, 2021; Taylor *et al.*, 2015). XNAs include α-L-threofuranosyl nucleic acids (TNAs), 2'-fluoroarabino nucleic acids (FANAs), arabino nucleic acids (ANAs), hexitol nucleic acids (HeNAs), and cyclohexene nucleic acids (CeNAs). To this day, HeNAs and CeNAs have not been used often, since both resulted in significantly lowered activity, but also faced problems during amplification (Taylor *et al.*, 2015; Huang and Liu, 2020). In addition, ANA modifications have also shown significant decrease or even loss in activity, leaving TNAs and FANAs as most promising modifications at the moment.

FANAs contain a fluorine atom at the 2' position of a 2'-deoxyarabinose sugar and appeared to improve RNA binding (Taylor and Holliger, 2021; Yan *et al.*, 2023a), increase resistance to nucleolytic degradation, and provide sufficient or elevated activity under physiological conditions as well as in presence of longer RNA substrates (Wang *et al.*, 2021; Taylor *et al.*, 2022; Gerber *et al.*, 2022). Due to enhanced duplex stability in FANA-RNA duplexes compared to unmodified ones, association is promoted. However, incorporating FANA into the catalytic core seems to determine the DRz's efficiency and clearly depends on nucleotide position (Wang *et al.*, 2021). In TNAs, the sugar moiety is replaced by a four-carbon α-L-threofuranose sugar, which is linked by 2',3'-phosphodiester bonds. TNA-modified DRz presented enhanced backbone stability against exonucleases and overall resilience to nucleases (Culbertson *et al.*, 2016). In a recent study, a combination of FANA, TNA, and DNA nucleotides demonstrated most promising results. DRz activity was increased by $\sim$ 50-fold under multiple turnover and physiological conditions and stability of the backbone structure was enhanced $>$ 100-fold under stringent nuclease conditions (Wang *et al.*, 2021).

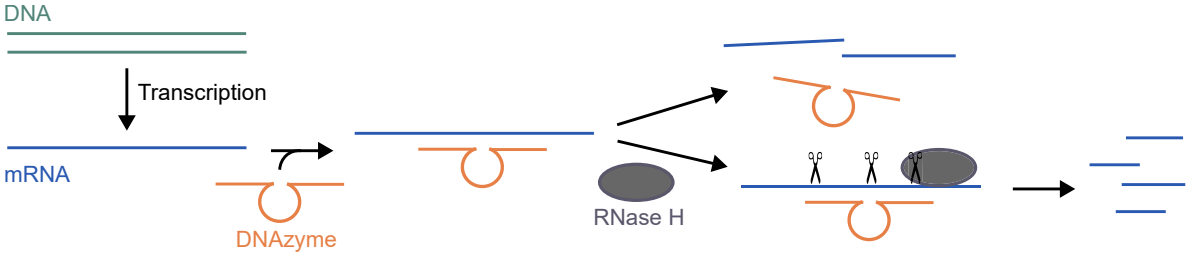

Figure 1.8: Schematic illustration of challenges in distinguishing mRNA knockdown mediated by a catalytically active DNAzyme and RNase H-mediated antisense effects. In case of the latter, the DNAzyme can be folded improperly, leaving it inactive. But the DNA-RNA hybrid is able to induce RNase H recruitment, resulting in mRNA degradation. Adapted from Taylor and Holliger (2021).

Yet, the incorporation of FANA into DRz fired and engaged an ongoing discussion, whether *in vivo* activity and RNA knockdown is truly the result of DRz-mediated cleavage or RNase H-dependent antisense effects (Yan *et al.*, 2023b; Larcher *et al.*, 2023; Taylor and Holliger, 2021; Young *et al.*, 2010, Figure 1.8). In this regard, DRz that contained a mix of FANA and DNA oligonucleotides were proposed to increase RNase H induction (Taylor and Holliger, 2021), since ANA and FANA are substrates of this enzyme (Damha *et al.*, 1998; Denisov *et al.*, 2001). During typical antisense-mediated knockdown, cellular RNase H is recruited by a RNA-DNA heteroduplex leading to the RNA's endonucleolytic degradation (Taylor and Holliger, 2021; Young *et al.*, 2010). Thus, the urge for rigorous controls is emphasized repeatedly. Here, DRz activity is often compared to an inactive variant, in which the sequence of the catalytic core is inverted (Wang *et al.*, 2021). Since voices claim significant impact on and changes in their tertiary structure due to sequence inversion, well-known point mutations are recommended to obtain inactivity instead (Taylor and Holliger, 2021; Zaborowska *et al.*, 2002). Alternatively, monitoring DRz activity at near physiological RNase H concentrations is also suggested (Spitale and Chaput, 2022).

1.5 Objective of this thesis

Due to their beneficial properties in applications, DNAzymes have attracted a lot of attention to become versatile tools. Within their functional diversity, RNA-cleaving DNAzymes, in particular, have shown great potential in biosensing (Gong *et al.*, 2015; McConnell *et al.*, 2021) and nucleic acid therapy (Xiao *et al.*, 2023; Larcher *et al.*, 2023). The most prominent and promising member is the 10-23 DNAzyme (Dz), of which few have entered clinical trials, for instance to aim at nasopharyngeal carcinomas (Cao *et al.*, 2014) or asthma (Krug *et al.*, 2017, section 1.3.2). However, its low activity in a cellular environment remains a major challenge in this field. Several factors have been proposed to prohibit the high catalytic activity observed in experiments carried out under *in vitro* conditions, which led to the current hypothesis of a multifaceted influence inside cells. But there is hardly any data on how the markedly different physicochemical surrounding in cells can impact DNAzyme function and structure.

Thus, the first objective of this thesis is to shed light on the effects caused by molecular crowding on the structure and activity of the Dz (Chapter 2, 3). Molecular crowding summarizes thermodynamic and kinetic consequences, which derive from the diversity of biomolecules and the densely packed environment in cells (Zhou *et al.*, 2008; Rivas and Minton, 2016). To mimic these crowded conditions, experiments will be carried out involving artificial and natural cosolutes. Various cosolutes and concentrations of such will be included in the study to simulate different degrees of a cell's divers properties. To understand how molecular crowding impacts the stability and activity of the Dz, measurements using denaturing urea polyacrylamide gel electrophoresis (urea-PAGE) and FRET-based cleavage assays will be carried out. Hereby, factors previously shown to influence the activity, such as ionic strength and cofactor requirement, will also be considered. The influence of crowded conditions on the structure of the Dz:RNA complex will be studied in detail using circular dichroism (CD) spectroscopy and small-angle X-ray scattering (SAXS). Moreover, fluorescence correlation spectroscopy (FCS) will be used to investigate the diffusion behaviour and determine the hydrodynamic radius of the Dz:RNA complex under cell-like conditions. In addition, physicochemical properties of crowded solutions will be determined to rationalize the observations from functional and structural analyses.

Experiments in chapter 3 will be performed with a Dz that has been designed to cleave the mRNA of the human prion protein (PrP) at position 839 (Dz839). According to computational predictions using a sequential folding algorithm (Victor *et al.*, 2018; Tafer *et al.*, 2008), the cleavage site is located within an mRNA stretch highly accessible for Dz hybridization. In humans, PrP causes the rare and rapidly progressive neurodegenerative Creutzfeldt-Jakob disease (CJD, Barnwal *et al.*, 2022). Since there is still no therapy for CJD treatment (Barnwal *et al.*, 2022), but studies in mice (Büeler *et al.*, 1993) indicated a promising potential for gene silencing methods, DNAzymes might serve as promising tools.

Since discrepancies between *in vitro* studies and *in vivo* experiments have been restricting the development of DNAzyme-based applications, improving *in vitro* approaches towards conditions that resemble cells is highly important. Here, chapter 2 provides a protocol for performing studies on DNAzymes under molecular crowding conditions. Detailed information on the handling of crowded solutions and the analytical methods, including urea-PAGE, FRET-based cleavage assays, and CD measurements will be revealed.

However, simulating a cell's complexity *in vitro* is a difficult task. Thus, understanding the advantages and disadvantages of experimental set ups that aim at mimicking a cell-like environment is of great interest. For this purpose, in a second objective, experimental set ups

of previous crowding studies with the focus on DNAzymes will be compared and discussed (Chapter 4). Here, the choice of cosolute, applied concentrations, buffer composition, and length of RNA substrate will be discussed in more detail. In addition, alternative, such as vesicle-based, systems will be introduced to resemble cell conditions. The compiled data is intended to highlight features that offer the potential for adjustment to facilitate gradually approximating conditions of higher complexity in prospective *in vitro* studies and to allow for a deeper understanding of molecular crowding effects.

Since the discovery of RNA-cleaving DNAzymes, designs and applications focused on targeting human pathogens. Nonetheless, other sectors such as agriculture (Nagaraja *et al.*, 2021; Tatineni and Hein, 2023) and fish farming (Baillon *et al.*, 2020; Mugimba *et al.*, 2021) as parts of the global food supply network are also greatly affected by viral infections that often face challenges in disease management. Here, the use of DNAzymes as preventive or therapeutic approach has not been reported so far. To explore the therapeutic potential of RNA-cleaving DNAzymes in aquaculture, the viral hemorrhagic septicemia virus (VHSV) will be selected as target (Chapter 5). This virus causes one of the most pathogenic diseases and lacks commercially available vaccines as treatment (World Organisation for Animal Health (OIE), 2021). In a third objective, 10-23 DNAzymes will be designed to bind and cleave the RNA sequence of the VHSV nucleocapsid protein, which is crucial for viral replication (Baillon *et al.*, 2020). To test selected DNAzymes for stability and activity, measurements using urea-PAGE will be carried out. Additional time resolved, urea-PAGE-based measurements will be performed to obtain first information on the speed of RNA cleavage. The initial data intends to provide a base to further evaluate the potential of DNAzymes to be applied in aquaculture.

2

Stability and Activity of the 10–23 DNAzyme Under Molecular Crowding Conditions

This chapter reflects content of the following publication.

Publication Information

Nina Kirchgässler, Hannah Rosenbach, and Ingrid Span

Published in: Steger, G., Rosenbach, H., Span, I. (eds) DNAzymes. Methods in Molecular Biology, vol 2439. Humana, New York, NY, pp 79–89, 28.02.2022

Chapter 6

Stability and Activity of the 10–23 DNAzyme Under Molecular Crowding Conditions

Nina Kirchgässler, Hannah Rosenbach, and Ingrid Span

Abstract

DNAzymes are biocatalysts that have been selected in vitro and their function inside cells (in vivo) is extremely low. Thus, almost all studies have been carried out in diluted solutions (in vitro). The cellular presence of molecules such as amino acids, polypeptides, alcohols, and sugars introduces forces that modify the kinetics and thermodynamics of DNAzyme-mediated catalysis. The crowded intracellular environment referred to as molecular crowding can be mimicked by adding high concentrations of natural or synthetic macromolecules to the reaction conditions. Here, we investigate the activity of the 10–23 DNAzyme and the stability of the DNAzyme:RNA complex under molecular crowding conditions. Therefore, we use a Förster resonance energy transfer (FRET)-based activity assay in combination with denaturing urea polyacrylamide gel electrophoresis and circular dichroism (CD) spectroscopy.

Key words 10–23 DNAzyme, Deoxyribozymes, Circular dichroism (CD) spectroscopy, Denaturation temperature, Förster resonance energy transfer (FRET), Molecular crowding, Polyethylene glycol (PEG)

1 Introduction

Deoxyribozymes (DNAzymes) are single-stranded, catalytically active DNA sequences. They were isolated using in vitro selection and they are capable of accelerating a broad spectrum of chemical reactions [1–3]. Although DNAzymes are highly active in vitro, only poor in vivo activity has been reported so far [4, 5]. The conditions in biochemical experiments (in vitro) and inside cells (in vivo) vary strongly (Fig. 1) and could be the reason for the discrepancy between in vitro activity and performance in cells. While in vitro experiments are performed in highly diluted solutions and under strictly controlled conditions, the in vivo environment is dominated by a diversity of macromolecules such as nucleic acids, proteins, organelles, osmolytes, and metabolites, creating crowded and heterogeneous conditions [6, 7]. The concentration of cellular molecules (ranging from 50 to 400 g/L) not only allows

Gerhard Steger et al. (eds.), *DNAzymes: Methods and Protocols*,
Methods in Molecular Biology, vol. 2439, https://doi.org/10.1007/978-1-0716-2047-2_6,

80 Nina Kirchgässler et al.

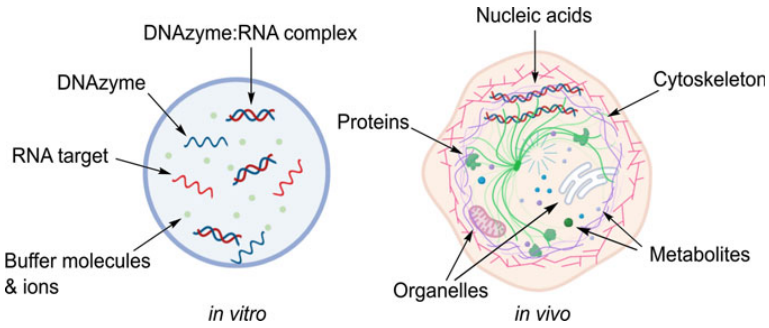

Fig. 1 Schematic illustration of the conditions of biochemical experiments (in vitro) and inside the cell (in vivo). In vitro experiments (left panel) are carried out in diluted, homogeneous solutions under controlled conditions. The environment in vivo (right panel) is highly condensed due to the presence of cellular organelles and a diversity of macromolecules, such as proteins, sugars, osmolytes, and nucleic acids, with concentrations between 50 and 400 g/L.

for crosstalk between them, but also affects solution properties, increases volume exclusion effects, unspecific interactions, and steric repulsion [8, 9]. The crowded intracellular environment referred to as molecular crowding affects the structure of biomolecules, their interactions, thermodynamics and kinetics of chemical reactions [10, 11].

The addition of high concentrations of natural and synthetic macromolecules, such as dextran and polyethylene glycol (PEG), to the reaction mixture enables molecular crowding to be mimicked in vitro [11–14]. In general, agents preferably used for molecular crowding analysis in vitro provide a high solubility in water, do not cause a degradation or precipitation of the molecule of interest and do not show higher binding affinities than water [15, 16]. The activity of DNAzymes and the stability of the DNAzyme:RNA complex under such conditions in vitro can be analyzed, e.g., by fluorescence-based activity assays and circular dichroism (CD) spectroscopy. Activity assays using fluorescence-labeled RNA targets in combination with denaturing polyacrylamide gel electrophoresis (PAGE) allow to distinguish between uncleaved and cleaved molecules, and potentially also degradation products. Addition of 6 to 8 M of urea to the polyacrylamide gel enables the denaturation of secondary and tertiary DNA and RNA structures, thus providing nucleic acid separation by size. This setup can be used to analyze the activity and specificity of DNAzymes as well as the stability of its RNA target. The resolution of this method is very high and enables the detection of length differences of one nucleotide [17, 18].

DNAzyme activity can also be measured by Förster resonance energy transfer (FRET) assays. These measurements require a double-labeled an RNA target containing a fluorophore at one

end and a quencher molecule at the other end. Here, metal ion-dependent DNAzyme-induced RNA cleavage leads to an increase in fluorescence allowing for time-resolved measurements and calculation of the observed rate constant k_{obs} [19].

CD spectroscopy is a very sensitive method to obtain information on the secondary structure and to determine the denaturation temperature of biomolecules. It exploits the chirality of molecules and the resulting difference in the absorption of right and left polarized light (ellipticity) [20]. The axial chirality of nucleic acids can be used to analyze structural conformation [21]. An additional implementation of temperature gradients allows an analysis of the denaturation behavior, since denaturation of nucleic acids results in an increase in absorbance close to 260 nm with increasing temperature [22, 23].

Here, we use different high molecular weight polymers and an osmolyte (Fig. 2) to simulate different degrees of volume exclusion effects. Hereby, we selected polymers of high molecular weight ranging from 3 to 20 kDa, as well as the polysaccharide dextran T500 (500 kDa). In addition, DNAzyme activity has been monitored in the presence of ethylene glycol (EG) and the osmolyte ectoine covering low molecular substances that also define the cellular environment and change solution properties [16]. Ectoine naturally accumulates in the cytoplasm of halophilic microorganisms aiming to protect cells from osmotic stress and to stabilize biomolecules [24, 25].

Here, we provide a protocol for the analysis of the catalytic activity of the 10–23 DNAzyme and the denaturation behavior of the DNAzyme:RNA complex under different molecular crowding concentrations using a variety of crowding agents.

2 Materials

Prepare all solutions using ultrapure water (obtained with a resistivity of 18.2 MΩ cm at 25 °C). Unless indicated otherwise, prepare and store all reagents at room temperature.

2.1 Analysis of Construct Stability and Specificity

1. Reaction buffer: 500 mM Tris(hydroxymethyl)aminomethane (Tris)–HCl pH 7.5 (*see* **Notes 1** and **2**).
2. 4 M NaCl in water.
3. 8 mM Ethylenediaminetetraacetic acid (EDTA) in water.
4. 10 mM $MgCl_2$ in water.
5. Thermocycler.
6. Tabletop centrifuge.
7. Crowding agents.

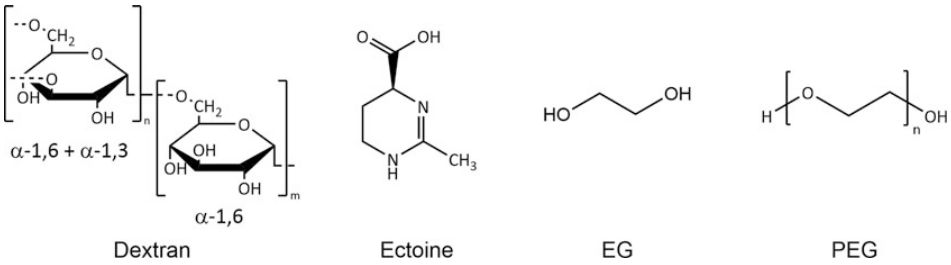

Fig. 2 Chemical structures of agents commonly used to mimic molecular crowding conditions

50% (w/v) PEG 3000, 3350, 4000, 6000, 8000, and 20,000 in Tris–HCl pH 7.5.

50% (w/v) EG in Tris–HCl pH 7.5.

50% (w/v) Ectoine in Tris–HCl pH 7.5.

50% (w/v) Dextran T500 in Tris–HCl pH 7.5.

8. DNAzyme and RNA targets.

   100 μM 10–23 DNAzyme (Dz) in water.

   100 μM simply labeled RNA target, containing 6-carboxyfluorescein (6-FAM) at the 5′-end (T_6-FAM), in water.

   100 μM dual labeled RNA target, containing 6-FAM at the 5′-end and Black Hole Quencher 1 (BHQ-1) at the 3′-end (T_FRET), in water.

   100 μM unlabeled RNA target (T) in water.

   100 μM stabilized RNA target (T_2′F) in water; the 2′ hydroxyl group (2′-OH) of the unpaired nucleotide is substituted by a fluorine atom to prevent RNA cleavage.

   All oligonucleotides can be stored at −20 °C (*see* **Notes 3** and **4**).

2.2 Urea Polyacrylamide Gel (18%)

1. 10× Tris-borate-EDTA (TBE) buffer: 0.89 M Tris, 0.89 M boric acid, 20 mM EDTA pH 8.0 (autoclaved). Prepare 1 L solution. Use water for dilution to 1× TBE buffer.
2. 40% acrylamide/bis-acrylamide solution (19:1) (store at 4 °C).
3. Urea (Molecular Biology Grade).
4. 10% Ammonium persulfate (APS) in water (store at −20 °C).
5. *N*,*N*,*N*′,*N*′-Tetramethyl-ethylenediamine (TEMED) (store at 4 °C).
6. 2× RNA gel loading dye: 9.4 mL formamide, 500 mM EDTA, 2 mg bromophenol blue, and 2 mg xylene cyanol (store at −20 °C).

7. Casting frame and glass plates (inner and outer plate) to obtain gels, two spacer stripes, and a 14-well comb (*see* **Note 5**).
8. Vertical electrophoresis cell and power supply.
9. Metal plate and clamps (*see* **Note 6**).
10. Nucleic acid gel staining agent.
11. Rocker.
12. Gel documentation system.

2.3 CD Spectroscopy

1. Reaction buffer: 500 mM Tris–HCl pH 7.5.
2. 4 M NaCl in water.
3. 8 mM EDTA in water.
4. 100 μM Dz in water (*see* **Note 4**).
5. 100 μM RNA target (T or T_2′F) in water (*see* **Note 4**).
6. Thermocycler.
7. Tabletop centrifuge.
8. Cuvette: quartz cuvette, 1 mm path length, for use with CD spectrometer.
9. CD spectrometer with a temperature control system, suitable to run temperature gradients.

3 Methods

3.1 Activity Assay for Stability Analysis

A control sample consisting of only RNA and a sample consisting of the DNAzyme:RNA complex have been analyzed for each condition.

1. Set up a reaction mixture in 50 mM Tris–HCl pH 7.5 with a final volume of 10 μL in a 1.5 mL reaction tube and add 0.4 μM Dz, 0.4 μM RNA target (T_6-FAM or T), and a crowding agent (*see* **Note 7**). Mix and incubate for 5 min at 73 °C (*see* **Notes 8** and **9**).
2. Centrifuge the sample for 4 s at 2000 × *g* to ensure that the entire solution is at the bottom of the tube and incubate for 10 min at room temperature.
3. Add 1 μL of 10 mM $MgCl_2$ to the reaction mixture and incubate for 3 h at 37 °C (*see* **Note 10**).
4. Centrifuge the sample for 4 s at 2000 × *g* and add 10 μL of 2× RNA gel loading dye. Mix and incubate for 10 min at 95 °C, then centrifuge again for 4 s at 2000 × *g*.

3.2 18% Urea-PAGE

1. During the 3 h incubation (*see* Subheading 3.1, **step 3**), prepare the 18% polyacrylamide gel. First, put a stirring bar in a 50 mL glass cylinder. Weigh 7 M of urea (12.61 g) and transfer

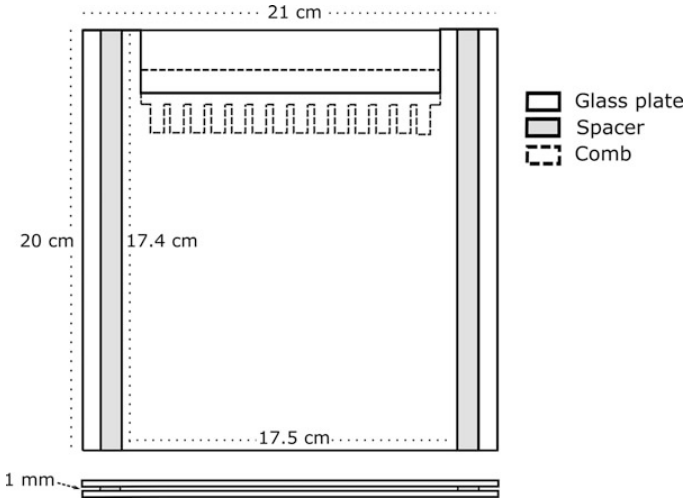

Fig. 3 Schematic representation of an 18% urea polyacrylamide gel. Two glass plates of 21 × 20 cm in size are sealed and held together by clamps. Two spacer stripes (1.2 × 20 cm) are placed between these plates to obtain gels with 17.5 × 17.4 cm in size and 1 mm in thickness. The comb contains 14 wells, each well with a filling capacity of 20 μL

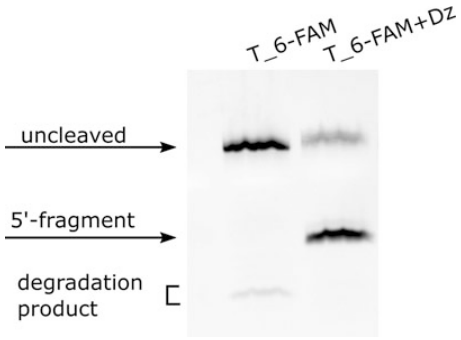

Fig. 4 Example of an urea-PAGE with samples consisting of RNA (T_6-FAM) and DNAzyme:RNA complex (T_6-FAM + Dz). The samples were incubated for 3 h at 37 °C prior to PAGE analysis, gel electrophoresis was carried out for 50 min, and the nucleic acids were visualized using fluorescence detection of the 6-carboxyfluorescein dye. While DNAzyme-mediated RNA cleavage results in two cleavage products, only the 5′-labeled fragment can be detected

it to the cylinder. Add 13.5 mL of the 40% acrylamide/bis-acrylamide solution (19:1) and 3 mL 10× TBE buffer. Heat the reaction mixture for a few seconds in a microwave until it becomes slightly warm. Seal the cylinder and stir until the urea is completely dissolved. Add water to a total volume of 30 mL.

Add 30 µL (0.1%, v/v) TEMED and 300 µL (0.1%, w/v) APS, then mix shortly. Transfer the solution to a prepared casting frame and insert a 14-well comb immediately without introducing air bubbles (Fig. 3). Wait until the gel is polymerized (approximately 1 h at room temperature).

2. After polymerization, transfer the gel to a vertical electrophoresis system. Place a metal plate in front of the gel and fix the setup using clamps.
3. Fill the buffer reservoirs with 1× TBE buffer without allowing the buffer to touch the metal plate.
4. Remove the comb and flush the wells with 1× TBE buffer.
5. Pre-run the gel for 30 min at 20 W to reduce temperature inhomogeneity throughout the gel. Flush the wells again with buffer prior to sample loading.
6. Add 20 µL of sample per gel lane (*see* **Note 11**).
7. Run the gel for 50 min at 20 W until the dye bromophenol blue has passed the first third of the gel.
8. For experiments with samples containing the fluorescence-labeled RNA target T_6-FAM, place the gel directly (do not remove the glass plates, since it poses the risk of damaging the gel) into the gel documentation system. Fluorescence bands become visible by excitation with blue light at 495 nm (Fig. 4). For experiments with non-fluorescent targets (T or T_2′F, used for CD spectroscopy), carefully remove the gel from the glass plates with the help of a spatula or a similar tool. Carefully transfer the gel to a tray filled with 150 mL 1× TBE buffer and 50 µL nucleic acid gel staining agent and cover the tray. Incubate on a rocker for 1 h at room temperature. After 1 h, place the gel into a gel documentation system. The stained nucleic acids become visible by excitation with UV light (302 nm).

3.3 Determining the Denaturation Temperature Using CD Spectroscopy

All samples are prepared with a total volume of 250 µL.

1. Mix 25 µM Dz and 25 µM RNA target (T or T_2′F) with 0.1 mM EDTA and incubate for 5 min at 73 °C (*see* **Note 8**).
2. Centrifuge the samples for 4 s at 2000 × *g* and incubate for 10 min at room temperature.
3. Transfer the entire sample into a cuvette (avoid air bubbles) and seal it (*see* **Notes 12** and **13**).
4. Record CD spectra from 190 nm to 320 nm in the temperature range of 20 °C to 73 °C. Record the sample's ellipticity, absorbance, and voltage applied to the photomultiplier. To provide a good signal to noise ratio at a complex concentration of 25 µM, perform measurements with ten accumulations. Set the scan rate to

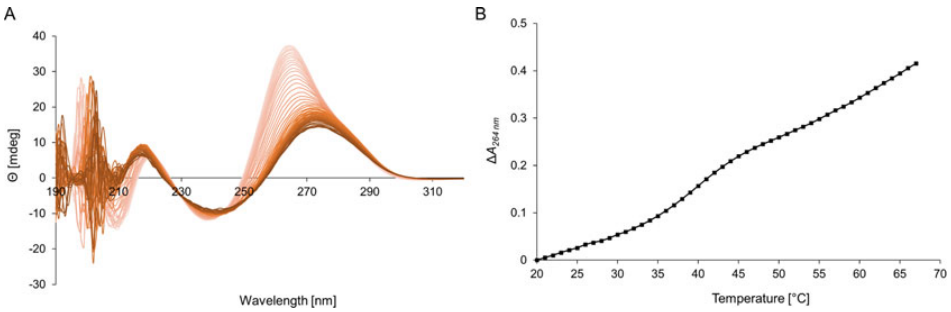

Fig. 5 Determining the denaturation temperature using CD spectroscopy. (**a**) CD spectra of the DNAzyme:RNA complex in absence of molecular crowding conditions collected in the temperature range from 20 to 73 °C. (**b**) Increase in absorbance at 264 nm (ΔA_{264nm}) with $\Delta A = A_T - A_{20\ °C}$ as a function of the temperature T

100 nm/min with a heating rate of maximally 1 °C/min. Collect data each nm and with a temperature interval of at least 1 °C.

5. Determine the denaturation temperature T_m of the DNAzyme:RNA complex in absence of molecular crowding agents by monitoring the CD signal at 264 nm. This wavelength was selected as the band in the CD spectrum (Fig. 5a) reveals the greatest impact of the temperature increase. Plot the absorbance difference at 264 nm (ΔA_{264nm}) with $\Delta A = A_T - A_{20\ °C}$ against the temperature (Fig. 5b). T_m refers to half height of the sigmoidal denaturation curve. For further analysis of denaturation curves, we refer to the literature [22, 23, 26].
6. After measurement, transfer the sample to a 1.5 mL reaction tube (store at −20 °C). For subsequent analysis by urea-PAGE (*see* Subheading 3.2), dilute the sample to a final concentration of 10 μM using 50 mM Tris pH 7.5. Use 10 μL of the sample and add 10 μL 2× RNA loading dye and follow the instructions (*see* Subheading 3.2).

4 Notes

1. Prior to buffer preparation, make sure to decontaminate all materials to minimize the risk of RNA degradation by RNases. All surfaces, including benchtops, pipettes, glassware, pH electrodes, and benchtop instruments, should be treated with a commercially available RNase decontamination agent. Alternatively, glassware can be heated for at least 4 h at 180 °C prior to usage.
2. Reaction buffer (stock solution): 1 M Tris pH 7.5. Weigh 24.22 g Tris and transfer to a 400 mL glass beaker. Add

150 mL water to a 250 mL graduated cylinder and transfer to the glass beaker. Dissolve and transfer to the cylinder. Add water to a volume of 180 mL, mix, and adjust the pH with HCl. Fill up to 200 mL with water. For experimental approaches and dissolving of crowding agents, prepare dilutions of 500 mM and 50 mM Tris pH 7.5.

3. For activity assays, prepare one stock solution of 4 μM Dz and one stock solution of 4 μM RNA target. Use water to dilute the samples.
4. Store nucleic acid solutions on ice during the experiments and long-term at −20 °C.
5. Regarding gel preparation, glass plates of 21 × 20 cm were used to obtain gels of 17.5 × 17.4 cm in size and 1 mm in thickness, containing 30 mL of mixture.
6. The metal plate should cover two-thirds of the glass plate to ensure a consistent temperature throughout the gel.
7. The cellular environment was mimicked by using the following concentration ranges: 0 to 0.18 g/mL for all PEG variants and EG, 0 to 0.004 g/mL for dextran T500 and 0 to 0.15 g/mL for ectoine.
8. Mix the sample gently. **Attention**: with increasing PEG size the solution's viscosity increases notably. Adapt the speed of mixing to prevent air bubbles.
9. During sample preparation, consider the volume of $MgCl_2$ needed for catalysis. Metal cofactors are added immediately prior to the 3 h incubation at 37 °C.
10. Use a piece of aluminum foil or something similar to cover the samples, thus reducing photobleaching effects on the label's fluorescence.
11. The addition of 10 μL 2× RNA loading dye in the remaining lanes is optional.
12. Prior to sample transfer, clean the CD cuvette with a special cleaning solution for optical equipment (in- and outside) and dry in a stream of nitrogen gas or air.
13. CD spectroscopic measurements are performed without adding any metal cofactors to prevent RNA cleavage, thus enabling the analysis of the DNAzyme:RNA complex.

References

1. Xiang Y, Lu Y (2014) DNA as sensors and imaging agents for metal ions. Inorg Chem 53:1925–1942. https://doi.org/10.1021/ic4019103
2. Baum DA, Silverman SK (2008) Deoxyribozymes: useful DNA catalysts in vitro and in vivo. Cell Mol Life Sci 65:2156–2174. https://doi.org/10.1007/s00018-008-8029-y
3. Breaker RR, Joyce GF (1994) A DNA enzyme that cleaves RNA. Chem Biol 1:223–229. https://doi.org/10.1016/1074-5521(94)90014-0
4. Rosenbach H, Victor J, Etzkorn M, Steger G, Riesner D, Span I (2020) Molecular features and metal ions that influence 10-23 DNAzyme activity. Molecules 25:11–21. https://doi.org/10.3390/molecules25133100
5. Victor J, Steger G, Riesner D (2018) Inability of DNAzymes to cleave RNA in vivo is due to limited Mg^{2+} concentration in cells. Eur Biophys J 47:333–343. https://doi.org/10.1007/s00249-017-1270-2
6. Ellis RJ (2001) Macromolecular crowding: obvious but underappreciated. Trends Biochem Sci 26:597–604. https://doi.org/10.1016/S0968-0004(01)01938-7
7. Zimmerman SB, Minton AP (1993) Macromolecular crowding: biochemical, biophysical, and physiological consequences. Annu Rev Biophys Biomol Struct 22:27–65
8. DasGupta S (2020) Molecular crowding and RNA catalysis. Org Biomol Chem 18:7724–7739. https://doi.org/10.1039/d0ob01695k
9. Zhou H-X, Rivas G, Minton AP (2008) Macromolecular crowding and confinemen: biochemical, biophysical, and potential physiological consequences. Annu Rev Biophys 37:375–397. https://doi.org/10.1146/annurev.biophys.37.032807.125817
10. Minton AP (2001) The influence of Macromolecular crowding and macromolecular confinement on biochemical reactions in physiological media. J Biol Chem 276:10577–10580. https://doi.org/10.1074/jbc.R100005200
11. Paudel BP, Fiorini E, Börner R, Sigel RKO, Rueda DS (2018) Optimal molecular crowding accelerates group II intron folding and maximizes catalysis. Proc Natl Acad Sci U S A 115:11917–11922. https://doi.org/10.1073/pnas.1806685115
12. Paudel BP, Rueda D (2014) Molecular crowding accelerates ribozyme docking and catalysis. J Am Chem Soc 136:16700–16703. https://doi.org/10.1021/ja5073146
13. Azri A, Giamarchi P, Grohens Y, Olier R, Privat M (2012) Polyethylene glycol aggregates in water formed through hydrophobic helical structures. J Colloid Interface Sci 379:14–19. https://doi.org/10.1016/j.jcis.2012.04.025
14. Tyrrell J, Weeks KM, Pielak GJ (2015) Challenge of mimicking the influences of the cellular environment on RNA structure by PEG-induced Macromolecular crowding. Biochemistry 54:6447–6453. https://doi.org/10.1021/acs.biochem.5b00767
15. Fiorini E, Börner R, Sigel RKO (2015) Mimicking the in vivo environment - the effect of crowding on RNA and biomacromolecular folding and activity. Chimia (Aarau) 69:207–212. https://doi.org/10.2533/chimia.2015.207
16. Nakano SI, Miyoshi D, Sugimoto N (2014) Effects of molecular crowding on the structures, interactions, and functions of nucleic acids. Chem Rev 114:2733–2758. https://doi.org/10.1021/cr400113m
17. Summer H, Grämer R, Dröge P (2009) Denaturing urea polyacrylamide gel electrophoresis (urea PAGE). J Vis Exp 3–5. https://doi.org/10.3791/1485
18. Albright LM, Slatko BE (2001) Denaturing polyacrylamide gel electrophoresis. Curr Protoc Nucleic Acid Chem Appendix 3:1–5. https://doi.org/10.1002/0471142905.hga03fs00
19. Rosenbach H, Borggräfe J, Victor J, Wuebben C, Schiemann O (2021) Influence of monovalent metal ions on metal binding and catalytic activity of the 10–23 DNAzyme. Biol Chem 402:99–111. https://doi.org/10.1515/hsz-2020-0207
20. Kypr J, Kejnovská I, Bednářová K, Vorlíčková M (2012) Circular dichroism spectroscopy of nucleic acids. Compr Chiroptical Spectrosc 2:575–586. https://doi.org/10.1002/9781118120392.ch17
21. Kypr J, Kejnovská I, Renčiuk D, Vorlíčková M (2009) Circular dichroism and conformational polymorphism of DNA. Nucleic Acids Res 37:1713–1725. https://doi.org/10.1093/nar/gkp026
22. Riesner D, Römer R (1973) Thermodynamics and kinetics of conformational transitions in oligonucleotides and tRNA. In: Duchesne J (ed) Structural studies on nucleic acids and other biopolymers. Academic Press, Cambridge, pp 237–318

23. Schmitz M, Tinoco I (2000) Thermodynamics of formation of secondary structure in nucleic acids. In: Di Cera E (ed) Thermodynamics in biology. Oxford University Press, New York, pp 131–176
24. Pastor JM, Salvador M, Argandoña M, Bernal V, Reina-Bueno M, Csonka LN, Iborra JL, Vargas C, Nieto JJ, Cánovas M (2010) Ectoines in cell stress protection: uses and biotechnological production. Biotechnol Adv 28: 782–801. https://doi.org/10.1016/j.biotechadv.2010.06.005
25. Czech L, Hermann L, Stöveken N, Richter AA, Höppner A, Smits SHJ, Heider J, Bremer E (2018) Role of the Extremolytes Ectoine and Hydroxyectoine as stress protectants and nutrients: genetics, Phylogenomics, biochemistry, and structural analysis. Genes (Basel) 9:1–58. https://doi.org/10.3390/genes9040177
26. Serra MJ, Turner DH (1995) Predicting thermodynamic properties of RNA. Methods Enzymol 259:242–261. https://doi.org/10.1016/0076-6879(95)59047-1

3

MOLECULAR CROWDING: IMPACTS ON THE ACTIVITY OF THE 10-23 DNAZYME

This chapter reflects content of the following manuscript.

3.1 Manuscript information

Nina Kirchgässler, Hannah Rosenbach, Ralf Biehl, Gerhard Steger, Richard Börner, and Ingrid Span

In preparation

3.2 Abstract

The growing number of approved nucleic acid therapeutics illustrates the potential to treat diseases by targeting their genetic blueprints *in vivo*. The 10-23 DNAzyme is capable of cleaving a wide range of target RNA with high selectivity. However, its poor performance *in vivo* restricts its therapeutic application as gene silencing agent. Studies on ribozymes have shown that the crowded environment in cells and associated effects can impact ribozyme folding and thermostability, resulting in a change in activity. This opens up the question whether DNAzymes are also affected by molecular crowding. Here, we investigate the functional and structural influence of molecular crowding conditions on the 10-23 DNAzyme. The stability and activity of a PrP-specific 10-23 DNAzyme were examined in presence of PEG, dextran, and osmolytes. Our results indicate that osmolytes decrease DNAzyme activity in a concentration-dependent manner, while certain PEG and dextran concentrations promote activity. To rationalize our observations, we studied the cosolutes' effect on physicochemical solution properties and the structure of the DNAzyme:RNA complex using FCS and SAXS. The data reveal that enhanced activity is observed under conditions where a combination of physicochemical properties matches an 'optimum' that seems to be dependent on the metal ion cofactor. Structural influence under such conditions is indicated less. We propose that a certain degree of molecular crowding is required to favor a state, which allows for higher catalytic turnover. In addition, we show that the requirement for magnesium and manganese as a cofactor remains unchanged under the conditions applied. Our work contributes to a better understanding of how the cellular environment affects DNAzyme structure and function.

3.3 Introduction

In 1994, Breaker and Joyce (1994) have found catalytically active, single-stranded DNA molecules by *in vitro* selection, called deoxyribozymes or DNAzymes. Adopting a three-dimensional structure allows DNAzymes to catalyze a broad spectrum of reactions (Chandrasekar and Silverman, 2013; Silverman, 2008; Zhou *et al.*, 2017a; Zhang, 2018; Hollenstein, 2015). Properties such as small in size, affordable in synthesis, diversity in modifications, and programmability made DNAzymes attract attention. Despite their diversity, RNA-cleaving DNAzymes in particular emerged to function as an alternative approach in nucleic acid therapeutics (Larcher *et al.*, 2023; Karnati *et al.*, 2014; Thomas *et al.*, 2021).

Nowadays, one of the most prominent RNA-cleaving DNAzymes is the 10-23 DNAzyme (Dz, for reviews see Larcher *et al.*, 2023; Yan *et al.*, 2023a; Rosenbach *et al.*, 2020b). Structurally, it consists of a 15 nt catalytic core flanked by two substrate binding arms, which may vary in length and sequence (usually 9–12 nt), but have to hybridize to the complementary RNA substrate of interest. To perform RNA cleavage, the Dz requires divalent cations (M^{2+}), such as Mg^{2+} or Mn^{2+}, and a purine-pyrimidine junction (5'–RY–3') as cleavage site with an efficiency order of AU = GU $\geq$ GC $\gg$ AC (Figure 3.1A, B). Mechanistically, the Dz is predicted to perform cleavage of a phosphodiester bond via an acid-base mechanism (Santoro and Joyce, 1998; Borggräfe *et al.*, 2023), similar to the 8-17 DNAzyme (Cortés-Guajardo *et al.*, 2021; Cepeda-Plaza and Peracchi, 2020; Cepeda-Plaza *et al.*, 2018).

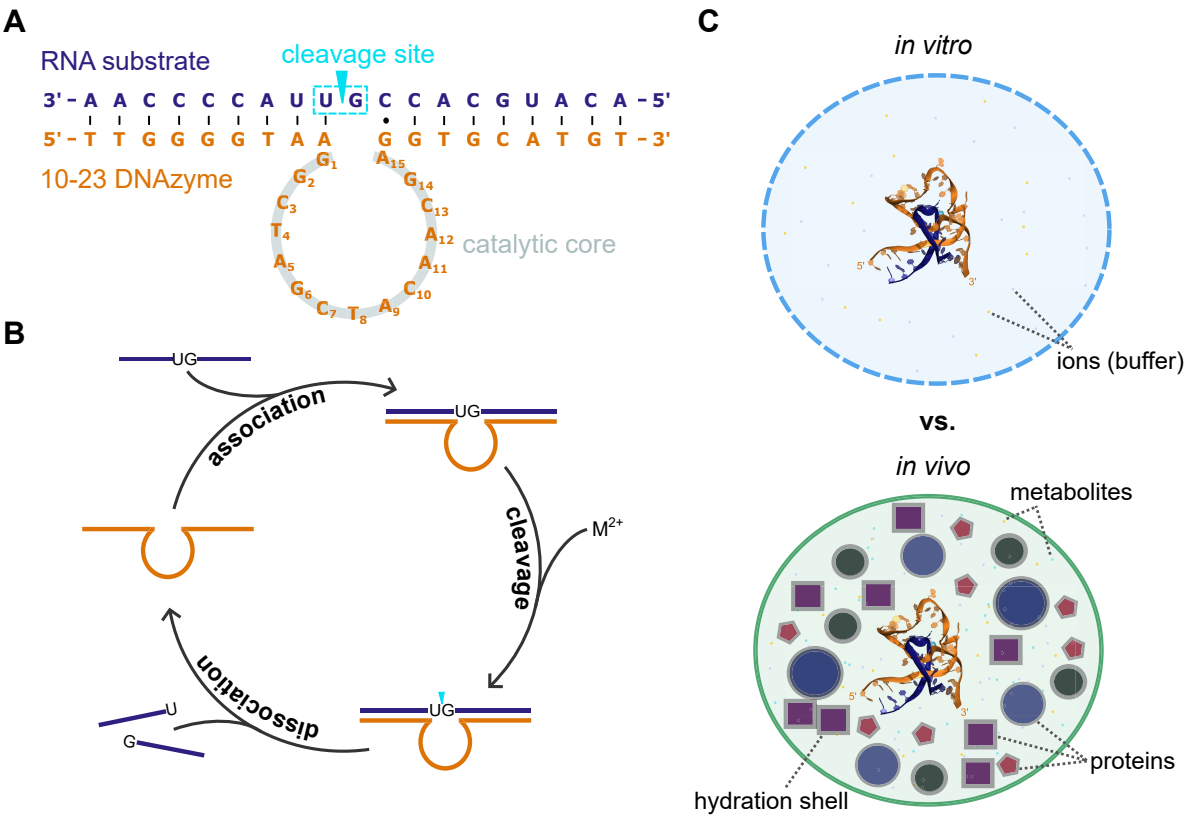

Figure 3.1: **A** Secondary structure of the 10-23 DNAzyme used in this study (Dz^{WT}) in complex with its RNA substrate. **B** Catalytic cycle of the 10-23 DNAzyme, which illustrates cleavage under multiple turnover. After association of the Dz and RNA substrate by complementary base pairing, site-specific cleavage is induced depending on divalent cations M^{2+}. Finally, the DNAzyme dissociates from the cleaved RNA to enter a new cycle. Modified after Rosenbach *et al.* (2020b). **C** Simplified illustration of differences between analyses on the DNAzyme:RNA complex (PDB 7PDU, Borggräfe *et al.*, 2021) under *in vitro* and *in vivo* conditions.

Since their discovery, the spectrum of DNAzymes in terms of function and catalysis (e. g. phosphorylation, amide hydrolysis, and Diels-Alder reaction) broadened immensely for *in vitro*-based applications (Silverman, 2016; Zhang, 2018). To this day, however, the use of DNAzymes in cells is limited due to a) a poor understanding of the catalytic mechanism and b) low *in vivo* activity (Garn and Renz, 2017; Etzkorn and Span, 2023). Although first DNAzymes were reported that have entered clinical trials (e. g. Cho *et al.*, 2013; Krug *et al.*, 2017), therapeutic success remains rare claiming several challenges: susceptibility to degradation by nucleases (Xiao *et al.*, 2023), hampered accessibility of the target sequence by RNA folding (Taylor *et al.*, 2022), low availability of free cofactors ($[Mg^{2+}] \approx 0.5 - 1\,\mathrm{mM}$, Victor *et al.* (2018)), and activity modulating properties by monovalent ions (Rosenbach *et al.*, 2021).

The latest modification studies on DNAzymes aim at addressing these limitations by partially modifying the backbone, sugar, and base of nucleotides, so-called xeno nucleic acids (XNAs). First attempts show progress in improved *in vivo* activities, thus providing a promising toolbox for the future (Wang *et al.*, 2021; Taylor *et al.*, 2022; Gerber *et al.*, 2022). A certainly lasting challenge is differentiating RNA knockdown effects by targeted DNAzyme activity from RNase H-induced antisense effects (Taylor and Holliger, 2021; Zhou *et al.*, 2022; Rivory *et al.*, 2006), leaving room for further optimization and reliable controls.

For several years now, questions pointed towards potential effects on DNAzyme activity by molecular crowding in cells. In general, the term molecular crowding often summarizes

effects resulting from macromolecular crowding, thus volume exclusion, confinement, and adsorption with thermodynamic and kinetic consequences. Since cells comprise a diversity of macromolecules, which generate a densely packed and heterogeneous environment, *in vivo* conditions differ clearly from experimentally controlled *in vitro* conditions (Feig *et al.*, 2017; Miyoshi and Sugimoto, 2008; Zhou, 2008b; Zimmerman and Minton, 1993, Figure 3.1C). With this, several studies on double-stranded DNA and RNA, proteins, and ribozymes reported impacts on e. g. mobility, water reactivity, folding, and intermolecular interactions (Paudel *et al.*, 2018; Kuznetsova *et al.*, 2014; Fiorini *et al.*, 2015; Nakano *et al.*, 2008; DasGupta, 2020; Nakano *et al.*, 2014b). Since the extent to which a biomolecule is affected by molecular crowding depends, amongst others, on its size and shape, this raises the question if DNAzymes are also affected by it.

In this study, we aim at simulating molecular crowding conditions *in vitro* using polyethylene glycol (PEG), dextran, and osmolytes as cosolutes and investigate their influence on DNAzyme function and structure. We hope that our results will provide first insights whether effects associated with molecular crowding interfere with DNAzyme activity that will help to better understand *in vivo* restrictions.

3.4 Material and Methods

3.4.1 Oligonucleotide sequences

DNA and RNA oligonucleotides were commercially obtained from biomers.net (Ulm, Germany). Single-labeled RNA substrates used in the stability assay followed by denaturing urea polyacrylamide gel electrophoresis (PAGE) contained a 6-carboxyfluorescein (6-FAM) molecule at the 5'-end. Single-labeled RNA substrates used for fluorescence correlation spectroscopy (FCS) measurements contained an Atto647N molecule at the 5'-end. RNA substrates in Förster resonance energy transfer (FRET)-based cleavage assays were double-labeled with a 6-FAM molecule at the 5'-end and the Black Hole Quencher-1 (BHQ-1) at the 3'-end. In terms of FCS and small-angle x-ray scattering (SAXS) studies, the RNA substrate was additionally stabilized by substituting the 2'-OH group of the ribose moiety of the guanosine at the cleavage site with a fluorine atom (2'F) to avoid cleavage (Rosenbach *et al.*, 2021; Borggräfe *et al.*, 2021). The Dz used in this study was designed to specifically bind the human prion protein (PrP) mRNA and perform cleavage at position 839 (Victor *et al.*, 2018). The sequences for Dz and RNA substrates are listed in Table 3.1.

Table 3.1: Sequences of Dz and RNA substrates used in this study. X=2'-F-dG

Construct	Sequence (5'–3')
Dz^{WT}	TTGGGGTAAGGCTAGCTACAACGAGGTGCATGT
Dz^{A5C}	TTGGGGTAAGGCTCGCTACAACGAGGTGCATGT
$T^{2'F}$	ACAUGCACCXUUACCCCAA
T^{FAM}	6-FAM-AAAACAUACACCGUUACCCCAACCA
T^{FRET}	6-FAM-ACAUGCACCGUUACCCCAA-BHQ-1
$T^{Atto647N}$	Atto647N-AAAACAUACACCXUUACCCCAACCA

3.4.2 Cosolutes to simulate crowded conditions

Cosolutes to simulate crowded conditions *in vitro* were obtained commercially and used at concentrations of 0.03, 0.07, 0.11, 0.15 and 0.18 g/mL, respectively. The concentration range was selected according to published studies (Paudel *et al.*, 2018; Fiorini *et al.*, 2015) and estimated total concentrations of biomolecules in cells ($50-400$ g/L, Zimmerman and Minton (1993)). Samples containing osmolytes were prepared either with betaine (BioUltra, ≥ 99 %, Sigma-Aldrich, St. Louis, MO, USA) or ectoine (≥ 95 %, HPLC, Sigma-Aldrich, St. Louis, MO, USA). In addition, we used ethylene glycol (EG, ≥ 99 %, Muskegon, MI, USA) and different variants of polyethylene glycol (PEG) with average molecular weights ($M_{\mathrm{W,\,av}}$) of 200 (PEG 200, for synthesis), 600 (PEG 600, for synthesis), 1000 (PEG 1000, for synthesis), 3000 (PEG 3000, BioUltra), 3350 (PEG 3350, BioUltra), 4000 (PEG 4000, for synthesis), 6000 (PEG 6000, BioUltra), 8000 (PEG 8000, BioUltra), and 20000 (PEG 20000, (stabilized) for synthesis). PEG 200 to 8000 were obtained from Sigma-Aldrich (St. Louis, MO, USA) and PEG 20000 from Merck (Darmstadt, Germany). In terms of polysaccharides, dextran 5000 (dex 5000, $M_{\mathrm{W,\,av}} = 5$ kDa) and 12000 (dex 12000, $M_{\mathrm{W,\,av}} = 12$ kDa, analytical standard for GPC, Sigma-Aldrich, St. Louis, MO, USA) were used. Stocks were prepared as 50 % (g/mL) solutions in either water (18.2 MΩ) or 50 mM tris(hydroxymethyl)aminomethane hydrochloride (Tris-HCl), pH 7.5.

3.4.3 Stability assay with single-labeled RNA substrates followed by denaturing urea-PAGE

Stability assays were performed with 0.4 µM 6-FAM-labeled RNA substrate and 0.4 µM Dz (single-turnover) in 50 mM Tris-HCl, pH 7.5 in presence and absence of 100 mM sodium chloride (NaCl) and cosolute. Prior to cleavage, RNA substrate and Dz were denatured in buffer without Mg^{2+} at 73 °C for 5 min, followed by an incubation of 10 min at room temperature for renaturation. RNA cleavage was induced with 1 mM magnesium chloride ($MgCl_2$) and incubated for 3 h at 37 °C. Samples taken for further analysis were quenched in 94 % (v/v) formamide, 25 mM ethylenediamine tetraacetic acid (EDTA), pH 8.0, 0.02 % (w/v) Bromphenol blue, and 0.02 % (w/v) Xylene cyanol and heated at 95 °C for 10 min. Sample separation was carried out using 18 % polyacrylamide gels with 7 M urea buffered with Tris-borate EDTA buffer (TBE) for 45 min at 20 W (Kirchgässler *et al.*, 2022). Prior to sample separation by gel electrophoresis, gels were preheated for 30 min at 20 W to avoid temperature inhomogeneities. 6-FAM labeled RNA substrates were detected and visualized by fluorescence, which allows detection of uncleaved RNA substrates and one of two cleavage products that contains the 6-FAM molecule at the 5'-end (5'-fragment). In case of unlabeled RNA substrates, visualization was provided by staining in TBE buffer that contains a dilution of 1:30,000 of GelRed nucleic acid gel stain (10,000X in H_2O, Biotium, Fremont, CA, USA) for 1 h at room temperature. Images were acquired using the ChemiDoc MP System (Bio-Rad, Hercules, CA, USA).

3.4.4 FRET-based cleavage assay

Cleavage assays were carried out using a double-labeled RNA substrate (T^{FRET}, Table 3.1). Metal ion-induced RNA cleavage allows detection of an increase in fluorescence over time. Assays were performed with final concentrations of 0.1 µM RNA substrate and 0.1 µM Dz (single-turnover) in 50 mM Tris-HCl, pH 7.5 and 0.1 mM EDTA with different concentrations of cofactors ($MgCl_2$: 0.5, 3 and 5 mM; manganese(II) chloride ($MnCl_2$) : 0.5 mM) at 37 °C. Measurements were carried out in presence and absence of 100 mM NaCl and cosolute.

0.8 µM RNA substrate and Dz were denatured in buffer for 5 min at 73 °C, followed by an incubation of 10 min at room temperature to allow renaturation. Samples were prepared at higher concentrations to facilitate complex formation. Initial denaturation was performed in either presence or absence of NaCl, but absence of cosolute and $MgCl_2$ or $MnCl_2$. During renaturation, different cosolute concentrations were added to the wells of a 384-well non-binding microplate (Greiner Bio-One, Kremsmünster, Austria) in buffer and a total volume of 15 µL. Nucleic acid stocks were diluted with buffer to a construct concentration of 0.2 µM. Next, 20 µL of solution were added to the wells. Each measurement included a control that contained the RNA substrate only in absence of cosolute. The plate was sealed with tape (Polyolefin Acrylate, Thermo Scientific, Waltham, MA, USA), placed inside the plate reader (CLARIOstar Plus, BMG Labtech, Ortenberg, Germany), and equilibrated to 37 °C for 30 min. Prior to measurement, the sealing tape was removed and RNA cleavage was induced by automatic injection of 5 µL of cofactor stock solution ($MgCl_2$ or $MnCl_2$) after 15 cycles of measurement. Data points were acquired with cycle times of either 8 s (0.05 mM $MgCl_2$), 7 s (0.1 mM $MgCl_2$), 6 s (0.2 mM $MgCl_2$), 5 s (0.3 mM $MgCl_2$), 4 s (0.5 mM $MgCl_2$ and 0.01 mM $MnCl_2$), 3 s (0.05 mM $MnCl_2$), 2 s (3 and 5 mM $MgCl_2$, 0.1, 0.2 and 0.25 mM $MnCl_2$), or 1 s (0.3, 0.4 and 0.5 mM $MnCl_2$) depending on the speed of reaction. Assays in competition with ATP were carried out with 0, 0.2, 0.5, 0.8, 1, 1.5 and 2 mM ATP at 0.5 mM $MgCl_2$ in 50 mM Tris-HCl, pH 7.5, 0.1 mM EDTA, and 100 mM NaCl. Measurements were performed with 1000 cycles and excitation and emission wavelength were set to $\lambda_{ex} = 484\,nm$ and $\lambda_{em} = 530\,nm$.

Experimental data was fitted and plotted using graphics layout engine (GLE, `https://glx.sourceforge.io/`). Fluorescence intensity curves were fitted using

$$F(t) = F_{max} \cdot (1 - e^{-k_{obs}\Delta t}) + F_{min} \tag{3.1}$$

with F_{max} and F_{min} as the maximum and minimum fluorescence in curves, k_{obs} as the observed rate constant, and $\Delta t = t - t_{injection}$ as the time difference after subtraction of RNA only fluorescence and data correction for a time-dependent linear decrease in fluorescence, most likely due to photobleaching.

To evaluate the impact of molecular crowding on Dz activity, the relative rate constant $k_{rel,i}$ was calculated

$$k_{rel,i} = \frac{k_{obs,i}}{k_{obs,\,no\,cosolute}} \tag{3.2}$$

3.4.5 FCS for diffusion analysis

Sample preparation for FCS analyses was carried out in sets of RNA substrate only (T) and Dz:RNA complex (TDz) for each tested condition using the stabilized RNA substrate $T^{Atto647N}$ (Table 3.1). In absence of cosolute, stocks containing 400 nM of $T^{Atto647N}$ and Dz^{WT} in 50 mM Tris-HCl, pH 7.5 and 0.1 mM EDTA were incubated for 5 min at 73 °C for denaturation, followed by an incubation of 10 min at room temperature to facilitate complex formation. Subsequently, stocks of T and TDz were diluted 1:10 with 50 mM Tris-HCl, pH 7.5 and 0.1 mM EDTA. Samples were prepared separately in reaction tubes with total volumes of 210 µL. Here, cosolutes and buffer were added first. 10.5 µL of diluted stock of T or TDz were added immediately before measurement to reach a final concentration of 2 nM. Samples were mixed thoroughly and 200 µL each were transferred into wells of sterile NuncTM Lab-TekTM II chambered coverglass systems (8 chambers, Nunc, Thermo Scientific, Rochester, NY, USA). Closed sample chambers were incubated for 20 min at 37 °C prior to measurement. The following conditions have been analyzed and were selected presenting all three types of cosolutes, different degrees of volume exclusion, and Dz activity: 50 mM Tris-HCl, pH 7.5 and 0.1 mM EDTA (buffer only), 0.03 g/mL PEG 4000, 0.07 g/mL PEG 3000 and 3350, 0.11 g/mL PEG 8000, 0.15 g/mL PEG 200, 600, 3000, and 4000, and 0.18 g/mL betaine, ectoine, dextran 12000, EG, and PEG 20000.

FCS data were collected using an Olympus FLUOVIEW FV3000 (Olympus Europa SE & Co. KG, Hamburg, Germany) confocal laser scanning microscope with a high numerical aperture objective (UPLSAPO60XW/1.2). The microscope is equipped with a multichannel picosecond event timer (HydraHarp 400, PicoQuant) for single-point time correlated single photon counting (TCSPC) measurements. Samples were excited using a 640 nm CW laser (OBIS, Coherent) and the fluorescence signal was split for its polarization using a polarizing beamsplitter. The parallel and perpendicular signal was detected using two identical bandpass filters (690/70, AHF Analysentechnik, Germany) in front of two avalanche photodiodes (SPCM-AQRH-14-TR module, Excelitas Technologies) to enable detector cross-correlation and afterpulse correction. FCS measurements were performed at 37 °C and with a laser intensity of 16.7 μW. All conditions (see above) were measured in triplicates ($n = 3$) to check for reproducibility, of which each measured triplicate consists of five measurements. From data of the obtained time traces, cross-correlation curves were calculated using the SymPhoTime 64 software (PicoQuant, Berlin, Germany). The cross-correlation curve of five independent measurements was averaged and fitted. The fitting model $G(\tau)$ accounts for the free diffusion of the molecule of interest within and the signal fluctuations due to the population of a potential triplet state of the used fluorophore (Lakowicz, 2006; Yu *et al.*, 2021) according to

$$G(\tau) = \frac{1}{N}\left(1 + \frac{T}{1-T}\exp\left(-\frac{t}{\tau_T}\right)\right)\left(1 + \left(\frac{t}{\tau_D}\right)^b\right)^{-1}\left(1 + S^2\left(\frac{t}{\tau_D}\right)^b\right)^{-\frac{1}{2}} \tag{3.3}$$

with N as average number of molecules within the confocal volume, T as triplet fraction, τ_D as diffusion time, τ_T as characteristic correlation time of the triplet state, b as anomalous or subdiffusion exponent due to molecular crowding (Höfling and Franosch, 2013), and $S = 0.2$ as structure factor, i. e., the aspect ratio of the 3D gaussian approximation of the confocal volume. The triplet fraction accounts for the varying population of the triplet state of the fluorophore used. We calibrated the confocal volume using a dye with known diffusion coefficient D and calculated the focus radius $R_0 = \sqrt{4D\tau_D}$ using the diffusion coefficient of Atto655 with $D_{37\,^\circ\mathrm{C}} = 5.62 \cdot 10^{-10}$ m^{2}s^{-1} (Müller *et al.*, 2008) due to structural similarity between Atto655

and Atto647. We determined $b = 1$ with calibration measurements of the free dye, as expected. In the presence of cosolutes, however, we found $b = 0.9$, which we attribute to subdiffusion of the nucleic acid molecules in the crowded solution. The offset of the autocorrelation curve has been found to be zero. The Stokes radius, thus, hydrodynamic radius r_h of the molecule of interest was calculated according to Stokes-Einstein

$$r_h = \frac{4k_B T \tau_D}{6\pi\eta R_0^2} \tag{3.4}$$

with k_B as Boltzmann constant, T the absolute temperature and $\eta(T)$ as the experimentally determined dynamic viscosity of the crowded solution.

3.4.6 Calculation of r_h, r_g, and cavity size D

For determining the size of PEG particles, the radius of gyration r_g was calculated based on light scattering results (Devanand and Selser, 1991) following the equation

$$r_{\mathrm{g,\,PEG}}[\mathrm{nm}] = 0.0215 \cdot M_\mathrm{W}^{0.583\pm0.031} \approx 0.195 \left(\frac{M_{\mathrm{W,\,cosolute}}}{M_{\mathrm{W,\,monomer}}} \right)^{0.583} \tag{3.5}$$

with $M_{\mathrm{W,\,monomer}} \approx 44\,\mathrm{g/mol}$ and considering volume exclusion effects, thus no overlap of cosolutes. The theoretical relation between the according hydrodynamic radius r_h and r_g for a linear polymer in a good solvent is $r_\mathrm{h}/r_\mathrm{g} = 0.64$ (Teraoka, 2002; Linegar *et al.*, 2010). r_h for PEG particles was calculated based on Devanand and Selser (1991)

$$r_{\mathrm{h,\,PEG}}[\mathrm{nm}] = 0.0145 \cdot M_\mathrm{W}^{0.571\pm0.009} \approx 0.126 \left(\frac{M_{\mathrm{W,\,cosolute}}}{M_{\mathrm{W,\,monomer}}} \right)^{0.571} \tag{3.6}$$

Hydrodynamic radii r_h for dextran molecules were calculated based on previous experiments by Hernández *et al.* (2017)

$$r_{\mathrm{h,\,dextran}}[\mathrm{nm}] = 0.0422 \cdot M_\mathrm{W}^{0.4453} \tag{3.7}$$

with M_W as the average molecular weight of the cosolute particle.

The theoretical, average distance between cosolutes (cavity size, D) was calculated based on the assumption of a simplified hard sphere model (Kang *et al.*, 2015),

$$D \approx \left(\frac{4}{3}\pi \right)^{1/2} \frac{r_\mathrm{g}}{\varphi^{1/3}} x \tag{3.8}$$

where φ is the volume fraction of all cosolute particles in solution, which depends on size of the particle, its number in solution, and its mass concentration.

$$\varphi = \frac{4}{3}\pi r_\mathrm{g}^3 \frac{N_\mathrm{A}}{M_{\mathrm{W,\,cosolute}}} \frac{m}{V} \tag{3.9}$$

The correction factor x is introduced to adjust differences between r_g and r_h, which was determined empirically for cosolutes EG (5.8), PEG 1000 (2.8), PEG 8000 (1.3), and PEG 35000 (0.65) in a previous ribozyme-based approach (unpublished). Theoretical correction factors

for the remaining PEG variants in this study have been calculated according to the fit model

$$x = y_0 + A_1 \cdot \exp\left(-\frac{(M_{\mathrm{W,\,cosolute}} - x_0)}{t_1}\right) + A_2 \cdot \exp\left(-\frac{(M_{\mathrm{W,\,cosolute}} - x_0)}{t_2}\right) \tag{3.10}$$

with $y_0 = 0.65851$, $A_1 = 2.0757$, $x_0 = 62$, $t_1 = 6999.927$, $A_2 = 3.0757$, and $t_2 = 387.688$.

3.4.7 Structural analysis by SAXS

Small-angle X-ray Scattering (SAXS) measurements were performed with final concentrations of 5 g/mL of Dz:RNA complex. In absence of cosolute and $MgCl_2$, Dz and RNA substrate ($T^{2'F}$) were denatured in 50 mM Tris-HCl, pH 7.5, 0.1 mM EDTA, and 100 mM NaCl at 73 °C for 5 min, followed by an incubation of 10 min at room temperature. Next, cosolutes or $MgCl_2$ dissolved in 50 mM Tris-HCl, pH 7.5, 0.1 mM EDTA, and 100 mM NaCl were added to reach the final complex concentration for measurement.

SAXS experiments were performed at the Jülich Center for Neutron Science (JCNS) at Forschungszentrum Jülich, Germany. The instrument "Ganesha-Air" from SAXSLAB/XENOCS was used. The X-ray source is a D2-MetalJet (Excillum) with Ga–Kα radiation (wavelength $\lambda = 0.134\,14\,\mathrm{nm}$). The data were acquired with a position-sensitive detector (PILATUS 300 K, Dectris). After calibration with silver behenate, the distance from the sample to the detector was set to cover a Q-range of $0.1 - 6\,\mathrm{nm}^{-1}$. Temperature was set to 20 °C.

The radius of gyration r_g was determined by a fit to the measured intensity

$$I(Q) = I_0 \exp\left(-\frac{1}{3}Q^2 r_\mathrm{g}^2\right) \tag{3.11}$$

for Qr_g using the Guinier model (Feigin and Svergun, 1987) with magnitude of the scattering vector

$$Q = 4\pi \sin(\Theta/2)\lambda^{-1} \tag{3.12}$$

and scattering angle Θ.

Ellipsoidal scattering formfactor $P(Q)$ for a sphere with semiaxes $r_\mathrm{a} = eR$ (axis of revolution) and $r_\mathrm{b} = R$, $e = r_\mathrm{a}/r_\mathrm{b}$ and contrast $\Delta\rho$ to the solvent (Pedersen, 1997) is

$$P(Q) = (\Delta\rho)^2 \int_0^{\pi/2} F_{\mathrm{sphere}}^2\big(Q, r(R,e,a)\big) \sin\alpha \, \mathrm{d}\alpha \tag{3.13}$$

with

$$r(R,e,a) = R(\sin^2\alpha + e^2\cos^2\alpha)^{\frac{1}{2}} \tag{3.14}$$

and

$$F_{\mathrm{sphere}}(Q,r) = \frac{3\big(\sin(Qr) - Qr\cos(Qr)\big)}{(Qr)^3} \tag{3.15}$$

The double Yukawa potential of a particle with radius r at a position r' is

$$\frac{V(r)}{kT} = \begin{cases} \infty & \text{if } r \leq 1 \\ -K_1 \left[\frac{\exp^{-z_1(r-1)}}{r}\right] - K_2 \left[\frac{\exp(-z_2(r-1))}{r}\right] & \text{if } r > 1 \end{cases} \tag{3.16}$$

with z_i as inverse screening length and potential K_i at the surface. For $K > 0$ we have attraction while $K < 0$ means repulsion. Liu *et al.* described the corresponding structure factor $S(Q)$ within the MSA closure (Liu *et al.*, 2005). Data analysis was done using the Python-based tool Jscatter (Biehl, 2019).

3.4.8 Analysis of physicochemical solution properties

All physicochemical solution properties in presence and absence of cosolutes were determined in 50 mM Tris-HCl, pH 7.5 and 0.1 mM EDTA with samples prepared in triplicates ($n = 3$) and at 37 °C, respectively. Density measurements have been performed using a DM450M densiometer (Anton-Paar, Ostfildern-Scharnhausen, Germany). Determining the dynamic and kinematic viscosity of solutions was carried out using a rolling ball viscosimeter Lovis 2000 M (Anton-Paar, Ostfildern-Scharnhausen, Germany), a glass capillary (short) with a diameter of 1.59 mm (uncalibrated), and a steel ball of 1.5 mm diameter in size and 7.69 $\mathrm{g/cm^3}$ in density (Mat no 73109, steel: 1.4125, Anton-Paar, Ostfildern-Scharnhausen, Germany). Prior to measurement, calibration was performed with water (18.2 MΩ) at 20 °C and a maximal variation coefficient of 0.1 %. In terms of pH analyses, samples were incubated for 4 h at 37 °C prior to measurement. pH values were determined using a standard pH meter (FiveEasy, Mettler-Toledo, Gießen, Germany) and glass combination electrode (REF 238140, BioTrode, Hamilton, Bonaduz, Switzerland).

3.5 Results

3.5.1 Impact of cosolutes on DNAzyme activity and stability

To investigate effects of molecular crowding on the 10-23 DNAzyme, we used a variant that cleaves the mRNA of the PrP protein (for sequence see Figure 3.1A, Victor *et al.*, 2018) and simulated crowded conditions *in vitro* using polymer-based cosolutes (PEG and dextran, DasGupta, 2020; Mardoum *et al.*, 2018), the PEG monomer EG as well as the osmolytes betaine and ectoine.

3.5.1.1 Oligonucleotides provide sufficient stability

To ensure sufficient stability of the oligonucleotides in presence of crowding, we performed assays in presence of the maximum cosolute concentration selected in this study, 0.18 g/mL, with subsequent analysis by urea-PAGE (Figure 3.2, S1). All samples that contain the RNA substrate only (T) do not show additional bands besides the uncleaved molecule, which indicates construct stability under the conditions used for this analysis. In samples containing the RNA substrate and DNAzyme (TDz), bands indicate site-specific cleavage without further degradation of the fluorescent cleavage product. Taken together, the results indicate that all tested cosolutes and conditions provide oligonucleotide stability and were considered for further analysis.

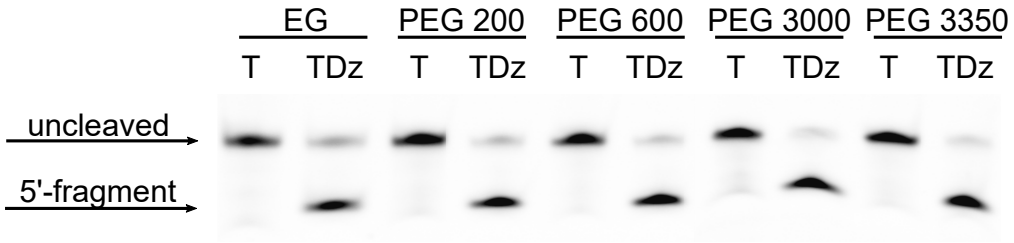

Figure 3.2: Urea-PAGE of samples after stability analysis in presence of 0.18 g/mL of cosolute. Conditions were analyzed in pairs of equally treated samples containing the RNA substrate only (T) and the DNAzyme:RNA complex (TDz). Assays were performed using the T^{FAM} and Dz^{WT} constructs (Table 3.1). Fluorescence detection and visualization of 6-FAM labeled RNA substrates and the 5' cleavage fragment.

3.5.1.2 Crowded conditions alter DNAzyme activity

As a next step, we investigated the effect of a large variety of crowded conditions on DNAzyme activity and performed FRET-based cleavage assays under single-turnover conditions with cosolute concentrations of 0.03, 0.07, 0.11, 0.15 and 0.18 g/mL. Since Dz-mediated cleavage can be performed in presence of different metal ions that demonstrated diverging impact at near physiological conditions in previous studies (0.5 mM M^{2+}, 100 mM NaCl, Rosenbach *et al.*, 2021), assays were performed in presence of Mg^{2+} (Figure 3.3, S2) and Mn^{2+} (Figure S3).

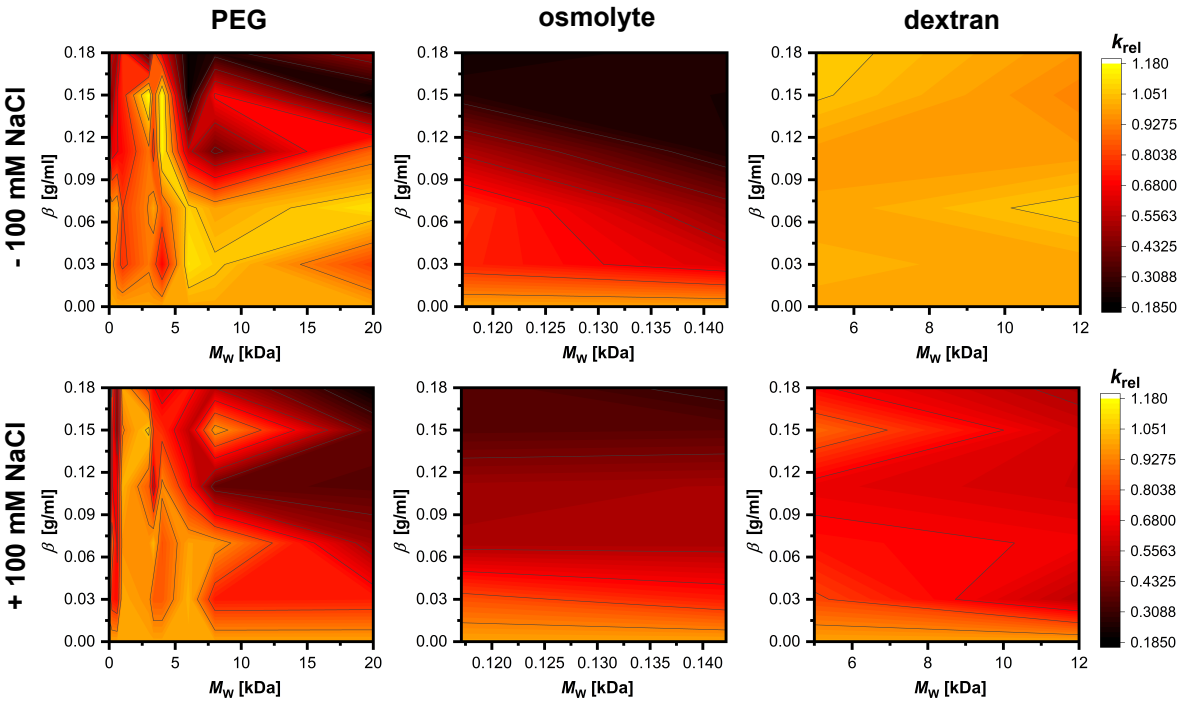

Figure 3.3: Effects of crowded conditions on Dz activity in presence and absence of 100 mM NaCl at 0.5 mM $MgCl_2$. Dz activity was determined in FRET-based cleavage assays in presence of PEG, osmolyte or dextran. Relative rate constants $k_{\mathrm{rel},i}$ (Equation 3.2) are based on determined rate constants $k_{\mathrm{obs},n=14} = (0.0048 \pm 0.0008)\,\mathrm{s}^{-1}$ and $k_{\mathrm{obs},n=14} = (0.0095 \pm 0.0017)\,\mathrm{s}^{-1}$ with and without 100 mM NaCl, respectively.

From the cleavage assays, we are able to observe different impacts on Dz activtiy depending on cosolute type, size, and concentration. In most cases, our data show that increasing cosolute concentrations lead to a decrease in Dz activity. Interestingly, in presence of certain conditions containing PEG and dextran we observe promoting effects on activity ($k_{\mathrm{rel}} > 1.10$). Considering Mg^{2+}-induced cleavage, favoring conditions include PEG variants $< 6\,\mathrm{kDa}$ and concentrations of 0.11 and $0.15\,\mathrm{g/mL}$ in absence of NaCl (Figure 3.3). In presence of NaCl, promoting conditions diverge slightly and include cosolute concentrations of 0.07 and $0.15\,\mathrm{g/mL}$ (Figure S2). Here, however, the extent, to which Dz activity is increased, is less than in absence of NaCl. k_{rel} has its maximum value of 1.07 at $0.07\,\mathrm{g/ml}$ of PEG 3350. In presence of Mn^{2+}, promoting conditions shift to cosolute concentrations $\leq 0.07\,\mathrm{g/mL}$, but appear to be similar for approaches with and without NaCl (Figure S3A, B). In general, PEG variants with $> 6\,\mathrm{kDa}$ result in decreased Dz activity at concentrations $\geq 0.11\,\mathrm{g/mL}$. Crowding simulated by the osmolytes betaine and ectoine result in a concentration-dependent decrease in Dz activity regardless of the respective cofactor, but with greater impact by ectoine (Figure 3.3, S3A). Samples that contain dextran, on the other hand, show maintained or even enhanced activity in absence of NaCl. Promoting effects on activity are only observed in presence of dex 12000 and for Mn^{2+}-induced cleavage at concentrations of 0.07 and $0.15\,\mathrm{g/mL}$ (Figure S3). Addition of NaCl result in fluctuations in activity with an overall greater impact by dex 12000 and in particular for Mg^{2+}-induced catalysis.

3.5.1.3 Cofactor requirement and competition with ATP

Previous studies on ribozymes presented a decrease in cofactor requirement in presence of cosolutes that facilitated catalysis at near physiological concentrations (Paudel *et al.*, 2018; DasGupta *et al.*, 2023). Since low cofactor availability and competition with ATP for free Mg^{2+} are suggested to challenge DNAzyme approaches *in vivo*, we questioned the influence of molecular crowding on the Dz's cofactor requirement (Figure 3.4, S3D) and ability to compete with ATP (Figure S5). Assays were performed in presence of crowded conditions that promoted Dz activity the most. The cofactor requirement was analyzed using FRET-based cleavage assays using $MgCl_2$ and $MnCl_2$ concentrations of $0-5\,\mathrm{mM}$ and $0-0.6\,\mathrm{mM}$, from which we observe that a crowded environment did not evidently change cofactor requirement, at least for the conditions tested here. In absence as well as presence of NaCl, crowded conditions indicate no clear change in requirement for Mg^{2+}. Only presence of $0.15\,\mathrm{g/mL}$ of PEG 4000 demonstrate a slight increase in activity at $MgCl_2$ concentrations $\leq 0.5\,\mathrm{mM}$ compared to the buffer only. With Mn^{2+} as cofactor, presence of cosolutes results in an increase in activity between $0.4-0.6\,\mathrm{mM}$ $MnCl_2$, below, there is no difference compared to the buffer only sample.

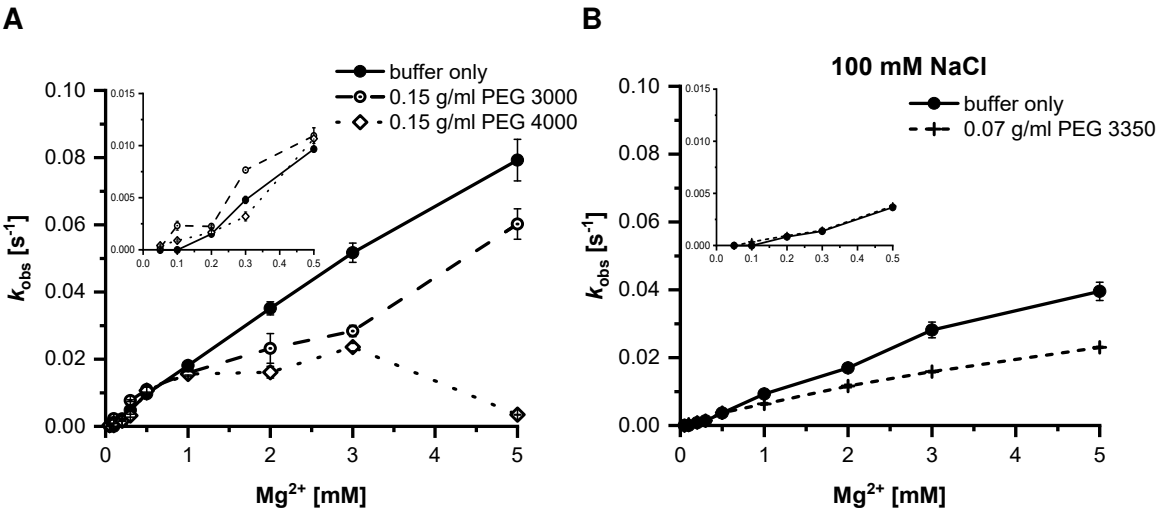

Figure 3.4: Cofactor-dependent rate constants in presence of crowded conditions with most activity enhancing properties: $0.15\,\mathrm{g/mL}$ of PEG 3000 and PEG 4000 in absence (**A**) and $0.07\,\mathrm{g/mL}$ of PEG 3350 in presence of 100 mM NaCl (**B**). Measurements were performed in a range of $0.05-5\,\mathrm{mM}$ $MgCl_2$.

ATP-competition assays revealed an ATP-dependent decrease in Dz activity in absence of crowding (Figure S5), supporting the data published by Victor *et al.* (2018). The same tendency also applies for all selected crowded conditions. Interestingly, Dz activity is less impacted by ATP when a crowded environment is mimicked by larger PEG. Here, activity at $0.18\,\mathrm{g/mL}$ PEG 20000 is hampered less compared to measurements with $0.15\,\mathrm{g/mL}$ PEG 600. Thus, we suggest that the extent of changes in solution properties determines diffusion-dependent binding of Mg^{2+} to either ATP or the Dz:RNA complex.

3.5.1.4 Activity in presence of osmolytes depending on ionic strength

Our data show that increasing concentrations of osmolytes enhance activity impairment. In absence of NaCl and presence of $0.18\,\mathrm{g/mL}$ betaine or ectoine, Dz activity is decreased to $22-26\,\%$ ($0.5\,\mathrm{mM}$ $MgCl_2$) or to $26\,\%$ (betaine) or rather $7\,\%$ (ectoine, $0.5\,\mathrm{mM}$ $MnCl_2$) of

the activity in absence of crowding. Assays in presence of 100 mM NaCl indicate, however, that the extent, to which osmolytes hamper Dz activity, changes (Figure 3.3, S3). Thus, we questioned the effect's dependence on ionic strength. FRET-based cleavage assays were performed in presence of NaCl concentrations ranging from $0-750\,\mathrm{mM}$ (Figure 3.5). To evaluate changes depending on ionic strength, relative rate constants (Equation 3.2) were determined in relation to Dz activity in absence of crowding and NaCl ($k_{\mathrm{obs},\,0}$).

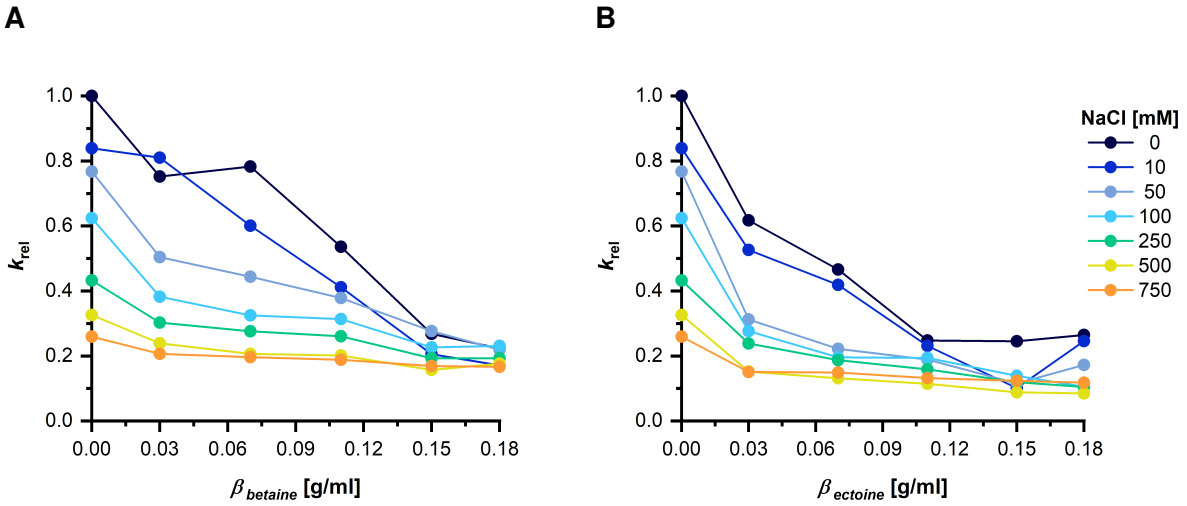

Figure 3.5: Effect of osmolytes on Dz activity depending on ionic strength. Analyses were performed by FRET-based cleavage assays at 0.5 mM $MgCl_2$. Relative Dz activity in presence of different concentrations of betaine (**A**) or ectoine (**B**). k_{rel} was calculated based on $k_{\mathrm{obs},\,0} = 0.009\,58\,\mathrm{s}^{-1}$ for experiments with ectoine and betaine.

Here, elevated levels of monovalent ions seem to lower the concentration-dependent effect of both osmolytes on catalysis. Sole presence of Na^+-ions resulted in a decrease in activity of 75 % at 750 mM NaCl. Assays in presence of betaine (Figure 3.5A) indicated a gradual reduction in Dz activity with increasing NaCl concentration. Only $0.07\,\mathrm{g/mL}$ betaine in absence and $0.03\,\mathrm{g/mL}$ in presence of 10 mM NaCl seem to have less impact. Samples containing ectoine, however, not only resulted in a clear decrease in activity of -40 % at $0.03\,\mathrm{g/mL}$ of ectoine (0 mM NaCl, Figure 3.5B), but also indicated an even greater impact, when NaCl is increased from 10 mM to 50 mM.

3.5.2 Complex size under crowded conditions

So far, we were able to observe that Dz activity is altered in presence of crowded conditions, but without a reduction or change in cofactor requirement. Since crowding studies in general stated altered solution properties as one central cause with thermodynamic and kinetic consequences, we further pursued investigations that target physicochemical solution properties and the Dz:RNA complex's diffusion behaviour and size, of which the latter are intended to help rationalize our observations with structural data.

3.5.2.1 Physicochemical properties of crowded solutions

We determined the physicochemical solution properties in absence of the Dz:RNA complex and aimed at investigating changes within the Dz's environment by crowding. Here, we performed density (Figure 3.6A), viscosity (Figure 3.6B, Table S1), and pH measurements (Figure 3.6C). In the latter, conditions were selected to cover all cosolute types and different degrees of Dz activity. We observed a strong increase in viscosity at high concentrations of large cosolutes, while the density and pH were less affected. Thus, we propose that viscosity-related effects potentially have a greater impact on Dz-mediated cleavage.

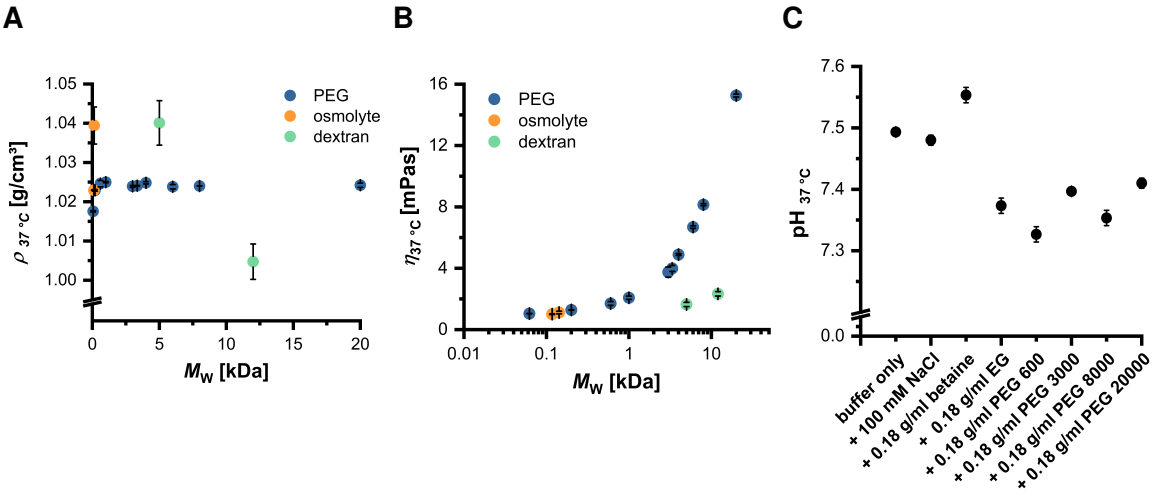

Figure 3.6: Changes in physicochemical solution properties in presence of cosolutes. **A** Density ρ of crowded solutions at 0.18 g/mL of cosolute and 37 °C. $\rho_{\text{buffer only, 37 °C}} = (0.9952 \pm 0.0003)\,\text{g/cm}^3$. **B** Dynamic viscosity η of crowded solutions at 0.18 g/mL of cosolute and 37 °C. $\eta_{\text{buffer only, 37 °C}} = (0.7025 \pm 0.0015)$ mPa·s. **C** pH of crowded solutions at 37 °C. Conditions were selected to cover different degrees of Dz activity.

Density measurements showed a maximum shift of 5 % ($\Delta\rho = 0.045\,\text{g/cm}^3$) at 0.18 g/mL of dex 5000 compared to the buffer only sample ($\rho_{\text{buffer, 37 °C}} = (0.995\,19 \pm 0.000\,32)\,\text{g/cm}^3$ (Figure 3.6A). In contrast, the solution's viscosity changed profoundly with increasing size of cosolute (Figure 3.6B). Here, 0.18 g/mL of PEG 20000 increased the viscosity to the largest extent to (15.2610 ± 0.0929) mPa·s (21-fold) compared to the buffer only sample ($\eta_{\text{buffer, 37 °C}} = (0.7025 \pm 0.0015)$ mPa·s, Figure 3.6B). Measurements of the pH did not result in considerable changes with maximum shifts of $\Delta\text{pH} = -0.17$ (0.18 g/mL PEG 600) and $\Delta\text{pH} = +0.05$ (0.18 g/mL betaine, Figure 3.6C).

3.5.2.2 Cosolute size and concentration limit accessible volume

As an increase in cosolute concentration and size not only affects the viscosity, but also determines the volume available between two cosolute molecules, we calculated the theoretical, average distance between them (cavity size, D) under the assumption of a hard sphere model. With this, we aim at investigating the extent, to which steric influence may impact Dz:RNA complex mobility and size. Determining D requires information on the hydrodynamic radius r_h (Figure S6A, equation 3.6 and 3.7) and radius of gyration r_g (Figure S6B, equation 3.5), which have been calculated based on previous studies (Section 3.4.6). Since PEG is one of the best characterized and most frequently used polymers for crowding analyses, D was determined only for the variants used here (Figure S6C, equation 3.8, 3.9, and 3.10, Table S2). In this study, D was assumed to be 100 nm for the buffer only sample. Borggräfe *et al.* (2021)

published a first structure of the precatalytic Dz:RNA complex using the same Dz, except for one base substitution within the catalytic core, and presented a size of approximately 50 Å in diameter. Taking this into account, D does not reach the proposed complex size for the most tested cosolutes and respective concentrations. However, the size is approximated, which includes D between five and six nm, or even smaller at $\geq 0.11\,\mathrm{g/mL}$ of EG, $0.18\,\mathrm{g/mL}$ of PEG 200, PEG 600, PEG 1000, and PEG 6000, $\geq 0.15\,\mathrm{g/mL}$ of PEG 8000, and $\geq 0.11\,\mathrm{g/mL}$ of PEG 20000. In general, the calculated values of D cover a size range of $\sim 4.4 - 11.2\,\mathrm{nm}$.

Since structural information by NMR spectroscopy did not include a crowded environment, we performed fluorescence correlation spectroscopy (FCS) and small-angle X-ray scattering (SAXS) experiments to obtain and compare new structural insights in presence of cosolutes. Due to a lack of information to calculate D for betaine, ectoine, and dex 12000, we assumed that $D(0.18\,\mathrm{g/mL\ betaine}) = D(0.18\,\mathrm{g/mL\ ectoine}) = D(0.18\,\mathrm{g/mL\ EG})$ and $D(0.18\,\mathrm{g/mL\ dextrane\ 1200}) = D(0.11\,\mathrm{g/mL\ PEG\ 8000})$.

3.5.2.3 Changes in solution properties impact Dz:RNA complex size

Diffusion analyses by FCS were carried out to determine the constructs' diffusion time τ_D (Figure S7, equation 3.3) and consequently the hydrodynamic radius r_h (Figure 3.7, equation 3.4). The data indicate a dependence between r_h and τ_D for T and TDz with cosolute size (Figure 3.7E, S7C), concentration, and eventually associated solution properties η (Figure 3.7D, S7B) and D (Figure 3.7C, S7A).

In absence of crowding, the Dz:RNA complex is slightly smaller than the RNA substrate alone ($r_{\mathrm{h,\,TDz}} = (2.09 \pm 0.37)\,\mathrm{nm}$, $r_{\mathrm{h,\,T}} = (2.50 \pm 0.17)\,\mathrm{nm}$). Here, τ_D of T is $(0.193 \pm 0.025)\,\mathrm{ms}$ and of TDz is $(0.161 \pm 0.029)\,\mathrm{ms}$ (Figure S7). In correlation with cosolute size and concentration, τ_D increases for T and TDz to a similar extent and reaches a maximum at $0.18\,\mathrm{g/mL}$ PEG 20000 ($\tau_{\mathrm{D,\,T}} = (1.380 \pm 0.108)\,\mathrm{ms}$, $\tau_{\mathrm{D,\,TDz}} = (1.429 \pm 0.150)\,\mathrm{ms}$). Under crowded conditions that contain PEG as cosolute, our data do not indicate a direct link between changes in r_h and solution properties such as D (Figure 3.7C) and η (Figure 3.7D), which makes us assume that further environmental factors impact Dz:RNA complex size. On the contrary, presence of betaine and ectoine as well as EG slightly increases $r_{\mathrm{h,\,TDz}}$ to a maximum of $r_{\mathrm{h,\,TDz}} = (2.38 \pm 0.09)\,\mathrm{nm}$ at $0.18\,\mathrm{g/mL}$ of ectoine. Interestingly, of all tested samples, $0.18\,\mathrm{g/mL}$ of dex 12000 ($\eta = 2.33\,\mathrm{mPa{\cdot}s}$) led to the strongest compaction of T and TDz ($r_{\mathrm{h,\,T}} = (0.55 \pm 0.03)\,\mathrm{nm}$, $r_{\mathrm{h,\,TDz}} = (0.54 \pm 0.01)\,\mathrm{nm}$), although Dz activity was not affected significantly ($k_\mathrm{rel} = 0.97$, Figure 3.7A). Even though FCS measurements have been performed in absence of Mg^{2+} or Mn^{2+}, conditions that demonstrated promoting effects on Mg^{2+}-induced Dz activity ($k_\mathrm{rel} > 1.10$, Figure 3.3) resulted in $r_{\mathrm{h,\,TDz}}$ between 1.81 and 2.0 nm (Figure 3.7A, 3.7B). Here, D is 6.51 nm. In presence of NaCl, D of favoring conditions shifts slightly and ranges between 6.51 and 8.41 nm. In contrast, conditions that promoted Dz activity with Mn^{2+} as cofactor ($k_\mathrm{rel} \geq 1.10$, Figure S3) demonstrate a $r_{\mathrm{h,\,TDz}}$ between 2.12 and 2.22 nm and include D of 8.40 and 11.1 nm (Figure S8). In presence of NaCl, $0.03\,\mathrm{g/ml}$ of PEG 4000 as the most promoting condition ($k_\mathrm{rel} = 1.13$) underlines an apparent preference of D of 11.1 nm with Mn^{2+} as cofactor. Overall, the data indicate that a hydrodynamic radius of $\sim 1 - 2.22\,\mathrm{nm}$ applies for different degrees of Dz activity ($k_\mathrm{rel} = 0.4\text{-}1.17$). In this regard, it is interesting that a $r_{\mathrm{h,\,TDz}}$ within a range of $\sim 1.81 - 2.22\,\mathrm{nm}$ can correspond to a $k_\mathrm{rel} < 0.3$ as well as > 1.0 for Mg^{2+} and Mn^{2+}. Additionally, we observe that crowded conditions that cause the Dz:RNA complex to compact and result in $r_{\mathrm{h,\,TDz}}$ of $< 1\,\mathrm{nm}$ restrict activity, which mainly occurs in presence of cosolutes with $M_\mathrm{W} > 5\,\mathrm{kDa}$.

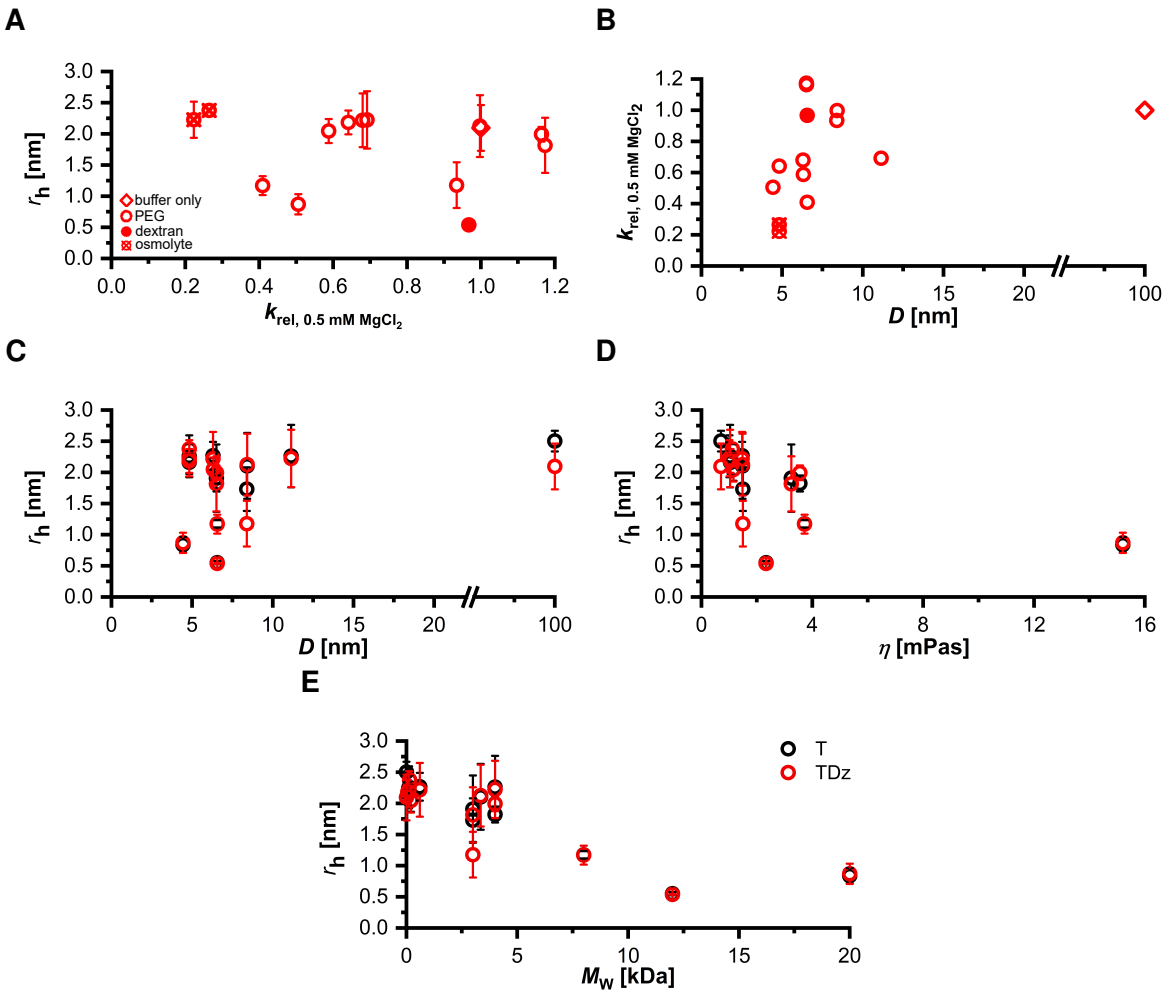

Figure 3.7: Hydrodynamic radius r_h of RNA substrate (T) and Dz:RNA complex (TDz) in absence and presence of cosolutes determined by FCS. **A** r_h[nm] of TDz in comparison to Dz activity as k_{rel} (Equation 3.2) at 0.5 mM $MgCl_2$ ($k_{obs,n=14} = (0.0095 \pm 0.0017)\,s^{-1}$). **B** Dz activity as k_{rel} at 0.5 mM $MgCl_2$ in relation to cavity size D. **C** r_h depending on cavity size D. **D** r_h depending on solution viscosity at 37 °C. **E** r_h depending on M_W of the respective cosolute.

Aiming for additional information on Dz:RNA complex size and shape, we performed SAXS measurements (Figure 3.8). Analyses in presence of $MgCl_2$ were further carried out using the A5C variant (Dz^{A5C}, Table 3.1). Substitution of the catalytic core residue A5 disrupts the palindromic sequence within the catalytic core and prevents homodimer formation (Borggräfe *et al.*, 2021). A comparison of both sequences will indicate whether samples contain complex species differing from the active complex that influence model predictions. We observe an elongated shape for the Dz:RNA complex with only small deviations between samples in absence and presence of crowding. In addition, our data reveal a slightly smaller size for the Dz:RNA complex containing the A5C variant than the wild type DNAzyme (Dz^{WT}).

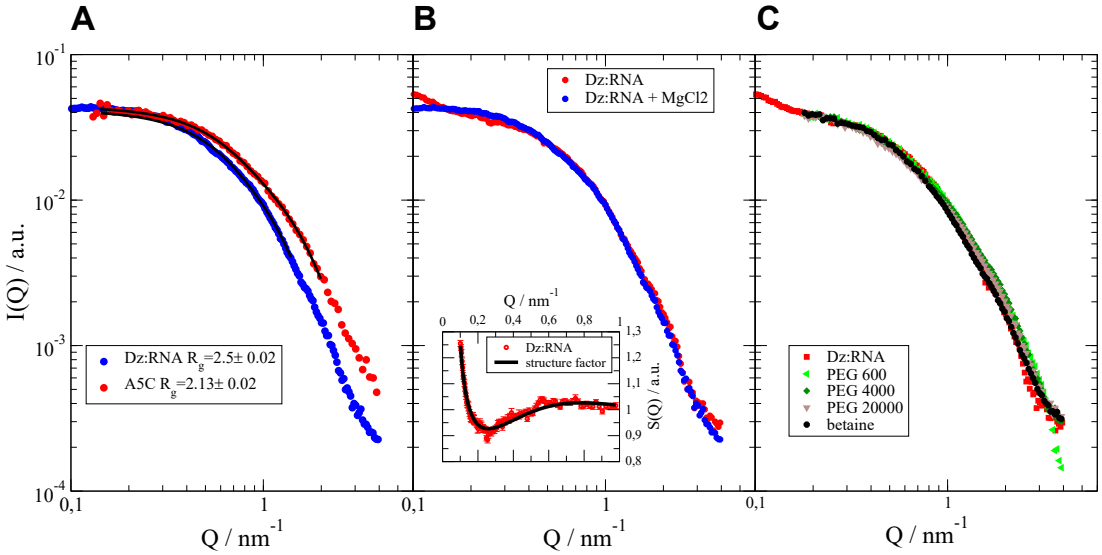

Figure 3.8: SAXS scattering intensities $I(Q)$ in dependence upon scattering vector Q. **A** Comparison of the Dz:RNA complex that either contains the Dz^{WT} (blue) or the Dz^{A5C} variant (red) in presence of 5 mM $MgCl_2$. Black lines show a fit with an ellipsoid of revolution form factor. **B** Comparison of the Dz^{WT}:RNA complex in absence (blue) and presence (red) of 5 mM $MgCl_2$. The inset shows the structure factor responsible for the deviation with and without $MgCl_2$. **C** Comparison of Dz^{WT}:RNA complex in absence (red) and presence of the respective cosolute: 0.15 g/ml of PEG 600 and PEG 4000 as well as 0.18 g/ml of PEG 20000 and betaine. PEG is known to be nearly matched in water that it is not seen in SAXS (Thiyagarajan *et al.*, 1995).

In presence of 5 mM $MgCl_2$, the Dz^{A5C}:RNA complex shows a more compact state ($r_g = 2.1\,\text{nm}$) than the Dz^{WT}-containing construct ($r_g = 2.5\,\text{nm}$, Figure 3.8A). A ratio of $r_g/r_h \approx 1.2$ compared to $r_g/r_h \approx 0.77$ for a solid sphere indicates already an elongated shape. Assuming an ellipsoidal shape, the Perrin friction factor indicates an aspect ratio ~ 5 (Perrin, 1934). Fitting an ellipsoidal formfactor to the scattering data in Figure 3.8A results in half axes $r_a = (5.00 \pm 0.05)\,\text{nm}$, $r_b = (1.08 \pm 0.01)\,\text{nm}$ for the Dz^{A5C}:RNA complex and half axes $r_a = (5.37 \pm 0.05)\,\text{nm}, r_b = (1.49 \pm 0.01)\,\text{nm}$ for the Dz^{WT}:RNA complex, which supports the assumption of an elongated shape. While a diameter of $2r_b$ equals roughly the diameter of DNA with $1.8 - 2.3\,\text{nm}$, the total length of $2r_a$ can only be reached with a strongly stretched configuration of 19 bp. Nevertheless, an elongated structure of the complex can be assumed.

In Figure 3.8B, the Dz^{WT}:RNA complex in absence of $MgCl_2$ presents a deviation from samples with $MgCl_2$, which we observe from a higher scattering intensity $I(Q)$ at lowest scattering vector Q and lower values near $0.2\,\text{nm}^{-1}$. This deviation is characteristic for a structure factor due to interparticle interactions with a short-range attraction and long-range repulsion. The structure factor $S(Q)$ for the Dz^{WT}:RNA complex can be determined using the complex's sample with 5 mM $MgCl_2$ as a formfactor (see Figure 3.8A for comparison) and dividing the measured $I(Q)$ by this formfactor $F(Q)$ according to $I(Q) = S(Q)F(Q)$. The extracted structure factor $S(Q)$ (see inset in Figure 3.8B) shows good agreement with a two Yukawa structure factor with a short range attractive and long-range repulsive component. Exchange of Na^+ at the complex by Mg^{2+} seems to reduce attraction and repulsion. Figure 3.8C compares the scattering patterns of the Dz^{WT}:RNA complex with different cosolutes in the solution. In presence of betaine, the complex shows only a small deviation to the sample without crowding. In presence of PEG, smaller deviations for $Q > 1\,\text{nm}^{-1}$ might indicate that conformational changes are much smaller than the difference between the Dz^{WT}:RNA and Dz^{A5C}:RNA complex in Figure 3.8A.

3.6 Discussion

High specificity, low cost in synthesis, and flexibility in design made DNAzymes as molecular tools gain attention, of which especially RNA-cleaving variants were considered promising to function as gene silencing agents. However, low *in vivo* activity remains a major challenge in cell-based Dz applications, in which effects by molecular crowding have been proposed to contribute (Paudel and Rueda, 2014; Paudel *et al.*, 2018; Victor *et al.*, 2018; DasGupta, 2020; Rosenbach *et al.*, 2021). Studies on ribozymes revealed changes in activity, cofactor requirement, and folding, in which crowding favored their activity at physiological relevant Mg^{2+} concentrations (Nakano *et al.*, 2008) and promoted formation and stabilization of a compact and active conformation (Paudel *et al.*, 2018). Thus, shedding light on possible effects by molecular crowding on the 10-23 DNAzyme is of great relevance for a fundamental understanding of Dz catalysis and for improving Dz by introducing chemical modifications. In this study we focus on functional analyses, changes in physicochemical solution properties, and the structure and shape of the Dz:RNA complex. Crowded conditions were mimicked using different concentrations of polymers PEG and dextran, EG, and osmolytes betaine and ectoine. With this approach we aim at covering different molecule properties and degrees of molecular crowding to achieve conditions that resemble a cell's divers composition.

In comparison to polymers PEG and dextran, our activity assays demonstrate a concentration-dependent impact on Dz activity in presence of betaine and ectoine. The two exhibit zwitterionic properties with strong water binding at neutral pH (Bownik and Stępniewska, 2016; Kurz, 2008). As the presence of both did not significantly change the density (Figure 3.6A), viscosity (Figure 3.6B), and pH (Figure 3.6C), we propose altered water activity as possible cause for activity impairment. Since both molecules are small in size, they are assumed less likely to influence cleavage by volume exclusion. Former *in vitro* studies using betaine revealed destabilization of nucleic acids depending on the GC-content, with preferred accumulation around single-stranded DNA (Hong *et al.*, 2004; Swinefus *et al.*, 2013; Vasudevamurthy *et al.*, 2009). Since the Dz's catalytic core provides unpaired GC nucleotides exposed to the surface, betaine may be able to interact at multiple sites. Similar to its derivative hydroxyectoine, ectoine is suggested to prefer negatively charged surfaces leading, if bound, to strong, unspecific interactions, which occur within the first hydration shell (Meyer *et al.*, 2017; Oprzeska-Zingrebe *et al.*, 2018). Presence of both molecules resulted in a slight increase in r_h for the Dz:RNA complex ($+0.132\,\text{nm}$ at $0.18\,\text{g/mL}$ betaine, $+0.282\,\text{nm}$ at $0.18\,\text{g/mL}$ ectoine; Figure 3.7). This in combination with their interaction potential makes consider complex dehydration and consequently elongation as possible cause. Due to their zwitterionic character and concentration-dependent impact, we questioned the effect's dependence on ionic strength (Figure 3.5). From cleavage assays in presence of different Na^+ concentrations we observe less impact by the two osmolytes at elevated Na^+ levels. As Na^+ ions are proposed to compete with Mg^{2+} for binding sites (Rosenbach *et al.*, 2021), their sole presence is sufficient to diminish Dz activity.

In contrast, our activity assays in presence of PEG and dextran indicate that single crowded conditions promote activity (Figure 3.3), which matches observations in ribozyme-based analyses (Paudel *et al.*, 2018; DasGupta *et al.*, 2023; Paudel and Rueda, 2014). Presence of the monomer EG, on the other hand, led to a concentration-dependent decrease in Dz activity. Previous studies on nucleic acids and ribozymes also assigned osmolytic properties and effects to EG, PEG 200, and PEG 600, by altering water activity (Adams and Znosko, 2019; DasGupta, 2020; DasGupta *et al.*, 2023; Ghosh *et al.*, 2020). Based on our activity measurements,

we assume similar effects for Mg^{2+}- (Figure 3.3) and Mn^{2+}-induced (Figure S2) cleavage. Crowded conditions that promote Dz activity contain PEG variants with $M_W > 1\,kDa$, of which most solutions include PEG 3000 and PEG 4000. However, preferred conditions seem to differ between Mg^{2+}- and Mn^{2+}-induced catalysis. Assays in presence of Mg^{2+} highlight an enhanced activity at $0.11 - 0.15\,g/mL$ of cosolute (Figure 3.3), whereas the range shifts to $0.03 - 0.07\,g/mL$ in presence of Mn^{2+} (Figure S2). But in presence of NaCl, lower cosolute concentrations seem to be beneficial, as $0.07\,g/ml$ of PEG 3350 provided the most promoting surrounding with Mg^{2+} as cofactor and $0.03\,g/ml$ of PEG 4000 with Mn^{2+}. Depending on the respective cofactor, Rosenbach *et al.* (2021) already predicted an altered interplay between ions, which the authors assigned to the metal ion's properties. Our activity data also imply that effects by molecular crowding change depending on the cofactor. Analyses, for example, by Nakano *et al.* (2008) demonstrated a lowered cofactor requirement for the hammerhead ribozyme in presence of crowding. Our activity assays, however, show that even the most promoting crowded conditions did not change the Dz's cofactor requirement (Figure S3, S2). Although ATP competition assays indicate that altered solution properties in presence of larger PEG molecules improve diffusion-dependent Mg^{2+}-binding to Dz, limited cofactor availability remains a considerable *in vivo* challenge (Figure S5).

To elucidate how crowding promotes Dz activity, we first focused on the physicochemical properties density, viscosity, pH, and the theoretical, average distance between cosolutes D (Figure 3.6, S6). Since none of the crowded solutions presented significant changes in pH and density, we suggest that viscosity-related alterations contribute in elevating Dz activity. Here, 'optima' provide similar solution viscosities for one cofactor (Figure 3.6, 3.3, S2). In this regard, the size and concentration of the respective cosolute not only affects the solution's viscosity, but also determines the average distance between two cosolute molecules (Figure S6), thus the volume available to the Dz:RNA complex. This makes structural information necessary to better understand steric influence by volume exclusion, which we addressed using FCS (Figure 3.7) and SAXS (Figure 3.8). From our FCS data we observe that a $r_{h,\,TDz} \sim 1.81 - 2.0\,nm$ in combination with D of $6.50\,nm$ is associated with activity favoring conditions for Mg^{2+}-induced catalysis (Figure 3.7A, 3.7B). In presence of NaCl, preferences in D extend to $8.41\,nm$. For Mn^{2+}-induced RNA cleavage, promoting conditions are associated with $D \sim 8.40 - 11.1\,nm$ and $r_{h,\,TDz} \gtrsim 2.0\,nm$ (Figure S8). Under conditions with NaCl, an 'optimum' cavity size seems to be $11.14\,nm$. In general, conditions that cause the Dz:RNA complex to compress to a $r_{h,\,TDz}$ below $1\,nm$ tend to restrict activity. This accounts for high concentrations of larger PEG molecules ($0.18\,g/mL$ PEG 20000, Figure 3.7E), which we assign to a higher degree of volume exclusion, thus an increased potential of steric repulsion (Dupuis *et al.*, 2014; Sugimoto, 2014; Kilburn *et al.*, 2010). Although we observe that certain combinations of viscosity and D can create a favoring surrounding, our data do not indicate a correlation between physicochemical properties and the corresponding r_h of the Dz:RNA complex. This makes us believe that other environmental factors, for instance osmotic pressure (DasGupta, 2020) or dielectric properties (Nasir and Al Ahmad, 2020; Fiorini *et al.*, 2015), also impact the DNAzyme, which should be evaluated. In addition, since we see that one $r_{h,\,TDz}$ can account for different degrees in Dz activity, we propose that Dz:RNA complex structure is impacted less by molecular crowding. This is also supported by the SAXS data, which indicated only small deviations in the Dz:RNA complex in presence of crowded conditions (Figure 3.8). Besides, the results show that interparticle interactions for the Dz:RNA complex change in presence of $MgCl_2$. The published data by Borggräfe *et al.* (2021) revealed that after binding of monovalent ions to the complex, its saturation with Mg^{2+} is required to achieve structural arrangements that result in the active conformation. Taken both observations

into account, this raises the question how the complex behaves structurally under crowded conditions in a cofactor-bound state, as FCS measurements were performed in absence of Mg^{2+} and Mn^{2+}.

For the first time we show that also the activity of the Dz is impacted in presence of a more cell-like surrounding, which is indicated to be dependent on the cosolute's properties and correlates with a previous study on the 8-17 DNAzyme variant 17E by Nakano *et al.* (2017). In addition, we provide first information on structural changes of the Dz:RNA complex under crowded conditions and highlight that cosolute concentration is one critical factor for Dz activity. To the best of our knowledge, this has not been shown for the Dz in presence of the selected cosolutes yet. The mentioned study by Nakano *et al.* (2017) supports the significance of cofactor concentration. By testing 10, 20 and 30 % of PEG 200, PEG 8000, and EtOH on DNAzyme activity and stability, they were able to observe that the extent, to which both are altered depends on the cosolute concentration. Here, catalytic activity and DNA stability presented a high level of correlation (Nakano *et al.*, 2017). In this study, we point out that few crowded conditions are able to promote Dz activity that we assume achieve a catalytically relevant degree of structural adaption of the Dz:RNA complex, although indicated as minor according to the FCS and SAXS data. But since FCS measurements were performed in absence of cofactor, further analysis is required to resolve structural influences by crowding. Despite, when we aim to connect Dz:RNA complex size to promoting conditions in Mg^{2+}- or Mn^{2+}-induced cleavage, $r_{h,\,TDZ}$ tendencies slightly differ between the two metal ions. Since both ions presented different interplays with monovalent ions during catalysis (Rosenbach *et al.*, 2021), this raises the question of cofactor-dependent conformational differences between Dz:RNA complexes that would explain variations in the preference of crowded conditions that needs to be evaluated further.

Based on our data, we refer to observations by Paudel *et al.* (2018) and also propose that the cavity size mediated by crowding influences Dz efficiency. But we have to note, that D calculations include a correction factor, whose underlying concept needs to be reviewed for the rest of the PEG variants in this study. Since cavity size distribution here is assumed homogeneous, but is most likely heterogeneous, given the molecular diversity in cells, this further questions whether the impact on Dz activity changes in a heterogeneous environment. Assays in this study were performed with pre-formed complexes under single-turnover. Although we suggest that the above mentioned alterations in complex size and solution properties will negatively impact complex association and dissociation under multiple turnover, validation is required. Our FCS data did not show notable differences between T and TDz under crowded conditions (Figure 3.7, S7). At this point, this leaves us to speculate that the RNA substrate and Dz:RNA complex are affected to a similar extent, despite size differences and estimated volume occupancy. Since FCS analyses have been performed based on the fluorescence of the single-labeled RNA substrate, further investigations are required to exclude multiple species in TDz samples. Despite first structural insights in this study, high resolution structural data is mandatory that would provide important insights into the reaction mechanism and contribute to a better understanding of conformational changes within the Dz:RNA complex that result from interactions with the respective cosolute. In this regard, possible rearrangements of catalytically relevant residues within the catalytic core are of great interest. Moreover, detailed structural data will also help understand the observed differences between Mg^{2+}- and Mn^{2+}-based approaches.

3.7 Acknowledgements

We thank apl. Prof. Dr. M. Schmitt from the Institute for Physical Chemistry I at Heinrich-Heine-Universität Düsseldorf for providing access to the densiometer to perform density analyses. We would also like to acknowledge the Center for Advanced Imaging (CAi) at Heinrich-Heine-Universität Düsseldorf for providing access to the facilities' microscope and especially apl. Prof. Dr. S. Weidtkamp-Peters for the assist and support with setting up the FCS experiments. Funding for instrumentation: Olympus FV3000 Confocal Laserscanning Microscope: DFG- INST 1358/44-1 FUGB.

3.8 Supporting data

3.8.1 Supporting figures

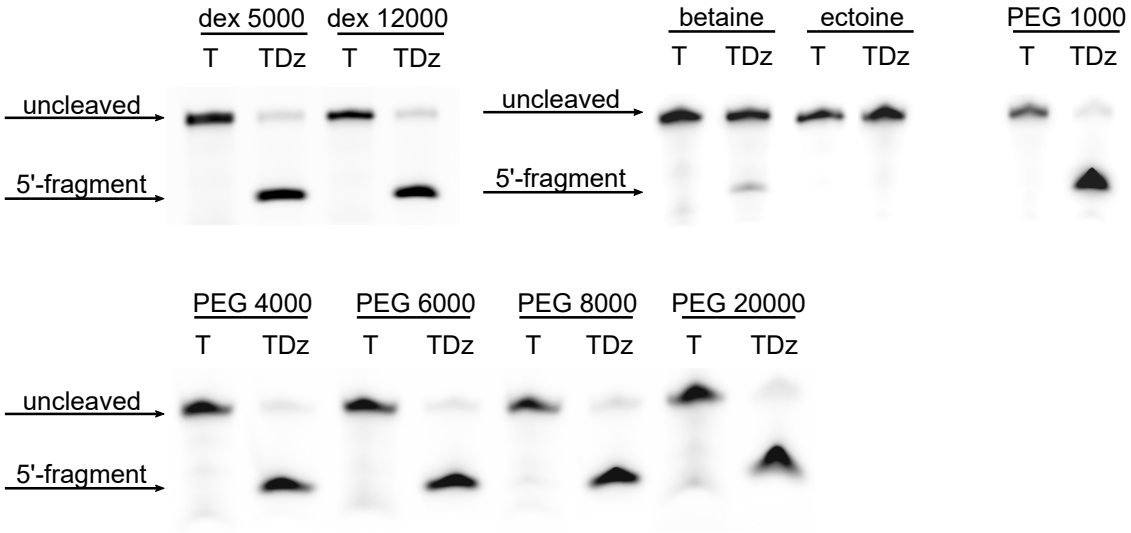

Figure S1: Urea-PAGE of samples after stability analysis in presence of 0.18 g/mL of the remaining cosolutes. Conditions were analyzed in pairs of equally treated samples containing the RNA substrate only (T) and the DNAzyme:RNA complex (TDz). Assays were performed using the T^{FAM} and Dz^{WT} constructs (Table 3.1). Fluorescence detection and visualization of 6-FAM labeled RNA substrates and the 5' cleavage fragment.

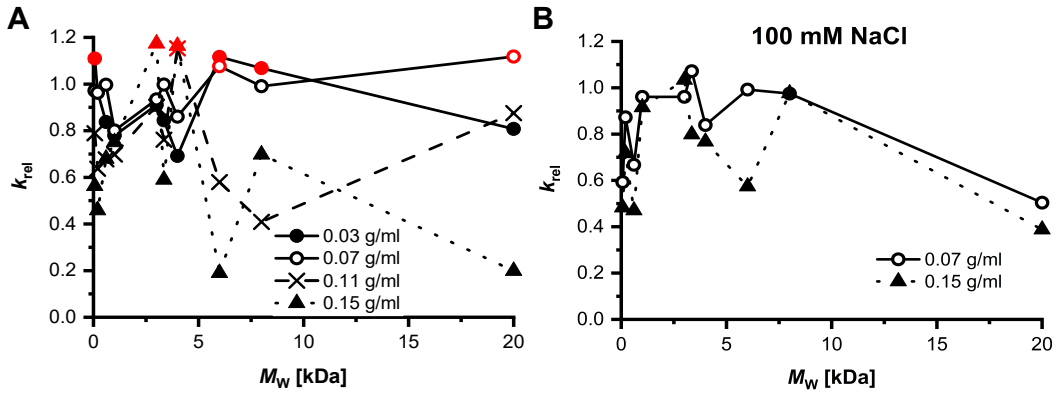

Figure S2: Selection of cosolute concentrations that included conditions with promoting properties on Dz activity at 0.5 mM $MgCl_2$. **A** k_{rel} of respective concentrations of PEG variants in absence of NaCl. Promoting conditions with $k_{rel} \geq 1.10$ are marked in red (•). **B** k_{rel} for 0.07 and 0.15 g/mL of PEG variants in presence of 100 mM NaCl. Promoting conditions include 0.07 g/ml of PEG 3350 ($k_{rel} = 1.07$) and 0.15 g/ml of PEG 3000 ($k_{rel} = 1.03$).

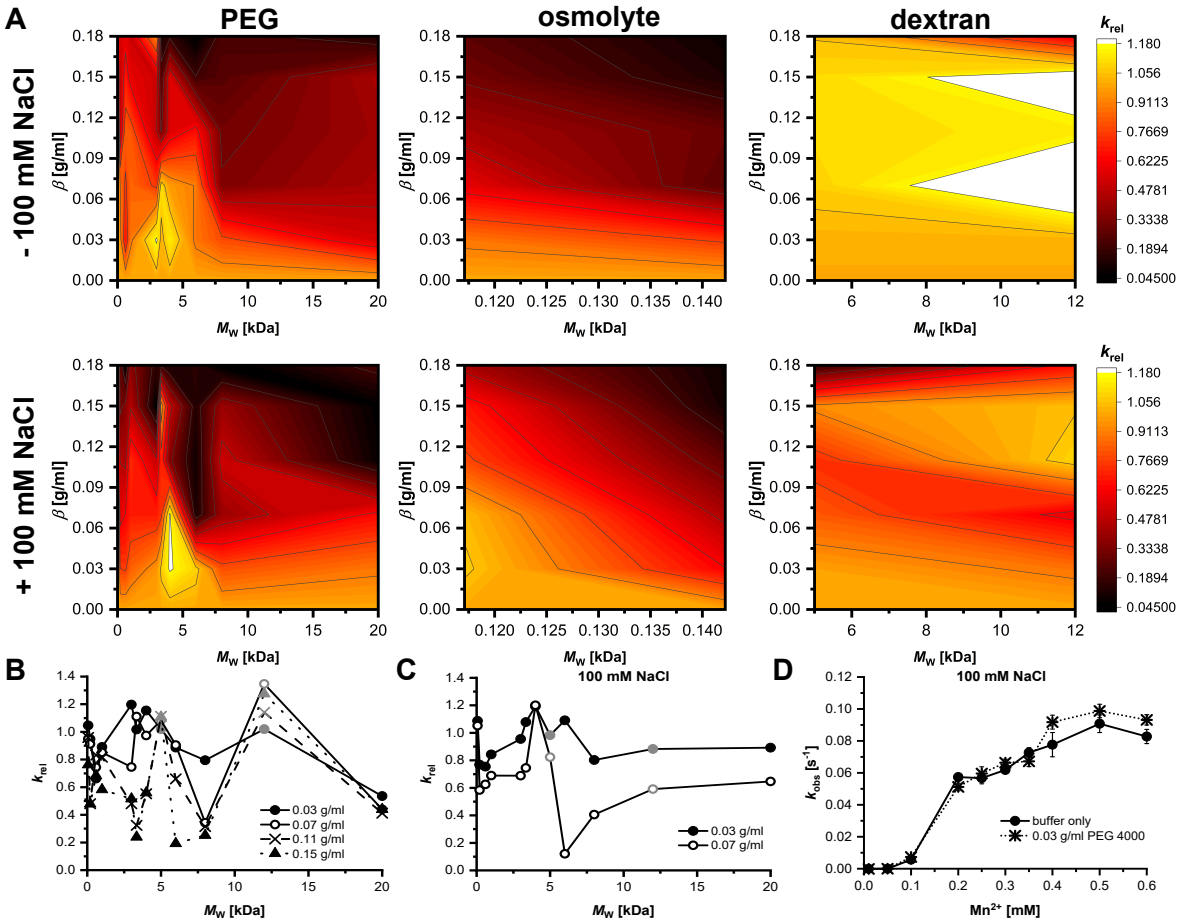

Figure S3: Effects of crowded conditions on Dz activity in presence and absence of 100 mM NaCl at 0.5 mM $MnCl_2$. Dz activity was determined in FRET-based cleavage assays. **A** Relative activity in presence of either PEG, osmolytes betaine and ectoine or dextran. Relative rate constants k_{rel} (Equation 3.2) are based on determined rate constants $k_{obs,n=14} = (0.1050 \pm 0.0299)\,s^{-1}$ and $k_{obs,n=14} = (0.0459 \pm 0.0076)\,s^{-1}$ with and without 100 mM NaCl, respectively. **B** k_{rel} for different concentrations of PEG and dextran in absence of NaCl that include promoting conditions on Dz activity. Samples containing dextran are highlighted in grey (•). Conditions that enhanced Dz activity ($k_{rel} > 1.10$) include: 0.03 g/mL PEG 3000, PEG 3350, and PEG 4000; 0.07 g/mL PEG 3350 and dextran 12000; 0.11 and 0.15 g/mL dextran 5000 and 12000. **C** k_{rel} for different concentration of PEG and dextran variants in presence of 100 mM NaCl. Samples containing dextran are highlighted in grey (•). Conditions that that enhance Dz activity ($k_{rel} > 1.10$) include: 0.03 and 0.07 g/mL PEG 4000. **D** Dz activity as $k_{obs}[s^{-1}]$ in absence of crowder (buffer only) and presence of 0.03 g/mL of PEG 4000 (most promoting condition, $k_{rel} = 1.13$) at $MnCl_2$ concentrations $0.01 - 0.6$ mM and 100 mM NaCl.

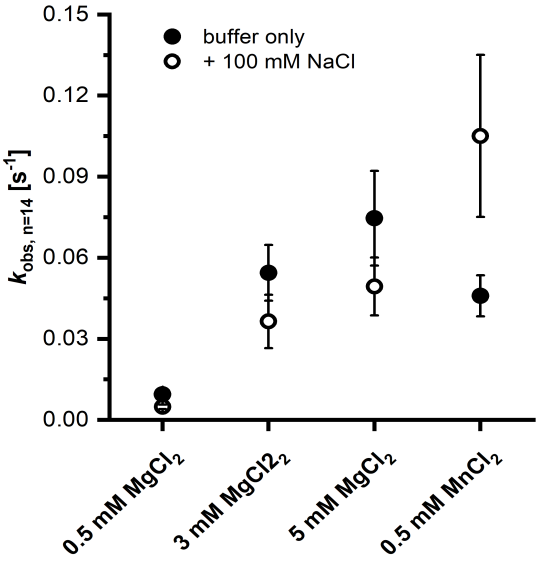

Figure S4: Dz activity depending on M^{2+} concentration. Mean values of $k_{obs}[s^{-1}]$ for Dz activity in buffer only with and without 100 mM NaCl. Mean values were calculated based on $n = 14$ samples, respectively.

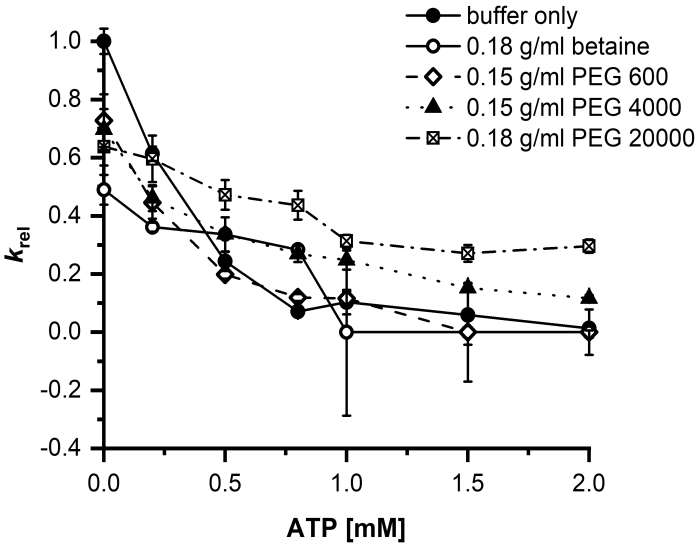

Figure S5: Dz activity in presence of crowding and competition with ATP at 0.5 mM $MgCl_2$ and 100 mM NaCl. Rate constants (k_{obs}) were put into relation to the activity in absence of cosolute and ATP (k_{rel}, equation 3.2) with 100 mM NaCl ($k_{obs,\ n=3} = (0.0035 \pm 0.0001)\,s^{-1}$).

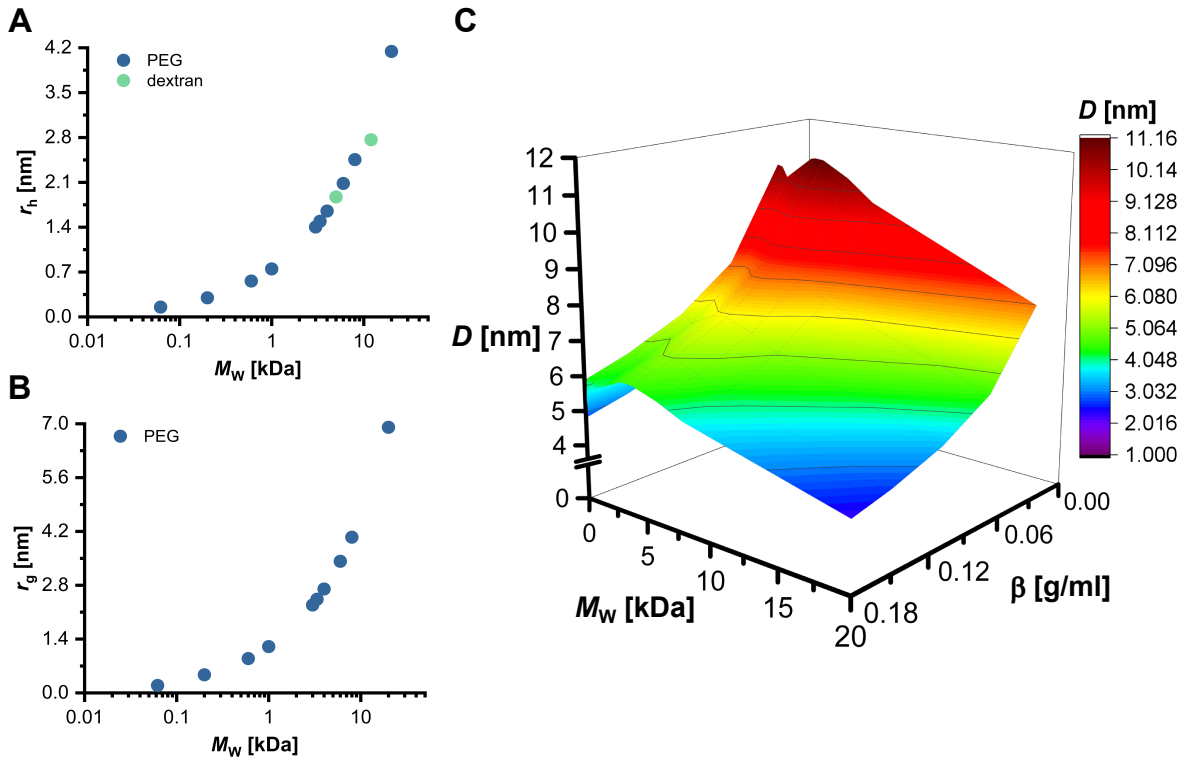

Figure S6: Hydrodynamic radius (r_h, **A**), radius of gyration (r_g, **B**), and theoretical, average distance between cosolutes (D, **C**) depending on M_W and concentration. **A** r_h were calculated based on equations 3.6 and 3.7. **B** r_g of PEG were calculated based on equation 3.5. **C** D between PEG molecules in solution was calculated based on the r_g and under the assumption of a hard sphere model (Equation 3.9, 3.8, and 3.10). D in buffer only is assumed to be 100 nm.

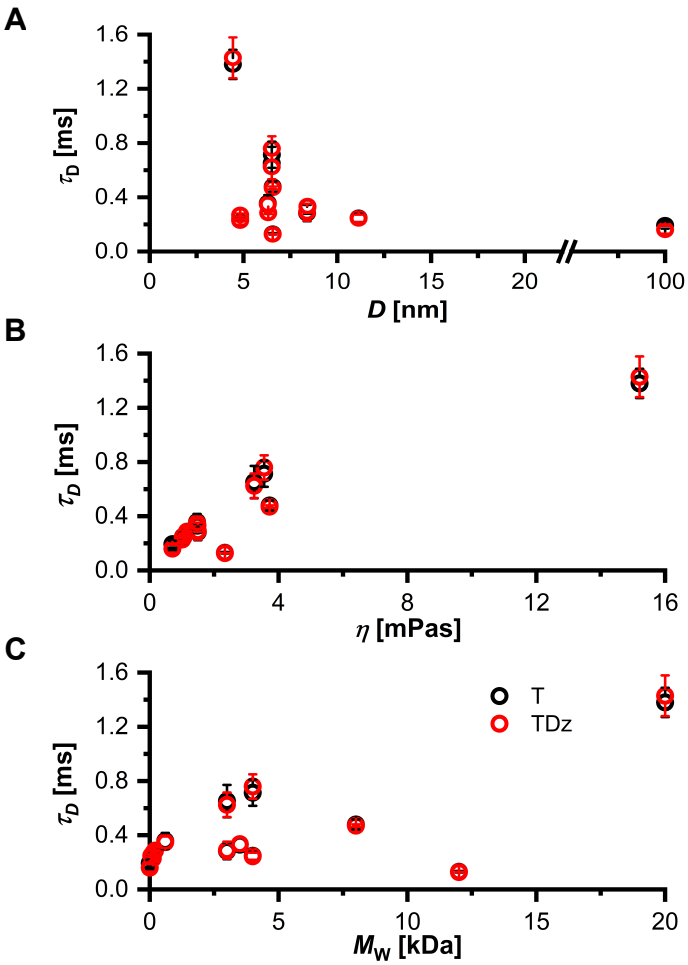

Figure S7: Diffusion time τ_D of RNA substrate (T) and Dz:RNA complex (TDz) in absence and presence of cosolutes determined by FCS. **A** τ_D depending on cavity size D. **B** τ_D depending on the viscosity of crowded solutions determined at 37 °C. **C** τ_D depending on M_W of the respective cosolute.

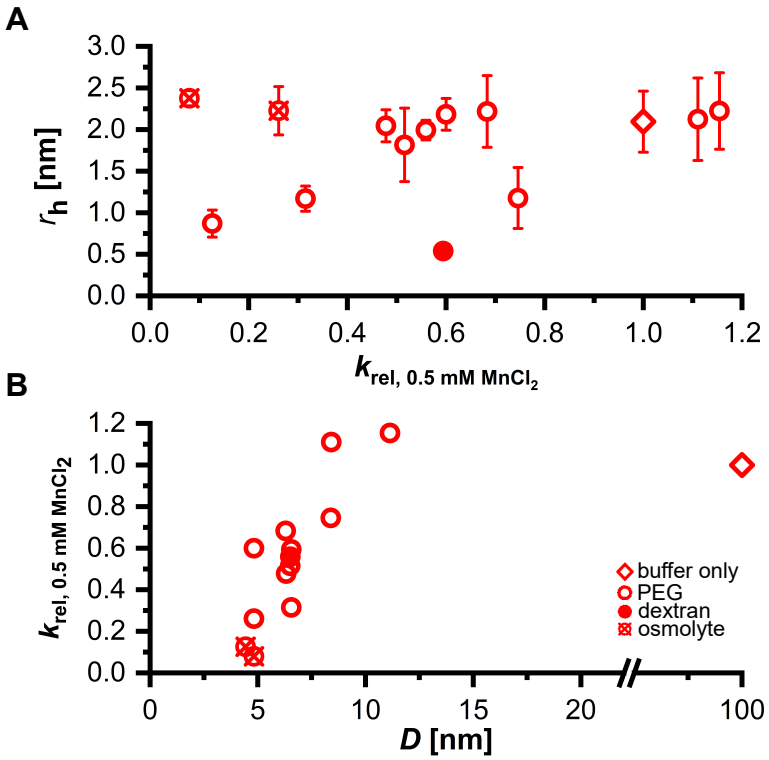

Figure S8: Comparison of the Dz:RNA complex's hydrodynamic radius r_h, D, and relative Dz activity for Mn^{2+}-induced RNA cleavage. **A** r_h[nm] of TDz in comparison to k_{rel} at 0.5 mM $MnCl_2$. **B** k_{rel} at 0.5 mM $MnCl_2$ depending on cavity size D.

3.8.2 Supporting tables

Table S1: Density ρ and dynamic viscosity η at 37 °C of additional samples used in FCS measurements with cosolute concentrations less than 0.18 g/mL.

Sample	$\rho_{37\,°C}$ [g/cm^3]	$\eta_{37\,°C}$ [mPas]
PEG 200, 0.15 g/mL	1.0181 ± 0.00003	1.1553 ± 0.00262
PEG 600, 0.15 g/mL	1.0199 ± 0.00075	1.4672 ± 0.08475
PEG 3000, 0.07 g/mL	1.0061 ± 0.00002	1.4940 ± 0.00535
PEG 3000, 0.15 g/mL	1.0191 ± 0.00008	3.2453 ± 0.00094
PEG 3350, 0.07 g/mL	1.0063 ± 0.00005	1.4797 ± 0.01674
PEG 4000, 0.03 g/mL	1.0004 ± 0.00016	1.0320 ± 0.00216
PEG 4000, 0.15 g/mL	1.0197 ± 0.00017	3.5538 ± 0.26721
PEG 8000, 0.11 g/mL	1.0125 ± 0.00058	3.7220 ± 0.05645

Table S2: D of all used PEG variants at a concentration range of $0.03 - 0.18$ g/mL.

$M_{W,\,PEG}$ [kDa]	D [nm]				
	0.03 g/mL	0.07 g/mL	0.11 g/mL	0.15 g/mL	0.18 g/mL
0.062	8.764	6.607	5.683	5.125	4.823
0.2	10.81	8.147	7.007	6.319	5.947
0.6	10.76	8.115	6.980	6.295	5.923
1	10.47	7.895	6.791	6.124	5.763
3	11.13	8.389	7.216	6.507	6.123
3.35	11.16	8.413	7.237	6.526	6.141
4	11.14	8.398	7.224	6.514	6.130
6	10.71	8.078	6.949	6.266	5.897
8	10.11	7.622	6.556	5.912	5.564
20	8.056	6.074	5.225	4.711	4.434

4

EXTENDING CROWDING *in vitro*

This chapter reflects content of the following manuscript.

4.1 Manuscript information

Nina Kirchgässler and Ingrid Span

In preparation

4.2 Abstract

For approximately four decades, investigations on effects on biomolecules and thermodynamics mediated by the cell's environment have gained increasing attention. In recent years, RNA-cleaving DNAzymes have attracted interest in the field of nucleic acid therapeutics, but their insufficient *in vivo* activity led to a search for possible causes within cellular systems. Although *in vitro* simulations of such conditions by using synthetic or natural cosolutes have been the standard approach so far, cellular relevance is reviewed. Here, we compare experimental set ups with analyses focussing on DNAzymes and discuss future alternatives.

4.3 Introduction

In the early 1980s, introducing effects on a macromolecule's thermodynamics mediated by volume exclusion gained a lot of attention (Minton, 1981). Since conditions in physiological probes are far from those in diluted solutions, the environmental impact, for instance, on equilibria, kinetics, solution properties, and interactions has been questioned (Zimmerman and Minton, 1993). Over the years, the investigation of such conditions evolved into a growing research field and 'macromolecular crowding', 'macromolecular confinement', and 'macromolecular adsorption' became essential terms (Minton, 1981; Zimmerman and Minton, 1993; Minton, 1992; Gnutt and Ebbinghaus, 2016; Rivas and Minton, 2016; Minton, 2006; Zhou *et al.*, 2008). As analyses in cells are hampered by their complexity, experimental approaches aim at designing simplified cell conditions and mimic them *in vitro* using artificial or natural cosolutes (Murade and Shubeita, 2019; Fiorini *et al.*, 2015; DasGupta, 2020; Kuznetsova *et al.*, 2014; Nakano *et al.*, 2014b).

For the past decades, crowding studies have been performed on proteins (Cino *et al.*, 2012; Ellis and Minton, 2006; Cheung *et al.*, 2005; Minh *et al.*, 2006; Kuznetsova *et al.*, 2014; Sasaki *et al.*, 2007; Christiansen *et al.*, 2013; Zhou, 2008a) and nucleic acids (DNA and RNA, Nakano *et al.*, 2004, 2014b; Kurz, 2008; Yu *et al.*, 2016; Tateishi-Karimata *et al.*, 2013; Sugimoto, 2014; Singh and Singh, 2016), including members with catalytic activity, so called biocatalysts. Protein-based catalysts are generally referred to as enzymes (Figure 4.1A) and RNA- or DNA-based biomolecules are called ribozymes (Figure 4.1B, Walter and Engelke, 2002; Desai *et al.*, 2014; Paudel and Rueda, 2014; Nakano *et al.*, 2008; Paudel *et al.*, 2018; DasGupta, 2020; DasGupta *et al.*, 2023) or DNAzymes (Figure 4.1C, Gao *et al.*, 2015; Wang *et al.*, 2023; Rudeejaroonrung *et al.*, 2020). Analyses showed different changes in thermal stability, folding, and catalytic activity depending on the biomolecule and cosolute type, size, and concentration used.

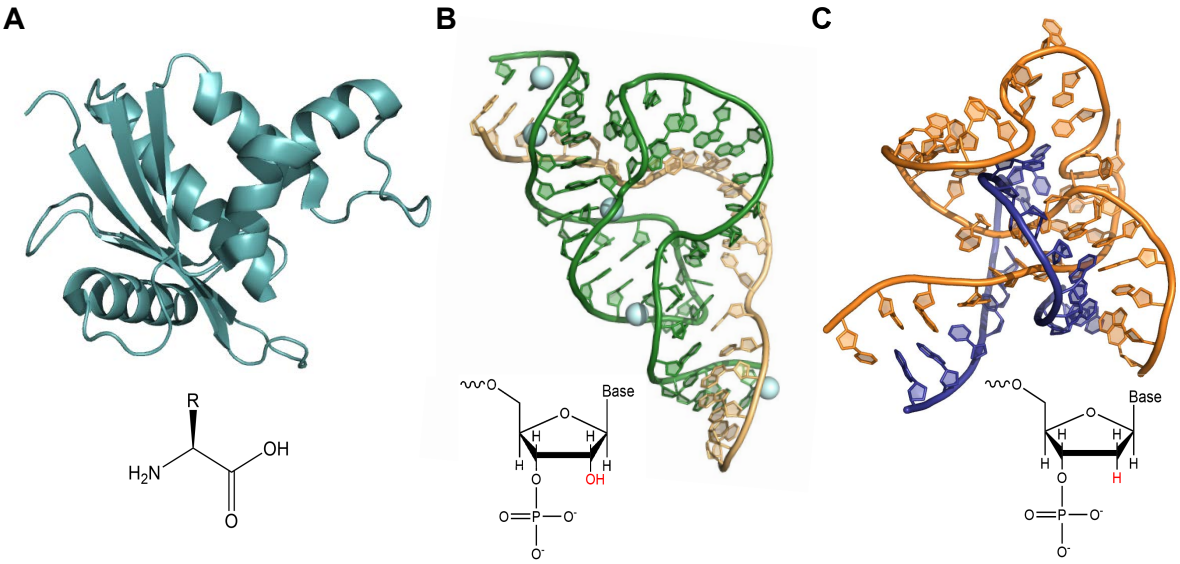

Figure 4.1: Comparison of architecture and composition of biocatalysts. Illustration of the tertiary structure (top) and the chemical structure of the respective building block (bottom). **A** Tertiary structure of the enzyme RNase H (PDB 6VRD). Secondary structure elements such as α-helices and β-sheets (arrows) are highlighted. The enzyme consists of a polypeptide chain with amino acids as building blocks. Each amino acid is characterized by its unique side chain (R). **B** Three-dimensional (3D) structure of the hammerhead ribozyme (green) in complex with an RNA substrate (beige) (PDB 2OEU). The single-stranded RNA sequence of the ribozyme adopts a catalytically active conformation upon binding of a complementary RNA substrate. The complex is stabilized by metal ions, here Mn(II) (lightblue spheres). Ribozyme and RNA substrate consist out of ribonucleotides. **C** 3D structure of the RNA-cleaving 10-23 DNAzyme (orange) in a pre-catalytic complex conformation with a complementary RNA substrate (blue) (PDB 7PDU). The complex is a DNA:RNA hybrid, in which the DNAzyme consists of deoxyribonucleotides, which are missing the 2' hydroxyl group (2'-OH) at the ribose moiety.

DNAzymes and especially RNA-cleaving variants (Figure 4.1C) are on the rise being an attractive alternative to present nucleic acid therapeutics, but face poor *in vivo* activity as a profound challenge (Larcher *et al.*, 2023; Thomas *et al.*, 2021; Xiao *et al.*, 2023; Silverman, 2016). Hence, questions were directed towards the potential contribution of the cell's environment to low *in vivo* success (Zhang, 2018; Etzkorn and Span, 2023; Victor *et al.*, 2018; Rosenbach *et al.*, 2020b, 2021). Even though *in vitro* studies have been the main approach so far, voices review their cellular relevance. In this perspective, we briefly introduce RNA-cleaving DNAzymes, summarize and discuss, which experimental set ups and cosolutes have been used to mimic *in vivo* conditions with focus on recent insights on DNAzymes, and finally outline possible adjustments and alternatives for prospective *in vitro* approaches.

4.4 Nucleic acid catalysts

In nature, the main role of DNA and RNA is the storage and/or transfer of genetic information, whereby RNA as a non-coding molecule also plays a key role in the regulation of gene expression (Minchin and Lodge, 2019). For the first time, in 1981, Cech *et al.* introduced catalytic RNA molecules, better known as ribozymes, that acquire catalytic activity after adopting a 3D structure (Cech *et al.*, 1981; Kruger *et al.*, 1982). Today, various ribozymes in size and shape are known with central functions in, e. g. protein synthesis, intron splicing or mRNA regulation (Westhof and Lescoute, 2008; Walter and Engelke, 2002; Serganov and Patel, 2007; Müller *et al.*, 2016). Due to similarities in chemical composition between

DNA and RNA (Figure 4.1B, C), the existence of DNA catalysts was questioned. To this day, however, catalytically active DNA molecules have not been found in nature (Sednev *et al.*, 2022).

In 1994, Breaker and Joyce presented the first DNA catalyst, better known as DNAzyme, using *in vitro* selection methodology (Breaker and Joyce, 1994). Since then, the number of DNAzymes and their reaction scope increased significantly (Silverman, 2016; Morrison *et al.*, 2018; Hollenstein, 2015; Ma and Liu, 2020). Due to advantages, such as low cost in synthesis, high specificity, and almost limitless design (Nguyen *et al.*, 2023), especially RNA-cleaving DNAzymes gained a lot of attention to function as gene silencing agents (Thomas *et al.*, 2021). These DNAzymes catalyze the site-specific cleavage of a phosphodiester bond via a proposed general acid-base mechanism depending on divalent metal ions (M^{2+}, e. g. Mg^{2+} and Mn^{2+}) similar to the hammerhead ribozyme (Borggräfe *et al.*, 2021, 2023; Cepeda-Plaza and Peracchi, 2020; Cortés-Guajardo *et al.*, 2021). The two most extensively studied variants are the 8-17 and 10-23 DNAzyme, named after the respective selection round and clone number from which they derive (Silverman, 2016; Santoro and Joyce, 1997).

However, low *in vivo* compared to high *in vitro* performance is still a major challenge for their success in cells. For the past years, scientists focused on identifying and testing modification strategies on DNAzymes to improve limitations such as biostability and requirement of metal ions (Etzkorn and Span, 2023; Huang and Liu, 2020; Wang *et al.*, 2021; Gerber *et al.*, 2022; Taylor *et al.*, 2022; Nguyen *et al.*, 2023), but very little is known about how a cell's environment impacts their activity.

4.5 Molecular Crowding - inside a cell

In general, *in vitro* analyses are performed in highly diluted solutions with experimental parameters under strict control (Foffi *et al.*, 2013). On the contrary, $5-40\,\%$ of the cellular volume is occupied by a diversity of macromolecules such as proteins, nucleic acids, lipids, and metabolites ($50-400\,\mathrm{g/L}$) creating a heterogeneous and densely packed surrounding (Ellis and Minton, 2003; Feig *et al.*, 2017; Miyoshi and Sugimoto, 2008, Figure 4.2). Besides, each compartment differs in density and composition, which generates highly organized micro-environments with different sets of specific and non-specific interactions likely to impact biochemical equilibria, kinetics, and isomerizations (Minton, 2006; Zhou *et al.*, 2008; Model *et al.*, 2021; Murade and Shubeita, 2019). But since cells undergo continuous cell cycles and adapt towards external or internal stimuli, in which cell dry mass and volume change differently, each micro-environment is dynamic (Model *et al.*, 2021; Mir *et al.*, 2011; Tzur *et al.*, 2009; Gnutt and Ebbinghaus, 2016). Hence, already small changes in cell volume hugely effect the spatial distribution of molecules, the compartment's physiochemical properties, and eventually thermodynamics. Important physical and chemical properties of a macromolecule's surrounding are, for instance the dielectric constant, osmotic pressure, density, viscosity, and water activity (Nakano *et al.*, 2017; Nakano and Sugimoto, 2017; Ghosh *et al.*, 2020; Nakano *et al.*, 2012; Adams and Znosko, 2019).

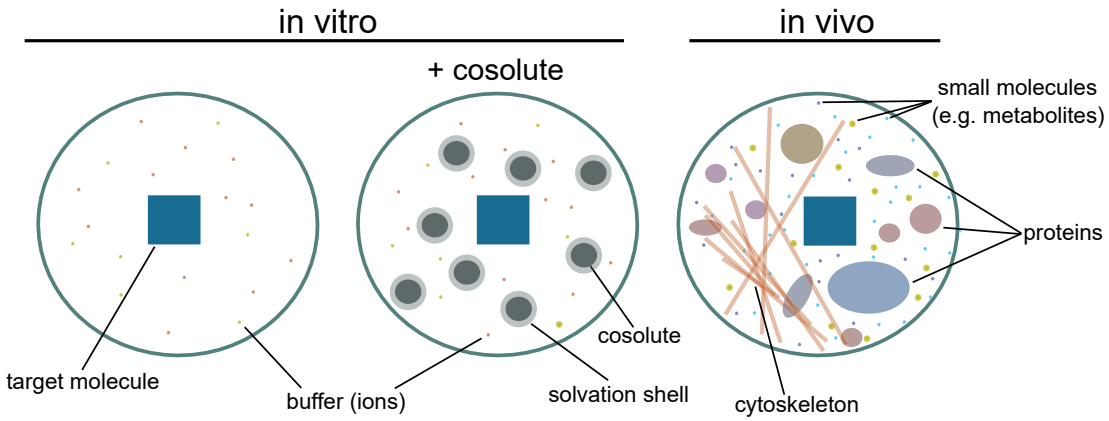

Figure 4.2: Simplified illustration of diluted conditions in absence and presence of cosolutes *in vitro* in comparison to a cellular environment (*in vivo*).

As a result of non-specific interactions, three phenomena can be summarized by the term 'molecular crowding' (MC, used here as an umbrella term): 'macromolecular crowding', 'macromolecular confinement', and 'macromolecular adsorption' (Minton, 2006; Zhou *et al.*, 2008; Zimmerman and Minton, 1993). Firstly, 'macromolecular crowding' is associated with effects resulting from volume exclusion by soluble macromolecules. In crowded solutions that contain high total volume fractions of molecules, each molecule occupies a specific volume, which is size- and shape-dependent and is no longer available to others (volume exclusion). This introduces the most universal non-specific interaction of steric repulsion (Minton, 2006; Zhou *et al.*, 2008; Rivas and Minton, 2016). Secondly, 'macromolecular confinement' summarizes effects on the chemical potential, free energy, and reactivity of a soluble macromolecule enclosed in a 'cavity' mediated by volume exclusion. In cells, such interstitial spaces result from immobile or confining structures such as membranes or the cytoskeleton in the cytoplasm (Minton, 2006, 1992; Zhou *et al.*, 2008). Lastly, 'macromolecular adsorption' describes the event of non-specific adsorption of a molecule to a surface, when its net charge is opposite to the cell structure in close proximity (Minton, 2006).

All mentioned phenomena not only induce steric effects, but also other non-specific interactions such as electrostatic interactions (repulsion or attraction) or hydrophobic interactions (DasGupta, 2020; Zhou *et al.*, 2008; Sugimoto, 2014; Nakano *et al.*, 2014b).

4.6 Mimicking crowded conditions *in vitro*

Considering a cell's interior, scientists aim at mimicking crowded conditions *in vitro* to provide a more cell-like surrounding. To this day, the most common cosolutes (Figure 4.3) are synthetic polymers such as polyethylene glycol (PEG), its monomer ethylene glycol (EG, Tyrrell *et al.*, 2015; Sasaki *et al.*, 2007; Nakano *et al.*, 2017; Nakano and Sugimoto, 2017; Paudel *et al.*, 2018), and branched polysaccharides such as dextran (Wang *et al.*, 2023; Nakano *et al.*, 2009) and their derivatives (e. g. Ficoll, Nakano *et al.*, 2012). The term cosolute describes a solute that exists in a solution together with another one. As PEG, dextran, and Ficoll are commercially available in various molecular weights, different degrees of MC can be mimicked easily. Besides, also compatible solutes, for instance alcohols (e. g. sorbitol, glycerol), amines (e. g. trimethylamine-*N*-oxide (TMAO)), amino acids, and their derivatives become more frequent in studies (DasGupta, 2020; Nakano *et al.*, 2014a; Kurz, 2008; DasGupta *et al.*, 2023; Nakano

et al., 2012; Tateishi-Karimata *et al.*, 2013). Moreover, some studies also include proteins for crowding simulation, in which bovine serum albumin is used often (BSA, Murade and Shubeita, 2019; Paudel and Rueda, 2014).

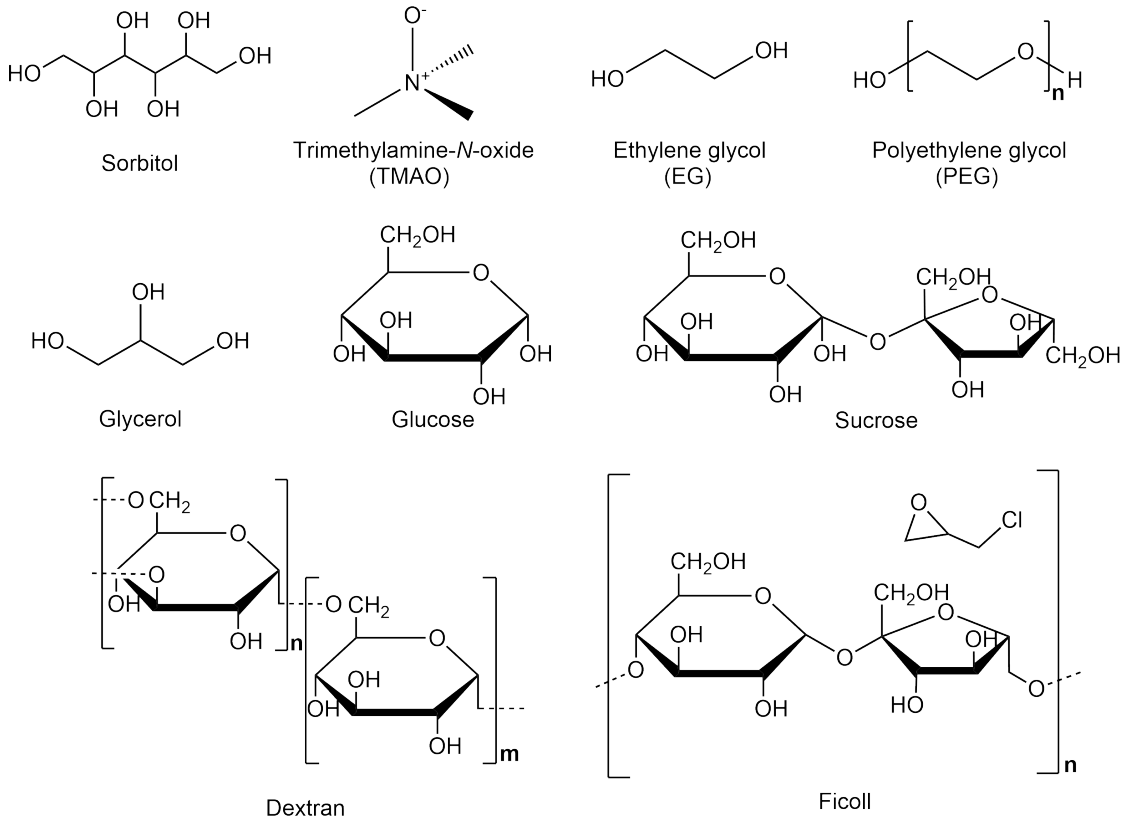

Figure 4.3: Structures of commonly used cosolutes to mimic a crowded, cell-like environment *in vitro*.

Applicable for analysis, cosolutes should satisfy the following requirements: high solubility in water, do not cause degradation or precipitation of the molecule of interest, and should not prevent interactions of water and ions (Fiorini *et al.*, 2015; Nakano *et al.*, 2014b). In addition, the neutral charge of PEG and dextran variants mostly favors their use, which is suggested to lower direct interactions between the respective biomolecule and cosolute (Fiorini *et al.*, 2015).

Based on collected observations, scientists tend to roughly categorise molecules used for simulating a crowded environment according to their suggested effect on biomolecules. Larger polymers, including PEG variants with $M_W \gtrsim 1000\,\mathrm{Da}$, dextran or Ficoll are thought to mainly take influence via space limitation and volume exclusion effects, thus assuming an entropic and less enthalpic impact (Adams and Znosko, 2019; Kilburn *et al.*, 2010; DasGupta *et al.*, 2023; Dupuis *et al.*, 2014). Consequences that result from restriction of conformational entropy by volume exclusion (only repulsive) are occasionally referred to as hard interactions (DasGupta, 2020; Silverstein and Slade, 2019; Wang *et al.*, 2012). On the opposite, EG, low molecular PEG variants with $M_W \lesssim 1000\,\mathrm{Da}$, and other small molecules are assumed to function as osmolytes in solution with predominant enthalpic influence including changes in water activity. Members are sometimes referred to as small-molecule cosolutes or small-molecule crowding (Nakano *et al.*, 2012; Adams and Znosko, 2019; Nakano *et al.*, 2014b,a). Here, changes in chemical interactions, e. g. ionic and hydrophobic, that lead to alterations in enthalpy are

sometimes referred to as soft interactions (DasGupta, 2020; Silverstein and Slade, 2019; Wang *et al.*, 2012).

Another category tends to summarize interactions mediated by proteins, which are supposed to be unspecific with the biomolecule of interest, when the respective protein is not considered as direct interaction partner (Yoshikawa *et al.*, 2010; Wang *et al.*, 2012; Nashimoto, 2000).

4.7 The environmental impact on nucleic acid catalysts - comparison of experimental setups

Accumulating results of MC studies *in vitro* that focus on nucleic acids show altering effects depending on oligonucleotide length, nucleobase composition, shape, and the respective cosolute selected as well as its concentration (Ghosh *et al.*, 2020; Tateishi-Karimata *et al.*, 2013; Adams and Znosko, 2019; Spink and Chaires, 1999; Nakano *et al.*, 2014b). During such approaches, effects on hydrogen bonding, base stacking, conformation, and the availability as well as interaction with water (hydration) and metal ions are of special interest. All of the above are crucial for folding, stability, and function of nucleic acids (Tateishi-Karimata *et al.*, 2013).

After several studies on RNA (Yu *et al.*, 2016; Adams and Znosko, 2019; Pincus *et al.*, 2008; Nakano *et al.*, 2014b), DNA duplexes (Nakano *et al.*, 2014b; Singh and Singh, 2016; Miyoshi and Sugimoto, 2008), and ribozymes (Paudel *et al.*, 2018; Rahman *et al.*, 2018; Desai *et al.*, 2014; Nakano *et al.*, 2009; Paudel and Rueda, 2014; Kilburn *et al.*, 2010) presented changes in thermostability, distribution of folding states, activity, and, for the latter, a reduction in M^{2+}-requirement in presence of cosolutes, recent results also demonstrate an influence on RNA-cleaving DNAzymes (Rudeejaroonrung *et al.*, 2020; Wang *et al.*, 2023; Gao *et al.*, 2015; Nakano *et al.*, 2017, Kirchgässler *et al.* in preparation). As in previous designs, a crowded environment was mimicked with one cosolute at a time and varying concentrations of such. For instance, Wang *et al.* (2023) used different sizes of PEG as well as the the cationic comb-type polymer poly(L-lysine)-*graft*-dextran (PLL-*g*-Dex) to mimic crowding. They observed an accelerating effect on the catalytic activity of a Na^{+}-dependent DNAzyme in presence of PEG and PLL-*g*-Dex, which was attributed to a decrease in dielectric constant and changes in electrostatic interactions (Wang *et al.*, 2023).

In a recent study, Kirchgässler *et al.* performed assays in presence of several different cosolutes: PEG (average molecular weight $M_{\mathrm{W,\,av}} = 0.2 - 20\,\mathrm{kDa}$), dextran ($M_{\mathrm{W,\,av}} =$ 5 and 12 kDa), EG as well as osmolytes betaine and ectoine (Kirchgässler *et al.* in preparation). One the one hand, their results indicate a decrease in DNAzyme activity, when small molecule cosolutes with osmolytic properties are present. On the other hand, DNAzyme activity is enhanced in presence of certain conditions that indicate to combine a favored set of physicochemical properties, which seem to depend on the respective metal ion involved in catalysis. As this also involves different preferences in average distances between two cosolute molecules, this study supports the hypothesis of an 'ideal' cavity size by Paudel *et al.* to achieve an increase in activity (Paudel *et al.*, 2018). Although all findings contribute to an important basis for understanding nucleic acids in crowded environments, the experimental design of *in vitro* approaches is continuously reviewed towards cellular relevance.

4.7.1 One cosolute at a time

To our knowledge, the vast majority of crowding studies (e. g. Wang *et al.*, 2023; Paudel *et al.*, 2018; Nakano *et al.*, 2012) performs analyses in presence of one cosolute at a time. For science, of course, simplification provides the clear advantage of categorizing and distinguishing multidimensional effects, whether being functional or structural on the molecule of interest, or causing alterations in chemical and physical properties of the surrounding solution. In cells, however, a diversity of biomolecules specifies a compartment's or micro-environment's properties (Model *et al.*, 2021), in which unilateral influences by one biomolecule are unlikely.

4.7.2 Variation in concentration and use of different cosolute types

All approaches are usually carried out in presence of different cosolute concentrations. Most of the time, these range between 5 and 20 wt% (e. g. Wang *et al.*, 2023; Nakano *et al.*, 2017; Desai *et al.*, 2014), which is in agreement with estimated total concentrations of biomolecules in cells of $50-400\,\mathrm{g/L}$ (Ellis and Minton, 2003). This setup allows for concentration-dependent investigations of above mentioned impacts and, if present, identification of possible optima (Paudel *et al.*, 2018). Especially effects mediated by volume exclusion can be regulated using this setup, since cosolute size and concentration limit the volume available to others. This effect is more pronounced for larger cosolutes (Minton, 1981; Hall and Minton, 2003; Paudel *et al.*, 2018; Kilburn *et al.*, 2010). However, cellular concentrations of biomolecules are not static, but alter dynamically according to, for example, the cell cycle, thus creating a heterogeneous distribution of available spaces (Gnutt and Ebbinghaus, 2016).

Besides changing concentrations, it is useful to compare different cosolute types and sizes, which to our knowledge, is the case in all *in vitro* crowding studies. Depending on the respective properties, changes in and extents of effects can be compared directly, distinguished, and, if possible, assigned specifically. In this regard, monomers are often used as direct comparison, e. g. EG for PEG (Nakano *et al.*, 2012, 2017; Fiorini *et al.*, 2015) and glucose for dextran.

4.7.3 Ionic strength

Despite achieving a certain degree of complexity by using cosolutes, parameters such as volume, pH, temperature, and ion concentrations still remain under high control. Considering DNAzymes, Na^+-, K^+-, and Mg^{2+}-ion concentrations are of particular interest (Rosenbach *et al.*, 2020b, 2021). In cells, the concentration of free Mg^{2+} is approximately $0.5-1\,\mathrm{mM}$ (Pechlaner and Sigel, 2012), which often is far from the concentrations applied in ribozyme- and DNAzyme-based crowding studies due to their higher requirement of them (Gao *et al.*, 2015; Paudel *et al.*, 2018; Fiorini *et al.*, 2015; Nakano *et al.*, 2017). In mammalian cells, the concentration of monovalent ions such as Na^+ and K^+ is 10 mM and 140 mM, respectively (Pechlaner and Sigel, 2012). Studies within recent years performed experiments approximating such concentrations in order to simulate an environment closer to physiological conditions (Wang *et al.*, 2023; Gao *et al.*, 2015; Nakano *et al.*, 2017; Rudeejaroonrung *et al.*, 2020). Often, however, only one type of monovalent ion is present alongside catalytically relevant divalent cations. Since simulations suggested different interactions of monovalent ions with different regions of nucleic acids (Cheng *et al.*, 2006), buffers with multiple ions should be

considered for an experimental set up. Rarely, studies include different salt concentrations and thus ionic strength-dependent effects, which in cells occur in the event of opening and closing of ion channels. Some approaches aim at simulating such influences by varying, for instance, Na^+ concentrations (Spink and Chaires, 1999; Nakano *et al.*, 2014a, Kirchgässler *et al.* in preparation).

4.7.4 Size of RNA substrates

To date, published studies on DNAzymes under cell-like conditions were performed with short RNA substrates of 19 to 30 nucleotides (nt) in length (Wang *et al.*, 2023; Gao *et al.*, 2015; Nakano *et al.*, 2017; Rudeejaroonrung *et al.*, 2020). Such strategies are also frequently found in ribozyme-based approaches (Rahman *et al.*, 2018; Desai *et al.*, 2014). Although short RNA sequences are low in synthesis cost and potentially facilitate the design depending on the experimental requirements, they do not include secondary or higher structures, thus RNA folding in general, that appear common and critical for longer or full-length sequences in nature (Leamy *et al.*, 2016; Pan and Sosnick, 2006; Zemora and Waldsich, 2010; Zhang *et al.*, 2022). Secondary structures, however, when transferred to a cell-like environment with increased volume exclusion, may not only interfere with the accessibility of potential cleavage sites, thus a DNAzyme's hybridization efficiency, but also, with the extent of steric impacts.

To obtain first ideas of an RNA sequence's structure, tools such as RNAstructure (Reuter and Mathews, 2010), Mfold (Zuker, 2003) or the ViennaRNA package (Gruber *et al.*, 2015; Lorenz *et al.*, 2011) provide structural predictions based on the nearest neighbour model (Tinoco *et al.*, 1971, 1973). However, thermodynamic parameters have been determined in buffer containing 1 M NaCl (SantaLucia *et al.*, 1996; Xia *et al.*, 1998; Sugimoto *et al.*, 1995), excluding crowded conditions. First parameters adapted to a crowded environment (40 wt% PEG 200, 100 mM NaCl) for DNA duplexes were published by Ghosh *et al.* in 2020 (Ghosh *et al.*, 2020).

4.7.5 Neglecting water in volume exclusion

In terms of volume exclusion, observations associated with it are usually attributed to the added cosolute. But every molecule, in particular water, occupies a volume as well, which usually is neglected in crowding studies (Sharp, 2015). However, water plays a pivotal role in cells with strict regulation. It is either found ordered, then mostly osmolytically inactive, or unordered/free (Sugimoto, 2014), which should be taken into account. Hence, it is advised to adapt applied models to describe molecular crowding.

Altogether, the comparison of molecular crowding studies demonstrates a variety of core factors that justify consideration and adjustment to gradually approximate even more cell-like conditions *in vitro*. On the one hand, construct design and buffer composition-especially the concentration of monovalent and divalent ions-should meet physiological demands to mimic natural nucleic acid-ion interactions and include consequences due to folding. On the other hand, the selection and applied concentration of respective cosolutes is crucial, since it determines the surrounding's properties that impact the DNAzyme:RNA complex.

4.8 Outlook

MC studies *in vitro* have proven to be an important first step in exploring the effects of complex cellular systems and understanding a molecule's biological behavior, here of DNAzymes in particular. But "simplicity" in experiments, mostly performing analyses in presence of one cosolute at a time, certainly is just the beginning in bridging the gap between *in vitro* and *in vivo*. Thus, future experiments require additional models with increased complexity to gradually enhance the levels of heterogeneity and effects on solution properties and interactions (Foffi *et al.*, 2013).

In this context, cell-like structures or artificial cells, such as cell-sized vesicle-in-vesicle structures (VIV, Zong *et al.*, 2017), capsules (e. g. liposomes, hydrogel particles, coacervates, and polymerosomes, Elani, 2021), and cell-sized aqueous/aqueous microdroplets (CAMDs, Nakatani *et al.*, 2018), but also hybrid cell systems (Elani *et al.*, 2018) present emerging tools (Figure 4.4).

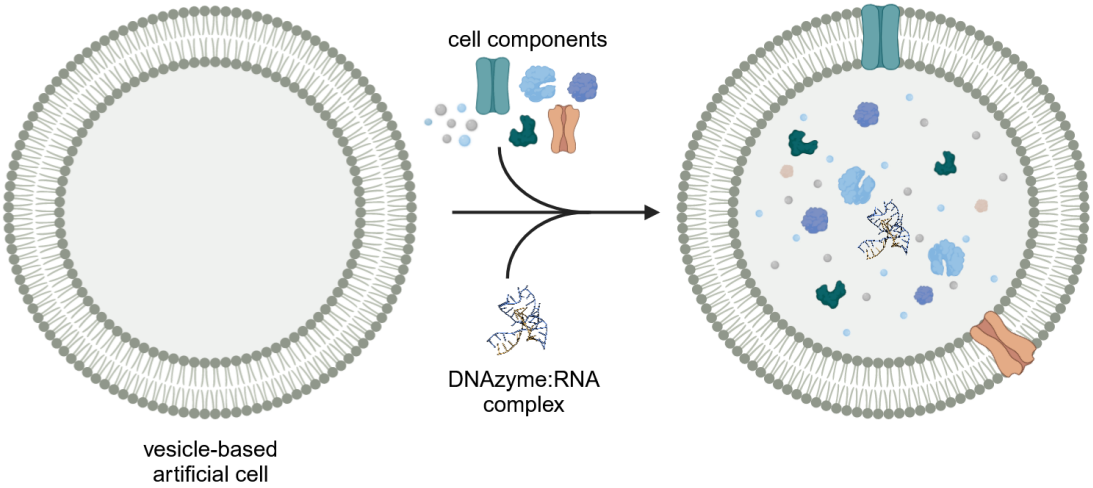

Figure 4.4: Example of an artificial cell system to investigate the properties of a DNAzyme:RNA complex (PDB 7PDU) under crowded conditions of higher complexity. Created with BioRender.com.

They provide flexibility in functionalization with biomolecular components like enzymes, nucleic acids, and transmembrane structures by changing their inner composition (Elani, 2021). In addition, the use of analyses in presence of cell lysates might be considered (Gnutt *et al.*, 2015). As a benefit, such approaches increase the complexity and mimic a cell's composition outside a closed cell system. Though, they simultaneously raise the difficulty in differentiating single interactions, which needs to be addressed in experimental designs and outlines the balancing act that studies on molecular crowding effects have to manage. One option to target the limitations of short RNA substrates and to facilitate analyses in presence of longer or even full length RNA substrates is to synthesize the respective molecules using *in vitro* transcription, by which quantities of μg to mg can be achieved (Beckert and Masquida, 2010). This method further provides the option, for example, to use copper-catalyzed alkyne-azide cycloaddition (CuAAC)-compatible nucleotides. Such, when added to the reaction and incorporated into the desired oligonucleotide sequence, provide the option to subsequently label and modify the RNA substrate with functional groups or fluorophores to match experimental requirements (Fantoni *et al.*, 2021). However, it has to be mentioned that their incorporation and thus the respective label position is random. Of course, synthesis costs depend on molecule size, desired quantity, and additional effort for the implementation of modifications.

5

DESIGN OF RNA-CLEAVING DNAZYMES TO TARGET THE VIRAL HEMORRHAGIC SEPTICAEMIA VIRUS (VHSV)

5.1 Introduction

Every year, continuous growth in aquaculture and the fish farming industry to meet global needs is hampered severely by infectious diseases. Those are mainly attributed to RNA viruses, which can spread easily due to often favoring conditions in intensive aquaculture (Kang *et al.*, 2012; Balmer *et al.*, 2018). Viral infections have been causing significant losses, thus serious economic consequences, with an increasing number of outbreaks in recent years. The main destructive pathogen threatening farming in Europe is the viral hemorrhagic septicaemia virus (VHSV, Gomez-Casado *et al.*, 2011; Garver *et al.*, 2011; Pereiro *et al.*, 2016; Escobar *et al.*, 2017; Skall *et al.*, 2005). VHSV causes viral hemorrhagic septicaemia (VHS, Marroquí *et al.*, 2007), which is also known and listed as a viral infection by the World Organisation for Animal Health (WOAH, founded as OIE, `https://www.woah.org/en/disease/viral-haemorrhagic-septicaemia/`). Nowadays, VHSV has been detected in more than 50 different marine and freshwater species, including rainbow trout, salmon, sea bream, sea bass, carp, and turbot, of which rainbow trout accounts for the most farmed freshwater fish in Europe (Cieslak *et al.*, 2016; Gomez-Casado *et al.*, 2011).

VHSV belongs to the genus *Novirhabdoviridiae* and is an enveloped, bullet-shaped virus (Figure 5.1A) that contains a non-segmented negative-sense (−) single-stranded RNA genome of $\sim$ 11 kb (Clark *et al.*, 2019; Jonstrup *et al.*, 2009). Thus, the genome acts as a complementary template and needs to become double-stranded first by synthesizing the corresponding positive strand to obtain the respective mRNA sequence for protein synthesis (Payne, 2017; Clark *et al.*, 2019). The genome consists of six genes, of which five code for structural proteins: nucleocapsid protein (N), phosphoprotein(P), matrix protein (M), surface glycoprotein (G), and large polymerase protein (L). The sixth gene encodes a unique nonvirion protein (NV). These are arranged in the order 3'-N-P-M-G-NV-L-5' (Figure 5.1B, Snow *et al.*, 2004; Schütze *et al.*, 1999; Dadar, 2020).

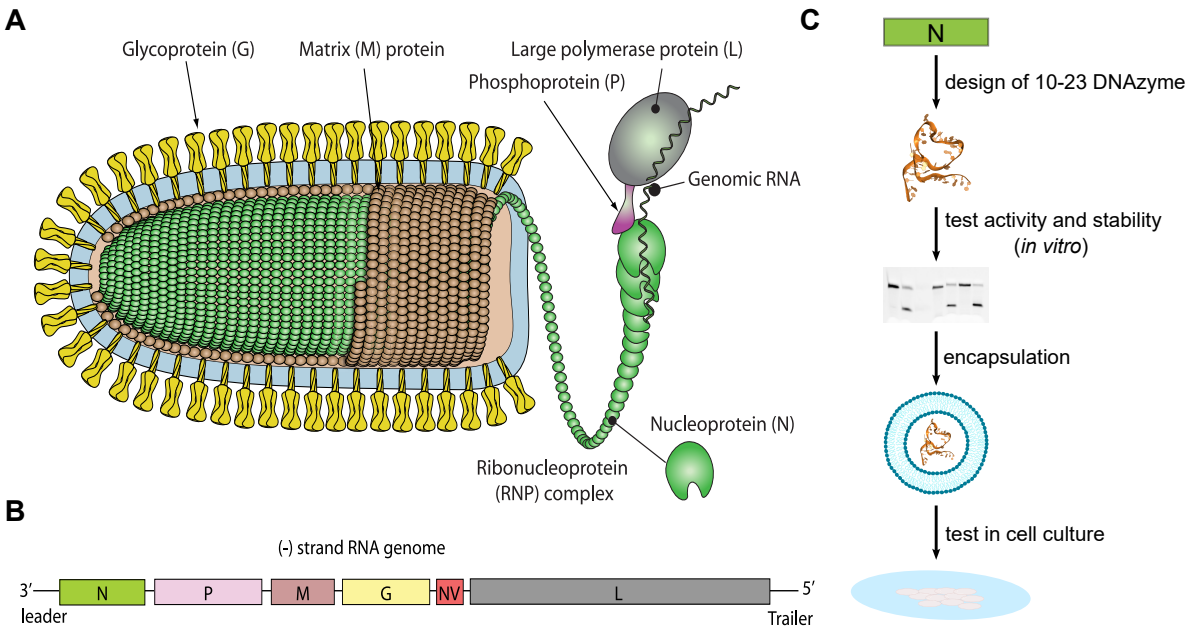

Figure 5.1: A Shape and structure of a *Novirhabdovirus* virion (e.g. VHSV). **B** Composition of a negative-sense linear-stranded RNA genome found in *Novirhabdovirus* such as VHSV with five genes encoding for structural proteins (nucleoprotein (N), phosphoprotein (P), matrix protein (M), glycoprotein (G), and large polymerase protein or RNA-dependent RNA polymerase (L)) and a sixth nonvirion (NV) protein. Figures **A, B** are obtained from: `https://viralzone.expasy.org/76?outline=all_by_species`, SwissBioPics, Swiss-Prot group, Swiss Institute of Bioinformatics. **C** Experimental strategy to target VHSV with RNA-cleaving DNAzymes: selection of target gene (here *N*-gene), design of 10-23 DNAzymes (PDB 7PDU), test activity and stability *in vitro*, encapsulation of the selected 10-23 DNAzyme into nanoparticles (liposomes or polymerosomes), and test on infected fish cells in cell culture.

As a result of phylogenetic analyses, mostly based on the sequences of the nucleocapsid or matrix protein, VHSV isolates are categorized into four different genotypes (I–IV). Here, certain genotypes exist more frequent in discrete geographical areas than others (Pereiro *et al.*, 2016; Jonstrup *et al.*, 2009). Genotype I comprises VHSV isolates from European freshwater and a marine group from the Baltic sea. Genotypes II and III include marine isolates in Europe and genotype IV is found primarily in North America and East Asia. In addition, genotypes I and IV are further subdivided into subgenotypes Ia–Ie and IVa and IVb (Pereiro *et al.*, 2016; Jonstrup *et al.*, 2009; Snow *et al.*, 2004). Symptomatically, VHS causes severe tissue changes such as necrotic degeneration of kidneys, spleen, liver, and intestines. In addition, common symptoms comprise lethargy, abnormal swimming behaviour, darkening of the skin, anemia, a bloated abdomen, bulging eyes, and haemorrhages on skin, eyes, internal organs, and gills (Pereiro *et al.*, 2016; Cieslak *et al.*, 2016; Ammayappan and Vakharia, 2009; Gadd, 2013; World Organisation for Animal Health (OIE), 2021).

In general, VHS can take three courses: acute, subacute, and chronic (Faisal *et al.*, 2012), which result in different percentages of mortality. The highest mortality of close to 100 % occurs during acute infections (Cieslak *et al.*, 2016). However, the extent of infection and symptoms seem to depend on various factors such as affected genotype, fish species and age, and additional external factors such as temperature, salt concentration, pH, and degree of water hardness (Gadd, 2013; Escobar *et al.*, 2017). In this regard, VHSV virions, which define as single viral particles outside a cell, seem to not appear or spread randomly across geographical areas (Escobar *et al.*, 2017). Transmission of virions is considered by either contact with urine or other reproductive fluids, contact with virion-contaminated water or with infected fish (Gadd, 2013; Cieslak *et al.*, 2016).

The main concern regarding fish pathogens is the lack of effective and specific therapeutics or universally applied measures for prevention (Gomez-Casado *et al.*, 2011; Pereiro *et al.*, 2016; Zhang *et al.*, 2021). High losses not only result from the course of infection, but also as consequence of current preventive measures (Cieslak *et al.*, 2016). Thus, there is an urgent need for treatment options. Although investigations on vaccines have been performed with promising antiviral effects for approximately four decades (Lorenzen and LaPatra, 2005; Ma *et al.*, 2019), none have yet been used on a large scale, are commercially available, or have been approved internationally, but often remain on a laboratory scale (Gomez-Casado *et al.*, 2011; Pereiro *et al.*, 2016). A general challenge in developing a suitable treatment is to cover a broad spectrum of genotypes, since simultaneous occurrence in one area is very likely (Gomez-Casado *et al.*, 2011). Current prophylactic measures include probiotics, immunostimulation or disinfection (Pereiro *et al.*, 2016; World Organisation for Animal Health (OIE), 2021). The first two are applied and achieved by targeted diet manipulation to strengthen a fish's immune system (Pereiro *et al.*, 2016). On the other hand, disinfection is carried out, for example, by UV irradiation of water or the use of chemicals such as chlorine or sodium hypochlorite (World Organisation for Animal Health (OIE), 2021). Studies within the past years provided alternative ideas by showing promising antiviral properties of plant extracts (Park *et al.*, 2017) or synthetic light-activated substances (Balmer *et al.*, 2018).

Nevertheless, new approaches are highly required that should meet general prerequisites of simple administration (injection, dissolvable in water, orally, or as immersion, Gomez-Casado *et al.*, 2011), cost-effectiveness on a large scale, minimal side effects, and no harm to the treated species and environment (Zhang *et al.*, 2021; Ma *et al.*, 2019). Since the discovery of artificial DNA molecules with catalytic activity (DNAzymes) in the early 1990s (Breaker and Joyce, 1994), especially RNA-cleaving DNAzymes emerge as promising tools for targeted gene silencing (Yan *et al.*, 2023a; Xiao *et al.*, 2023). The two most extensively studied variants are the 8-17 and 10-23 DNAzyme (Silverman, 2016). Despite rare *in vivo* success with ongoing challenges, optimization and modification strategies of recent years show promising progress (Etzkorn and Span, 2023; Wang *et al.*, 2021; Taylor *et al.*, 2022). So far, DNAzyme applications *in vivo* focus on targeting pathogens that threaten humans (Yan *et al.*, 2023a). Studies in the field of animal health and fish farming in particular, in which DNAzymes are used for a therapeutic purpose, are not known.

Therefore, the aim of this project is to design several 10-23 DNAzymes (Dz) that target VHSV and test their activity and stability *in vitro*. The mRNA sequence of the nucleocapsid protein (N) is used as RNA substrate during the design, which, besides encapsidation of the RNA genome, plays a key role in virus replication and is the first protein synthesized during the cycle (Baillon *et al.*, 2020; Gomez-Casado *et al.*, 2011). Subsequently, which is no longer part of this chapter, selected Dz with appropriate *in vitro* activity and stability will be encapsulated into lipid nanoparticles and further tested on infected fish cells in cell culture (Figure 5.1C).

5.2 Material and Methods

5.2.1 Design of a 10-23 DNAzyme

The mRNA sequence of gene *N* plus ≈ 20 nt on each side (nt 141 - 1410) of the VHSV isolate Fi13 (GenBank AC Y18263, Schütze *et al.*, 1999) was used as RNA target. In addition, the design of Dz was carried out to potentially target multiple VHSV isolates. Thus, Dz were also selected according to hybridization sites with high sequence identity between different isolates, at maximum two nt difference in a stretch of ≤ 20 nt. Additional isolates were selected randomly from the subgenogroup Ia, since this subcategory has been the main cause for outbreaks in rainbow trout farming in Europe for the past decades (Cieslak *et al.*, 2016; Panzarin *et al.*, 2020; Cano *et al.*, 2021): GenBank AC MW507000.1, MT162452, MT162447, MT162445, MN038327, MK829686, MK829391, MN038338, MK829681, MN856666, and D00687.

As a temperature of 15 °C has proven to be appropriate for VHSV replication (Cho *et al.*, 2019), Dz were designed with a desired melting temperature (T_m) of substrate binding arms of 15 °C using the following methods:

- perl script PROB.PL (Steger and Victor, 2022), which is based on RNAPLFOLD (Bernhart *et al.*, 2006; Tafer *et al.*, 2008) from the ViennaRNA package (Lorenz *et al.*, 2011). Calculations were performed with cleavage sites GU and AU. The accessibility of potential cleavage sites was calculated and ranked by the mean probability u_{10} (probability of a sequence of length $l = 10$ to be unpaired centered at a GU or AU) with parameters restricted to a maximum distance of pairing nucleotides $L = 40$ and a length of sliding window $W = 80$.
- free online tool DNAzymeBuilder (Mohammadi-Arani *et al.*, 2022) with settings: cleavage position GU and AU, type 10-23, pH > 7, reaction RNA transesterification cleavage, yield $80 - 100\,\%$, cofactor Mg^{2+}.

5.2.2 Oligonucleotides

DNA and RNA oligonucleotides were obtained from biomers.net (Ulm, Germany). Single-labeled RNA substrates used in the stability as well as time-resolved activity assay contained a 6-carboxyfluorescein (6-FAM) molecule at the 5'-end. The sequences for Dz and RNA substrates are listed in Table 5.1. The cleavage position of respective Dz in the construct and genome sequence are listed in Table 5.2.

Table 5.1: Sequences of 10-23 DNAzymes (Dz) and RNA substrates(T). The sequence in lower case is the cataytic core of the Dz. The sequence in bold is the part of T complementary to the binding arms of the respective Dz.

Construct	Sequence (5'– 3')
Dz^{137}	CACCAACAggctagctacaacgaACACGATGA
Dz^{612}	GATGAAggctagctacaacgaGCATAG
Dz^{1063}	CTCTCCAAggctagctacaacgaCCTCTCG
T^{137}	6-FAM-**UCAUCGUGUAUGUUGGUG**
T^{612}	6-FAM-CCU**CUAUGCGUUCAUC**CUG
T^{1063}	6-FAM-UA**CGAGAGGAUUGGAGAG**

Table 5.2: Cleavage site and position (cp) of selected 10-23 DNAzymes.

DNAzyme	cleavage site	cp construct [nt]	cp genome [nt]
Dz^{137}	AU	137	278
Dz^{612}	GU	612	753
Dz^{1063}	AU	1063	1204

5.2.3 Stability assay followed by denaturing urea-PAGE

Stability assays were performed with 0.4 µM 6-FAM-labeled RNA substrate and 0.4 µM Dz in 50 mM Tris-HCl, pH 7.5. Prior to cleavage, RNA substrate and Dz were denatured in buffer without $MgCl_2$ at 73 °C for 5 min and subsequently renatured for 10 min at room temperature. RNA cleavage was induced with 1 mM $MgCl_2$ and samples were incubated for 3 h at 15 °C. Samples taken for further analysis by denaturing urea polyacrylamide gel electrophoresis (PAGE) were quenched in 94 % (v/v) formamide, 25 mM EDTA (pH 8.0), 0.02 % (w/v) Bromphenol blue, and 0.02 % (w/v) Xylene cyanol and heated at 95 °C for 10 min. Samples were separated by size using 18 % polyacrylamide gels (prepared with ROTIPHORESE Gel 40 (19:1) acrylamide/bis-acrlyamide solution, Carl Roth, Karlsruhe, Germany) that contain 7 M urea buffered with Tris-borate EDTA buffer (TBE; 89 mM Tris, 89 mM boric acid, and 2 mM EDTA, pH 8.0) for 45 min at 20 W. Prior to sample separation, gels were preheated for 30 min at 20 W to avoid temperature inhomogeneities. Detection of 6-FAM-labeled RNA substrates by fluorescence allowed the visualization of uncleaved RNA and one of two cleavage products, which contains the 6-FAM molecule at the 5'-end (5'-fragment). Images were acquired using the ChemiDoc MP System (Bio-Rad, Hercules, CA, USA).

5.2.4 Time-resolved cleavage assay (urea-PAGE-based)

Assays were performed with 0.4 µM 6-FAM-labeled RNA substrate and 0.4 µM Dz in 50 mM Tris-HCl, pH 7.5. Prior to cleavage, RNA substrate and Dz were denatured in buffer without $MgCl_2$ at 73 °C for 5 min and subsequently renatured for 10 min at room temperature. RNA cleavage was induced with 0.5 mM $MgCl_2$ and samples were taken after 10, 20, 30, 60, 90, 120, 180, 300, 420, 600, 1800, 3600 and 10 800 s respectively. Samples were quenched and separated by urea-PAGE as in section 5.2.3.

DNAzyme activity was quantified relatively using the Image Lab software by Bio-Rad (Bio-Rad, Hercules, CA, USA). The percentage of cleaved RNA was determined by the ratio of band intensity of the 5'-fragment to the band intensity of uncleaved RNA in the RNA substrate only (T) sample.

5.3 Results

5.3.1 Design and selection of DNAzymes

Dz were designed to target the mRNA that codes for the nucleocapsid protein (N) based on the VHSV isolate Fi13 (GenBank AC Y18263). RNA cleavage is performed between a purine–pyrimidine junction, with GU and AU sequences most preferred. Since local RNA secondary structures are expected to influence DNAzyme hybridization efficiency, a sequential folding algorithm (ViennaRNA package, see section 5.2.1) was used to calculate and rank the accessibility of potential cleavage sites within the mRNA according to the mean probability u_{10}, so that sequences of 10 nt in length centered at a GU or AU are unpaired.

Depending on a Dz's predicted monomeric and homodimeric structure, hybridization site (degree of sequence identity between isolates), and predicted cleavage site accessibility, three potential cleavage sites were selected for stability and activity analyses: at positions 137, 612, and 1063 with low pairing probability u_{10} of 0.030, 0.007, and 0.026, respectively (Figure 5.2). Regarding Dz structure prediction, candidates were preferred when a) monomers contain a low degree of or no internal structures, such as hairpin helices, and b) complementary sequences in homodimers are restricted to the catalytic core region.

Dz that perform cleavage at selected positions are called Dz137, Dz612, and Dz1063 and short RNA targets (19 nt) that resemble stretches of the corresponding mRNA and contain the required cleavage sequence are called T137, T612, and T1063, respectively. Dz612 was the most promising variant, which resulted from design approaches using the online tool DNAzymeBuilder (Section 5.2.1).

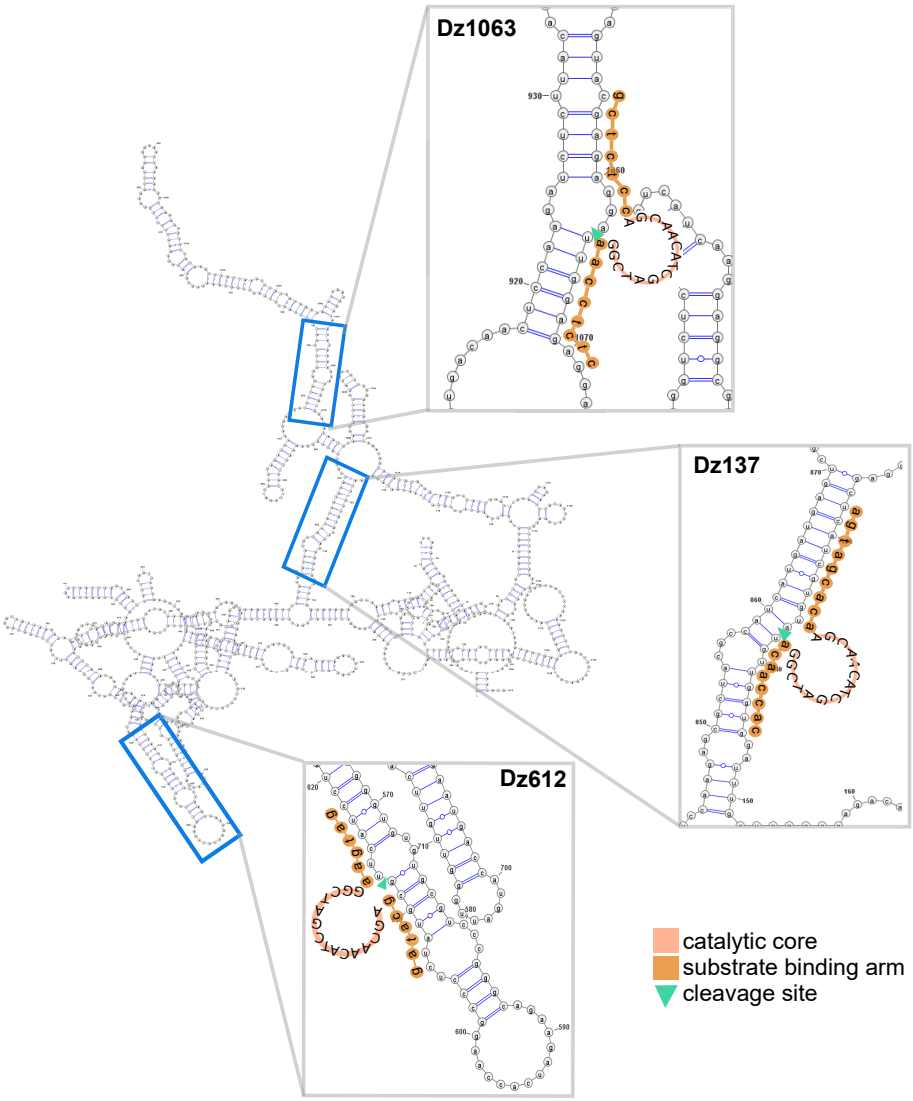

Figure 5.2: Predicted RNA structure by RNAFOLD (Hofacker *et al.*, 1994) of the sequence (nt 141 - 1410) including the sequence for the nucleocapsid protein (N) (nt 168 - 1382) as target sequence of the VHSV isolate Fi13 (GenBank AC Y18263). Cleavage and hybridization sites of Dz137, Dz612, and Dz1063 are highlighted. Visualization of RNA structure predictions with VARNA (Darty *et al.*, 2009).

5.3.2 Successful cleavage of short RNA substrates

First, Dz and RNA target stability was tested to exclude undesired degradation and unspecific site reactions. Oligonucleotides were incubated in presence of 1 mM $MgCl_2$ for 3 h at 15 °C. Samples containing the RNA substrate only (T) showed no additional bands, except for the uncleaved RNA substrate, indicating sufficient stability without degradation. Samples containing the respective Dz (TDz) showed site-specific cleavage without unspecific site reactions, since only one band attributed to the fluorescent 5'-cleavage product was detected (Figure 5.3). Remaining fluorescence of uncleaved RNA in all TDz samples indicates a cleavage efficiency of less than 100 % within 3 h.

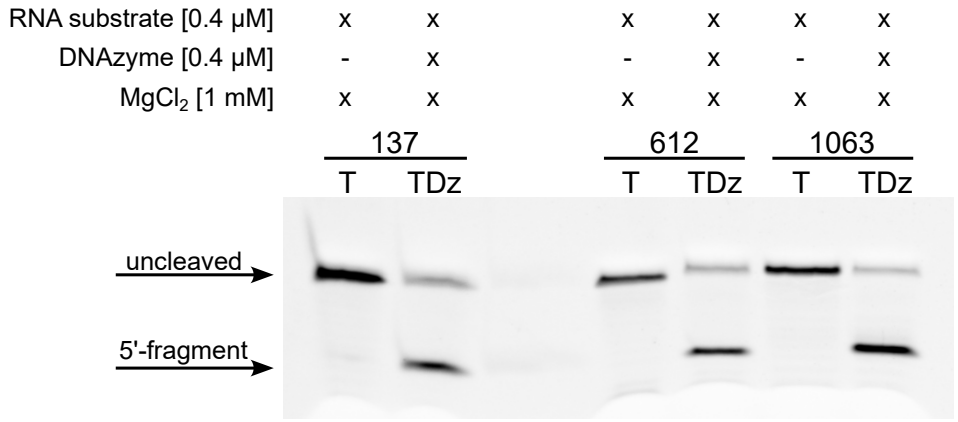

Figure 5.3: Urea-PAGE of samples after stability analysis. Oligonucleotides were tested in sets of samples containing the RNA substrate only (T) and the Dz:RNA complex (TDz).

To obtain information on the speed of reaction, time-resolved cleavage assays were performed next. Cleavage was induced by addition of 0.5 mM $MgCl_2$. In a first attempt, selected cofactor concentrations were used based on free Mg^{2+} concentrations in mammalian cells ($Mg^{2+}_{free} \sim 0.5 - 1$ mM, Pechlaner and Sigel (2012)). Samples were taken within a range of 10 to 10 800 s (= 3 h) after induction (Figure 5.4A). Subsequently, the fluorescence intensity of cleaved RNA (5'-fragment) was quantified relatively and the respective percentage was calculated (Section 5.2.4, Figure 5.4B).

Relative quantification of fluorescence intensity resulted roughly in 34 %, 5 %, and 83 % of cleaved RNA for Dz137, Dz612, and Dz1063, respectively, after 3 h of incubation at 15 °C. To this point, Dz1063 shows the highest activity in 50 mM Tris-HCl, pH 7.5 at 0.5 mM $MgCl_2$. Applying a monoexponential fit (see section 3.4.4, equation 3.1) provides first information on the observed rate constant (k_{obs}) with which the reaction takes place. In a first approximation, k_{obs} is 0.000 89 s^{-1} for the Dz1063.

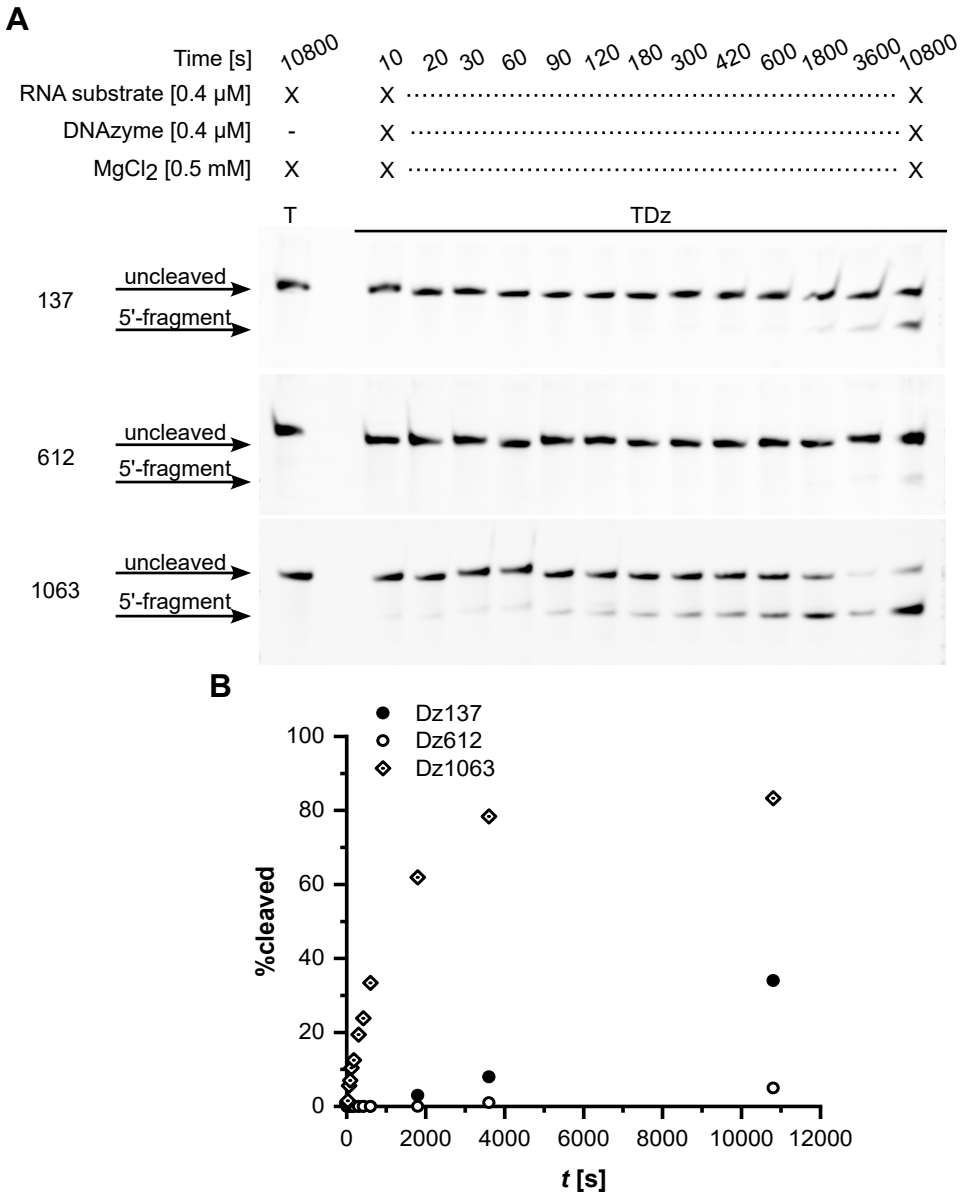

Figure 5.4: A Urea-PAGE of samples taken during the time-resolved cleavage assay for Dz137, Dz612, and Dz1063. **B** Percentage of cleaved RNA substrate depending on time in seconds for Dz137, Dz612, and Dz1063.

5.4 Discussion

The annual loss of fish in aquaculture due to infectious diseases such as VHS is a persistent challenge that can only be fought to a limited extent by present strategies (Pereiro *et al.*, 2016; Ma *et al.*, 2019). RNA-cleaving DNAzymes, like the 10-23 DNAzyme, provide an attractive alternative. Thus, the aim of this project is to design Dz that target the nucleocapsid protein of VHSV and test them *in vitro* at first. In initial experiments, all RNA substrates showed sufficient stability and the three selected Dz performed site-specific cleavage excluding any undesired site reactions (Figure 5.3). Time-resolved assays highlight Dz1063 to be the most active variant so far (Figure 5.4). During the design, Dz612 was thought to be promising due to its shorter substrate binding arms of 6 nt each, which considered facilitated dissociation after cleavage at 15 °C. However, Dz612 demonstrated very low activity compared to the other two tested Dz. So either the predicted melting temperature T_m of the binding arms is lower

than demanded, which would shift the equilibrium towards dissociation and hamper efficient hybridization, or is higher, which would impair dissociation. The latter would impact catalysis under multiple turnover. Here, for further investigation and evaluation, cleavage assays at different temperatures or with altered binding arm lengths are reasonable.

The results presented here are first impressions that selected Dz are stable and are capable of performing site-specific cleavage, but require further experiments prior to tests in aquaculture. Assays were performed at pH 7.5, which is included in the desired pH range of fish farming (pH 6.5 to 9), but does not cover it. Thus, cleavage assays at different pH values are recommended, since pH changes most likely interfere with Dz efficiency (Kasprowicz *et al.*, 2017). Furthermore, experiments were carried out at 0.5 mM $MgCl_2$, which does not necessarily have to reflect the free concentration of Mg^{2+} in fish cells (Brucka-Jastrzêbska and Kawczuga, 2011; Shearer, 1989). Thus, assays in presence of different Mg^{2+}-concentrations may be of interest as well that approximate conditions of the desired application site (e. g. tissue). In addition, experiments were carried out with short RNA substrates of 19 nt in length, which excludes RNA folding and presence of secondary structures that naturally occur for longer or full length sequences (Zhang *et al.*, 2022). In consequence, Dz activity needs to be analyzed with longer RNA substrates, which also provides information whether the structural predictions and calculated probability of cleavage site accessibility during the design were correct. Otherwise, additional Dz need to be selected and tested for activity.

During the design, calculations were performed at 15 °C, since this temperature appeared to be appropriate for VHSV replication. However, RNAFOLD and RNAPLFOLD usually use thermodynamic parameters at 37 °C as default, which allow for better structure predictions (Lorenz *et al.*, 2011). Thus, predictions at 15 °C may be less accurate than at 37 °C and may impact experimental observations.

Recent studies on Dz focus on implementing different modifications in order to overcome *in vivo* limitations such as biostability (risk of degradation) or the requirement of high cofactor concentrations (Etzkorn and Span, 2023). In this regard modifications, such as 2'-deoxy-2'-fluoro-D-arabinonucleic acid (FANA), α-L-threofuranosyl nucleic acid (TNA), 2'-O-methyl-RNA, or phosphorthioates show promising results (Wang *et al.*, 2021; Taylor *et al.*, 2022; Nguyen *et al.*, 2023). Therefore, introducing modifications should also be considered and tested when targeting VHSV mRNA, since risk of degradation and other factors also apply for Dz under marine and freshwater conditions.

As the number and accessibility of potential cleavage sites (AU and GU) within the gene *N* was limited to 10 using the ViennaRNA package, additional target sequences of other viral proteins could be considered for Dz design as well to expand the number of potential candidates.

5.5 Acknowledgements

I would like to acknowledge PD Dr. Anna Becker and Prof. Dr. Kathrin Castiglione from the Department Chemistry and Bioengineering (CBI) and chair Bioprocess Engineering (BVT) at the Friedrich Alexander University Erlangen-Nürnberg for cooperating with us on this project and providing information on VHSV and the experimental idea on how to target viruses in aquaculture.

6

General Discussion

6.1 Molecular crowding and prospectives

Center of attention in this thesis is the RNA-cleaving 10-23 DNAzyme, which presented as one of the most promising DNAzymes (Montserrat Pagès *et al.*, 2023). Encouraged by their beneficial properties, RNA-cleaving DNAzymes were considered to function as gene silencing agents in nucleic acid therapy (Xiao *et al.*, 2023). These include flexibility in design due to their artificial character, target specificity, and low costs in synthesis, since lacking the 2'-OH at the ribose moiety makes DNAzymes less prone to hydrolysis compared to ribozymes (Javadi-Zarnaghi and Höbartner, 2020). However, low *in vivo* activity limits their success in cells (Larcher *et al.*, 2023), whereby previous studies suggest low Mg^{2+} availability and competition with ATP (Victor *et al.*, 2018) as well as activity modulating properties by monovalent ions (Rosenbach *et al.*, 2021) as causes. Recently, effects mediated by molecular crowding are suspected to contribute as well. As information on how a cell's environment is able to interfere with DNAzyme function and structure is scarce, this thesis addresses this question.

For this purpose, a crowded cell environment was mimicked *in vitro* using a variety of natural and artificial cosolutes, including various sizes of polymers PEG and dextran, the monomer EG, and osmolytes betaine and ectoine (Chapter 2, 3, Figure 4.3). With this, our strategy was to cover different degrees of molecular crowding and to achieve a kind of molecule diversity to approximate cells. Since previous reports have shown that the highest activity can be achieved in the presence of Mg^{2+} and Mn^{2+} as cofactor (Joyce, 2001), therefore, this study also characterized the effect of the cosolutes on metal ion dependency. Here, a 10-23 DNAzyme variant that is able to bind and cleave the mRNA of the human prion protein at position 839, Dz839, is used as model. By applying a combination of spectroscopic and structural methods as well as analytical approaches to determine physicochemical solution properties, it was possible to observe that a cell-like environment is able to change DNAzyme activity. Here, a decrease or even increase in activity depends on the cosolute type, but also on the physicochemical conditions mediated by a respective cosolute concentration, in which preferences seem to differ between Mg^{2+} and Mn^{2+} (Chapter 3). The outcome of this first part emphasizes the importance to continue investigating molecular crowding effects on DNAzyme performance.

Despite the great interest in molecular crowding and promising progress made here, investigating and simulating such conditions *in vitro* is challenging. That is why this thesis

includes a protocol that provides instructions on how to simulate crowded conditions, given the cosolutes used here, how to handle crowded solutions, and how to investigate the DNAzyme's function and structure in presence of them (Chapter 2). In addition, we compare and discuss previous crowding studies according to their experimental set ups in a second part of this thesis (Chapter 4). The purpose is to outline possibilities for experimental adjustments that will help improve resembling cells *in vitro* on the long term. Considering a cell's molecular diversity, each micro-environment is imagined to comprise an individual degree of heterogeneity and set of interactions (Minton, 2006). As the majority of so far performed studies mimics crowded conditions with one cosolute at a time (e. g. DasGupta *et al.*, 2023; Rudeejaroonrung *et al.*, 2020, section 4.7.1), which is assumed to create rather homogeneous conditions, more comprehensive results in a heterogeneous, more-cell like environment could be obtained by mixing cosolutes or using artificial cell systems (Zong *et al.*, 2017; Elani, 2021, Figure 4.4) instead. However, the key challenge is to gradually achieve an elevated level of system complexity, manage molecule diversity, and provide an experimental design that allows sophisticated analysis and tracing back of single effects. Besides cosolute type and number applied, the comparison of previous studies allowed to outline further parameters, such as buffer composition (Section 4.7.3) and RNA substrate length (Section 4.7.4) as options for improvement to gain even deeper insights.

As stated above, the main goal of this thesis is to evaluate the potential impact of molecular crowding on the activity of the 10-23 DNAzyme. Despite the assigned lower degree in crowding complexity, we chose to use one cosolute at a time, since there is no comparable data available for the tested cosolutes on the activity and structure of the 10-23 DNAzyme. To evaluate the cosolute's impact on activity, relative rate constants k_{rel} were determined based on rate constants obtained from cleavage assays (Equation 3.2). In addition, effects were compared in presence and absence of near physiological, intracellular concentrations of monovalent ions and between cofactors Mn^{2+} and Mg^{2+}. From them, we first show that the type and size of cosolute impact DNAzyme activity differently (Figure 3.3, S3). While osmolytes betaine and ectoine led to a reduced activity, PEG and dextran variants demonstrated an enhancing as well as restricting influence. This is in good agreement with previous findings on the hammerhead ribozyme (Nakano *et al.*, 2014a) and the 8-17 DNAzyme variant 17E (Nakano *et al.*, 2017), in which smaller PEG molecules or molecules, in general, that tend to have osmolytic properties result in a decrease in activity, while larger cosolutes tend to increase activity. Our data further reveal, that besides the type and size of cosolute, its respective concentration determines DNAzyme activity. Previous studies on a Na^{+}-dependent DNAzyme demonstrated a mainly promoting effect in presence of PEG and dextran, in which activity was further elevated with increasing cosolute concentrations (Wang *et al.*, 2023). Contrary to these, studies by Paudel *et al.* (2018) on the group II intron ribozyme D135 showed that some concentrations are able to promote, while others tend do decrease activity. Tested conditions included EG, PEG 1000, PEG 8000, PEG 35000, and dextran 10000 at a concentration range of $0-0.2\,\mathrm{g/mL}$ (Paudel *et al.*, 2018). For the 10-23 DNAzyme, the activity data followed the second approach (Figure 3.3, S2, S3), whereby betaine and ectoine solely decreased DNAzyme activity in a concentration-dependent manner, while PEG- and dextran-based conditions highlighted certain conditions with promoting properties, at which $k_{\mathrm{rel}} > 1.10$. We have set this limit as a criterion to take account for fluctuations during measurement. We further show that crowding preferences differ between cofactors Mg^{2+} and Mn^{2+} as well as in presence and absence of NaCl. In absence of NaCl, conditions that favored Mg^{2+}-induced cleavage include cosolute concentrations $\gtrsim 0.11\,\mathrm{g/mL}$ (Figure S2),

while conditions shift to $\lesssim 0.11\,\mathrm{g/mL}$ with Mn^{2+} as cofactor (Figure S3B, C). Interestingly, both tendencies mostly included cosolutes PEG 3000 and PEG 4000. In presence of NaCl, however, preferences further shifted to lower concentrations, at which $0.07\,\mathrm{g/ml}$ of PEG 3350 promoted DNAzyme activity the most with Mg^{2+} as cofactor ($k_{\mathrm{rel}} = 1.07$) and $0.03\,\mathrm{g/ml}$ of PEG 4000 with Mn^{2+} ($k_{\mathrm{rel}} = 1.13$). Similar to Paudel *et al.*, the results presented here indicate that DNAzyme activity can be promoted not at one, but multiple 'optima'. But in contrast to their observations, our data do not indicate one single condition that results in maximum activity, at least for measurements performed in absence of NaCl. In presence of NaCl, however, our data showed fewer promoting conditions (Figure 3.3, S3). In their studies, 10 % of PEG 8000 is highlighted as optimum for the group II intron ribozyme (Paudel *et al.*, 2018). The observed differences between cofactors Mn^{2+} and Mg^{2+} engage into previous findings by Rosenbach *et al.* (2021), in which Na^{+} was able to promote activity with Mn^{2+} as cofactor, but decreased it in presence of Mg^{2+}. The authors were able to trace it back to competition of Mg^{2+} and Na^{+} for binding sites, whereas Na^{+} induced cooperative binding of Mn^{2+} to the DNAzyme:RNA complex (Rosenbach *et al.*, 2021). Consequently, we demonstrate that these mediatory properties transfer to a crowded environment, but it simultaneously raises the question, which factors determine respective crowded 'optima'. With regard to both osmolytes, we intend to attribute the concentration-dependent restriction in DNAzyme activity to nucleic acid destabilization, as it has been shown previously for calf thymus DNA (Rees *et al.*, 1993; Rajendrakumar *et al.*, 1997). However, measurements additionally indicated a change in the extent, to which both influence activity, in absence and presence of NaCl. As osmolytes provide vital function in response to cellular stress including salinity (Blose *et al.*, 2011), their influence on DNAzyme activity depending on ionic strength was further investigated (Figure 3.5). The results showed that elevated Na^{+}-levels were sufficient enough to decrease DNAzyme activity and consequently lowered the additional influence of both osmolytes. Although the assays have been carried out with Mg^{2+} as cofactor, which states a decrease in activity by Na^{+} according to the previously mentioned studies, the same tendency was found in assays with Mn^{2+} (Figure 3.5). These findings not only strongly support the suggestion of monovalent ion as *in vivo* limitation, but also consider molecules with osmolytic properties as another one. To shed light on how crowding is able to promote biocatalysis, several studies on ribozymes revealed that a crowded environment is able to lower their Mg^{2+}-requirement (DasGupta *et al.*, 2023; Paudel *et al.*, 2018; Nakano *et al.*, 2009; Desai *et al.*, 2014), which is of great interest due to a low concentration of free Mg^{2+} *in vivo* (Pechlaner and Sigel, 2012). As an example, Mg^{2+}-requirement of an RNA ligating ribozyme was reduced to approximately a five-fold in presence of 19 % of PEG 1000, which caused a five-fold increase in activity at 1 mM Mg^{2+} (DasGupta *et al.*, 2023). However, we were not able to observe changes in cofactor requirement at crowded conditions that promoted DNAzyme activity the most, neither for Mg^{2+} (Figure 3.4) nor Mn^{2+} (Figure S3D). At this point, this leaves limited cofactor availability as considerable *in vivo* limitation (Victor *et al.*, 2018) and potentially requires modification strategies (see section 1.4.2) for improving the performance of the 10-23 DNAzyme. This is further supported by the ATP competition assays (Figure S5), in which an increase in solution viscosity by larger cosolutes is able to slightly enhance DNAzyme activity, suggesting less Mg^{2+} bound to ATP, but does not sufficiently lower diffusion-dependent Mg^{2+}-binding to ATP.

To rationalize the obtained activity data, our strategy included the determination of physicochemical solution properties (Figure 3.6, S6, Table S1, S2) and the collection of structural information (Figure 3.7, S7, S8, 3.8), of which the latter has not been reported for DNAzymes under crowded conditions yet. From a previous study (Gonzalez-Tello *et al.*, 1994), density

and viscosity measurements of PEG variants revealed a significant increase in viscosity, but less changes in density. As the same tendency also applied for the tested cosolutes here, with no further impact on pH (Figure 3.6), observed effects on DNAzyme activity are mainly attributed to changes in viscosity at this point. With regard to solution properties under crowded conditions, Paudel *et al.* (2018), as mentioned before, made the interesting observation, that maximum activity for the group II intron ribozyme D135 is observed at 10 % of PEG 8000. Above and beyond this condition, activity tends to be hindered. As the authors simultaneously observe a favor in compact folded conformations by single-molecule FRET (smFRET) measurements, they propose an ideal cavity size D between cosolutes that in size depends on the respective cosolute concentration and is able to favor a state that facilitates catalysis (Paudel *et al.*, 2018). Combining the data obtained from cleavage assays and the theoretically calculated cavity sizes (Figure 3.6C), we also observe D, at which DNAzyme activity is promoted (Figure 3.7B, S8). Again, the preference in D differs between Mg^{2+} and Mn^{2+} as cofactors, which with respect to the activity data emphasizes the importance of unveiling metal ion function in and structural influence on catalysis. Moreover, the data indicate that favored cavity sizes slightly change between approaches in absence and presence of NaCl, which corresponds to the differences in preferred cosolute concentrations stated above. In presence of NaCl, promoting conditions account for slightly larger D as in absence of NaCl, which includes cavity sizes of $6.51 - 8.40\,\mathrm{nm}$ with Mg^{2+} as cofactor and $\sim 11.1\,\mathrm{nm}$ with Mn^{2+}. But, in terms of D calculation, we have to mention that applied correction factors have been calculated based on an empirical model (Section 3.4.6) that requires validation prior to further evaluate the significance of cavity size distribution on DNAzyme activity.

Regardless, pursuing investigations included FCS (Figure 3.7) and SAXS (Figure 3.8) measurements to investigate if changes in DNAzyme activity result from structural alterations that would explain cavity size preferences. As mentioned above, Paudel *et al.* (2018), but also other studies (Desai *et al.*, 2014; Kilburn *et al.*, 2010; Rahman *et al.*, 2018), observed a more compact state of ribozymes in presence of crowding. For the 10-23 DNAzyme, the DNAzyme:RNA complex is compacted to half of its initial size at high concentrations of large polymers with $M_W \geq 8\,\mathrm{kDa}$. However, these conditions, which correspond to $r_{h,\,TDz} \lesssim 1.0\,\mathrm{nm}$, tend to restrict DNAzyme activity. We assigned these observations to too elevated levels of volume exclusion, thus steric repulsion, as larger PEG molecules are thought to mainly take influence by such effects (Kilburn *et al.*, 2010). On the contrary, conditions that resulted in hydrodynamic radii between ~ 1.30 and $2.2\,\mathrm{nm}$ were associated with different degrees of DNAzyme activity. Although we imagine that, based on the persisting differences between cofactors Mg^{2+} and Mn^{2+}, also the hydrodynamic radius of the DNAzyme:RNA complex will differ between the two, we are not able to verify it, as FCS measurements have been carried out in absence of Mg^{2+} and Mn^{2+}. Since the NMR structure published by Borggräfe *et al.* demonstrated that cofactor binding induces conformational changes for complex activation (Borggräfe *et al.*, 2023), it is likely to assume that $r_{h,\,TDz}$ will change in presence of Mg^{2+} and Mn^{2+}. Consequently, we are not able to draw conclusions whether molecular crowding is able to favor a more compact state of the 10-23 DNAzyme that facilitates activity. At this point, the data indicate that DNAzyme activity is impacted less by structural changes due to a crowded environment, which is supported by the SAXS data (Figure 3.8). However, these observations tend to agree with findings by Paudel *et al.* (2018), as they did observe ribozyme compaction, but could not identify or correlate it to an optimal condition. Although the SAXS data indicate less structural influence by crowding, we have to note that they also indicate the presence of multiple species within the samples, which complicates data interpretation. As the samples contain a high complex concentration ($5\,\mathrm{g/mL}$), dimer formation is facilitated. Despite

comparative measurements using the A5C variant (Figure 3.8A), in which the palindromic sequence within the catalytic core is disrupted to prevent dimer formation (Borggräfe *et al.*, 2021), the data also indicate multiple species here. Thus, further analysis is required to distinguish between different species and to better investigate changes of the DNAzyme:RNA complex as a monomer.

Given the concentration differences of DNAzyme:RNA complex between cleavage assays (100 nM) and FCS measurements (2 nM), the question of a stable complex was raised for the latter. Although samples have been prepared with stock concentrations of 400 nM to ensure complex formation, DNAzyme activity has not been validated at 2 nm yet. Here, neither obtained diffusion times (Figure S7) nor calculated hydrodynamic radii by FCS (Figure 3.7) were able to provide sufficient information, since variations between measurements were too large to resolve differences in size, especially for crowded conditions containing cosolutes of $M_W \leq 5$ kDa. It should also be noted that, according to literature, FCS generally requires a difference in diffusion times of a factor of > 1.6 to distinguish two molecules (Meseth *et al.*, 1999), which is not fulfilled according to the determined diffusion times of our constructs (< 1). To exclude mixed species in DNAzyme samples (TDz) that would impact data evaluation and r_h calculation, cleavage assays were performed with a final complex concentration of 2 nm (data not shown). However, fluorescence intensities of < 50 were inconclusive and did not allow to calculate a rate constant and eventually an assumption of an active and stable complex. Thus, in a new attempt, complex verification shall be provided using Pulsed Interleaved Excitation-Fluorescence Cross-Correlation Spectroscopy (PIE-FCCS, data not shown). For this purpose, the DNAzyme is additionally labeled with the fluorophore Cy3b at its 5'-end. As RNA substrate, the Atto647N-labeled and stabilized variant is used again (Table 3.1). Thus, the complex contains two dyes in close proximity. FCCS setups allow to determine whether two differently labeled species diffuse together, as the cross-correlation function between two channels is directly proportional to the fraction of the co-diffusing particles that carry both fluorophores simultaneously (Weidemann and Schwille, 2013). In addition, PIE facilitates distinguishing between cross-correlation and direct excitation by making use of pulsed lasers, whose pulses are adjusted to ensure that the fluorescence of each dye after excitation can be recognized and is fully decayed prior to the excitation of the second dye (Müller *et al.*, 2005). Measurements and data evaluation are in preparation. As an alternative approach, single-molecule FRET experiments can also be considered that allow the analysis of conformational dynamics and interactions of individual biomolecules (Sasmal *et al.*, 2016; Paudel *et al.*, 2018).

To further pursue behavioural investigations on the DNAzyme:RNA complex under molecular crowding conditions, this work aims to use CD spectroscopy to determine the melting temperature T_m (see chapter 2, Kypr *et al.*, 2009, data not shown). By this, a decrease in T_m in presence of crowding would suggest effects on association, whereas an increase in T_m proposes effects on complex dissociation, which is of relevance under multiple turnover conditions. A previous study on the hammerhead ribozyme demonstrated that EG and low molecular PEG, including PEG 200 and PEG 600, decreased duplex stability, which the authors explained by specific interactions with single-stranded bases and reduced water activity (Nakano *et al.*, 2014a). A different approach on double-stranded DNA agrees with this, but additionally states an increase in stability in presence of PEG molecules PEG 3400 and PEG 8000 (Spink and Chaires, 1999). Based on the activity data presented in this thesis, we would have expected comparable results for the 10-23 DNAzyme. Unfortunately, we were not able to determine T_m for the DNAzyme:RNA complex due to poor data quality and measurement inconsistencies (data not shown). During the experiments, we faced bubble formation as limitation at high

temperatures of the applied temperature gradient ($15 - 95\,^{\circ}C$). To address this, preformed DNAzyme:RNA complexes in buffer were treated with argon for 5 min prior to measurement to displace oxygen within the sample. However, sufficient data quality could not be achieved to determine T_m. Additional measures included an exchange in buffer and cuvette, cleaning of the respective cuvette, and the use of new RNA substrate, DNAzyme, and cosolute stocks. Despite all efforts, data quality could not be improved sufficiently. Thus, CD measurements have not been continued to this point.

Although the data provided here do not indicate a correlation between DNAzyme activity and the hydrodynamic radius of the DNAzyme:RNA complex, it is reasonable to believe that catalytically relevant residues within the catalytic core (Borggräfe *et al.*, 2021) are rearranged conformationally by molecular crowding, which would explain changes in activity. However, FCS and SAXS do not provide the resolution required for this purpose. In this regard, high resolution structural data is required prospectively to further rationalize our observations and shed light on the differences between Mn^{2+}- and Mg^{2+}-bound states. Such information is of great interest anyway, since the published NMR structure has been determined in absence of crowded conditions (Borggräfe *et al.*, 2021). Nonetheless, SAXS and FCS presented different advantages that made us choose both methods to obtain a very first glance at structural influences by molecular crowding, which we did successfully. FCS presented beneficial due to its short analysis time, high spatial and temporal resolution, and high sensitivity at the level of a single molecule. Moreover, small sample volume and low nanomolar construct concentrations are advantageous to minimize oligonucleotide usage (Yu *et al.*, 2021). Although SAXS measurements required a significantly higher complex concentration ($5\,g/mL$) compared to FCS, this method appeared advantageous as it provides structural information on a nanoscale level that allows to analyse liquid samples without the requirement of a crystal (Bauch and Rosenkranz, 2017). In addition, SAXS provides direct structural information and complements indirect information provided by FCS. To obtain high resolution structural information, applicable approaches include e. g. NMR spectroscopy or X-ray crystallography. Albeit, it has to be mentioned that both approaches turn out more difficult for the analysis of nucleic acids than for proteins. In NMR spectroscopy, the limited number of DNA and RNA building blocks restricts the resolution and dispersion of chemical shifts, which results in overlapping signals that impede spectra assignments (Al-Hashimi, 2013). But strategies, such as isotope labeling, advanced to address such issues (Plavec, 2022). Making use of X-ray crystallography, on the other hand, is challenged due to the negatively charged phosphate backbone of nucleic acids, which often results in crystals of poor long-range order. Here, promising progress has been made using NA-binding proteins as modules to facilitate NA crystallization, such as the U1A protein (Ferré-D'Amaré, 2016; Rosenbach *et al.*, 2020a). As additional approach, molecular dynamics (MD) simulations should be considered (Ostrowska *et al.*, 2019). Previous attempts that used MD simulations for crowding analyses include proteins (Feig *et al.*, 2017) and DNA duplexes (Hong *et al.*, 2020).

Altogether, this thesis is able to provide first information that the activity of the 10-23 DNAzyme is impacted by a crowded surrounding. Yet, we are convinced that several other physicochemical properties of a cell-like environment determine DNAzyme performance as well, which require exploring to gain a deeper understanding.

6.2 Antiviral potential of the 10-23 DNAzyme

As molecular crowding is an universal phenomenon, though it will most likely appear in different degrees depending on the respective cell type and composition, understanding its potential to influence biocatalysis is of great interest far beyond applications on humans. Hence, overcoming *in vivo* limitations may also trigger the use of DNAzymes in other fields. To this day, research on DNAzymes that aims for a therapeutic use focuses, amongst others (Yan *et al.*, 2023a), on cancer-associated genes (e. g. Shen *et al.*, 2013; Cho *et al.*, 2013), viral infections (e. g. Xie *et al.*, 2006; Reyes-Gutiérrez and Alvarez-Salas, 2009), and cardiovascular (Iversen *et al.*, 2001) or central nervous system diseases (Mastroyiannopoulos *et al.*, 2010) that threaten humans. In biosensing, a second field of interest, a majority of DNAzyme designs aims for the detection of metal ions that are predominantly assigned as environmental threat (Zhou *et al.*, 2017b, section 1.3.3). Recent applications also involve the detection of pathogenic bacteria (Ma *et al.*, 2021), which proved to be advantageous for the monitoring of food contaminations (Yousefi *et al.*, 2018). In this thesis, fish farming as one part of global food supply is suggested to profit from the potential of RNA-cleaving DNAzymes (Chapter 5). Although first reports emerged that include DNAzyme-based biosensors to detect plant (Wang *et al.*, 2019b) or fish (Gu *et al.*, 2019) pathogens, the use of RNA-cleaving DNAzymes as a preventive or therapeutic measure against viral infections in such has not been reported so far. Since aquaculture faces the challenge of insufficient options to eliminate the dissemination of aquatic viral infections (Kibenge, 2019), the need for alternatives is emphasized. In a collaboration project, one of the most concerning fish pathogens, the VHSV, is selected as target virus, to which no widely approved treatment is available (World Organisation for Animal Health (OIE), 2021). In this part of this thesis, the design of stable and active DNAzymes is the main goal. The design of 10-23 DNAzymes led to the selection of three candidates Dz137, Dz612, and Dz1063 (Figure 5.2), which were tested for stability and activity at 15 °C, the optimum temperature for VHSV replication. Urea-PAGE-based assays revealed that all candidates are stable and perform site-specific cleavage, which excludes undesired site reactions (Figure 5.3). Initial time-resolved assays in 50 mM Tris-HCl, pH 7.5 and 0.5 mM $MgCl_2$ highlighted Dz1063 to be the most active candidate with an approximate rate constant of $0.000\,89\,s^{-1}$ (Figure 5.4). Herewith, for the first time, I provide three potential DNAzymes that are able to bind and cleave VHSV-RNA, but require further analyses prior to tests in cell culture. In this regard, incorporation of modifications (Section 1.4.2) is considered to counteract known *in vivo* limitations, such as biostability, in early stages of exploring the potential of DNAzymes in fish farming.

Based on our results, another sector we recommend exploring, in which the high target affinity, cleavage-site specificity, and low cytotoxicity of DNAzymes (Xiao *et al.*, 2023) may present beneficial, is agriculture. As mentioned before, there have been no reports so far, in which DNAzymes have been used therapeutically on plants. In plants, viral infections also are a major threat, affecting their metabolism, appearance, and consequently yield, which already led to severe economic losses (Anikina *et al.*, 2023; Tatineni and Hein, 2023; Nagaraja *et al.*, 2021). Even though various strategies that aim at viral resistance have evolved over time, such as genome editing, immunization or thermotherapy, long-term efficiency, phytotoxicity, and social controversies towards transgenic plants portray some of the challenges (Rubio *et al.*, 2020; Anikina *et al.*, 2023). Thus, RNA-cleaving DNAzymes may provide an alternative. Here, viruses of interest with a worldwide distribution may be the *Maize Dwarf Mosaic Virus* (MDMV, Kannan *et al.*, 2018) or the *Cucumber Mosaic Virus* (CMV, Jacquemond, 2012).

In comparison to DNAzyme-based applications on human cells, however, the potential use of DNAzymes in plants or fish includes new features that require examination prior. For example, humans are homoiotherm, thus their body temperature is maintained within a range of $\sim 37\,^{\circ}\mathrm{C}$, regardless of the environment's temperature. On the contrary, plants and fish are exposed to a variety of temperatures throughout the year, at which for example the body temperature of fish as poikilothermic animals adapts to the water's temperature (Clausen, 1934; Sokolova, 2008). Thus, a pool of DNAzymes that contains a variety of optimum temperatures to perform cleavage would most likely be required. In addition, concepts of application have to be evaluated, for instance on the surface of plants, in water or soil, or in fish. If spread in water or soil, DNAzymes must not harm other organisms or the environment. If considering, for example, a surface-based application on plants, the photostability of DNAzymes in presence of sunlight-based ultraviolet (UV) radiation needs to be investigated, as UV light is known to cause nucleic acid damage (Roy, 2017; Wurtmann and Wolin, 2009).

With regard to therapeutic applications against human pathogens, I was involved in the design of 10-23 DNAzymes against the human immunodeficiency virus type 1 (HIV-1, data not shown). HIV attacks CD4 cells of the immune system and can lead, if untreated, to acquired immunodeficiency syndrome (AIDS, Justiz Vaillant and Gulick, 2022). Even though symptoms associated with HIV infections and AIDS have been able to be decelerated or suppressed by the use of antiretroviral drugs (Justiz Vaillant and Gulick, 2022; Seitz, 2016), we aim to exploit the promising properties and advances in knowledge of RNA-cleaving DNAzymes as well as modifications against HIV. Here to mention, none of the DNAzymes in clinical trials include a variant targeting HIV. So far, known reports of DNAzymes in connection with cleaving HIV-RNA include: Dash and Banerjea (2004); Jakobsen *et al.* (2007); Sugiyama *et al.* (2010); Singh *et al.* (2012). To begin with, Dash and Banerjea designed 10-23 DNAzymes that target the most conserved regions in the HIV genome that code for the p24 group-specific antigen (Gag) and negative regulating factor (Nef) protein (Dash and Banerjea, 2004). The p24 Gag is the capsid protein, which is involved in virion–host cell interactions (Rossi *et al.*, 2021), and the Nef protein influences, amongst others, viral replication (Seitz, 2016). The authors report on active variants that are able to perform cleavage at cellular relevant Mg^{2+} concentrations (Dash and Banerjea, 2004). In a different approach, Jakobsen *et al.* chose the 5'-UTR of the HIV genome as target sequence, which contains several functional elements. DNAzymes were tested unmodified and LNA-modified (LNAzymes, see section 1.4.2) *in vitro* and *in vivo*. The comparison of different nucleic acid constructs revealed LNAzymes to be the most effective in RNA knockdown, despite facing significant cell toxicity as side effect (Jakobsen *et al.*, 2007). Singh *et al.*, on the other hand, used the mRNA of the HIV integrase as target sequence, which is responsible for integrating the proviral genome into the human genome (Singh *et al.*, 2012). Two of the three selected candidates were found highly active *in vitro* and provided sufficient inhibition of gene expression *in vivo* (Singh *et al.*, 2012). Lastly, Sugiyama *et al.* describe HIV-1 reverse transcription-dependent lentiviral vector-transduced DNAzymes to inhibit viral replication (Sugiyama *et al.*, 2010). The RNA sequence of the envelope (*env*) reading frame was used as target, which codes for proteins crucial in virus-to-cell-attachment. DNAzymes were designed based on the 10-23 variant and were found active as well as able to inhibit HIV replication in cell culture (Sugiyama *et al.*, 2010).

In our approach, 10-23 DNAzymes were designed based on an infectious cDNA clone of HIV-1, pNL4-3 (GenBank AC M19921, Adachi *et al.*, 1986). The entire sequence of the *gag* polyprotein gene, which includes coding sequences for the inner structural proteins (capsid, matrix, and nucleoprotein and p6 *gag*, Seitz, 2016; Waheed and Freed, 2012), was

used as target. Herewith, the intend is to aim at multiple sites at once. The design was carried out using the script by Steger and Victor (2022), which is based on RNAPLFOLD (see section 5.2.1). Candidates were selected according to a desired melting temperature T_m of 37 °C, the average body temperature of humans (Mäkinen and Jussila, 2014). In addition, the experimentally determined structure of the HIV-1 genome (Watts *et al.*, 2009) was taken into account to compare predictions regarding cleavage site accessibility. Moreover, this comparison facilitates the selection of DNAzymes that are potentially better suited to perform cleavage in presence of full-length mRNA. Subsequently, the three DNAzymes Dz502, Dz513, and Dz1274, which are named according to their cleavage position within the RNA sequence, were tested towards stability and activity using urea-PAGE (see section 5.2.3, 5.2.4). Complementary RNA substrates were of 19 nt in length. All three demonstrated sufficient stability and site specific-cleavage activity under near physiological conditions (50 mM Tris-HCl, pH 7.5, 100 mM NaCl, and 0.5 mM $MgCl_2$) at 37 °C. Time-resolved assays and relative quantification highlighted Dz502 to be the most active under the tested conditions ($\sim$ 84 % of cleaved RNA), which presented an approximate rate constant of $0.00053\,s^{-1}$. With this, I was able to obtain three different DNAzymes that may have the potential to target HIV. As mentioned for the VHSV-DNAzymes, future analyses will include chemically modified versions of the selected candidates and tests in presence of longer RNA substrates to approximate cell conditions and evaluate their potential for *in vivo* tests.

7

BIBLIOGRAPHY

Achenbach J, Chiuman W, Cruz R, Li Y. DNAzymes: From Creation In Vitro to Application In Vivo. Curr Pharm Biotechnol. 2005; 5(4):321–336. doi: 10.2174/1389201043376751.

Adachi A, Gendelman HE, Koenig S, Folks T, Willey R, Rabson A, Martin MA. Production of acquired immunodeficiency syndrome-associated retrovirus in human and nonhuman cells transfected with an infectious molecular clone. Journal of Virology. 1986; 59(2):284–291. doi: 10.1128/jvi.59.2.284-291.1986.

Adams MS, Znosko BM. Thermodynamic characterization and nearest neighbor parameters for RNA duplexes under molecular crowding conditions. Nucleic Acids Res. 2019; 47(7):3658–3666. doi: 10.1093/nar/gkz019.

Akhtar S, Hughes MD, Khan A, Bibby M, Hussain M, Nawaz Q, Double J, Sayyed P. The delivery of antisense therapeutics. Adv Drug Deliv Rev. 2000; 44(1):3–21. doi: 10.1016/S0169-409X(00)00080-6.

Al-Hashimi HM. NMR studies of nucleic acid dynamics. Journal of Magnetic Resonance. 2013; 237:191–204. doi: 10.1016/j.jmr.2013.08.014.

Ali MM, Aguirre SD, Lazim H, Li Y. Fluorogenic DNAzyme probes as bacterial indicators. Angew Chemie - Int Ed. 2011; 50(16):3751–3754. doi: 10.1002/anie.201100477.

Ali MM, Brown CL, Jahanshahi-Anbuhi S, Kannan B, Li Y, Filipe CDM, Brennan JD. A Printed Multicomponent Paper Sensor for Bacterial Detection. Sci Rep. 2017; 7(1):1–10. doi: 10.1038/s41598-017-12549-3.

Ammayappan A, Vakharia VN. Molecular characterization of the great lakes viral hemorrhagic septicemia virus (VHSV) isolate from USA. Virol J. 2009; 6:1–16. doi: 10.1186/1743-422X-6-171.

Anikina I, Kamarova A, Issayeva K, Issakhanova S, Mustafayeva N, Insebayeva M, Mukhamedzhanova A, Khan SM, Ahmad Z, Lho LH, Han H, Raposo A. Plant protection from virus: a review of different approaches. Frontiers in Plant Science. 2023; 14:1–12. doi: 10.3389/fpls.2023.1163270.

Baillon L, Mérour E, Cabon J, Louboutin L, Vigouroux E, Alencar ALF, Cuenca A, Blanchard Y, Olesen NJ, Panzarin V, Morin T, Brémont M, Biacchesi S. The Viral Hemorrhagic Septicemia Virus (VHSV) Markers of Virulence in Rainbow Trout (Oncorhynchus mykiss). Front Microbiol. 2020; 11(October):1–17. doi: 10.3389/fmicb.2020.574231.

Balmer BF, Getchell RG, Powers RL, Lee J, Zhang T, Jung ME, Purcell MK, Snekvik K, Aguilar HC. Broad-spectrum antiviral JL122 blocks infection and inhibits transmission of aquatic rhabdoviruses. Virology. 2018; 525(September):143–149. doi: 10.1016/j.virol.2018.09.009.

Barnwal S, Jha G, Sola SC, Anand P, Shariff SY. Creutzfeldt-Jakob Disease: A Case Report and Literature Review for Understanding the Big Picture. Cureus. 2022; 14(11):9–14. doi: 10.7759/cureus.31303.

Bauch J, Rosenkranz R. SAXS - Röntgenkleinwinkelstreuung. In: *Physikalische Werkstoffdiagnostik* Springer Berlin Heidelberg; 2017.p. 54–55. doi: 10.1007/978-3-662-53952-1_27.

Baum DA, Silverman SK. Deoxyribozymes: Useful DNA catalysts in vitro and in vivo. Cell Mol Life Sci. 2008; 65(14):2156–2174. doi: 10.1007/s00018-008-8029-y.

Beaucage SL, Caruthers MH. Deoxynucleoside phosphoramidites-A new class of key intermediates for deoxypolynucleotide synthesis. Tetrahedron Lett. 1981; 22(20):1859–1862. doi: 10.1016/S0040-4039(01)90461-7.

Beckert B, Masquida B. Synthesis of RNA by In Vitro Transcription. In: *Methods in Molecular Biology* Humana Press; 2010.p. 29–41. doi: 10.1007/978-1-59745-248-9_3.

Benny P, Raghunath M. Making microenvironments : A look into incorporating macromolecular crowding into in vitro experiments , to generate biomimetic microenvironments which are capable of directing cell function for tissue engineering applications. J Tissue Eng. 2017; 8:1–8. doi: 10.1177/2041731417730467.

Benson VL, Khachigian LM, Lowe HC. DNAzymes and cardiovascular disease. Br J Pharmacol. 2008; 154(4):741–748. doi: 10.1038/bjp.2008.145.

Bernhart SH, Hofacker IL, Stadler PF. Local RNA base pairing probabilities in large sequences. Bioinformatics. 2006; 22(5):614–615. doi: 10.1093/bioinformatics/btk014.

Bhagavan NV. Three-Dimensional Structure of Proteins. In: *Med. Biochem.*, 4 ed. Academic Press; 2002.p. 51–65. doi: 10.1016/B978-012095440-7/50006-8.

Biehl R. Jscatter, a program for evaluation and analysis of experimental data. PLOS One. 2019; 14:e0218789. doi: 10.1371/journal.pone.0218789.

Blose JM, Pabit SA, Meisburger SP, Li L, Jones CD, Pollack L. Effects of a Protecting Osmolyte on the Ion Atmosphere Surrounding DNA Duplexes. Biochemistry. 2011; 50(40):8540–8547. doi: 10.1021/bi200710m, pMID: 21882885.

Borggräfe J, Gertzen CGW, Viegas A, Gohlke H, Etzkorn M. The architecture of the 10-23 DNAzyme and its implications for DNA-mediated catalysis. FEBS J. 2023; 290(8):2011–2021. doi: 10.1111/febs.16698.

Borggräfe J, Victor J, Rosenbach H, Viegas A, Gertzen C, Wuebben C, Kovacs H, Gopalswamy M, Riesner D, Steger G, Schiemann O, Gohlke H, Span I, Etzkorn M. Time-resolved structural analysis of an RNA-cleaving DNA catalyst. Nature. 2021; 601(January):144–149.

Bownik A, Stępniewska Z. Ectoine as a promising protective agent in humans and animals. Archives of Industrial Hygiene and Toxicology. 2016; 67:260–265. doi: 10.1515/aiht-2016-67-2837.

Breaker RR, Emilsson GM, Lazarev D, Nakamura S, Puskarz IJ, Roth A, Sudarsan N. A common speed limit for RNA-cleaving ribozymes and deoxyribozymes. RNA. 2003; 9(8):949–957. doi: 10.1261/rna.5670703.

Breaker RR, Joyce GF. A DNA enzyme that cleaves RNA. Chem Biol. 1994; 1(4):223–229. doi: 10.1016/1074-5521(94)90014-0.

Breaker RR, Joyce GF. A DNA enzyme with Mg^{2+}-dependent RNA phosphoesterase activity. Chem Biol. 1995; 2(10):655–660. doi: 10.1016/1074-5521(95)90028-4.

Brucka-Jastrzêbska E, Kawczuga D. Level of magnesium in tissues and organs of freshwater fish. Journal of Elementology. 2011; 16(1):7–19. doi: 10.5601/jelem.2011.16.1.7-20.

Büeler H, Aguzzi A, Sailer A, Greiner RA, Autenried P, Aguet M, Weissmann C. Mice devoid of PrP are resistant to scrapie. Cell. 1993; 73(7):1339–1347. doi: 10.1016/0092-8674(93)90360-3.

Cai S, Chen X, Chen H, Zhang Y, Wang X, Zhou N. A fluorescent aptasensor for ATP based on functional DNAzyme/walker and terminal deoxynucleotidyl transferase-assisted formation of DNA-AgNCs. Analyst. 2023; 148(4):799–805. doi: 10.1039/d2an02006h.

Cairns MJ, Hopkins TM, Witherington C, Sun LQ. The influence of arm length asymmetry and base substitution on the activity of the 10-23 DNA enzyme. Antisense Nucleic Acid Drug Dev. 2000; 10(5):323–332. doi: 10.1089/oli.1.2000.10.323.

Cano I, Santos EM, Moore K, Farbos A, van Aerle R. Evidence of Transcriptional Shutoff by Pathogenic Viral Haemorrhagic Septicaemia Virus in Rainbow Trout. Viruses. 2021; 13(6). doi: 10.3390/v13061129.

Cao Y, Yang L, Jiang W, Wang X, Liao W, Tan G, Liao Y, Qiu Y, Feng D, Tang F, Hou BL, Zhang L, Fu J, He F, Liu X, Jiang W, Yang T, Sun LQ. Therapeutic evaluation of epstein-barr virus-encoded latent membrane protein-1 targeted DNAzyme for treating of nasopharyngeal carcinomas. Mol Ther. 2014; 22(2):371–377. doi: 10.1038/mt.2013.257.

Carmi N, Balkhi SR, Breaker RR. Cleaving DNA with DNA. Proc Natl Acad Sci U S A. 1998; 95(5):2233–2237. doi: 10.1073/pnas.95.5.2233.

Caruthers MH. The chemical synthesis of DNA/RNA: Our gift to science. J Biol Chem. 2013; 288(2):1420–1427. doi: 10.1074/jbc.X112.442855.

Cech TR, Zaug AJ, Grabowski PJ. In vitro splicing of the ribosomal RNA precursor of tetrahymena: Involvement of a guanosine nucleotide in the excision of the intervening sequence. Cell. 1981; 27(3):487–496. doi: 10.1016/0092-8674(81)90390-1.

Cepeda-Plaza M, McGhee CE, Lu Y. Evidence of a General Acid-Base Catalysis Mechanism in the 8-17 DNAzyme. Biochemistry. 2018; 57(9):1517–1522. doi: 10.1021/acs.biochem.7b01096.

Cepeda-Plaza M, Peracchi A. Insights into DNA catalysis from structural and functional studies of the 8-17 DNAzyme. Org Biomol Chem. 2020; 18:1697–1709. doi: 10.1039/C9OB02453K.

Chakravarthy M, Aung-Htut MT, Le BT, Veedu RN. Novel Chemically-modified DNAzyme targeting Integrin alpha-4 RNA transcript as a potential molecule to reduce inflammation in multiple sclerosis. Sci Rep. 2017; 7(1):1–8. doi: 10.1038/s41598-017-01559-w.

Chandra M, Silverman SK. DNA and RNA can be equally efficient catalysts for carbon-carbon bond formation. J Am Chem Soc. 2008; 130(10):2936–2937. doi: 10.1021/ja7111965.

Chandrasekar J, Silverman SK. Catalytic DNA with phosphatase activity. Proc Natl Acad Sci U S A. 2013; 110:5315–5320. doi: 10.1073/pnas.1221946110.

Cheng Y, Korolev N, Nordenskiöld L. Similarities and differences in interaction of K^+ and Na^+ with condensed ordered DNA. A molecular dynamics computer simulation study. Nucleic Acids Res. 2006; 34(2):686–696. doi: 10.1093/nar/gkj434.

Cheng Z, Wei J, Gu L, Zou L, Wang T, Chen L, Li Y, Yang Y, Li P. DNAzyme-based biosensors for mercury (II) detection: Rational construction, advances and perspectives. J Hazard Mater. 2022; 431(March):128606. doi: 10.1016/j.jhazmat.2022.128606.

Chery J. RNA therapeutics: RNAi and antisense mechanisms and clinical applications. Postdoc J. 2016; 4(7):35–50. doi: 10.14304/surya.jpr.v4n7.5.

Cheung MS, Klimov D, Thirumalai D. Molecular crowding enhances native state stability and refolding rates of globular proteins. Proc Natl Acad Sci U S A. 2005; 102(13):4753–4758. doi: 10.1073/pnas.0409630102.

Chiba K, Yamaguchi T, Obika S. Development of 8–17 XNAzymes that are functional in cells. Chem Sci. 2023; 14(28). doi: 10.1039/d3sc01928d.

Chinnapen DJF, Sen D. A deoxyribozyme that harnesses light to repair thymine dimers in DNA. Proc Natl Acad Sci U S A. 2004; 101(1):65–69. doi: 10.1073/pnas.0305943101.

Cho EA, Moloney FJ, Cai H, Au-Yeung A, China C, Scolyer RA, Yosufi B, Raftery MJ, Deng JZ, Morton SW, Hammond PT, Arkenau HT, Damian DL, Francis DJ, Chesterman CN, Barnetson RSC, Halliday GM, Khachigian LM. Safety and tolerability of an intratumorally injected DNAzyme, Dz13, in patients with nodular basal-cell carcinoma: A phase 1 first-in-human trial (DISCOVER). Lancet. 2013; 381(9880):1835–1843. doi: 10.1016/S0140-6736(12)62166-7.

Cho SY, Protzman RA, Kim YO, Vaidya B, Oh MJ, Kwon J, Kim D. Elucidation of mechanism for host response to VHSV infection at varying temperatures in vitro and in vivo through proteomic analysis. Fish Shellfish Immunol. 2019; 88(August 2018):244–253. doi: 10.1016/j.fsi.2019.02.037.

Christiansen A, Wang Q, Cheung MS, Wittung-Stafshede P. Effects of macromolecular crowding agents on protein folding in vitro and in silico. Biophys Rev. 2013; 5(2). doi: 10.1007/s12551-013-0108-0.

Christopher A, Kaur R, Kaur G, Kaur A, Gupta V, Bansal P. MicroRNA therapeutics: Discovering novel targets and developing specific therapy. Perspect Clin Res. 2016; 7(2):68. doi: 10.4103/2229-3485.179431.

Cieslak M, Mikkelsen SS, Skall HF, Baud M, Diserens N, Engelsma MY, Haenen OLM, Mousakhani S, Panzarin V, Wahli T, Olesen NJ, Schütze H. Phylogeny of the viral hemorrhagic septicemia virus in European aquaculture. PLOS One. 2016; 11(10):1–18. doi: 10.1371/journal.pone.0164475.

Cino EA, Karttunen M, Choy WY. Effects of Molecular Crowding on the Dynamics of Intrinsically Disordered Proteins. PLOS One. 2012; 7(11). doi: 10.1371/journal.pone.0049876.

Clark DP, Pazdernik NJ, McGehee MR. Viruses, Viroids, and Prions. In: Clark DP, Pazdernik NJ, McGehee MR, editors. *Molecular Biology*, 3 ed. Academic Press; 2019.p. 749–792. doi: 10.1016/b978-0-12-813288-3.00024-0.

Clausen RG. Body Temperature of Fresh Water Fishes. Ecology. 1934; 15(2):139–144. doi: 10.2307/1932783.

Cortés-Guajardo C, Rojas-Hernández F, Paillao-Bustos R, Cepeda-Plaza M. Hydrated metal ion as a general acid in the catalytic mechanism of the 8-17 DNAzyme. Org Biomol Chem. 2021; 19(24):5395–5402. doi: 10.1039/d1ob00366f.

Cramer ER, Starcovic SA, Avey RM, Kaya AI, Robart AR. Structure of a 10-23 deoxyribozyme exhibiting a homodimer conformation. Commun Chem. 2023; 6:119. doi: 10.1038/s42004-023-00924-3.

Crooke ST. Molecular Mechanisms of Antisense Oligonucleotides. Nucleic Acid Ther. 2017; 27(2):70–77. doi: 10.1089/nat.2016.0656.

Cuenoud B, Szostak JW. A DNA metalloenzyme with DNA ligase activity. Nature. 1995; 375(6532):611–614. doi: 10.1038/375611a0.

Culbertson MC, Temburnikar KW, Sau SP, Liao JY, Bala S, Chaput JC. Evaluating TNA stability under simulated physiological conditions. Bioorganic Med Chem Lett. 2016; 26(10):2418–2421. doi: 10.1016/j.bmcl.2016.03.118.

Dadar M. Viral Hemorrhagic Septicemia Disease. In: Ennaji MM, editor. *Emerging and Reemerging Viral Pathogens* Academic Press; 2020.p. 705–715. doi: 10.1016/b978-0-12-819400-3.00031-4.

Damha MJ, Wilds CJ, Noronha A, Brukner I, Borokow G, Arion D, Parniak MA. Hybrids of RNA and arabinonucleic acids (ANA and 2' F-ANA) are substrates of ribonuclease H. J Am Chem Soc. 1998; 120(51):13545. doi: 10.1021/ja985535v.

Dana H, Chalbatani GM, Mahmoodzadeh H, Gharagouzlo E, Karimloo R, Rezaiean O, Moradzadeh A, Mazraeh A, Marmari V, Rashno MM, Mehmandoost N, Moazzen F, Ebrahimi M, Abadi SJ. Molecular Mechanisms and Biological Functions of siRNA. Int J Biomed Sci. 2017; 13(2):48–57. doi: 10.59566/ijbs.2017.13048.

Darty K, Denise A, Ponty Y. VARNA: Interactive drawing and editing of the RNA secondary structure. Bioinformatics. 2009; 25(15):1974–1975. doi: 10.1093/bioinformatics/btp250.

DasGupta S. Molecular crowding and RNA catalysis. Org Biomol Chem. 2020; 18(39):7724–7739. doi: 10.1039/d0ob01695k.

DasGupta S, Zhang S, Szostak JW. Molecular crowding facilitates ribozyme-catalyzed RNA assembly. ACS Cent Sci. 2023; 9:1670–1678. doi: 10.1021/acscentsci.3c00547.

Dash BC, Banerjea AC. Sequence-Specific Cleavage Activities of DNA Enzymes Targeted Against HIV-1 Gag and Nef Regions. Oligonucleotides. 2004; 14(1):41–47. doi: 10.1089/154545704322988049.

Denisov AY, Noronha AM, Wilds CJ, Trempe JF, Pon RT, Gehring K, Damha MJ. Solution structure of an arabinonucleic acid (ANA)/RNA duplex in a chimeric hairpin: Comparison with 2'-fluoro-ANA/RNA and DNA/RNA hybrids. Nucleic Acids Res. 2001; 29(21):4284–4293. doi: 10.1093/nar/29.21.4284.

Desai R, Kilburn D, Lee HT, Woodson SA. Increased ribozyme activity in crowded solutions. J Biol Chem. 2014; 289(5):2972–2977. doi: 10.1074/jbc.M113.527861.

Devanand K, Selser JC. Asymptotic behavior and long-range interactions in aqueous solutions of poly(ethylene oxide). Macromolecules. 1991; 24(22):5943–5947. doi: 10.1021/ma00022a008.

Dhuri K, Bechtold C, Quijano E, Pham H, Gupta A, Vikram A, Bahal R. Antisense oligonucleotides: An emerging area in drug discovery and development. J Clin Med. 2020; 9(6):1–24. doi: 10.3390/JCM9062004.

Doudna JA, Cech TR. The chemical repertoire of natural ribozymes. Nature. 2002; 418(6894):222–228. doi: 10.1038/418222a.

Dupuis NF, Holmstrom ED, Nesbitt DJ. Molecular-crowding effects on single-molecule RNA folding/unfolding thermodynamics and kinetics. Proc Natl Acad Sci U S A. 2014; 111(23):8464–8469. doi: 10.1073/pnas.1316039111.

Egli M, Manoharan M. Chemistry, structure and function of approved oligonucleotide therapeutics. Nucleic Acids Res. 2023; 51(6):2529–2573. doi: 10.1093/nar/gkad067.

Ekland EH, Bartel DP. RNA-catalysed RNA polymerization using nucleoside triphosphates. Nature. 1996; 382(6589):373–376. doi: 10.1038/382373a0.

El-Murr N, Maurel MC, Rihova M, Vergne J, Hervé G, Kato M, Kawamura K. Behavior of a hammerhead ribozyme in aqueous solution at medium to high temperatures. Naturwissenschaften. 2012; 99(9):731–738. doi: 10.1007/s00114-012-0954-9.

Elani Y. Interfacing Living and Synthetic Cells as an Emerging Frontier in Synthetic Biology. Angew Chemie - Int Ed. 2021; 60(11):5602–5611. doi: 10.1002/anie.202006941.

Elani Y, Trantidou T, Wylie D, Dekker L, Polizzi K, Law RV, Ces O. Constructing vesicle-based artificial cells with embedded living cells as organelle-like modules. Sci Rep. 2018; 8(1):1–9. doi: 10.1038/s41598-018-22263-3.

Ellington AD, Szostak JW. Selection in vitro of single- stranded DNA molecules that fold into specific ligand binding structures. Nature. 1992; 355(5):850–852. doi: 10.1038/355850a0.

Ellis RJ, Minton AP. Join the crowd. Nature. 2003; 425:27–28. doi: 10.1038/425027a.

Ellis RJ, Minton AP. Protein aggregation in crowded environments. Biol Chem. 2006; 387(5):485–497. doi: 10.1515/BC.2006.064.

Emilsson GM, Nakamura S, Roth A, Breaker RR. Ribozyme speed limits. RNA. 2003; 9(8):907–918. doi: 10.1261/rna.5680603.

Escobar LE, Kurath G, Escobar-Dodero J, Craft ME, Phelps NBD. Potential distribution of the viral haemorrhagic septicaemia virus in the Great Lakes region. J Fish Dis. 2017; 40(1):11–28. doi: 10.1111/jfd.12490.

Etzkorn M, Span I. RNA-Processing DNAzymes. In: Barciszewski J, editor. *RNA Structure and Function*, vol. 14 Cham: Springer International Publishing; 2023.p. 629–643. doi: 10.1007/978-3-031-36390-0_28.

Faisal M, Shavalier M, Kim RK, Millard EV, Gunn MR, Winters AD, Schulz CA, Eissa A, Thomas MV, Wolgamood M, Whelan GE, Winton J. Spread of the emerging viral hemorrhagic septicemia virus strain, genotype IVb, in Michigan, USA. Viruses. 2012; 4(5):734–760. doi: 10.3390/v4050734.

Fantoni NZ, El-Sagheer AH, Brown T. A Hitchhiker's Guide to Click-Chemistry with Nucleic Acids. Chemical Reviews. 2021; 121(12):7122—7154. doi: 10.1021/acs.chemrev.0c00928.

Feig M, Yu I, Wang Ph, Nawrocki G, Sugita Y. Crowding in Cellular Environments at an Atomistic Level from Computer Simulations. J Phys Chem B. 2017; doi: 10.1021/acs.jpcb.7b03570.

Feigin L, Svergun DI. Structure analysis by small-angle X-ray and neutron scattering, vol. 1. Taylor GW, editor, Springer New York; 1987. doi: 10.1007/978-1-4757-6624-0.

Ferré-D'Amaré AR. Use of the U1A Protein to Facilitate Crystallization and Structure Determination of Large RNAs. In: *Nucleic Acid Crystallography* Springer New York; 2016.p. 67–76. doi: 10.1007/978-1-4939-2763-0_6.

Fiorini E, Börner R, Sigel RKO. Mimicking the in vivo environment - The effect of crowding on RNA and biomacromolecular folding and activity. CHIMIA. 2015; 69(4):207–212. doi: 10.2533/chimia.2015.207.

Flynn-Charlebois A, Wang Y, Prior TK, Rashid I, Hoadley KA, Coppins RL, Wolf AC, Silverman SK. Deoxyribozymes with 2'-5' RNA ligase activity. J Am Chem Soc. 2003; 125(9):2444–2454. doi: 10.1021/ja028774y.

Foffi G, Pastore A, Piazza F, Temussi PA. Macromolecular crowding: Chemistry and physics meet biology (Ascona, Switzerland, 10–14 June 2012). Phys Biol. 2013; 10(4):10–14. doi: 10.1088/1478-3975/10/4/040301.

Fokina AA, Chelobanov BP, Fujii M, Stetsenko DA. Delivery of therapeutic RNA-cleaving oligodeoxyribonucleotides (deoxyribozymes): from cell culture studies to clinical trials. Expert Opin Drug Deliv. 2017; 14(9):1077–1089. doi: 10.1080/17425247.2017.1266326.

Fokina AA, Meschaninova MI, Durfort T, Venyaminova AG, François JC. Targeting insulin-like growth factor I with 10-23 DNAzymes: 2'-O-methyl modifications in the catalytic core enhance mRNA cleavage. Biochemistry. 2012; 51(11):2181–2191. doi: 10.1021/bi201532q.

Fokina AA, Stetsenko DA, François JC. DNA enzymes as potential therapeutics: Towards clinical application of 10-23 DNAzymes. Expert Opin Biol Ther. 2015; 15(5):689–711. doi: 10.1517/14712598.2015.1025048.

Förster T. Delocalized excitation and excitation transfer. In: Sinaoglu O, editor. *Modern Quantum Chemitry*, vol. 3 New York: Academic Press Inc.; 1965.p. 93–137.

Freund N, Taylor AI, Arangundy-Franklin S, Subramanian N, Peak-Chew SY, Whitaker AM, Freudenthal BD, Abramov M, Herdewijn P, Holliger P. A two-residue nascent-strand steric gate controls synthesis of 2'-O-methyl- and 2'-O-(2-methoxyethyl)-RNA. Nat Chem. 2023; 15(1):91–100. doi: 10.1038/s41557-022-01050-8.

Fusco DD, Dinallo V, Marafini I, Figliuzzi MM, Romano B, Monteleone G. Antisense oligonucleotide: Basic concepts and therapeutic application in inflammatory bowel disease. Frontiers in Pharmacology. 2019; 10. doi: 10.3389/fphar.2019.00305.

Gadd T. Fish Rhabdoviruses - VIRAL HAEMORRHAGIC SEPTICAEMIA VIRUS (VHSV) AND PERCH RHABDOVIRUS (PRV): STUDY OF VIRAL STRAINS AND THE DISEASE EPIDEMIOLOGY IN FINLAND. Academic dissertation, University of Helsinki; 2013.

Gao A, Tang CX, He XW, Yin XB. Electrochemiluminescent lead biosensor based on GR-5 lead-dependent DNAzyme for $Ru(phen)_3^{2+}$ intercalation and lead recognition. Analyst. 2013; 138(1):263–268. doi: 10.1039/c2an36398d.

Gao J, Shimada N, Maruyama A. Enhancement of deoxyribozyme activity by cationic copolymers. Biomater Sci. 2015; 3(2):308–316. doi: 10.1039/c4bm00256c.

Garibyan L, Avashia N. Research Techniques Made Simple: Polymerase Chain Reaction (PCR). J Invest Dermatol. 2013; 133(3):1–8. doi: 10.2807/ese.18.04.20382-en.

Garn H, Renz H. GATA-3-specific DNAzyme — A novel approach for stratified asthma therapy. Eur J Immunol. 2017; 47(1):22–30. doi: 10.1002/eji.201646450.

Garver KA, Hawley LM, McClure CA, Schroeder T, Aldous S, Doig F, Snow M, Edes S, Baynes C, Richard J. Development and validation of a reverse transcription quantitative PCR for universal detection of viral hemorrhagic septicemia virus. Dis Aquat Organ. 2011; 95(2):97–112. doi: 10.3354/dao02344.

Gerber PP, Donde MJ, Matheson NJ, Taylor AI. XNAzymes targeting the SARS-CoV-2 genome inhibit viral infection. Nat Commun. 2022; 13(1):6716. doi: 10.1038/s41467-022-34339-w.

Ghosh S, Takahashi S, Ohyama T, Endoh T, Tateishi-Karimata H, Sugimoto N, Sugimoto N. Nearest-neighbor parameters for predicting DNA duplex stability in diverse molecular crowding conditions. Proc Natl Acad Sci U S A. 2020; 117(25):14194–14201. doi: 10.1073/pnas.1920886117.

Gilbert W. Origin of Life: The RNA world. Nature. 1986; 319:618. doi: 10.1038/319618a0.

Gnutt D, Ebbinghaus S. The macromolecular crowding effect - From in vitro into the cell. Biol Chem. 2016; 397(1):37–44. doi: 10.1515/hsz-2015-0161.

Gnutt D, Gao M, Brylski O, Heyden M, Ebbinghaus S. Excluded-volume effects in living cells. Angew Chemie - Int Ed. 2015; 54(8):2548–2551. doi: 10.1002/anie.201409847.

Gomez-Casado E, Estepa A, Coll JM. A comparative review on European-farmed finfish RNA viruses and their vaccines. Vaccine. 2011; 29(15):2657–2671. doi: 10.1016/j.vaccine.2011.01.097.

Gong L, Zhao Z, Lv YF, Huan SY, Fu T, Zhang XB, Shen GL, Yu RQ. DNAzyme-based biosensors and nanodevices. Chem Commun. 2015; 51(6):979–995. doi: 10.1039/c4cc06855f.

Gonzalez-Tello P, Camacho F, Blazquez G. Density and Viscosity of Concentrated Aqueous Solutions of Polyethylene Glycol. Journal of Chemical and Engineering Data. 1994; 39(3):611–614. doi: 10.1021/je00015a050.

Greulich T, Hohlfeld JM, Neuser P, Lueer K, Klemmer A, Schade-Brittinger C, Harnisch S, Garn H, Renz H, Homburg U, Renz J, Kirsten A, Pedersen F, Müller M, Vogelmeier CF, Watz H. A GATA3-specific DNAzyme attenuates sputum eosinophilia in eosinophilic COPD patients: A feasibility randomized clinical trial. Respir Res. 2018; 19(1):1–10. doi: 10.1186/s12931-018-0751-x.

Gruber AR, Bernhart SH, Lorenz R. The ViennaRNA Web Services. In: Picardi E, editor. *RNA Bioinformatics*, vol. 1269 New York, NY: Humana Press; 2015.p. 307–326. doi: 10.1007/978-1-4939-2291-8_19.

Gu L, Yan W, Wu H, Fan S, Ren W, Wang S, Lyu M, Liu J. Selection of DNAzymes for Sensing Aquatic Bacteria: Vibrio Anguillarum. Anal Chem. 2019; 91(12):7887–7893. doi: 10.1021/acs.analchem.9b01707.

Guerrier-Takada C, Gardiner K, Marsh T, Pace N, Altman S. The RNA moiety of ribonuclease P is the catalytic subunit of the enzyme. Cell. 1983; 35(3):849–857. doi: 10.1016/0092-8674(83)90117-4.

Guo Y, Chen J, Cheng M, Monchaud D, Zhou J, Ju H. A Thermophilic Tetramolecular G-Quadruplex/Hemin DNAzyme. Angew Chemie - Int Ed. 2017; 56(52):16636–16640. doi: 10.1002/anie.201708964.

Hall D, Minton AP. Macromolecular crowding: Qualitative and semiquantitative successes, quantitative challenges. Biochimica et Biophysica Acta (BBA) - Proteins and Proteomics. 2003; 1649(2):127–139. doi: 10.1016/S1570-9639(03)00167-5.

He S, Qu L, Shen Z, Tan Y, Zeng M, Liu F, Jiang Y, Li Y. Highly specific recognition of breast tumors by an RNA-cleaving fluorogenic DNAzyme probe. Anal Chem. 2015; 87(1):569–577. doi: 10.1021/ac5031557.

He X, Zhou X, Liu Y, Wang X. Ultrasensitive, recyclable and portable microfluidic surface-enhanced raman scattering (SERS) biosensor for uranyl ions detection. Sensors Actuators, B Chem. 2020; 311(October 2019):127676. doi: 10.1016/j.snb.2020.127676.

Hernández S, Porter C, Thang X, Wei Y, Bhattacharyya D. Layer-by-layer assembled membranes with immobilized porins. RSC Adv. 2017; 88(7):56123–56136. doi: 10.1039/c7ra08737c.

Higgs PG, Lehman N. The RNA World: Molecular cooperation at the origins of life. Nat Rev Genet. 2015; 16(1):7–17. doi: 10.1038/nrg3841.

Hingorani KS, Gierasch LM. Comparing protein folding in vitro and in vivo: Foldability meets the fitness challenge. Curr Opin Struct Biol. 2014; 24(1):81–90. doi: 10.1016/j.sbi.2013.11.007.

Hofacker IL, Fontana W, Stadler PF, Bonhoeffer LS, Tacker M, Schuster P. Fast folding and comparison of RNA secondary structures. Monatshefte für Chemie Chem Mon. 1994; 125(2):167–188. doi: 10.1007/BF00818163.

Höfling F, Franosch T. Anomalous transport in the crowded world of biological cells. Reports on Progress in Physics. 2013; 76(4):46602. doi: 10.1088/0034-4885/76/4/046602.

Hollenstein M. DNA catalysis: The chemical repertoire of DNAzymes. Molecules. 2015; 20(11):20777–20804. doi: 10.3390/molecules201119730.

Hollenstein M, Hipolito CJ, Lam CH, Perrin DM. A self-cleaving DNA enzyme modified with amines, guanidines and imidazoles operates independently of divalent metal cations (M^{2+}). Nucleic Acids Res. 2009; 37(5):1638–1649. doi: 10.1093/nar/gkn1070.

Hong F, Schreck JS, Šulc P. Understanding DNA interactions in crowded environments with a coarse-grained model. Nucleic Acids Research. 2020; 48(19):10726–10738. doi: 10.1093/nar/gkaa854.

Hong J, Capp MW, Anderson CF, Saecker RM, Felitsky DJ, Anderson MW, Record MT. Preferential interactions of glycine betaine and of urea with DNA: Implications for DNA hydration and for effects of these solutes on DNA stability. Biochemistry. 2004; 43(46):14744–14758. doi: 10.1021/bi049096q.

Horning DP, Joyce GF. Amplification of RNA by an RNA polymerase ribozyme. Proc Natl Acad Sci U S A. 2016; 113(35):9786–9791. doi: 10.1073/pnas.1610103113.

Hu B, Zhong L, Weng Y, Peng L, Huang Y, Zhao Y, Liang XJ. Therapeutic siRNA: state of the art. Signal Transduct Target Ther. 2020; 5(1). doi: 10.1038/s41392-020-0207-x.

Huang PJJ, Liu J. In vitro Selection of Chemically Modified DNAzymes. ChemistryOpen. 2020; 9(10):1046–1059. doi: 10.1002/open.202000134.

Hughes RA, Ellington AD. Synthetic DNA synthesis and assembly: Putting the synthetic in synthetic biology. Cold Spring Harb Perspect Biol. 2017; 9(1). doi: 10.1101/cshperspect.a023812.

Iversen PO, Nicolaysen G, Sioud M. DNA enzyme targeting TNF-α mRNA improves hemodynamic performance in rats with postinfarction heart failure. American Journal of Physiology-Heart and Circulatory Physiology. 2001; 281(5):H2211–H2217. doi: 10.1152/ajpheart.2001.281.5.h2211.

Jacquemond M. Cucumber Mosaic Virus. Adv Virus Res. 2012; 84:439–504. doi: 10.1016/b978-0-12-394314-9.00013-0.

Jakobsen MR, Haasnoot J, Wengel J, Berkhout B, Kjems J. Efficient inhibition of HIV-1 expression by LNA modified antisense oligonucleotides and DNAzymes targeted to functionally selected binding sites. Retrovirology. 2007; 4:1–13. doi: 10.1186/1742-4690-4-29.

Javadi-Zarnaghi F, Höbartner C. Strategies for Characterization of Enzymatic Nucleic Acids. In: Seitz H, Stahl F, Walter JG, editors. *Catalytically Active Nucleic Acids*, 1 ed. Springer Cham; 2020.p. 37–58. doi: 10.1007/978-3-030-29646-9.

Jijakli K, Khraiwesh B, Fu W, Luo L, Alzahmi A, Koussa J, Chaiboonchoe A, Kirmizialtin S, Yen L, Salehi-Ashtiani K. The in vitro selection world. Methods. 2016; 106(2016):3–13. doi: 10.1016/j.ymeth.2016.06.003.

Jonstrup SP, Gray T, Kahns S, Skall HF, Snow M, Olesen NJ. FishPathogens.eu/vhsv: A user-friendly viral haemorrhagic septicaemia virus isolate and sequence database. J Fish Dis. 2009; 32(11):925–929. doi: 10.1111/j.1365-2761.2009.01073.x.

Joyce GF. RNA cleavage by the 10-23 DNA enzyme. Methods Enzymol. 2001; 341:503–517. doi: 10.1016/S0076-6879(01)41173-6.

Joyce GF. Forty years of in vitro evolution. Angew Chemie - Int Ed. 2007; 46(34):6420–6436. doi: 10.1002/anie.200701369.

Justiz Vaillant AA, Gulick PG, HIV and AIDS Syndrome. StatPearls [Internet]; 2022. Accessed: (23.02.2024). https://www.ncbi.nlm.nih.gov/books/NBK534860/.

Kang H, Pincus PA, Hyeon C, Thirumalai D. Effects of macromolecular crowding on the collapse of biopolymers. Phys Rev Lett. 2015; 114(6):1–5. doi: 10.1103/PhysRevLett.114.068303.

Kang SY, Kang JY, Oh MJ. Antiviral activities of flavonoids isolated from the bark of Rhus verniciflua stokes against fish pathogenic viruses In Vitro. J Microbiol. 2012; 50(2):293–300. doi: 10.1007/s12275-012-2068-7.

Kannan M, Ismail I, Bunawan H. Maize Dwarf Mosaic Virus: From Genome to Disease Management. Viruses. 2018; 10(9):1–23. doi: 10.3390/v10090492.

Karnati HK, Yalagala RS, Undi R, Pasupuleti SR, Gutti RK. Therapeutic potential of siRNA and DNAzymes in cancer. Tumour Biol. 2014; 35:9505–21. doi: 10.1007/s13277-014-2477-9.

Kashani-Sabet M. Ribozyme therapeutics. J Investig Dermatology Symp Proc. 2002; 7(1):76–78. doi: 10.1046/j.1523-1747.2002.19642.x.

Kasprowicz A, Stokowa-Sołtys K, Jeżowska-Bojczuk M, Wrzesiński J, Ciesiołka J. Characterization of Highly Efficient RNA-Cleaving DNAzymes that Function at Acidic pH with No Divalent Metal-Ion Cofactors. ChemistryOpen. 2017; 6(1):46–56. doi: 10.1002/open.201600141.

Khan S, Rehman U, Parveen N, Kumar S, Baboota S, Ali J. siRNA therapeutics: insights, challenges, remedies and future prospects. Expert Opin Drug Deliv. 2023; 20(9):1167–1187. doi: 10.1080/17425247.2023.2251890.

Khan S, Burciu B, Filipe CDM, Li Y, Dellinger K, Didar TF. DNAzyme-Based Biosensors: Immobilization Strategies, Applications, and Future Prospective. ACS Nano. 2021; 15(9):13943–13969. doi: 10.1021/acsnano.1c04327.

Kibenge FS. Emerging viruses in aquaculture. Current Opinion in Virology. 2019; 34:97–103. doi: 10.1016/j.coviro.2018.12.008.

Kilburn D, Roh JH, Guo L, Briber RM, Woodson SA. Molecular Crowding Stabilizes Folded RNA Structure by the Excluded Volume Effect. J Am Chem Soc. 2010; 132(17):8690–8696. doi: 10.1021/ja101500g.

Kirchgässler N, Rosenbach H, Span I. Stability and Activity of the 10–23 DNAzyme Under Molecular Crowding Conditions. In: Steger G, Rosenbach H, Span I, editors. *DNAzymes*, vol. 2439 of Methods in Molecular Biology New York, NY: Humana; 2022.p. 79–89. doi: 10.1007/978-1-0716-2047-2_6.

Krug N, Hohlfeld JM, Buhl R, Renz J, Garn H, Renz H. Blood eosinophils predict therapeutic effects of a GATA3-specific DNAzyme in asthma patients. J Allergy Clin Immunol. 2017; 140(2):625–628.e5. doi: 10.1016/j.jaci.2017.02.024.

Krug N, Hohlfeld JM, Kirsten AM, Kornmann O, Beeh KM, Kappeler D, Korn S, Ignatenko S, Timmer W, Rogon C, Zeitvogel J, Zhang N, Bille J, Homburg U, Turowska A, Bachert C, Werfel T, Buhl R, Renz J, Garn H, *et al.* Allergen-Induced Asthmatic Responses Modified by a GATA3-Specific DNAzyme. New England Journal of Medicine. 2015; 372(21):1987–1995. doi: 10.1056/NEJMoa1411776, pMID: 25981191.

Kruger K, Grabowski PJ, Zaug AJ, Sands J, Gottschling DE, Cech TR. Self-splicing RNA: Autoexcision and autocyclization of the ribosomal RNA intervening sequence of tetrahymena. Cell. 1982; 31(1):147–157. doi: 10.1016/0092-8674(82)90414-7.

Kumar B, Rajput R, Pati DR, Khanna M. Potent Intracellular Knock-Down of Influenza A Virus M2 Gene Transcript by DNAzymes Considerably Reduces Viral Replication in Host Cells. Mol Biotechnol. 2015; 57(9):836–845. doi: 10.1007/s12033-015-9876-z.

Kumar S, Jain S, Dilbaghi N, Ahluwalia AS, Hassan AA, Kim KH. Advanced Selection Methodologies for DNAzymes in Sensing and Healthcare Applications. Trends Biochem Sci. 2019; 44(3):190–213. doi: 10.1016/j.tibs.2018.11.001.

Kurreck J. Antisense technologies: Improvement through novel chemical modifications. Eur J Biochem. 2003; 270(8):1628–1644. doi: 10.1046/j.1432-1033.2003.03555.x.

Kurz M. Compatible solute influence on nucleic acids: many questions but few answers. Saline Syst. 2008; 4(1):1–14. doi: 10.1186/1746-1448-4-6.

Kuznetsova IM, Turoverov KK, Uversky VN. What macromolecular crowding can do to a protein. Int J Mol Sci. 2014; 15(12):23090–23140. doi: 10.3390/ijms151223090.

Kypr J, Kejnovska I, Renciuk D, Vorlickova M. Circular dichroism and conformational polymorphism of DNA. Nucleic Acids Research. 2009; 37(6):1713–1725. doi: 10.1093/nar/gkp026.

Lakowicz JR. Principles of fluorescence spectroscopy. 3 ed. New York: Springer; 2006. doi: 10.1007/978-0-387-46312-4.

Larcher LM, Pitout IL, Keegan NP, Veedu RN, Fletcher S. DNAzymes: Expanding the potential of nucleic acid therapeutics. Nucleic Acid Ther. 2023; 33:178–192. doi: 10.1089/nat.2022.0066.

Leamy KA, Assmann SM, Mathews DH, Bevilacqua PC. Bridging the gap between in vitro and in vivo RNA folding . Q Rev Biophys. 2016; 49:1–26. doi: 10.1017/s003358351600007x.

Lee B, Bo Kim K, Oh S, Sig Choi J, Park JS, Min DH, Kim DE. Suppression of hepatitis C virus genome replication in cells with RNA-cleaving DNA enzymes and short-hairpin RNA. Oligonucleotides. 2010; 20(6):285–296. doi: 10.1089/oli.2010.0256.

Lewin AS, Hauswirth WW. Ribozyme gene therapy: Applications for molecular medicine. Trends Mol Med. 2001; 7(5):221–228. doi: 10.1016/S1471-4914(01)01965-7.

Li J, Lu Y. A Highly Sensitive and Selective Catalytic DNA Biosensor for Lead Ions. J Am Chem Soc. 2000; 122:10466–10467. doi: 10.1021/ja0021316.

Li Y, Sen D. A catalytic DNA for porphyrin metallation. Nat Struct Biol. 1996; 3(9):743–747. doi: 10.1038/nsb0996-743.

Li Y, Breaker RR. Phosphorylating DNA with DNA. Proc Natl Acad Sci U S A. 1999; 96(6):2746–2751. doi: 10.1073/pnas.96.6.2746.

Li Y, Liu Y, Breaker RR. Capping DNA with DNA. Biochemistry. 2000; 39(11):3106–3114. doi: 10.1021/bi992710r.

Lilley DMJ. Mechanisms of RNA catalysis. Philos Trans R Soc B Biol Sci. 2011; 366(1580):2910–2917. doi: 10.1098/rstb.2011.0132.

Linegar KL, Adeniran AE, Kostko AF, Anisimov MA. Hydrodynamic radius of polyethylene glycol in solution obtained by dynamic light scattering. Colloid J. 2010; 72(2):279–281. doi: 10.1134/S1061933X10020195.

Liu C, Sheng Y, Sun Y, Feng J, Wang S, Zhang J, Xu J, Jiang D. A glucose oxidase-coupled DNAzyme sensor for glucose detection in tears and saliva. Biosens Bioelectron. 2015; 70:455–461. doi: 10.1016/j.bios.2015.03.070.

Liu J, Lu Y. A colorimetric lead biosensor using DNAzyme-directed assembly of gold nanoparticles. J Am Chem Soc. 2003; 125(22):6642–6643. doi: 10.1021/ja034775u.

Liu J, Lu Y. Fluorescent DNAzyme Biosensors for Metal Ions Based on Catalytic Molecular Beacons. In: Didenko VV, editor. *Fluoresc. Energy Transf. Nucleic Acid Probes. Methods Mol. Biol.* Houston: Humana Press; 2006.p. 275–288. doi: 10.1385/1-59745-069-3:275.

Liu K, Lat PK, Yu HZ, Sen D. CLICK-17, a DNA enzyme that harnesses ultra-low concentrations of either Cu^{+} or Cu^{2+} to catalyze the azide-alkyne 'click' reaction in water. Nucleic Acids Res. 2020; 48(13):7356–7370. doi: 10.1093/nar/gkaa502.

Liu Y, Chen WR, Chen SH. Cluster formation in two-Yukawa fluids. The Journal of Chemical Physics. 2005; 122(4). doi: 10.1063/1.1830433.

Lorenz R, Bernhart SH, Höner zu Siederdissen C, Tafer H, Flamm C, Stadler PF, Hofacker IL. ViennaRNA Package 2.0. Algorithms Mol Biol. 2011; 6(26):1–14. doi: 10.1186/1748-7188-6-26.

Lorenzen N, LaPatra SE. DNA vaccines for aquacultured fish. Rev sci tech Off int Epiz. 2005; 24(1):201–213. doi: 10.20506/rst.24.1.1565.

Ma J, Bruce TJ, Jones EM, Cain KD. A review of fish vaccine development strategies: Conventional methods and modern biotechnological approaches. Microorganisms. 2019; 7(11). doi: 10.3390/microorganisms7110569.

Ma L, Liu J. Catalytic Nucleic Acids: Biochemistry, Chemical Biology, Biosensors, and Nanotechnology. iScience. 2020; 23(1):100815. doi: 10.1016/j.isci.2019.100815.

Ma L, Liu J. DNAzymes as Biosensors. In: Müller S, Masquida B, Winkler W, editors. *Ribozymes*, vol. 2, 1 ed. Wiley-VCH GmBH; 2021.p. 685–720. doi: 10.1002/9783527814527.ch27.

Ma X, Ding W, Wang C, Wu H, Tian X, Lyu M, Wang S. DNAzyme biosensors for the detection of pathogenic bacteria. Sensors Actuators, B Chem. 2021; 331(January):129422. doi: 10.1016/j.snb.2020.129422.

MacFarlane LA, R Murphy P. MicroRNA: Biogenesis, Function and Role in Cancer. Curr Genomics. 2010; 11(7):537–561. doi: 10.2174/138920210793175895.

Mäkinen H, Jussila K. Cold-protective clothing: types, design and standards. In: *Protective Clothing* Elsevier; 2014.p. 3–38. doi: 10.1533/9781782420408.1.3.

Mardoum WM, Gorczyca SM, Regan KE, Wu TC, Robertson-Anderson RM. Crowding induces entropically-driven changes to DNA dynamics that depend on crowder structure and ionic conditions. Front Phys. 2018; 6:1–20. doi: 10.3389/fphy.2018.00053.

Marroquí L, Estepa A, Perez L. Assessment of the inhibitory effect of ribavirin on the rainbow trout rhabdovirus VHSV by real-time reverse-transcription PCR. Vet Microbiol. 2007; 122(1-2):52–60. doi: 10.1016/j.vetmic.2007.01.002.

Martick M, Scott WG. Tertiary Contacts Distant from the Active Site Prime a Ribozyme for Catalysis. Cell. 2006; 126(2):309–320. doi: 10.1016/j.cell.2006.06.036.

Mastroyiannopoulos NP, Uney JB, Phylactou LA. The application of ribozymes and DNAzymes in muscle and brain. Molecules. 2010; 15(8):5460–5472. doi: 10.3390/molecules15085460.

Matteucci MD, Caruthers MH. Synthesis of deoxyoligonucleotides on an isotactic polymer support. J. 1981; 103:3185–3191. doi: 10.1080/10601327308060485.

McConnell EM, Cozma I, Mou Q, Brennan JD, Lu Y, Li Y. Biosensing with DNAzymes. Chem Soc Rev. 2021; 50(16):8954–8994. doi: 10.1039/d1cs00240f.

McGhee CE, Loh KY, Lu Y. DNAzyme sensors for detection of metal ions in the environment and imaging them in living cells. Curr Opin Biotechnol. 2017; 45:191–201. doi: 10.1016/j.copbio.2017.03.002.

Meseth U, Wohland T, Rigler R, Vogel H. Resolution of Fluorescence Correlation Measurements. Biophysical Journal. 1999; 76(3):1619–1631. doi: 10.1016/s0006-3495(99)77321-2.

Meyer S, Schröter MA, Hahn MB, Solomun T, Sturm H, Kunte HJ. Ectoine can enhance structural changes in DNA in vitro. Sci Rep. 2017; 7(1):1–10. doi: 10.1038/s41598-017-07441-z.

Mills DR, Peterson RL, Spiegelman S. An extracellular Darwinian experiment with a self-duplicating nucleic acid molecule. Proc Natl Acad Sci U S A. 1967; 58(1):217–224. doi: 10.1073/pnas.58.1.217.

Min D, Xue S, Li H, Yang W. 'In-line attack' conformational effect plays a modest role in an enzyme-catalyzed RNA cleavage: A free energy simulation study. Nucleic Acids Res. 2007; 35(12):4001–4006. doi: 10.1093/nar/gkm394.

Minchin S, Lodge J. Understanding biochemistry: Structure and function of nucleic acids. Essays Biochem. 2019; 63(4):433–456. doi: 10.1042/EBC20180038.

Minh DDL, Chang CE, Trylska J, Tozzini V, McCammon JA. The influence of macromolecular crowding on HIV-1 protease internal dynamics. J Am Chem Soc. 2006; 128(18):6006–6007. doi: 10.1021/ja060483s.

Minton AP. Confinement as a determinant of macromolecular structure and reactivity. Biophys J. 1992; 63(4):1090–1100. doi: 10.1016/S0006-3495(92)81663-6.

Minton AP. Excluded Volume as a Determinant of Macromolecular Structure and Reactivity. Biopolymers. 1981; 20(1):2093–2120. doi: 10.1016/S0006-3495(80)84917-4.

Minton AP. How can biochemical reactions within cells differ from those in test tubes? J Cell Sci. 2006; 119(14):2863–2869. doi: 10.1242/jcs.03063.

Mir M, Wang Z, Shen Z, Bednarz M, Bashir R, Golding I, Prasanth SG, Popescu G. Optical measurement of cycle-dependent cell growth. Proc Natl Acad Sci U S A. 2011; 108(32):13124–13129. doi: 10.1073/pnas.1100506108.

Miyoshi D, Sugimoto N. Molecular crowding effects on structure and stability of DNA. Biochimie. 2008; 90:1040–1051. doi: 10.1016/j.biochi.2008.02.009.

Model MA, Hollembeak JE, Kurokawa M. Macromolecular crowding: A hidden link between cell volume and everything else. Cell Physiol Biochem. 2021; 55(S1):25–40. doi: 10.33594/000000319.

Mohammadi-Arani R, Javadi-Zarnaghi F, Boccaletto P, Bujnicki JM, Ponce-Salvatierra A. DNAzymeBuilder, a web application for in situ generation of RNA/DNA-cleaving deoxyribozymes. Nucleic Acids Res. 2022; 50(W1):W261–W265. doi: 10.1093/nar/gkac269.

Montserrat Pagès A, Hertog M, Nicolaï B, Spasic D, Lammertyn J. Unraveling the Kinetics of the 10–23 RNA-Cleaving DNAzyme. International Journal of Molecular Sciences. 2023; 24(18):13686. doi: 10.3390/ijms241813686.

Morrison D, Rothenbroker M, Li Y. DNAzymes: Selected for Applications. Small Methods. 2018; 2(3):1–12. doi: 10.1002/SMTD.201700319.

Mugimba KK, Byarugaba DK, Mutoloki S, Evensen O, Munang'andu HM. Challenges and Solutions to Viral Diseases of Finfish in Marine Aquaculture. Pathogens. 2021; 10(6):1–21. doi: 10.3390/pathogens10060673.

Müller CB, Loman A, Pacheco V, Koberling F, Willbold D, Richtering W, Enderlein J. Precise measurement of diffusion by multi-color dual-focus fluorescence correlation spectroscopy. EPL (Europhysics Letters). 2008; 83(4):46001. doi: 10.1209/0295-5075/83/46001.

Müller S, Appel B, Balke D, Hieronymus R, Nübel C. Thirty-five years of research into ribozymes and nucleic acid catalysis: Where do we stand today? F1000Research. 2016; 5(0):1–11. doi: 10.12688/F1000RESEARCH.8601.1.

Mullis K, Faloona F, Scharf S, Saiki R, Horn G, Erlich H. Specific enzymatic amplification of DNA in vitro: the polymerase chain reaction. Cold Spring Harb Symp Quant Biol. 1986; 51:263–273. doi: 10.1101/sqb.1986.051.01.032.

Murade CU, Shubeita GT. A molecular sensor reveals differences in macromolecular crowding between the cytoplasm and nucleoplasm. ACS Sensors. 2019; 4(7):1835–1843. doi: 10.1021/acssensors.9b00569.

Müller BK, Zaychikov E, Bräuchle C, Lamb DC. Pulsed Interleaved Excitation. Biophysical Journal. 2005; 89(5):3508–3522. doi: 10.1529/biophysj.105.064766.

Nagaraja A, Chethana BS, Jain AK. Biotic stresses and their management. In: Singh M, Sood S, editors. *Millets and Pseudo Cereals* Woodhead Publishing Series in Food Science, Technology and Nutrition, Woodhead Publishing; 2021.p. 119–142. doi: 10.1016/b978-0-12-820089-6.00007-0.

Nakano Si, Horita M, Kobayashi M, Sugimoto N. Catalytic activities of ribozymes and DNAzymes in water and mixed aqueous media. Catalysts. 2017; 7(12):1–14. doi: 10.3390/catal7120355.

Nakano Si, Karimata H, Ohmichi T, Kawakami J, Sugimoto N. The effect of molecular crowding with nucleotide length and cosolute structure on DNA duplex stability. J Am Chem Soc. 2004; 126(44):14330–14331. doi: 10.1021/ja0463029.

Nakano Si, Karimata HT, Kitagawa Y, Sugimoto N. Facilitation of RNA enzyme activity in the molecular crowding media of cosolutes. J Am Chem Soc. 2009; 131(46):16881–16888. doi: 10.1021/ja9066628.

Nakano Si, Kitagawa Y, Karimata HT, Sugimoto N. Molecular crowding effect on metal ion binding properties of the hammerhead ribozyme. Nucleic Acids Symp Ser (Oxf). 2008; 52(1):519–520. doi: 10.1093/nass/nrn263.

Nakano Si, Kitagawa Y, Miyoshi D, Sugimoto N. Hammerhead ribozyme activity and oligonucleotide duplex stability in mixed solutions of water and organic compounds. FEBS Open Bio. 2014; 4:643–650. doi: 10.1016/j.fob.2014.06.009.

Nakano Si, Miyoshi D, Sugimoto N. Effects of molecular crowding on the structures, interactions, and functions of nucleic acids. Chem Rev. 2014; 114(5):2733–2758. doi: 10.1021/cr400113m.

Nakano Si, Sugimoto N. Model studies of the effects of intracellular crowding on nucleic acid interactions. Mol Biosyst. 2017; 13(1):32–41. doi: 10.1039/c6mb00654j.

Nakano Si, Yamaguchi D, Tateishi-Karimata H, Miyoshi D, Sugimoto N. Hydration changes upon DNA folding studied by osmotic stress experiments. Biophys J. 2012; 102(12):2808–2817. doi: 10.1016/j.bpj.2012.05.019.

Nakatani N, Sakuta H, Hayashi M, Tanaka S, Takiguchi K, Tsumoto K, Yoshikawa K. Specific spatial localization of actin and DNA in a water/water microdroplet: Self-emergence of a cell-like structure. ChemBioChem. 2018; 19(13):1370–1374. doi: 10.1002/cbic.201800066.

Nashimoto M. Correct folding of a ribozyme induced by nonspecific macromolecules. Eur J Biochem. 2000; 267(9):2738–2745. doi: 10.1046/j.1432-1327.2000.01294.x.

Nasir N, Al Ahmad M. Cells Electrical Characterization: Dielectric Properties, Mixture, and Modeling Theories. Journal of Engineering. 2020; 2020:1–17. doi: 10.1155/2020/9475490.

Nedorezova DD, Fakhardo AF, Molden TA, Kolpashchikov DM. Deoxyribozyme-Based DNA Machines for Cancer Therapy. ChemBioChem. 2020; 21(5):607–611. doi: 10.1002/cbic.201900525.

Nelson KE, Bruesehoff PJ, Lu Y. In vitro selection of high temperature Zn^{2+}-dependent DNAzymes. J Mol Evol. 2005; 61(2):216–225. doi: 10.1007/s00239-004-0374-3.

Nguyen K, Malik TN, Chaput JC. Chemical evolution of an autonomous DNAzyme with allele-specific gene silencing activity. Nat Commun. 2023; 14:1–11. doi: 10.1038/s41467-023-38100-9.

Nowakowski J, Shim PJ, Prasad GS, Stout CD, Joyce GF. Crystal structure of an 82-nucleotide RNA-DNA complex formed by the 10-23 DNA enzyme. Nat Struct Biol. 1999; 6(2):151–156. doi: 10.1038/5839.

O'Brien J, Hayder H, Zayed Y, Peng C. Overview of microRNA biogenesis, mechanisms of actions, and circulation. Frontiers in Endocrinology. 2018; 9:1–12. doi: 10.3389/fendo.2018.00402.

Oprzeska-Zingrebe EA, Meyer S, Roloff A, Kunte HJ, Smiatek J. Influence of compatible solute ectoine on distinct DNA structures: thermodynamic insights into molecular binding mechanisms and destabilization effects. Phys Chem Chem Phys. 2018; 20:25861–25874. doi: 10.1039/c8cp03543a.

Ostrowska N, Feig M, Trylska J. Modeling Crowded Environment in Molecular Simulations. Frontiers in Molecular Biosciences. 2019; 6. doi: 10.3389/fmolb.2019.00086.

Pan T, Sosnick T. RNA folding during transcription. Annu Rev Biophys Biomol Struct. 2006; 35:161–175. doi: 10.1146/annurev.biophys.35.040405.102053.

Panzarin V, Cuenca A, Gastaldelli M, Alencar ALF, Pascoli F, Morin T, Blanchard Y, Cabon J, Louboutin L, Ryder D, Abbadi M, Toffan A, Dopazo CP, Biacchesi S, Brémont M, Olesen NJ. VHSV Single Amino Acid Polymorphisms (SAPs) Associated With Virulence in Rainbow Trout. Front Microbiol. 2020; 11(August):1–17. doi: 10.3389/fmicb.2020.01984.

Park YJ, Moon C, Kang JH, Choi TJ. Antiviral effects of extracts from Celosia cristata and Raphanus sativus roots against viral hemorrhagic septicemia virus. Arch Virol. 2017; 162(6):1711–1716. doi: 10.1007/s00705-017-3270-z.

Paudel BP, Fiorini E, Börner R, Sigel RKO, Rueda DS. Optimal molecular crowding accelerates group II intron folding and maximizes catalysis. Proc Natl Acad Sci U S A. 2018; 115(47):11917–11922. doi: 10.1073/pnas.1806685115.

Paudel BP, Rueda D. Molecular crowding accelerates ribozyme docking and catalysis. J Am Chem Soc. 2014; 136(48):16700–16703. doi: 10.1021/ja5073146.

Pauling L, Corey RB. A Proposed Structure For The Nucleic Acids. Proc Natl Acad Sci. 1953; 39(2):84–97. doi: 10.1073/pnas.39.2.84.

Payne S. Chapter 10 - Introduction to RNA Viruses. In: Payne S, editor. *Viruses* Academic Press; 2017.p. 97–105. doi: 10.1016/B978-0-12-803109-4.00010-6.

Pechlaner M, Sigel RKO. Characterization of metal ion-nucleic acid interactions in solution. In: *Interplay between Met. Ions Nucleic Acids* Springer; 2012.p. 1–42. doi: 10.1007/978-94-007-2172-2.

Pedersen JS. Analysis of small-angle scattering data from colloids and polymer solutions: modeling and least-squares fitting. Adv Colloid Interface Sci. 1997; 70:171–210. doi: 10.1016/S0001-8686(97)00312-6.

Peng H, Li XF, Zhang H, Le XC. A microRNA-initiated DNAzyme motor operating in living cells. Nat Commun. 2017; 8(1). doi: 10.1038/ncomms14378.

Pereiro P, Figueras A, Novoa B. Turbot (*Scophthalmus maximus*) vs. VHSV (Viral Hemorrhagic Septicemia Virus): A review. Frontiers in Physiology. 2016; 7:1–10. doi: 10.3389/fphys.2016.00192.

Perrin F. Mouvement brownien d'un ellipsoide-I. Dispersion diélectrique pour des molécules ellipsoidales. J Phys Radium. 1934; 5:497–511. doi: 10.1051/jphysrad:01934005010049700.

Pfeiffer F, Tolle F, Rosenthal M, Brändle GM, Ewers J, Mayer G. Identification and characterization of nucleobase-modified aptamers by click-SELEX. Nat Protoc. 2018; 13(5):1153–1180. doi: 10.1038/nprot.2018.023.

Pincus DL, Hyeon C, Thirumalai D. Effects of trimethylamine N-Oxide (TMAO) and crowding agents on the stability of RNA hairpins. J Am Chem Soc. 2008; 130(23):7364–7372. doi: 10.1021/ja078326w.

Pine AC, Brooke GN, Marco A. A computational approach to identify efficient RNA cleaving 10-23 DNAzymes. NAR Genomics Bioinforma. 2023; 5(1):1–9. doi: 10.1093/nargab/lqac098.

Plavec J. NMR Study on Nucleic Acids. In: *Handbook of Chemical Biology of Nucleic Acids* Springer Nature Singapore; 2022.p. 1–44. doi: 10.1007/978-981-16-1313-5_8-1.

Pradeepkumar PI, Höbartner C, Baum DA, Silverman SK. DNA-catalyzed formation of nucleopeptide linkages. Angew Chemie - Int Ed. 2008; 47(9):1753–1757. doi: 10.1002/anie.200703676.

Przybilski R, Hammann C. The hammerhead ribozyme structure brought in line. ChemBioChem. 2006; 7(11):1641–1644. doi: 10.1002/cbic.200600312.

Rahman MM, Matsumura S, Ikawa Y. Effects of molecular crowding on a bimolecular group I ribozyme and its derivative that self-assembles to form ribozyme oligomers. Biochem Biophys Res Commun. 2018; 507(1-4):136–141. doi: 10.1016/j.bbrc.2018.10.188.

Raina M, Ibba M. tRNAs as regulators of biological processes. Front Genet. 2014; 5(1):1–14. doi: 10.3389/fgene.2014.00171.

Rajendrakumar CSV, Suryanarayana T, Reddy AR. DNA helix destabilization by proline and betaine: possible role in the salinity tolerance process. FEBS Letters. 1997; 410(2-3):201–205. doi: 10.1016/s0014-5793(97)00588-7.

Rees WA, Yager TD, Korte J, von Hippel. Betaine can eliminate the base pair composition dependence of DNA melting. Biochemistry. 1993; 32:137–44. doi: 10.1021/bi00052a019.

Reuter JS, Mathews DH. RNAstructure: Web servers for RNA secondary structure prediction and analysis. BM. 2010; 11:1–9. doi: 10.1093/nar/gkt290.

Reyes-Gutiérrez P, Alvarez-Salas LM. Cleavage of HPV-16 E6/E7 mRNA mediated by modified 10-23 deoxyribozymes. Oligonucleotides. 2009; 19(3):233–242. doi: 10.1089/oli.2009.0193.

Rivas G, Minton AP. Macromolecular Crowding In Vitro, In Vivo, and In Between. Trends Biochem Sci. 2016; 41(11):970–981. doi: 10.1016/j.tibs.2016.08.013.

Rivory L, Tucker C, King A, Lai A, Goodchild A, Witherington C, Gozar MM, Birkett DJ. The DNAzymes Rs6, Dz13, and DzF have potent biologic effects independent of catalytic activity. Oligonucleotides. 2006; 16(4):297–312. doi: 10.1089/oli.2006.16.297.

Robertson MP, Joyce GF. Origins of the RNA world. Cold Spring Harb Perspect Biol. 2012; 4:1–22. doi: 10.1017/cbo9780511626180.013.

Rosenbach H, Borggräfe J, Victor J, Wuebben C, Schiemann O. Influence of monovalent metal ions on metal binding and catalytic activity of the 10 – 23 DNAzyme. Biol Chem. 2021; 402(1):99–111. doi: 10.1515/hsz-2020-0207.

Rosenbach H, Victor J, Borggräfe J, Biehl R, Steger G, Etzkorn M, Span I. Expanding crystallization tools for nucleic acid complexes using U1A protein variants. Journal of Structural Biology. 2020; 210(2):107480. doi: 10.1016/j.jsb.2020.107480.

Rosenbach H, Victor J, Etzkorn M, Steger G, Riesner D, Span I. Molecular Features and Metal Ions That Influence 10-23 DNAzyme Activity. Molecules. 2020; 25:11–25. doi: 10.3390/molecules25133100.

Rossi E, Meuser ME, Cunanan CJ, Cocklin S. Structure, Function, and Interactions of the HIV-1 Capsid Protein. Life. 2021; 11(2):100. doi: 10.3390/life11020100.

Roth A, Breaker RR. An amino acid as a cofactor for a catalytic polynucleotide. Proc Natl Acad Sci U S A. 1998; 95(11):6027–6031. doi: 10.1073/pnas.95.11.6027.

Roy S. Impact of UV Radiation on Genome Stability and Human Health. In: *Ultraviolet Light in Human Health, Diseases and Environment* Springer International Publishing; 2017.p. 207–219. doi: 10.1007/978-3-319-56017-5_17.

Rubio L, Galipienso L, Ferriol I. Detection of Plant Viruses and Disease Management: Relevance of Genetic Diversity and Evolution. Frontiers in Plant Science. 2020; 11:1–23. doi: 10.3389/fpls.2020.01092.

Rudeejaroonrung K, Hanpanich O, Saito K, Shimada N, Maruyama A. Cationic copolymer enhances 8-17 DNAzyme and MNAzyme activities. Biomater Sci. 2020; 8(14):3812–3818. doi: 10.1039/d0bm00428f.

SantaLucia J, Allawi HT, Seneviratne PA. Improved Nearest-Neighbor Parameters for Predicting DNA Duplex Stability†. Biochemistry. 1996; p. 3555–3562. doi: 10.1021/bi951907q.

Santoro SW, Joyce GF. A general purpose RNA-cleaving DNA enzyme. Proc Natl Acad Sci U S A. 1997; 94(9):4262–4266. doi: 10.1073/pnas.94.9.4262.

Santoro SW, Joyce GF. Mechanism and utility of an RNA-cleaving DNA enzyme. Biochemistry. 1998; 37(38):13330–13342. doi: 10.1021/bi9812221.

Sasaki Y, Miyoshi D, Sugimoto N. Regulation of DNA nucleases by molecular crowding. Nucleic Acids Res. 2007; 35(12):4086–4093. doi: 10.1093/nar/gkm445.

Sasmal DK, Pulido LE, Kasal S, Huang J. Single-molecule fluorescence resonance energy transfer in molecular biology. Nanoscale. 2016; 8(48):19928–19944.

Schubert S, Kurreck J. Ribozyme- and Deoxyribozyme-Strategies for Medical Applications. Curr Drug Targets. 2005; 5(8):667–681. doi: 10.2174/1389450043345092.

Schubert S, Gül DC, Grunert HP, Zeichhardt H, Erdmann VA, Kurreck J. RNA cleaving '10-23' DNAzymes with enhanced stability and activity. Nucleic Acids Res. 2003; 31(20):5982–5992. doi: 10.1093/nar/gkg791.

Schütze H, Mundt E, Mettenleiter TC. Complete genomic sequence of viral hemorrhagic septicemia virus, a fish rhabdovirus. Virus Genes. 1999; 19(1):59–65. doi: 10.1023/A:1008140707132.

Sednev MV, Liaqat A, Höbartner C. High-Throughput Activity Profiling of RNA-Cleaving DNA Catalysts by Deoxyribozyme Sequencing (DZ-seq). J Am Chem Soc. 2022; 144(5):2090–2094. doi: 10.1021/jacs.1c12489.

Seferos DS, Prigodich AE, Giljohann DA, Patel PC, Mirkin CA. Polyvalent DNA Nanoparticle Conjugates Stabilize Nucleic Acids. Nano Lett. 2009; 9(1):308–311. doi: 10.1021/nl802958f.Polyvalent.

Seitz R. Human Immunodeficiency Virus (HIV). Transfusion Medicine and Hemotherapy. 2016; 43(3):203–222. doi: 10.1159/000445852.

Serganov A, Patel DJ. Ribozymes, riboswitches and beyond: Regulation of gene expression without proteins. Nat Rev Genet. 2007; 8(10):776–790. doi: 10.1038/nrg2172.

Sharp KA. Analysis of the size dependence of macromolecular crowding shows that smaller is better. Proc Natl Acad Sci U S A. 2015; 112(26):7990–7995. doi: 10.1073/pnas.1505396112.

Shearer KD. Whole body magnesium concentration as an indicator of magnesium status in rainbow trout (*Salmo gairdneri*). Aquaculture. 1989; 77(2-3):201–210. doi: 10.1016/0044-8486(89)90202-0.

Shen L, Zhou Q, Wang Y, Liao W, Chen Y, Xu Z, Yang L, Sun LQ. Antiangiogenic and Antitumoral Effects Mediated by a Vascular Endothelial Growth Factor Receptor 1 (VEGFR-1)-Targeted DNAzyme. Molecular Medicine. 2013; 19(1):377–386. doi: 10.2119/molmed.2013.00090.

Sidorov AV, Grasby JA, Williams DM. Sequence-specific cleavage of RNA in the absence of divalent metal ions by a DNAzyme incorporating imidazolyl and amino functionalities. Nucleic Acids Res. 2004; 32(4):1591–1601. doi: 10.1093/nar/gkh326.

Silverman SK. In vitro selection, characterization, and application of deoxyribozymes that cleave RNA. Nucleic Acids Res. 2005; 33(19):6151–6163. doi: 10.1093/nar/gki930.

Silverman SK. Pursuing DNA catalysts for protein modification. Acc Chem Res. 2015; 48(5):1369–1379. doi: 10.1021/acs.accounts.5b00090.

Silverman SK. Catalytic DNA: Scope, Applications, and Biochemistry of Deoxyribozymes. Trends Biochem Sci. 2016; 41(7):595–609. doi: 10.1016/j.tibs.2016.04.010.

Silverman SK. Catalytic DNA (deoxyribozymes) for synthetic applications-current abilities and future prospects. Chemical Communications. 2008; p. 3467–3485. doi: 10.1039/b807292m.

Silverstein TP, Slade K. Effects of Macromolecular Crowding on Biochemical Systems. J Chem Educ. 2019; 96(11):2476–2487. doi: 10.1021/acs.jchemed.9b00399.

Singh A, Singh N. Molecular crowding effects on stability of DNA double helix. AIP Conf Proc. 2016; 1728(May). doi: 10.1063/1.4946179.

Singh N, Ranjan A, Sur S, Chandra R, Tandon V. Inhibition of HIV-1 Integrase gene expression by 10-23 DNAzyme. Journal of Biosciences. 2012; 37(3):493–502. doi: 10.1007/s12038-012-9216-4.

Skall HF, Olesen NJ, Mellergaard S. Viral haemorrhagic septicaemia virus in marine fish and its implications for fish farming – a review. Journal of Fish Diseases. 2005; 28(9):509–529. doi: 10.1111/j.1365-2761.2005.00654.x.

Snow M, Bain N, Black J, Taupin V, Cunningham CO, King JA, Skall HF, Raynard RS. Genetic population structure of marine viral haemorrhagic septicaemia virus (VHSV). Dis Aquat Organ. 2004; 61(1-2):11–21. doi: 10.3354/dao061011.

Sokolova I. Poikilotherms. In: Jørgensen SE, Fath BD, editors. *Encyclopedia of Ecology* Oxford: Academic Press; 2008.p. 2851–2854. doi: 10.1016/b978-008045405-4.00536-x.

Spink CH, Chaires JB. Effects of hydration, ion release, and excluded volume on the melting of triplex and duplex DNA. Biochemistry. 1999; 38(1):496–508. doi: 10.1021/bi9820154.

Spitale RC, Chaput JC. Reply to: On gene silencing by the X10-23 DNAzyme. Nature Chemistry. 2022; 14:859–861. doi: 10.1038/s41557-022-00983-4.

Steger G, Victor J. Design of a DNAzyme. In: Steger G, Rosenbach H, Span I, editors. *DNAzymes*, vol. 2439 of Methods in Molecular Biology New York: Humana Press; 2022.p. 47–63. doi: 10.1007/978-1-0716-2047-2_4.

Sugimoto N. Noncanonical Structures and Their Thermodynamics of DNA and RNA Under Molecular Crowding: Beyond the Watson–Crick Double Helix. In: Hancock R, Jeon KW, editors. *New Models of the Cell Nucleus: Crowding, Entropic Forces, Phase Separation, and Fractals*, vol. 307 of International Review of Cell and Molecular Biology Academic Press; 2014.p. 205–273. doi: 10.1016/b978-0-12-800046-5.00008-4.

Sugimoto N, Nakano Si, Katoh M, Matsumura A, Nakamuta H, Ohmichi T, Yoneyama M, Sasaki M. Thermodynamic Parameters To Predict Stability of RNA/DNA Hybrid Duplexes. Biochemistry. 1995; 34(35):11211–11216. doi: 10.1021/bi00035a029.

Sugimoto N, Okumoto Y, Ohmichi T. Effect of metal ions and sequence of deoxyribozymes on their RNA cleavage activity. J Chem Soc, Perkin Trans 2. 1999; p. 1381–1386. doi: 10.1039/a901461f.

Sugiyama R, Hayafune M, Habu Y, Yamamoto N, Takaku H. HIV-1 RT-dependent DNAzyme expression inhibits HIV-1 replication without the emergence of escape viruses. Nucleic Acids Research. 2010; 39(2):589–598. doi: 10.1093/nar/gkq794.

Swinefus JJ, Menssen RJ, Kohler JM, Schmidt EC, Thomas AL. Quantifying the Temperature Dependence of Glycine Betaine RNA Duplex Destabilization. Biochemistry. 2013; 52(5):1–20. doi: 10.1021/bi400765d.

Tafer H, Ameres SL, Obernosterer G, Gebeshuber CA, Schroeder R, Martinez J, Hofacker IL. The impact of target site accessibility on the design of effective siRNAs. Nat Biotechnol. 2008; 26(5):578–583. doi: 10.1038/nbt1404.

Takahashi H, Hamazaki H, Habu Y, Hayashi M, Abe T, Miyano-Kurosaki N, Takaku H. A new modified DNA enzyme that targets influenza virus a mRNA inhibits viral infection in cultured cells. FEBS Lett. 2004; 560(1-3):69–74. doi: 10.1016/S0014-5793(04)00073-0.

Tanner NK. Ribozymes: The characteristics and properties of catalytic RNAs. FEMS Microbiol Rev. 1999; 23(3):257–275. doi: 10.1016/S0168-6445(99)00007-8.

Tateishi-Karimata H, ichi Nakano S, Sugimoto N. Quantitative analyses of nucleic acid stability under the molecular crowding condition induced by cosolutes. Curr Protoc Nucleic Acid Chem. 2013; 53(1). doi: 10.1002/0471142700.nc0719s53.

Tatineni S, Hein GL. Plant Viruses of Agricultural Importance: Current and Future Perspectives of Virus Disease Management Strategies. Phytopathology. 2023; 113(2):117–141. doi: 10.1094/phyto-05-22-0167-rvw.

Taube T, Shalapour S, Seifert GJ, Pfau M, Henze G, Seeger K. Specific Inhibition of *BCR-ABL* Gene Expression in Acute Lymphoblastic Leukemia by Catalytic DNAzymes. Blood. 2005; 106(11):148–148. doi: 10.1182/blood.v106.11.148.148.

Taylor AI, Holliger P. On gene silencing by the X10-23 DNAzyme. Nat Chem. 2021; doi: 10.1038/s41557-022-00990-5.

Taylor AI, Pinheiro VB, Smola MJ, Morgunov AS, Peak-Chew S, Cozens C, Weeks KM, Herdewijn P, Holliger P. Catalysts from synthetic genetic polymers. Nature. 2015; 518(7539):427–430. doi: 10.1038/nature13982.Catalysts.

Taylor AI, Wan CJK, Donde MJ, Peak-Chew SY, Holliger P. A modular XNAzyme cleaves long, structured RNAs under physiological conditions and enables allele-specific gene silencing. Nat Chem. 2022; doi: 10.1038/s41557-022-01021-z.

Teraoka I. Dynamics of Dilute Polymer Solutions. In: *Polymer Solutions - An Introduction to Physical Properties* New York: John Wiley and Sons Inc.; 2002.p. 167–275. doi: 10.4324/9780203809075-32.

Thiyagarajan P, Chaiko D, Hjelm Jr R. A neutron scattering study of poly (ethylene glycol) in electrolyte solutions. Macromolecules. 1995; 28:7730–7736. doi: 10.1021/ma00127a020.

Thomas IBK, Gaminda KAP, Jayasinghe CD, Abeysinghe DT, Senthilnithy R. DNAzymes, novel therapeutic agents in cancer therapy: A review of concepts to applications. J Nucleic Acids. 2021; 2021. doi: 10.1155/2021/9365081.

Tinoco I, Borer PN, Dengler B, Levine MD. Improved Estimation of Secondary Structure in Ribonucleic Acids. Nat New Biol. 1973; 246:40–41. doi: 10.1038/newbio246040a0.

Tinoco I, Bustamante C. How RNA folds. J Mol Biol. 1999; 293(2):271–281. doi: 10.1006/jmbi.1999.3001.

Tinoco I, Uhlenbeck OC, Levine MD. Estimation of secondary structure in ribonucleic acids. Nature. 1971; 230(5293):362–367. doi: 10.1038/230362a0.

Tolle F, Brändle GM, Matzner D, Mayer G. A Versatile Approach Towards Nucleobase-Modified Aptamers. Angew Chemie - Int Ed. 2015; 54(37):10971–10974. doi: 10.1002/anie.201503652.

Travascio P, Bennet AJ, Wang DY, Dipankar S. A ribozyme and a catalytic DNA with peroxidase activity: Active sites versus cofactor-binding sites. Chem Biol. 1999; 6(11):779–787. doi: 10.1016/S1074-5521(99)80125-2.

Tuerk C, Gold L. Systematic Evolution of Ligands by Exponential Enrichment: RNA Ligands to Bacteriophage T4 DNA Polymerase. Science. 1990; 249(4968):505–510. doi: 10.1126/science.2200121.

Tyrrell J, Weeks KM, Pielak GJ. Challenge of Mimicking the Influences of the Cellular Environment on RNA Structure by PEG-Induced Macromolecular Crowding. Biochemistry. 2015; 54(42):6447–6453. doi: 10.1021/acs.biochem.5b00767.

Tzur A, Kafri R, LeBleu VS, Lahav G, Kirschner MW. Cell Growth and Size Homeostasis in Proliferating Animal Cells. Science. 2009; 325(5937):167–171. doi: 10.1126/science.1174294.

Uehata T, Takeuchi O. RNA Recognition and Immunity-Innate Immune Sensing and Its Posttranscriptional Regulation Mechanisms. Cells. 2020; 9(7):1701. doi: 10.3390/cells9071701.

Valadkhan S, Gunawardane LS. Role of small nuclear RNAs in eukaryotic gene expression. Essays Biochem. 2013; 54(1):79–90. doi: 10.1042/BSE0540079.

Van Lint S, Heirman C, Thielemans K, Breckpot K. From a chemical blueprint for protein production to an off-the-shelf therapeutic. Hum Vaccines Immunother. 2013; 9(2):265–274. doi: 10.4161/hv.22661.

Vasudevamurthy MK, Lever M, George PM, Morison KR. Betaine structure and the presence of hydroxyl groups alters the effects on DNA melting temperatures. Biopolymers. 2009; 91(1):85–94. doi: 10.1002/bip.21085.

Vester B, Lundberg LB, Sørensen MD, Babu BR, Douthwaite S, Wengel J. LNAzymes: Incorporation of LNA-type monomers into DNAzymes markedly increases RNA cleavage. J Am Chem Soc. 2002; 124(46):13682–13683. doi: 10.1021/ja0276220.

Victor J, Steger G, Riesner D. Inability of DNAzymes to cleave RNA in vivo is due to limited Mg^{2+} concentration in cells. Eur Biophys J. 2018; 47(4):333–343. doi: 10.1007/s00249-017-1270-2.

Wada A, Suyama A. Local stability of DNA and RNA secondary structure and its relation to biological functions. Prog Biophys Mol Biol. 1986; 47(2):113–157. doi: 10.1016/0079-6107(86)90012-X.

Waheed AA, Freed EO. HIV Type 1 Gag as a Target for Antiviral Therapy. AIDS Research and Human Retroviruses. 2012; 28(1):54–75. doi: 10.1089/aid.2011.0230.

Walter NG, Engelke DR. Ribozymes: Catalytic RNAs that cut things, make things, and do odd and useful jobs. Biologist. 2002; 49(5):199–203.

Wang B, Cao L, Chiuman W, Li Y, Xi Z. Probing the function of nucleotides in the catalytic cores of the 8-17 and 10-23 DNAzymes by abasic nucleotide and C3 spacer substitutions. Biochemistry. 2010; 49(35):7553–7562. doi: 10.1021/bi100304b.

Wang H, He D, Wu R, Cheng H, Ma W, Huang J, Bu H, He X, Wang K. A hybridization-triggered DNAzyme cascade assay for enzyme-free amplified fluorescence detection of nucleic acids. Analyst. 2019; 144(1):143–147. doi: 10.1039/c8an01796d.

Wang J, Huang H, Hanpanich O, Shimada N, Maruyama A. Cationic copolymer and crowding agent have a cooperative effect on a Na^{+}-dependent DNAzyme†. Biomater Sci. 2023; doi: 10.1039/d3bm01119d.

Wang M, Zhang H, Zhang W, Zhao Y, Yasmeen A, Zhou L, Yu X, Tang Z. In vitro selection of DNA-cleaving deoxyribozyme with site-specific thymidine excision activity. Nucleic Acids Res. 2014; 42(14):9262–9269. doi: 10.1093/nar/gku592.

Wang Y, Nguyen K, Spitale RC, Chaput JC. A biologically stable DNAzyme that efficiently silences gene expression in cells. Nat Chem. 2021; 13(4):319–326. doi: 10.1038/s41557-021-00645-x.

Wang Y, Sarkar M, Smith AE, Krois AS, Pielak GJ. Macromolecular crowding and protein stability. J Am Chem Soc. 2012; 134(40):16614–16618. doi: 10.1021/ja305300m.

Wang Y, Liu J, Zhou H. Visual detection of cucumber green Mottle Mosaic virus based on terminal deoxynucleotidyl transferase coupled with DNAzymes amplification. Sensors (Switzerland). 2019; 19(6). doi: 10.3390/s19061298.

Ward WL, Plakos K, Derose VJ. Nucleic acid catalysis: Metals, nucleobases, and other cofactors. Chem Rev. 2014; 114(8):4318–4342. doi: 10.1021/cr400476k.

Watts JM, Dang KK, Gorelick RJ, Leonard CW, Bess Jr JW, Swanstrom R, Burch CL, Weeks KM. Architecture and secondary structure of an entire HIV-1 RNA genome. Nature. 2009; 460(7256):711–716. doi: 10.1038/nature08237.

Weidemann T, Schwille P. Fluorescence Cross-Correlation Spectroscopy. In: Roberts GCK, editor. *Encyclopedia of Biophysics* Berlin, Heidelberg: Springer Berlin Heidelberg; 2013.p. 795–799. doi: 10.1007/978-3-642-16712-6_509.

Weinberg CE, Weinberg Z, Hammann C. Novel ribozymes: discovery, catalytic mechanisms, and the quest to understand biological function. Nucleic Acids Res. 2019; 47(18):9480–9494. doi: 10.1093/nar/gkz737.

Westhof E, Lescoute A. Ribozymes. In: Mahy BWJ, Van Regenmortel MHV, editors. *Encyclopedia of Virology*, 3 ed. Elsevier; 2008.p. 475–481. doi: 10.1016/B978-012374410-4.00495-7.

Wilson DS, Szostak JW. IN VITRO SELECTION OF FUNCTIONAL NUCLEIC ACIDS. Annu Rev Biochem. 1999; 68:611–647. doi: 10.1146/annurev.biochem.68.1.611.

Wong BC, Shahid U, Tan HS. Ribozymes as Therapeutic Agents against Infectious Diseases. In: Vlasova I, editor. *RNA Ther.*, vol. 11 Rijeka: IntechOpen; 2022.p. 1–23. doi: 10.5772/intechopen.107141.

Wong OY, Pradeepkumar PI, Silverman SK. DNA-catalyzed covalent modification of amino acid side chains in tethered and free peptide substrates. Biochemistry. 2011; 50(21):4741–4749. doi: 10.1021/bi200585n.

World Organisation for Animal Health (OIE). Infection with viral haemorrhagic septicaemia virus. In: *Man. Diagnostic Tests Aquat. Anim. 2021* World Organisation for Animal Health; 2021.p. 377–401.

Wu J, Yu Y, Wei S, Xue B, Zhang J. A DNAzyme-based electrochemical impedance biosensor for highly sensitive detection of Cu^{2+} ions in aqueous solution. Int J Electrochem Sci. 2017; 12(12):11666–11676. doi: 10.20964/2017.12.46.

Wu P, Hwang K, Lan T, Lu Y. A DNAzyme-gold nanoparticle probe for uranyl ion in living cells. J Am Chem Soc. 2013; 135(14):5254–5257. doi: 10.1021/ja400150v.

Wurtmann EJ, Wolin SL. RNA under attack: Cellular handling of RNA damage. Critical Reviews in Biochemistry and Molecular Biology. 2009; 44(1):34–49. doi: 10.1080/10409230802594043.

Xia T, and M E Burkard, Kierzek R, Schroeder SJ, Jiao X, Cox C, Turner DH. Thermodynamic parameters for an expanded nearest-neighbor model for formation of RNA duplexes with Watson-Crick base pairs. Biochemistry. 1998; 37(42):14719–14735. doi: 10.1021/bi9809425.

Xiang Y, Lu Y. DNA as sensors and imaging agents for metal ions. Inorg Chem. 2014; 53(4):1925–1942. doi: 10.1021/ic4019103.

Xiao L, Zhao Y, Yang M, Luan G, Du T, Deng S, Jia X. A promising nucleic acid therapy drug: DNAzymes and its delivery system. Frontiers in Molecular Biosciences. 2023; 10:1–16. doi: 10.3389/fmolb.2023.1270101.

Xiao Y, Rowe AA, Plaxco KW. Electrochemical detection of parts-per-billion lead via an electrode-bound DNAzyme assembly. J Am Chem Soc. 2007; 129(2):262–263. doi: 10.1021/ja067278x.

Xie YY, Zhao XD, Jiang LP, Liu HL, Wang LJ, Fang P, Shen KL, Xie ZD, Wu YP, Yang XQ. Inhibition of respiratory syncytial virus in cultured cells by nucleocapsid gene targeted deoxyribozyme (DNAzyme). Antiviral Research. 2006; 71(1):31–41. doi: 10.1016/j.antiviral.2006.02.011.

Xu ZJ, Yang LF, Sun LQ, Cao Y. Use of DNAzymes for cancer research and therapy. Chinese Sci Bull. 2012; 57(26):3404–3408. doi: 10.1007/s11434-012-5380-z.

Yan J, Ran M, Shen X, Zhang H. Therapeutic DNAzymes: From Structure Design to Clinical Applications. Adv Mater. 2023; 35(30):1–34. doi: 10.1002/adma.202300374.

Yan J, Ran M, Zhang H. A scientific debate: The sword that cleaves chaos of DNAzyme catalysis research. Biomed Technol. 2023; 4:21–23. doi: 10.1016/j.bmt.2023.01.004.

Yang H, Peng Y, Xu M, Xu S, Zhou Y. Development of DNA Biosensors Based on DNAzymes and Nucleases. Crit Rev Anal Chem. 2023; 53(1):161–176. doi: 10.1080/10408347.2021.1944046.

Yoshikawa K, Hirota S, Makita N, Yoshikawa Y. Compaction of DNA induced by like-charge protein: Opposite salt-effect against the polymer-salt-induced condensation with neutral polymer. J Phys Chem Lett. 2010; 1(12):1763–1766. doi: 10.1021/jz100569e.

Young DD, Lively MO, Deiters A. Activation and deactivation of DNAzyme and antisense function with light for the photochemical regulation of gene expression in mammalian cells. J Am Chem Soc. 2010; 132(17):6183–6193. doi: 10.1021/ja100710j.

Yousefi H, Ali MM, Su HM, Filipe CDM, Didar TF. Sentinel Wraps: Real-Time Monitoring of Food Contamination by Printing DNAzyme Probes on Food Packaging. ACS Nano. 2018; 12(4):3287–3294. doi: 10.1021/acsnano.7b08010.

Yu L, Lei Y, Ma Y, Liu M, Zheng J, Dan D, Gao P. A Comprehensive Review of Fluorescence Correlation Spectroscopy. Frontiers in Physics. 2021; 9. doi: 10.3389/fphy.2021.644450.

Yu T, Zhu Y, He Z, Chen SJ. Predicting Molecular Crowding Effects in Ion-RNA Interactions. J Phys Chem B. 2016; 120(34):8837–8844. doi: 10.1021/acs.jpcb.6b05625.Predicting.

Zaborowska Z, Fürste JP, Erdmann VA, Kurreck J. Sequence requirements in the catalytic core of the "10-23" DNA enzyme. J Biol Chem. 2002; 277(43):40617–40622. doi: 10.1074/jbc.M207094200.

Zaborowska Z, Schubert S, Kurreck J, Erdmann VA. Deletion analysis in the catalytic region of the 10-23 DNA enzyme. FEBS Lett. 2005; 579(2):554–558. doi: 10.1016/j.febslet.2004.12.008.

Zemora G, Waldsich C. RNA folding in living cells. RNA Biol. 2010; 7(6):634–641. doi: 10.4161/rna.7.6.13554.

Zhang J. RNA-cleaving DNAzymes: Old catalysts with new tricks for intracellular and in vivo applications. Catalysts. 2018; 8(11). doi: 10.3390/catal8110550.

Zhang J, Fei Y, Sun L, Zhang QC. Advances and opportunities in RNA structure experimental determination and computational modeling. Nat Methods. 2022; 19(10):1193–1207. doi: 10.1038/s41592-022-01623-y.

Zhang L, Zhang Y, Wei M, Yi Y, Li H, Yao S. A label-free fluorescent molecular switch for Cu^{2+} based on metal ion-triggered DNA-cleaving DNAzyme and DNA intercalator. New J Chem. 2013; 37(4):1252–1257. doi: 10.1039/c3nj41103f.

Zhang W, Chen X, Yu F, Li F, Li W, Yi M, Jia K. α-Lipoic Acid Exerts Its Antiviral Effect against Viral Hemorrhagic Septicemia Virus (VHSV) by Promoting Upregulation of Antiviral Genes and Suppressing VHSV-Induced Oxidative Stress. Virol Sin. 2021; 36(6):1520–1531. doi: 10.1007/s12250-021-00440-5.

Zhang XB, Kong RM, Lu Y. Metal ion sensors based on DNAzymes and related DNA molecules. Annu Rev Anal Chem. 2011; 4:105–128. doi: 10.1146/annurev.anchem.111808.073617.

Zhou HX. Effect of mixed macromolecular crowding agents on protein folding. Proteins. 2008; 72(4):1109–1113. doi: 10.1002/prot.22111.

Zhou HX, Rivas G, Minton AP. Macromolecular Crowding and Confinement : Biochemical , Biophysical , and Potential Physiological Consequences. Annu Rev Biophys. 2008; 37:375–397. doi: 10.1146/annurev.biophys.37.032807.125817.

Zhou HX. Protein folding in confined and crowded environments. Arch Biochem Biophys. 2008; 469:76–82. doi: 10.1016/j.abb.2007.07.013.

Zhou W, Ding J, Liu J. Theranostic dnazymes. Theranostics. 2017; 7(4):1010–1025. doi: 10.7150/thno.17736.

Zhou W, Saran R, Liu J. Metal Sensing by DNA. Chem Rev. 2017; 117(12):8272–8325. doi: 10.1021/acs.chemrev.7b00063.

Zhou Z, Sun W, Huang Z. 8-17 DNAzyme silencing gene expression in cells via cleavage and antisense. Molecules. 2022; 28:286. doi: 10.3390/molecules28010286.

Zimmerman SB, Minton AP. MACROMOLECULAR CROWDING: biochemical, biophysical, and physiological consequences. Annu Rev Biophys Biomol Struct. 1993; 22:27–65. doi: 10.1146/annurev.bb.22.060193.000331.

Zong W, Ma S, Zhang X, Wang X, Li Q, Han X. A Fissionable Artificial Eukaryote-like Cell Model. J Am Chem Soc. 2017; 139(29):9955–9960. doi: 10.1021/jacs.7b04009.

Zuker M. Mfold web server for nucleic acid folding and hybridization prediction. Nucleic Acids Res. 2003; 31(13):3406–3415. doi: 10.1093/nar/gkg595.

List of Figures

List of Tables

DECLARATION OF CONTRIBUTIONS

Stability and Activity of the 10-23 DNAzyme Under Molecular Crowding Conditions

Nina Kirchgässler[1], Hannah Rosenbach[1], and Ingrid Span[2,*]

Published in: **Methods in Molecular Biology**
Impact Factor (2022): 1.13
Contribution: 80 %

N.K. selected the references, prepared all figures, and wrote the first draft of the book chapter. All authors commented on the manuscript.

Molecular crowding: impacts on the activity of the 10-23 DNAzyme

Nina Kirchgässler[1], Hannah Rosenbach[1], Gerhard Steger[1], Ralf Biehl[3], Richard Börner[4], and Ingrid Span[2,*]

In preparation
Contribution: 68 %

All authors designed the experiments. N.K. performed all experiments shown in the article, except for the SAXS measurements and data analysis (R. Biehl) and FCS data analysis (R. Börner). N.K. prepared all figures and tables, except for Figure 3.8 (R. Biehl). N.K. wrote the first draft of the manuscript, except for material and method paragraphs regarding SAXS measurements and data analysis (R. Biehl) and FCS data analysis (R. Börner). The manuscript will be reviewed by all authors.

Extending crowding *in vitro*

Nina Kirchgässler[1] and Ingrid Span[2,*]

In Preparation
Contribution: 90 %

N.K. selected the references and wrote the first draft of the manuscript. N.K. prepared all figures and tables. N.K. and I.S. will finalize the manuscript.

[1] Heinrich Heine University Düsseldorf, Faculty of Mathematics and Natural Sciences, Institut für Physikalische Biologie, D-40225 Düsseldorf, Germany

[2] Department of Chemistry and Pharmacy, Bioinorganic Chemistry, Friedrich Alexander University Erlangen-Nürnberg, D-91058 Erlangen, Germany

[3] Juelich Centre for Neutron Science (JCNS) and Institute for Complex Systems (ICS), Forschungszentrum Jülich GmbH, D-52425 Jülich, Germany

[4] Laserinsitut Hochschule Mittweida, University of Applied Science Mittweida, D-09648 Mittweida, Germany

* Corresponding author
Department of Chemistry and Pharmacy, Bioinorganic Chemistry, Friedrich Alexander University Erlangen-Nürnberg, D-91058 Erlangen, Germany
ingrid.span@fau.de; Room A2.37; +49 9131 85-25428

DANKSAGUNG

Ich möchte mich recht herzlich bei meiner Erstgutachterin Frau Prof. Dr. Ingrid Span für die Möglichkleit zur Promotion in Ihrer Arbeitsgruppe und die herausfordernden Projekte, an denen ich mitwirken durfte, bedanken. Zusätzlich bedanke ich mich bei Frau Prof. Dr. Ilka Axmann für die Übernahme des Zweitgutachtens und den konstruktiven Austausch.

Herrn Prof. Dr. Dieter Willbold danke ich für die Bereitstellung der Labore und Verbrauchsmaterialien und, dass ich meine Promotion, trotz des Standortwechsels von Frau Prof. Dr. Ingrid Span nach Erlangen, an der Heinrich-Heine-Universität in Düsseldorf abschließen durfte.

Ein ganz besonderer Dank gilt Herrn apl. Prof. Dr. Ing. Gerhard Steger für seine stete Unterstützung, konstruktiven Diskussionen und tolle Zusammenarbeit im DNAzym-Projekt, aber vor allem auch für seine Hilfe bei Fragen und Antworten im Bereich Bioinformatik und LaTeX.

Darüber hinaus möchte ich mich bei allen aktuellen, besonders Melissa und Bianca, und ehemaligen Mitgliedern der Arbeitsgruppe Span für die Zusammenarbeit der letzten Jahre bedanken. Ein großer Dank gilt auch den Mitgliedern des IPB für ein freundliches Arbeitsklima und die Unterstützung im Laboralltag. Hervorheben möchte ich an dieser Stelle Astrid Wies, Robin Backer, Barbara Schulten, Linda Reineke und Joanna Zeyer, die als aktuelle und teils ehemalige IPB-Mitglieder dafür gesorgt haben, dass es im Labor läuft, Materialien beschafft werden und die mit Rat und Tat bei sämtlichen bürokratischen Belangen zur Seite standen.

Abseits des IPB danke ich auch meinen Kooperationspartnern für die Zusammenarbeit und fachliche Untersützung. Erwähnen möchte ich an dieser Stelle Prof. Dr. Richard Börner, apl. Prof. Dr. Stefanie Weidtkamp-Peters und Dr. Ralf Biehl.

Als Freundin und Kollegin möchte ich mich herzlich bei Celina für ihre Offenheit, die ideenreichen Gespräche und vielen lustigen und schönen Stunden während und abseits der Arbeit bedanken. Dankend erwähnen möchte ich zudem meine Kolleg*innen Sophia, Justin und Chris für eine sehr amüsante und abwechslungsreiche Zeit.

Für bedingungslose Untersützung und Zuspruch auf meinem gesamten Weg spreche ich meiner Familie, meinen Eltern Anita und Bruno, meinem Bruder Nick und meinen Freunden besonderen Dank aus. Ich möchte mich an dieser Stelle auch herzlichst bei meiner Freundin Anni für ihre Ruhe, Fürsorge und Unterstützung, vor allem in den letzten Monaten, bedanken. Ohne Euch hätte ich es nicht so weit geschafft!

EIDESSTATTLICHE ERKLÄRUNG

Ich versichere an Eides Statt, dass diese Dissertation von mir selbstständig und ohne unzulässige fremde Hilfe unter Beachtung der „Grundsätze zur Sicherung guter wissenschaftlicher Praxis an der Heinrich-Heine-Universität Düsseldorf“ erstellt worden ist. Die Arbeit wurde bisher keiner Prüfungsbehörde vorgelegt und auch noch nicht veröffentlicht. Ich habe bisher keinen erfolglosen Promotionsversuch unternommen.

Düsseldorf, den 4. März 2024

Nina Maria Kirchgässler